ISSN 0021-9673

VOL. 718 NO. 1 1 DECEMBER 1995

JOURNAL OF CHROMATOGRAPHY A

INCLUDING ELECTROPHORESIS AND OTHER SEPARATION METHODS

ELSEVIER

JOURNAL OF CHROMATOGRAPHY A

INCLUDING ELECTROPHORESIS AND OTHER SEPARATION METHODS

Scope. The *Journal of Chromatography* publishes papers on all aspects of **chromatography, electrophoresis** and other separation methods. Contributions consist mainly of research papers dealing with chromatographic theory, instrumental developments and their applications. Section *A* covers all areas except biomedical applications of separation science which are published in section *B: Biomedical Applications.*

Submission of Papers. The preferred medium of submission is on disk with accompanying manuscript. Manuscripts (in English; *four* copies are required) should be submitted to: Editorial Office of *Journal of Chromatography A*, P.O. Box 681, 1000 AR Amsterdam, Netherlands, Telefax (+31-20) 485 2304. Review articles are invited or proposed in writing to the Editors who welcome suggestions for subjects. An outline of the proposed review should first be forwarded to the Editors for preliminary discussion prior to preparation. Submission of an article is understood to imply that the article is original and unpublished and is not being considered for publication elsewhere. For copyright regulations, see below.

Subscription information. For 1996 Vols. 715–748 of *Journal of Chromatography A* (ISSN 0021-9673) are scheduled for publication. Subscription prices for *Journal of Chromatography A + B* (combined), or for section *A* or *B* are available upon request from the publisher. Subscriptions are accepted on a prepaid basis only and are entered on a calendar year basis. Issues are sent by surface mail except to the following countries where air delivery via SAL is ensured: Argentina, Australia, Brazil, Canada, China, Hong Kong, India, Israel, Japan, Malaysia, Mexico, New Zealand, Pakistan, Singapore, South Africa, South Korea, Taiwan, Thailand, USA. For all other countries airmail rates are available upon request. Claims for missing issues must be made within six months of our publication (mailing) date. Please address all your requests regarding orders and subscription queries to: Elsevier Science B.V., Journal Department, P.O. Box 211, 1000 AE Amsterdam, Netherlands. Tel.: (+31-20) 485 3642; Fax: (+31-20) 485 3598. Customers in the USA and Canada wishing information on this and other Elsevier journals, please contact Journal Information Center, Elsevier Science Inc., 655 Avenue of the Americas, New York, NY 10010, USA, Tel. (+1-212) 633 3750, Telefax (+1-212) 633 3764.

Abstracts/Contents Lists published in Analytical Abstracts, Biochemical Abstracts, Biological Abstracts, Chemical Abstracts, Chemical Titles, Chromatography Abstracts, Current Awareness in Biological Sciences (CABS), Current Contents/Life Sciences, Current Contents/Physical, Chemical & Earth Sciences, Deep-Sea Research/Part B: Oceanographic Literature Review, Excerpta Medica, Index Medicus, Mass Spectrometry Bulletin, PASCAL-CNRS, Referativnyi Zhurnal, Research Alert and Science Citation Index.

US Mailing Notice. *Journal of Chromatography A* (ISSN 0021-9673) is published weekly (total 52 issues) by Elsevier Science B.V., (Sara Burgerhartstraat 25, P.O. Box 211, 1000 AE Amsterdam, Netherlands). Annual subscription price in the USA US$ 6863.00 (US$ price valid in North, Central and South America only) including air speed delivery. Second class postage paid at Jamaica, NY 11431. **USA POSTMASTERS**: Send address changes to *Journal of Chromatography A*, Publications Expediting, Inc., 200 Meacham Avenue, Elmont, NY 11003. Airfreight and mailing in the USA by Publications Expediting.

Advertisements. The Editors of the journal accept no responsibility for the contents of the advertisements. Advertisement rates are available on request. Advertising orders and enquiries may be sent to *International:* Elsevier Science, Advertising Department, The Boulevard, Langford Lane, Kidlington, Oxford, OX5 1GB, UK; Tel: (+44) (0) 1865 843565; Fax: (+44) (0) 1865 843952. *USA and Canada:* Weston Media Associates, Dan Lipner, P.O. Box 1110, Greens Farms, CT 06436-1110, USA; Tel: (203) 261 2500; Fax: (203) 261 0101. *Japan:* Elsevier Science Japan, Ms Noriko Kodama, 20-12 Yushima, 3 chome, Bunkyo-Ku, Tokyo 113, Japan; Tel: (+81) 3 3836 0810; Fax: (+81) 3 3839 4344.

See inside back cover for Publication Schedule and Information for Authors.

0021-9673/95/$09.50

Printed in the Netherlands

VOL. 718, NO. 1 JOURNAL OF CHROMATOGRAPHY A 1 DECEMBER 1995

CONTENTS

(Abstracts/Contents Lists published in Analytical Abstracts, Biochemical Abstracts, Biological Abstracts, Chemical Abstracts, Chemical Titles, Chromatography Abstracts, Current Awareness in Biological Sciences (CABS), Current Contents/Life Sciences, Current Contents/Physical, Chemical & Earth Sciences, Deep-Sea Research/Part B: Oceanographic Literature Review, Excerpta Medica, Index Medicus, Mass Spectrometry Bulletin, PASCAL-CNRS, Referativnyi Zhurnal, Research Alert and Science Citation Index)

REGULAR PAPERS

Column Liquid Chromatography

Gas Chromatography

(Continued overleaf)

Contents (continued)

SHORT COMMUNICATION

JOURNAL OF CHROMATOGRAPHY A

VOL. 718 (1995)

JOURNAL OF CHROMATOGRAPHY A

INCLUDING ELECTROPHORESIS AND OTHER SEPARATION METHODS

ELSEVIER

Amsterdam – Lausanne – New York – Oxford – Shannon – Tokyo

0021-9673/95/$09.50

ELSEVIER

Journal of Chromatography A, 718 (1995) 1–8

JOURNAL OF CHROMATOGRAPHY A

Liquid chromatographic process identification using pulse testing techniques
Applications to column standardization and scale-up☆

Joseph C. Dalton[a], Shalabh Gupta[a], Mark D. Bruley[b], Kyung A. Kang[a], Duane F. Bruley[a]*

[a]*Department of Chemical and Biochemical Engineering, University of Maryland Baltimore County (UMBC), Baltimore, MD 21228, USA*

[b]*Synthesizer Inc., Columbia, MD 21045, USA*

First received 29 December 1994; revised manuscript received 6 June 1995; accepted 12 June 1995

Abstract

Transfer functions have been obtained from frequency response analysis via liquid chromatographic pulse testing and Bode diagrams. The system order of the transfer function, within the range tested, is dependent on the anion-exchange gel characteristics, and not on packing height or pulse sample size. It is also observed that as the activity of the anion-exchange gel decreased, the system order of the transfer function decreased. This unique identification strategy could have great potential for the design of automatic control systems, and the standardization of chromatographic systems for Food and Drug Administration process validation. The ultimate goal, however, would be to verify phenomenological models to facilitate process scale-up for the commercialization of bioproducts.

1. Introduction

Over the past 30 years, chromatography has developed into an indispensable technique for protein purification. With such widespread use, process identification, scale-up, and validation are primary focus issues. To date, most scale-up and validation techniques are still accomplished via "seat of the pants" modifications relying on the expertise and experience of the operators. In this work, a preliminary study has been made to apply the principles of frequency response analysis [1] to develop a transfer function for liquid chromatographic system identification.

Pulse testing, to obtain frequency response data, has long been accepted as a practical technique for process identification [2–5]. Chromatography has benefited from pulse testing for parameter evaluation [6–8], although the underlying assumptions for its use in physico-chemical parameter evaluation have not been the subject of a detailed investigation. Until now, transfer functions have not been used to model chromatographic systems. The advantage of using

* Corresponding author. Address for correspondence: Bioengineering Program, UMBC, ECS 202-A, 5401 Wilkens Avenue, Baltimore, MD 21228, USA.

☆ Presented at *the Workshop on Chromatography, Electrokinetics, and Separations in Porous Media, Gaithersburg, MD, 4–5 August 1994.*

0021-9673/95/$09.50
SSDI 0021-9673(95)00664-8

this technique is that the transfer function must empirically match both the phase angle and the magnitude ratio simultaneously, thus providing a system check that does not exist within the time domain. Therefore, by relating physical parameters to variables in the frequency domain of the transfer function [3–5], a potentially powerful tool for chromatographic system identification is employed.

2. Theory

The application of pulse testing to chromatography treats the system as a black box. Once the system is at equilibrium, a disturbance is added, and system response is recorded until re-equilibration.

The disturbance is the fundamental requirement for any process identification technique. While sinusoidal inputs are the classical disturbance, these are difficult to generate for processes like chromatography. The use of a single input pulse as the disturbance allows for a frequency response over a range of frequencies. With an appropriately sharp pulse, approximating a Dirac delta function, a wide range of response frequencies can be achieved. The pulse is small enough not to overload the column, thereby avoiding non-linear behavior. Non-linear operation using overloaded gradients have been under investigation by Guiochon and co-workers [9].

The system response is recorded as a function of time and then, using Fourier transforms [4,10], the data is reduced to the frequency domain,

$$F(\omega) = \int_{\infty}^{-\infty} f(t)\, e^{-j\omega t}\, dt \qquad (1)$$

where $f(t)$ is the time domain pulse data, $F(\omega)$ is the pulse data in the Fourier domain, t is the time, j is the imaginary number, and ω is the frequency. In theory, the integral would be over an interval from positive to negative infinity. For pulses, however, the interval begins and ends at zero. Thus, the integration time limits for both the input and output functions are zero. The system response in the Fourier domain is defined as the transfer function $G(\omega)$. A transfer function is a method of translating the dynamic behavior of a system's input and output signals into the Laplace or Fourier domain. Once in the Laplace or Fourier domain, mathematical calculations for exponential relationships, and interpretations on relationships become simpler. When the forcing frequency (ω) is substituted for s (Laplace variable), a transfer function in the frequency domain results:

$$G(\omega) = \frac{Y(\omega)}{X(\omega)} = \frac{\int_0^{T_y} y(t)\, e^{-j\omega t}\, dt}{\int_0^{T_x} x(t)\, e^{-j\omega t}\, dt} \qquad (2)$$

where T_x and T_y are the pulse input and output times, respectively.

When reducing experimental pulse data, the normalized input frequency content (NFC) is useful for discerning when the transformed data has become too noisy for use. The NFC is defined as:

$$NFC = \frac{\left| \int_0^{T_x} x(t)\, e^{-j\omega t}\, dt \right|}{\left| \int_0^{T_x} x(t)\, dt \right|} \qquad (3)$$

NFC can vary between values of 0 and 1, and decreases with increasing forcing frequency. As a rule-of-thumb, when the NFC falls below 0.3, results are deemed unstable. The sharper the input pulse, the greater the range of frequencies the response will cover before the NFC falls below 0.3. The NFC of a Dirac delta function is unity throughout the entire frequency domain, with a zero phase shift.

In the frequency domain, the system is represented by its magnitude ratio (MR) and its phase angle (ϕ). These quantities are defined as [4,5,11]:

$$MR = |G(i\omega)| = \sqrt{Re^2(\omega) + Im^2(\omega)} \quad (4)$$

$$\phi = \phi|_{G(\omega)} = \tan^{-1}\left[\frac{\mathrm{Im}(\omega)}{\mathrm{Re}(\omega)}\right] \quad (5)$$

After substitution of the Euler relationship

$$e^{-j\omega x} = \cos(\omega t) - j\sin(\omega t) \quad (6)$$

the real and imaginary contributions can be determined:

$$Re(\omega) = (AC + BD)/(C^2 + D^2) \quad (7a)$$

$$Im(\omega) = (AD - BC)/(C^2 + D^2) \quad (7b)$$

and the values A, B, C, and D are defined as:

$$A = \int_0^{T_y} y(t)\cos(\omega t)\,dt \quad (8a)$$

$$B = \int_0^{T_y} y(t)\sin(\omega t)\,dt \quad (8b)$$

$$C = \int_0^{T_x} x(t)\cos(\omega t)\,dt \quad (8c)$$

$$D = \int_0^{T_x} x(t)\sin(\omega t)\,dt \quad (8d)$$

The computation of these product integrals is carried out numerically using a Filon's Method Data Reduction Code [13]. Application of various quadrature methods such as the trapezoidal rule, Simpson's rule, approximation by linear or higher order curves followed by integration of the subsequent trigonometric functions are discussed in the literature [4,5]. Problems arise due to oscillations of the trigonometric functions at high frequencies. To offer a smooth approximation of the pulse curves, Filon [12] proposed a quadrature formula for the integrals based on approximation by parabolic segments as in Simpson's rule. However, Simpson's rule coefficients are replaced by functions of $\omega\Delta t$ [4]. The transformed, reduced data are plotted as magnitude ratio (MR) and phase angle (ϕ) versus frequency (ω), known as Bode diagrams. These Bode diagrams are analyzed using process control theory to yield transfer functions that empirically model the system.

The MR is the ratio of output to input peak amplitude for a specific frequency when using a direct sinusoidal forcing function. Input and output amplitudes may be measured directly from the time domain data. For pulse testing, the MR must be numerically calculated. For convenience, the input pulse has been approximated as the Dirac delta function.

When taking data from the strip chart recorder, the delay between the input pulse and the output response is typically defined as the pure transport delay, or time delay (θ_d) of the system. As read off the chromatogram, however, this value appears to have an analogous delay contribution. Influences such as pore diffusion and ionic sorption will probably contribute to increase the apparent time delay value. The actual time delay must be calculated from the flow-rate, intraparticular void fraction, column width and length, and column volume, or from a pulse test using a non-interacting protein or chemical. A calculated pure transport delay of approximately 600 s suggests that the strip chart recorder's total delay time of 900 s contains this analogous contribution. By reducing only the response data, the analogous delay contribution becomes apparent at high frequencies on the phase angle Bode plot. Therefore, the time delay analogue is back calculated from the Bode plots. To empirically fit transfer functions to systems with a non-integer order and an analogous time delay, the following equations were proposed:

$$\theta_a = \phi(\omega_i) + \sum_{k=1}^{int(n)} \tan^{-1}(\tau_k\omega_i) + (n - int[n])\tan^{-1}(\tau_n\omega_i) \quad (9)$$

where the subscripts i and k denote the value of the frequency or phase angle at specific points on the Bode diagram, a subscript n denotes a variable's value at the overall system order, t is the time constant ($1/\omega$) at each break point, $\phi(\omega_i)$ is the phase angle at a specified frequency, and θ_a is the time delay analogue. The overall transfer function of the system is calculated using:

$$G(s) = \frac{K_p \exp(-\theta_a s)}{\left(\prod_{k=1}^{int(n)} (\tau_k s + 1)\right)(\tau_n s + 1)^{(n - int(n))}} \quad (10)$$

where s is the Laplace variable and K_p is the steady-state gain of the system. The contributions of each integer order to the overall transfer function are multiplicative in the frequency domain.

3. Procedures

3.1. Materials

Equipment

The equipment consisted of a peristaltic pump (Pharmacia P-1, Piscataway, NJ, USA), 280 nm UV-detector (Pharmacia UV-1), fraction collector (Pharmacia FRAC-100), chart recorder (Pharmacia REC 102), Econo-columns of 10 cm height and 1.0 cm I.D. (Bio Rad, Melville, NY, USA), and silicon tubing (1.0 mm I.D.). The columns were placed with the filter at the same height as the fraction collector's tubing exit, negating any pressure heads. A 50-μl pipetter (Eppendorf North America) was used to insert the pulse into the column.

Chemicals

The wash buffer is 0.1 *M* phosphate buffer, at 7.5 pH. The elution buffer is 1.0 *M* NaCl + 0.1 *M* phosphate buffer, at 7.5 pH. The protein used to pulse the system is 1.0 mg/ml bovine serum albumin (BSA). All chemicals were purchased from Sigma (St. Louis, MO, USA) and meet ACS reagent standards.

Gels

Anion-exchange gels used were DEAE Sephadex, Q-Sepharose, Dowex (200–400 μm), and Dowex (50–100 μm). The gels were all purchased from Sigma.

3.2. Experimental protocol

Gel preparation

The dry gel is allowed to swell overnight in wash buffer. It is then packed into a column and allowed to settle by gravity to a specified height. Once the gel is settled, the column is equilibrated again with wash buffer and the packing height is visually verified. The column is equilibrated with elution buffer and re-equilibrated with wash buffer to remove contaminants and prepare for experimentation.

Experimental

The signal measured is 280 nm UV adsorbance and is directly related to protein concentration at the outlet of the column. Base-line deviations for wash and elution buffers were averaged and accounted for as a 'corrected' base line on the chromatogram. Deviations within 5% of the corrected base line are assumed to be at equilibrium conditions. The flow-rate from the peristaltic pump is held constant at 30 ml/h, except where otherwise noted. Once a column is equilibrated with wash buffer, the flow from the peristaltic pump is stopped, and the column is allowed to drain by gravity until the liquid level is 0.5 cm above the top of the anion-exchange gel packing. At this point the pulse, 50 μl of 1.0 mg/ml BSA, is injected into the top of the column. At the upper surface of the anion-exchange gel, where a thin layer will best simulate the Dirac delta function, the protein is allowed to adsorb via ion-exchange for 2 min. Washing with two column volumes of wash buffer verifies that the protein is bound to the anion-exchange matrix. Next, the protein is isocratically eluted with the elution buffer, and the experiment is concluded when equilibration with elution buffer is complete. All experiments were performed at room temperature (25°C).

Special conditions

DEAE Sephadex was observed to contract in the elution buffer. Although once re-equilibrated with the wash buffer, the gel would expand to its original packed height. Therefore, all packing heights referred to will be pre-elution. The pulsating mechanism of the peristaltic pump is assumed not to be a factor in the pulse tests, as the pulse is one of protein concentration, and not pressure.

3.3. Transfer function

Concentration versus time data (from the chromatogram) is transferred from the UV signal recorder output to a Filon's method data reduction program [13]. The resulting output from this program, in the frequency domain, is used to construct Bode plots. At frequencies high enough to generate oscillatory behavior ($\omega >$ 0.01 Hz), the results were discarded. These oscillations are attributed to the rule-of-thumb: when the normalized frequency content drops below its accepted minimum (NFC < 0.3), the reduced results become scattered [5].

The transfer function is constructed from the Bode plots (Figs. 1a, 1b) as follows: (1) the overall system order is determined from the final slope of the magnitude ratio (MR), (2) the break points are calculated from the intersection of the each asymptote for every integer step in the overall order and the final order, (3) the steady-state gain (K_p) is ascertained from the horizontal asymptote of the MR graph, (4) the time delay analogue (θ_a) is calculated from Eq. 9, and the overall transfer function is calculated using Eq. 10.

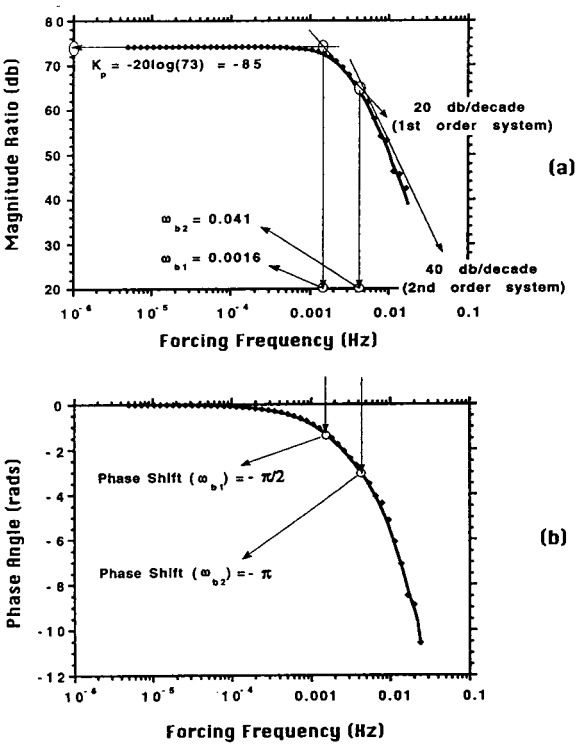

Fig. 1. (a) The magnitude ratio versus forcing frequency Bode plot of an experiment, displaying the log measurement of the breakpoints (ω_{b1} and ω_{b2}), system order (n) and steady-state gain (K_p). (b) The phase angle versus forcing frequency Bode plot of the same experiment, displaying the phase shift at the break points from (a).

4. Results

Transfer functions acquired from the tested systems enable us to empirically model the Bode plots. An example is a transfer function obtained from a 3-cm Sephadex column:

$$G(s) = \frac{-85\exp(-347s)}{(0.0016s + 1)(0.041s + 1)} \quad (11)$$

It was possible to reproduce the plots from the transfer functions alone (Figs. 2a, 2b) with minimal deviance on either magnitude ratio or phase angle plots versus forcing frequency.

The order of the system (n) was shown to be dependent on the type of anion-exchange gel (Table 1). When each gel was subjected to different packing heights and pulse sample sizes, the order remained constant (Table 1). The system order was reproducible for each experiment with nearly zero deviation for each gel type. A notable exception is that the order of DEAE Sephadex decreased with use as shown in Table 2. It is known that DEAE Sephadex loses activity with use, therefore it is hypothesized that the decrease with system order corresponds to a decrease in the activity of the gel.

The transport delay, timed from pulse elution to initial chromatogram response was equal to the time delay analogue (θ_a) calculated from the Bode plots (Eq. 9). The time delay analogue was reproducible ($\pm 5\%$), and has a linear relationship to the gel packing height of the column (not shown).

As the pulse strength increased, the steady-state gain of the system (K_p) increased as well (Table 1). Although this direct dependence was qualitatively consistent within our experiments, the steady-state gain varied up to 100% of the mean value for each experiment. While the

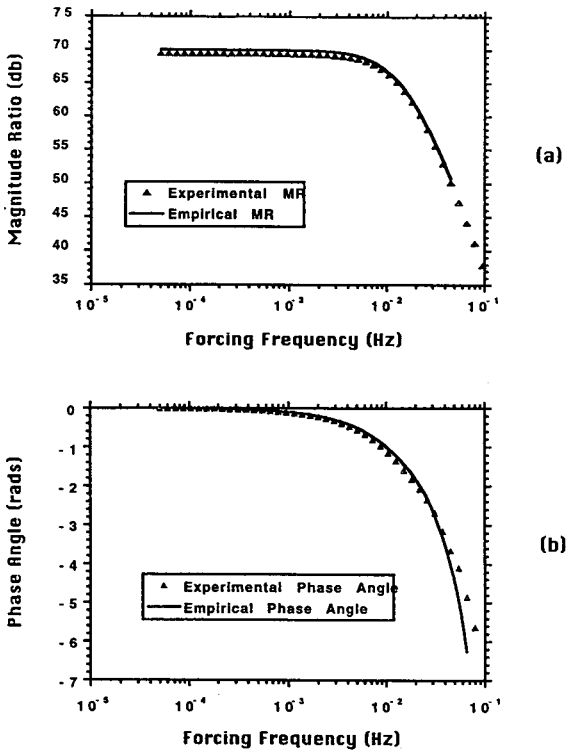

Fig. 2. (a) A comparison of the experimental magnitude ratio (MR) results with the empirical transfer function. (b) For the same experiment, a comparison of the experimental phase angle (ϕ) results with the empirical transfer function.

output of the system is quantifiable by the chromatogram, the input does not have a distinct measurement. The input pulse is assumed to be constant for all experiments (a Dirac delta function), but other contributing factors could lead to the discrepancies. When a method to quantify the input pulse is attained, the steady-state gain of the system should become more stable.

Table 2
The system order versus the age of the anion-exchange gel DEAE Sephadex

Packing height (cm)	System order	
	Initial two days	After four days
3	2	1.25
4	2	1.25
5	2	1.5

5. Conclusion

As a result of this preliminary study, transfer functions have been found to successfully identify properties of a chromatographic system where they have been empirically determined via Bode plots of pulse test experiments. Within the range of values tested, overall system order is dependent on the anion-exchange gel characteristics. In the frequency domain, there is a linear relationship between the time delay analogue of the system and the packing height of the column. This result would suggest that the time delay analogue represents the delay contributions of system characteristics, possibly from diffusion, dispersion, and kinetics. Tests on rate-limited systems would be enlightening in this area.

Table 1
The observed characteristics of anion-exchange gels investigated, including the steady-state gain (K_p), first break point (FBP), and the system order

Gel	Pulse 1[a]			Pulse 2[a]		
	K_p	FBP	Order	K_p	FBP	Order
Dowex (50–100)	7.93	227.36	1.50	20.0	398.0	1.50
Dowex (200–400)	3.16	159.15	1.50	25.0	227.4	1.50
Q-Sepharose	1.78	26.52	2.0	10.0	89.0	2.0
Sephadex (DEAE)	2.51	106.10	2.0	6.33	256.6	2.0

[a] Pulses 1 and 2 were performed with 0.15 mg and 0.32 mg of bovine serum albumin (BSA), respectively.

It is also observed that the steady-state gain of the system is dependent on the size of the pulse strength. For linear operating conditions, the steady-state gain of the transfer function should remain independent of the input pulse size. Research into a normalized input pulse strength is currently under way.

Proposed uses for transfer functions include phenomenological modeling, process control, and FDA validation. To be useful with phenomenological modeling, non-linearities within the system must be linearized over known dependent variable ranges. It is our goal that phenomenological models for individual systems can be verified using empirical transfer functions. Breaking down a transfer function into classical chromatographic principles also holds potential for the further identification of chromatography. A validated phenomenological model could then be used as a tool for scale-up calculations. Frequency response results utilized for process control would be a direct application of transfer functions. Automatic-control system design for chromatography would benefit greatly from easily obtainable transfer functions to represent the operational systems.

If non-linearities persist, and specific contributions from the time domain cannot be related to transfer functions, pulse testing still offers a viable mechanism to uniquely "fingerprint" a chromatographic system. This "fingerprint" could be used to verify the proper operation of the system, much like statistical process control techniques used today. As an actual pulse test on a system is not time or material restrictive, pulse testing could be used to standardize chromatographic processes and thus be an ideal mechanism to enhance FDA validation procedures.

Acknowledgements

This work was supported by The Whitaker Foundation–Special Opportunity Awards in Biomedical Engineering, Symbiosis of Biomedical and Bioprocess Engineering Utilizing Total Quality Management to Enhance Health Care Quality and Delivery, and Synthesizer Inc.

Nomenclature

dB	decibel
G	transfer function
Im	imaginary part of transfer function
i	ith frequency
j	jth component of system order
j	imaginary number
K_p	steady-state gain
MR	magnitude ratio
n	system order
NFC	normalized frequency content
Re	real part of transfer function
s	Laplace variable
t	time (s)
T_x	input pulse time (s)
T_y	output pulse time (s)
x	input variable (mg/ml) in time domain
X	transformed input in frequency domain
y	output variable (mg/ml) in time domain
Y	transformed output in frequency domain
ξ	damping coefficient
θ_a	time delay analogue (s)
θ_d	time delay (s)
ϕ	phase angle (rad)
τ	break point (s/rad)
ω	frequency (rad/s)

References

[1] D.F. Bruley and J.W. Prados, AIChE J., 11 (September) (1964) 612.
[2] S.J Lees and J. Hougen, J. Ind. Eng. Chem., 48 (1956) 1064–1068.
[3] C.I.J. Lewis, D.F. Bruley and D.H. Hunt, Ind. Eng. Chem. Process Des. Dev., 6 (July) (1967) 281.
[4] W.L. Luyben, Process Control, McGraw-Hill, New York, 1991, pp. 502–534.
[5] W.C. Clements, Jr. and K.B. Schnelle, Jr., Ind. Eng. Chem. Process Des. Dev. 2, No. 2 (April) (1963) 94–102.
[6] F.H. Arnold, H.W. Blanch and C.R. Wilke, Chem. Eng. J., 30 (1985) B25–B36.
[7] R.D. Whitley, J.M. Brown, N.P. Karajgikar and N. Wang, J. Chromatogr., 483 (1989) 263–287.

[8] J.L. Wade, A.F. Bergold and P.W. Carr, Anal. Chem., 59 (1987) 1286–1295.
[9] M.Z. El Fallah, S. Golshan-Shirazi and G. Guiochon, J. Chromatogr., 511 (1990) 1.
[10] K.A. Kang, D.F. Bruley, J.M. Londono and B. Chance, Ann. Biomed. Eng., 22 (1994) 240–252.
[11] D.R. Coughanowr, Process Systems Analysis and Control, McGraw-Hill, New York.
[12] L.N.G. Filon, Proc. R. Soc. Edinburgh, 49 (1928) 38.
[13] D.F. Bruley, Filon's Method Data Reduction Code, DuPont, 1975, unpublished.

ELSEVIER

Journal of Chromatography A, 718 (1995) 9–26

JOURNAL OF CHROMATOGRAPHY A

Optimization of chiral selectivity on cellulose-based high-performance liquid chromatographic columns using aprotic mobile-phase modifiers ☆

K.M. Kirkland

Zeneca Pharmaceuticals, A Business Unit of ZENECA, Wilmington, DE 19897, USA

First received 22 March 1995; revised manuscript received 30 May 1995; accepted 1 June 1995

Abstract

Tris-3,5-dimethyl phenyl carbamate-derivatized cellulose HPLC columns and other cellulose-based columns are popular for the direct separation of many racemic drugs and agrichemicals. These columns exhibit good efficiency and stability under well-controlled chromatographic conditions. Cellulose-based chiral columns also exhibit high sample-load capacity with normal-phase solvents, which is particularly advantageous for isolating purified solutes. Several investigators have reported that the stereoselectivity of these columns can be varied by changing the type and composition of alcohol modifiers in the mobile phase, and by altering temperature. We now find that separation selectivity and resolution can be significantly increased, and often optimized, by modifying the nonpolar mobile phase with certain aprotic solvents. The potential of this new separation dimension greatly increases the general applicability of cellulose-based columns for analytical and preparative separations of racemates. A simple, systematic scheme is proposed for optimizing the separation of enantiomeric drugs with the Chiralcel OD column.

1. Introduction

The HPLC separation of chiral compounds in pharmaceutical and agrichemical products is increasing in popularity because of regulatory and other concerns. Typically, useful HPLC separations of racemic mixtures are developed by scouting columns with different types of chirally-active stationary phases. However, such columns have proliferated to the point that it is difficult to chose a satisfactory mobile phase/column combination without considerable effort. Columns for analytical and preparative separations include the "Pirkle" type, ligand exchangers, inclusion-formation systems such as the cyclodextrins, various polysaccharide-based materials, and those based on various immobilized proteins. Systematic studies have defined the areas of best applications for these column types, and the experimental approaches for satisfactory results [1–5].

Previous studies in this laboratory have extensively utilized a silica-based column with an ovomucoid protein stationary phase (Ultron ES-OVM) for the analytical separation of a wide range of racemic drugs [6–8]. This column type often exhibits superior separations of racemic drugs with widely-differing characteristics [6]. Studies involving the effects of varying sepa-

☆ Presented at the *17th International Symposium on Column Liquid Chromatography, Hamburg, 9–14 May 1993.*

0021-9673/95/$09.50
SSDI 0021-9673(95)00633-8

ration parameters with this column have led to development of simple and systematic schemes for optimizing the separation of enantiomeric agents [7,8]. Unfortunately, however, immobilized protein columns all suffer from an inherent disadvantage: sample loadings must be kept small or the column will overload, degrading separation performance. This characteristic of immobilized protein columns seriously limits this column type for separations where purified enantiomers must be isolated. Limitations in the protein-based columns directed us to study cellulose-based columns for achieving both analytical and preparative separations. Although preparative separations are not a subject of this report, methods for optimizing separations of racemic mixtures are analogous for both analytical and preparative applications.

Cellulose-based columns have several potential advantages over protein-based columns for separating racemic mixtures. First, cellulose-based columns have higher sample loading capacity. Second, the low-boiling organic solvents typically used with these columns facilitate the isolation of purified solutes. Totally organic solvent systems used with cellulose-based columns are readily removed from purified fractions, simplifying problems with removing the buffered aqueous mobile phases used with protein-based columns. Third, the cellulose-based columns are broadly applicable to many compound types [4]. Fourth, commercially-available short columns of these materials rapidly equilibrate and allow faster separations for decreased method development time. Lastly, short cellulose columns are less expensive, permitting the practical survey of a range of column types at reasonable cost.

However, practical disadvantages of the cellulose-based columns had to be overcome in this study. There are many different types of cellulose-based chiral columns [9]. Which type might be the most promising so that the testing of all might not be required? Also, the chromatographic performance of cellulose-based columns is sensitive to water contamination in organic normal-phase solvents, requiring the use of dry sample and mobile-phase solvents. Lastly, another limitation of cellulose-based columns is that they generally have lower plate numbers (less efficient) than protein-based columns. This characteristic often dictates that selectivity factors (α) be maximized for optimum separations.

The need for maximizing the analysis and isolation of chiral compounds led us to study ways that α-values for cellulose-based columns could be rapidly optimized. Optimization usually involves selecting a mobile phase and other operating conditions that produce the highest α-value, while maintaining good column efficiency. As a background for our work, the studies of Okamoto et al. [10], Wainer et al. [11] and Shibata et al. [4] were useful in promoting insight for expanding the range of typically-used solvents for the cellulose-based columns. Traditionally, cellulose-based column manufacturers recommend that protic (proton donating) modifiers are to be used with non-polar mobile-phase carriers (e.g., hexane) to resolve enantiomers [9,12]. Precautionary statements furnished with columns warn of adverse effects on performance and stability if there are deviations from suggested mobile-phase compositions.

This study has identified that certain non-protic modifiers often can improve chiral separations. At times, an aprotic modifier can produce a useful separation that is not possible with traditional protic modifiers. Use of polar modifiers other than alcohols greatly expands the applicability of the cellulose-based columns, without apparent column stability difficulties.

Three main objectives of this study were defined. First, data were needed to identify and quantify the effects of using aprotic modifiers with cellulose-based chiral columns. Second, there was an internal need to resolve and preparatively isolate a proprietary racemic aryl-oxy-propionate mixture using a derivatized cellulosic column. Finally, a simple optimization strategy for using cellulose-based columns was desired so that future analytical and preparative separations could be quickly and effectively completed.

2. Experimental

Chiralcel OD and OJ columns (50 × 4.6 mm I.D.), Chiralcel OC, OF and OG columns (250 ×

4.6 mm I.D.) and all HPLC-grade solvents were from J.T. Baker (Phillipsburg, NJ, USA). The HPLC apparatus consisted of a Model 400 pump (ABI Analytical, Ramsey, NJ, USA), a Model 7125 loop sample injector (Rheodyne, Cotati, CA, USA), and a variable-wavelength UV detector (ABI, Model 783G). Chromatographic data were acquired and analyzed with a Multichrome system (version 2.0, VG Laboratory Systems, Manchester, UK). Detector output also was monitored with a strip-chart recorder (Model BD-41, Kipp and Zonen, Delft, Netherlands).

Proprietary drug candidates, designated aryloxy propionate "ester", aminotetralin, aminoquinuclidine and aryl carbamate, were synthesized by ZENECA Pharmaceuticals (Wilmington, DE, USA). The general structural characteristics of these compounds are shown in Fig. 1. Stock solutions of 1 mg/ml for these compounds were prepared in ethanol or methanol, followed by dilutions with hexane to a concentration of 10 μg/ml. Injection volumes were 10 μl. At least duplicate injections were made with all solutions to verify that columns were equilibrated and retentions reproducible.

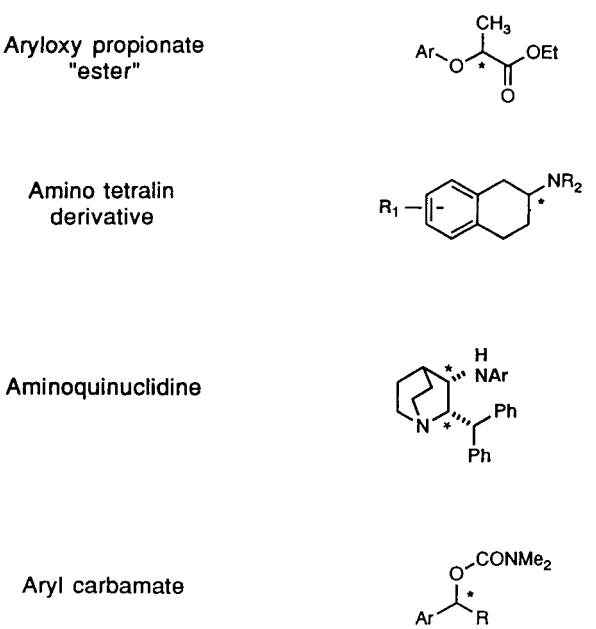

Fig. 1. Structures of compounds studied.

3. Results and discussion

For this study we chose to focus on the tris-3,5-dimethylphenylcarbamate column (Chiralcel OD), because of the large number of successful applications that have been successfully achieved with this stationary phase. Of 510 racemates tested, 229 (about 62%) were completely resolved with this column [13]. It has been indicated that 40% of the analytical sales and 70% of preparative isolations are performed with cellulose-based columns with this stationary phase [14]. However, other stationary phases are included in this study for comparison.

The mechanism for the enantioselectivity of carbamate–cellulose columns has been proposed by Okamoto and co-workers [4,13,15,16]. The suggested recognition processes with solutes include: (1) hydrogen bonding, (2) dipole–dipole interaction, (3) $\pi-\pi$ interactions, and (4) possible inclusion into chiral cavities [17]. Hydrogen-bonding plays a strong role in the selective chiral interaction process, and this interaction can occur at two potential sites of the carbamate functionality, as illustrated by the arrows in Fig. 2.

Hydrogen bonding is possible for both the solute and a protic (proton donating) modifier. This results in a competition between the solute and the protic solvent with the stationary phase for chiral recognition and separation resolution. For separations where hydrogen bonding pre-

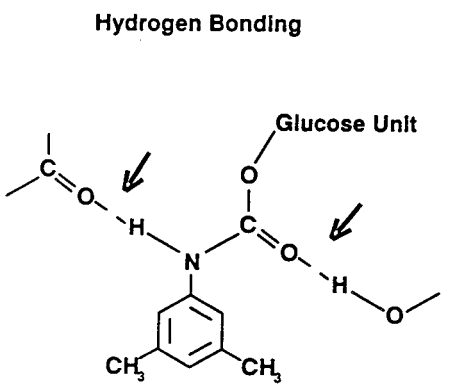

Fig. 2. Proposed mechanism for chiral recognition on cellulose–carbamate derivatives. Adapted from Ref. [10].

dominates, desired chiral interactions with solutes should then be facilitated by selecting a mobile-phase modifier that ineffectively competes by hydrogen bonding for chirally-active sites on the stationary phase. This postulation led to trials with aprotic solvents in the mobile phase to reduce hydrogen-bonding competition of the organic modifier with stationary-phase sites, compared to protic solvents.

Separations with the cellulose-based column packings have historically been performed with hexane carrier modified with various aliphatic alcohols. An interesting pattern is found for the resolution of the chiral "ester" compound (Fig. 1) on the popular Chiralcel OD column. Fig. 3A shows the effect of methanol, ethanol and 1-propanol modifiers in hexane. With this column, no resolution occurs with methanol and ethanol modifiers, but 1-propanol produces a resolution of about 0.9.

Fig. 3B shows that somewhat poorer resolution was obtained with 2-propanol as the modifier. But, as the size of the alcohol increased, resolution also increased, with *tert.*-butanol modifier giving the highest α-value. This effect may be based on the reduced capability of larger alcohols to compete for hydrogen-bonding sites because of steric limitations. (A higher concentration of this alcohol was required to maintain similar retention; a modest resolution increase may have occurred as a result of increased k' values). In spite of this higher α-value, resolution was somewhat lower for *tert.*-butanol compared to iso-butanol. This probably was the result of poorer column efficiency (plate number $N = 524$ for *tert.*-butanol; $N = 727$ for iso-butanol), which may be caused by less favorable kinetics with the solvated stationary phase. Highest column efficiency for the C_4 alcohols was found for 1-butanol, even though α (and resolution) values were lower. These results suggest that mobile-phase modifiers with reduced tendency to interact by hydrogen bonding with the modified cellulose stationary phase can provide higher enantiomeric resolution for compounds that also compete for these hydrogen-bonding, chirally-active sites.

An attempt was made to correlate some basic characteristic of alcohol modifiers to enantiomeric selectivity. No useful correlation was found with the solvent polarity parameter described by Snyder [18]. However, a reasonable correlation was obtained using the solvent strength parameter, ϵ^0, also described by Snyder for use in liquid–solid chromatography [19], as illustrated by the data in Fig. 4. This result supports a mechanism involving the competition of the solute and the modifying polar solvent for hydrogen bonding sites on the stationary phase. The interaction may be somewhat similar to the site-competition process now accepted as the mechanism for liquid–solid or adsorption chromatography [19].

Utilizing aprotic solvents as mobile-phase modifiers apparently reduces the competition of the solvent for the hydrogen-bonding sites on the chiral stationary phase, increasing the possibility of the solute to interact at these sites. The effect of aprotic mobile-phase modifiers with the Chiralcel OD column is shown in Fig. 5. Fig. 5A shows that acetonitrile and tetrahydrofuran produce no improvement over results with the protic modifiers in Fig. 3. This suggests that both acetonitrile and tetrahydrofuran are strongly held to hydrogen-bonding sites of the chiral stationary phase. However, as shown in Fig. 5A, the aprotic methyl-*tert.*-butyl ether modifier (MTBE) produced a resolution of 1.70. (Note that 25% of this solvent modifier was required to maintain comparable retention). This resolution of 1.70 significantly exceeds the best previously found with the alcohol modifiers ($R_s = 1.30$ for iso-butanol in Fig. 3B). Fig. 5B shows that aprotic methylene chloride and ethyl acetate modifiers both provide resolutions of > 1.2 for the chiral "ester". Methylene chloride exhibited the most favorable effect on column efficiency, producing the largest plate number of any solvent tested with this solute.

Based on use-recommendations by the manufacturer, we were concerned about the stability of the Chiracel OD column when employing aprotic solvent modifiers. Fig. 6 shows comparative chromatograms obtained with a fresh column and one with a history of about 400 sample injections, using a mobile phase of 25% methyl-

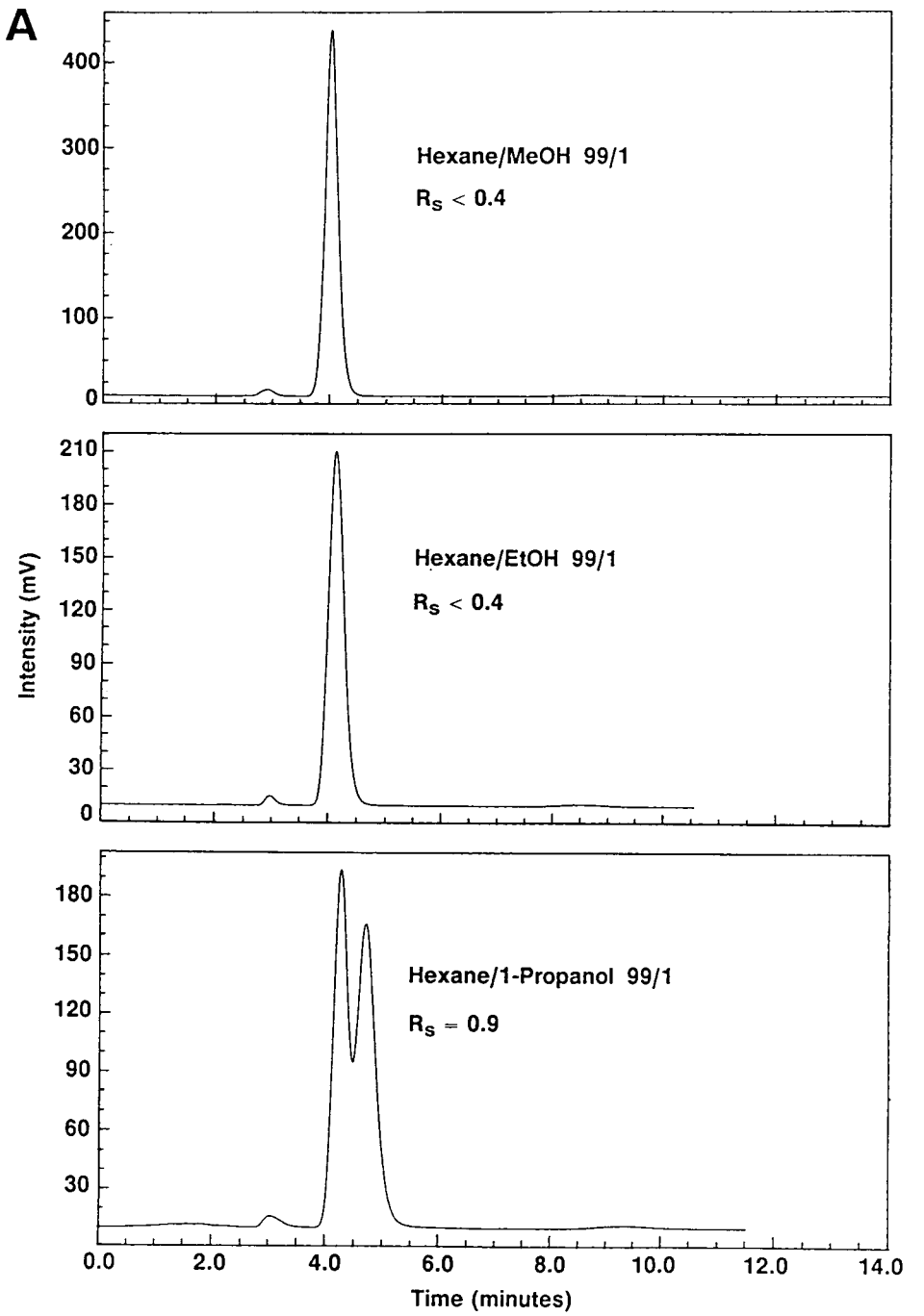

Fig. 3. Effect of protic mobile phase modifiers on resolution of chiral ester. Column, 50 × 4.6 mm I.D. Chiralcel OD; solute, "ester" in Fig. 2; flow-rate, 0.5 ml/min; temperature, ambient; UV detector, 230 nm. (A) Methanol, ethanol, 1-propanol modifiers; (B) 2-propanol, 1-butanol, isobutanol, *tert.*-butanol modifiers.

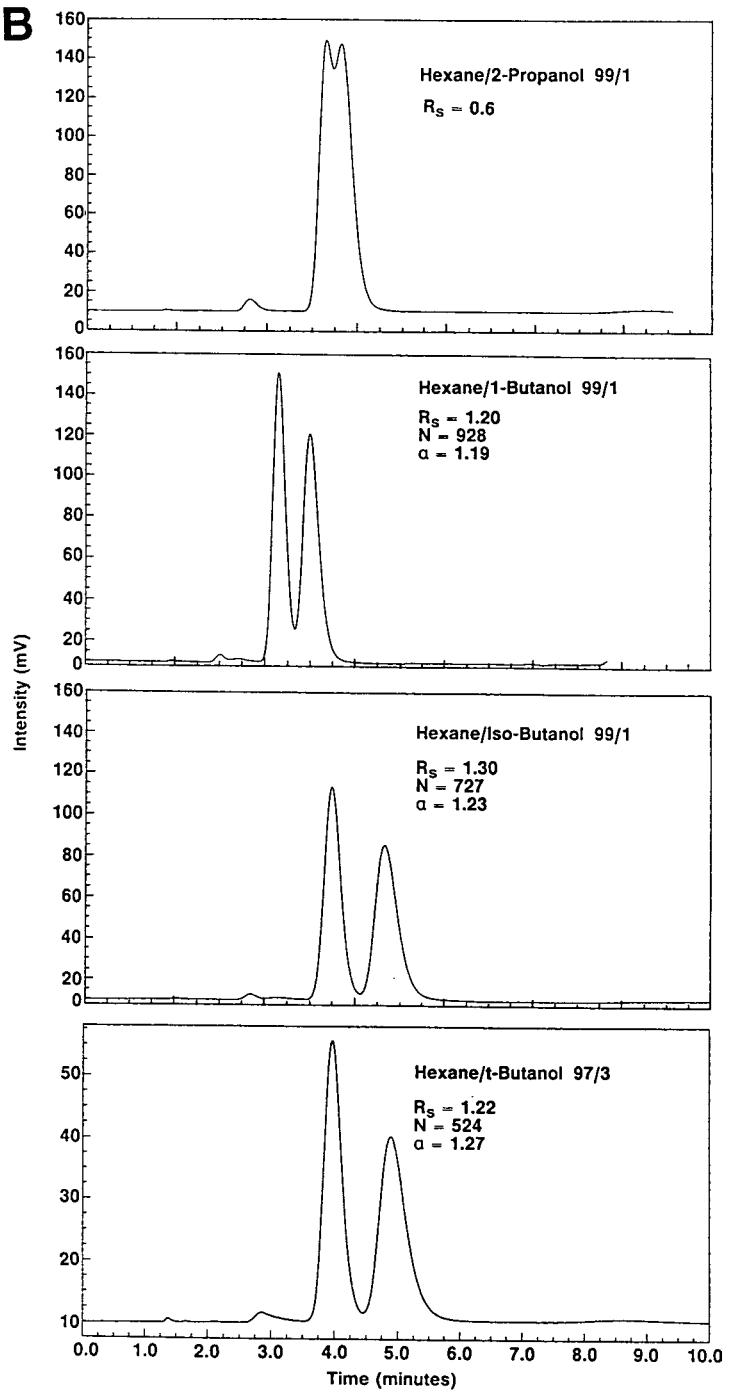

Fig. 3. (*continued*)

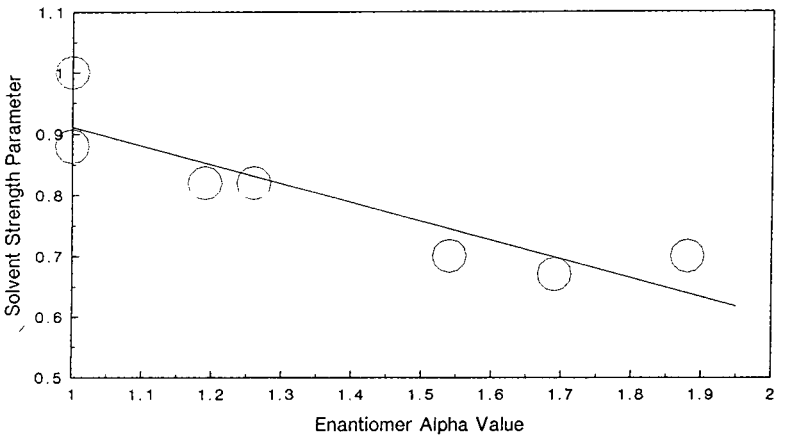

Fig. 4. Correlation of solvent strength ϵ^0 with selectivity α-values. Conditions of Fig. 3.

tert.-butyl ether–hexane. Essentially equivalent retention and resolution for the two columns suggest satisfactory column stability in such mobile phases. In obtaining the data for this study, we used compositions up to 50% methyl-*tert.*-butyl ether, 30% tetrahydrofuran, 10% methylene chloride and 10% ethyl acetate with the Chiracel OD column without column stability problems.

The short (5-cm) columns were used for method development because of convenience and cost. Comparative chromatograms for the racemic ester with 5- and 25-cm columns are given in Fig. 7. Curiously, with this mobile phase of 25% methyl-*tert.*-butyl ether in hexane, the expected five-fold increase in plate number was not obtained with the 25-cm column. The plate height for the 5-cm column was 0.00625 cm at a flow-rate of 0.5 ml/min, compared to 0.0202 for the 25-cm column at a flow-rate of 1.0 ml/min. We speculate that the shorter 5-cm column may have contained smaller particles, or was more efficiently packed.

A brief study was made on the batch-to-batch reproducibility for the 5-cm columns. Three different 5-cm columns of Chiracel OD (one used for these studies, two fresh columns) showed resolutions of 1.25 to 1.70 for the same enantiomers. No changes occurred in resolution for the initial column used in this study ($R_s = 1.70$ for these enantiomers). This finding suggests that, while these short columns are quite useful for research and certain method studies, they may not be sufficiently reproducible for regulatory (Good Laboratory/Manufacturing Procedures) operations.

Table 1 summarizes results of using different mobile phases with the Chiracel OD column in the resolution of enantiomers for the "ester" type drug. Again, the addition of acetonitrile to the ethanol–hexane mobile phase affected α-values very little. However, with aprotic acetonitrile modifier, column plate number increased dramatically, resulting in a significant increase in enantiomer resolution. We speculate that this higher plate number may result in better kinetics (mass transfer) with the lower-viscosity acetonitrile-modified mobile phase. This effect is well known in the reversed-phase separation of achiral compounds, where acetonitrile as mobile-phase modifier (instead of alcohols) decreases column back pressure and increases column plate number [20]. As shown in Table 1, adding methyl-*tert.*-butyl ether or ethyl acetate to the ethanol–hexane mobile phase had little effect on chiral resolution.

As shown by the Chiralcel OD data in Fig. 8 for the racemic aryl carbamate, α-values and separation resolution were highest when higher alcohols and methyl-*tert.*-butyl ether were used as mobile-phase modifiers. Interestingly, plate number was lowest and α value highest with

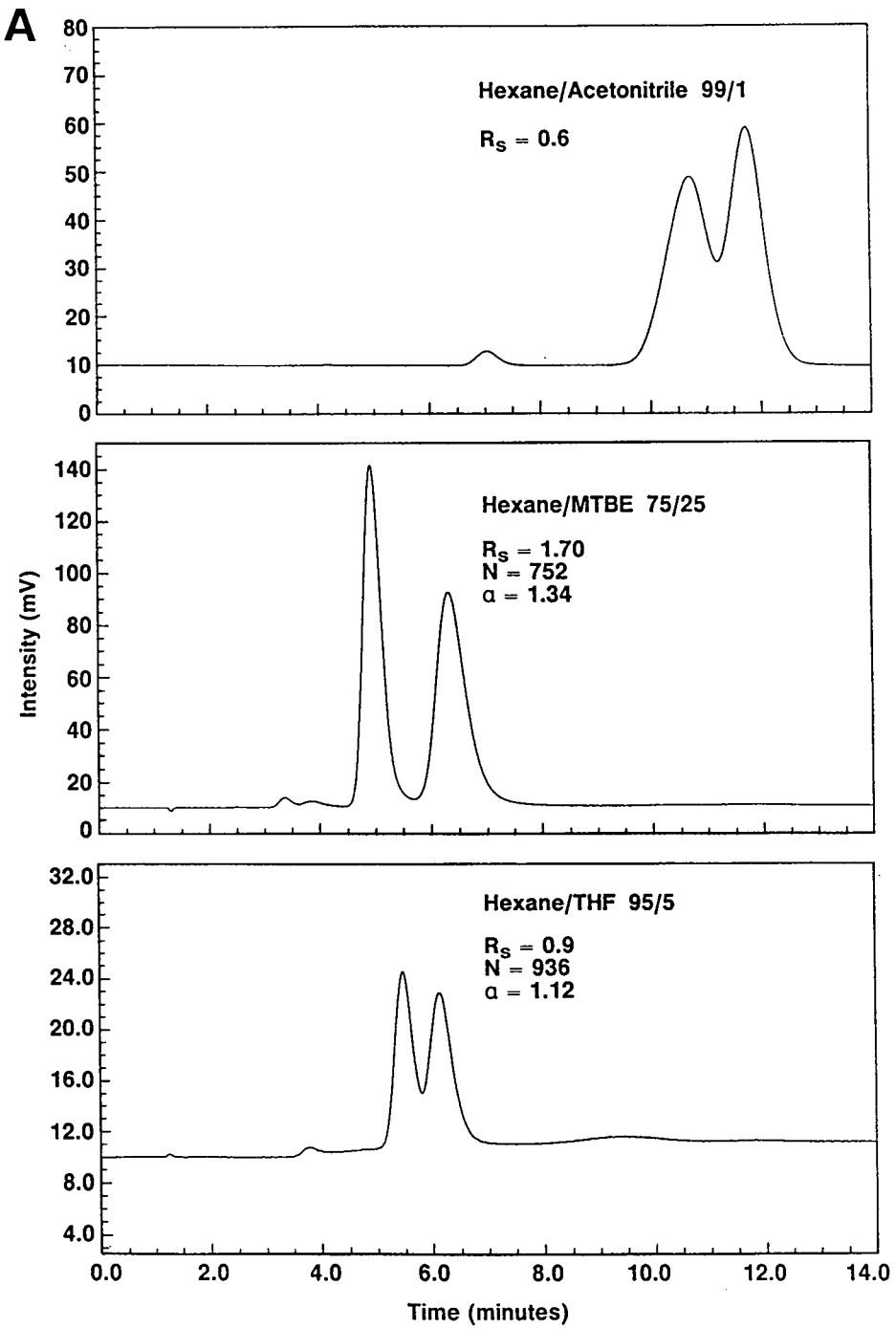

Fig. 5. Effects of aprotic modifiers on resolution of chiral ester. Conditions as for Fig. 3. (A) Acetonitrile, methyl-*tert.*-butyl ether (MTBE) and tetrahydrofuran (THF) modifiers; (B) methylene chloride ($MeCl_2$) and ethyl acetate (EtAc) modifiers.

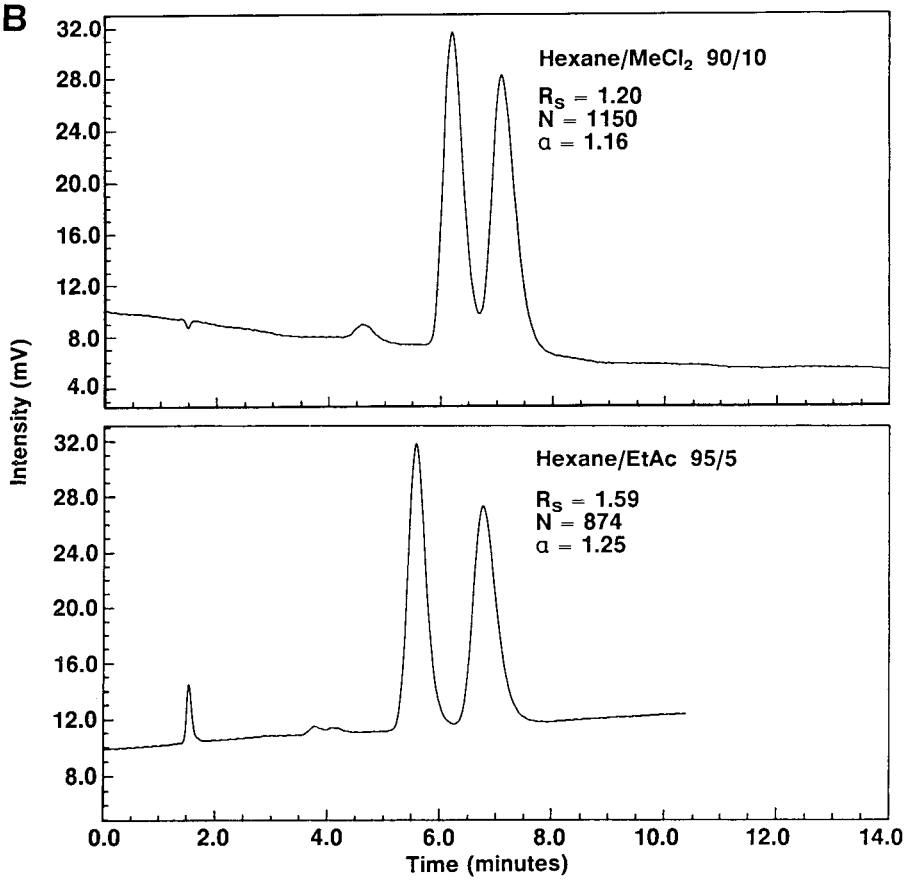

Fig. 5. (*continued*)

methyl-*tert.*-butyl ether as the modifier. These results are somewhat similar to those for the aryloxy propionate "ester" previously discussed.

However, aprotic mobile-phase modifiers are not required with the Chiracel OD column for adequate resolution of all racemates. For example, Table 2 gives retention data for three mobile phases tested with the amino-tetralin drug (Fig. 1). In this case, adding protic solvents such as acetonitrile and MTBE to the mobile phase improved the resolution of these enantiomers very little. Best separation was obtained with methanol, which has the strongest capability to interact with the chirally-active sites on the stationary phase by hydrogen bonding. The results in Tables 1 and 2 suggest, therefore, that hydrogen-bonding interactions are not a dominating feature of chiral interactions that affect enantiomeric selectivity for all drugs. Note that where the ethanol concentration exceeds 5% for proper elution, direct replacement with an aprotic solvent usually is not feasible.

A convenient method was sought for adjusting solvent strength for the Chiracel OD column when replacing protic with aprotic solvents for selectivity enhancement. As noted in Fig. 4, Snyder's solvent strength parameter, ϵ^0, seems to relate to α for the cellulose-based columns, suggesting that stronger solvents more effectively compete for chirally-active sites on the stationary phase than the solute. Based on limited data, it appears that ϵ^0-values for the amino bonded phase given by Snyder and Schunk [21] may be useful in relating the strength of one modifier to another. For example, the chiral ester drug

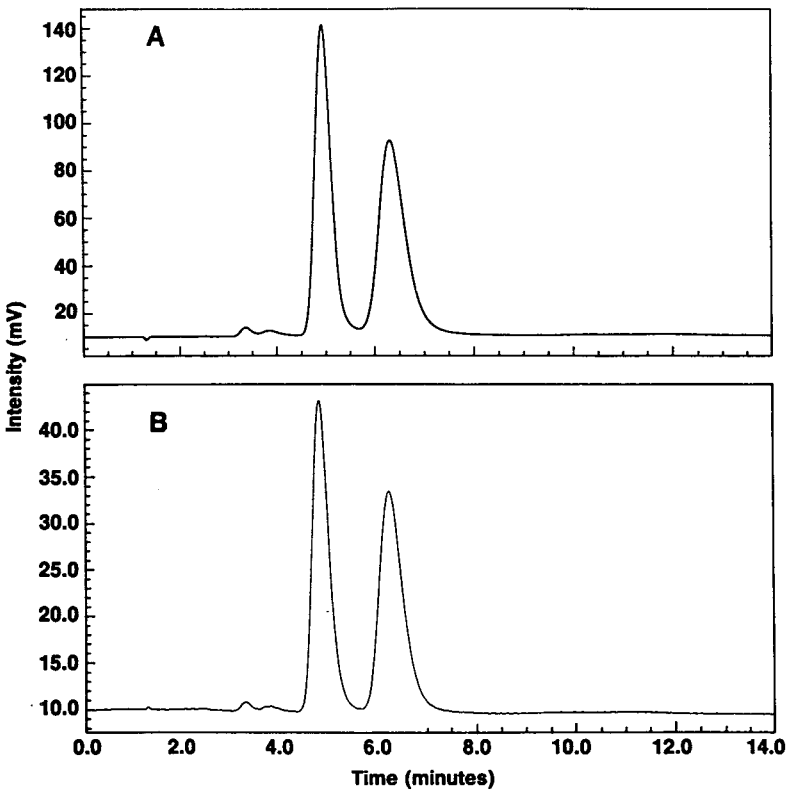

Fig. 6. Stability of cellulose-based chiral column in aprotic solvent-modified mobile phase. Column, 50 × 4.6 mm I.D. Chiralcel OD; solute, "ester" in Fig. 1; mobile phase, methyl-*tert.*-butyl ether–hexane (25:75, v/v); flow-rate, 0.5 ml/min; temperature, ambient; UV detector, 230 nm. (A) Fresh column; (B) after 400 sample injections.

shows about the same retention (k'-values) with 25% MTBE, 10% methylene chloride and 1% ethanol in hexane. According to Ref. [20], 28% MTBE, 11% methylene chloride and 1% ethanol in hexane all have a solvent strength parameter value of 0.04. These results suggest the possibility of using solvent strength values to characterize retention with the Chiralcel OD column, but more work in the area is needed.

What is the effect of aprotic modifiers on enantiomer resolution that can be expected for other carbamate stationary phases? As shown in Figs. 9A and 9B, no resolution was found for the enantiomers of the aryloxy propionate "ester" with Chiracel OC and OG columns when alcohol (protic) modifiers were used. Hexane modified with MTBE (aprotic) produced partial resolution with the Chiralcel OC column (Fig. 9A) and excellent resolution with the Chiracel OG column (Fig. 9B). For this drug, the Chiracel OF column produced the best results with methyl-*tert.*-butyl ether modifier (Fig. 9C).

The effect of various protic modifiers on the enantioselectivity of the Chiralcel OJ column is demonstrated in Fig. 10 for the chiral "ester" compound (Fig. 1). No separation of enantiomers occurred with 5% methanol as the modifier when using a 5-cm column (Fig. 10A). Ethanol and propanol at the same concentration produced resolutions of about 0.8 and 0.7, respectively. All of these solvents have strong hydrogen-bonding capabilities, with methanol the most polar and the most basic of the three. One could speculate that the sample has the most difficulty interacting with this chiral cellulose stationary phase in the presence of tightly-held methanol.

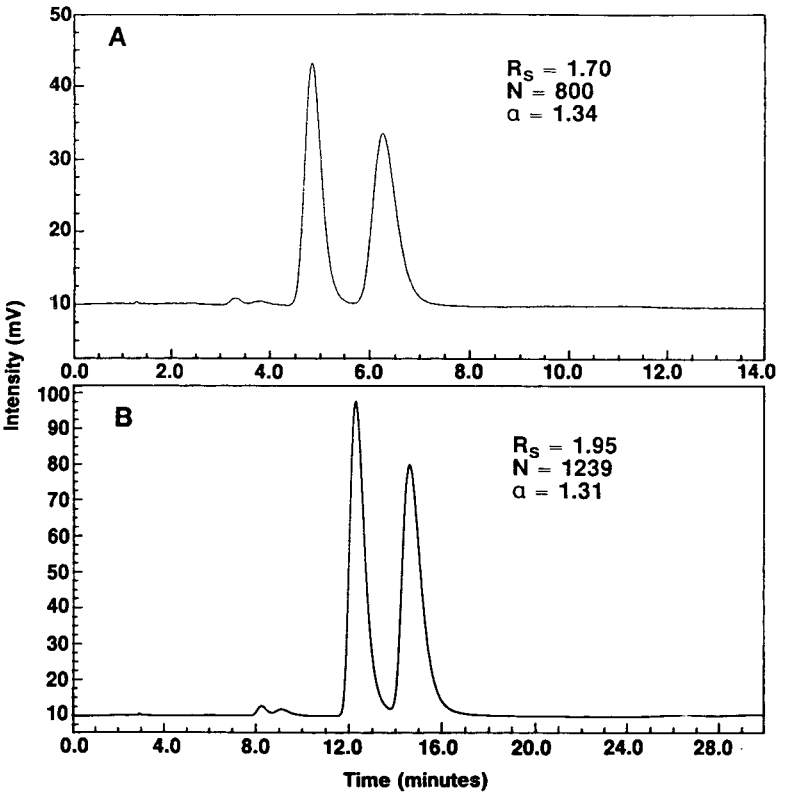

Fig. 7. Comparison of column configurations. Conditions of Fig. 6, except: (A) 250 × 4.6 mm I.D. column; flow-rate, 1.0 ml/min; (B) 50 × 4.6 mm I.D. column; flow-rate, 0.5 ml/min.

The desired chiral interaction occurs with ethanol as modifier, even though this is a more polar and more basic solvent than 1-propanol. The interactive process likely involves, but is not exclusively dependent on, hydrogen bonding. Note that increasing the steric bulk of the alcohol modifier or substituting the aprotic methyl-*tert.*-butyl ether solvent did not improve the resolution of the "ester" enantiomers on Chiracel OJ (Fig. 10B).

Based on the results of this study, a simple strategy was devised for optimizing chiral separations on the Chiralcel OD column. A synopsis of this strategy is given in Fig. 11. Ethanol-

Table 1
Summary of chromatographic data on candidate "ester" drug with Chiralcel OD column

Mobile phase (v/v)	k_1'	k_2'	Selectivity, α	Resolution, R_s	Plate number[a]
Hexane–ethanol (99:1)	2.63	3.23	1.23	1.18	1348
Hexane–ethanol–acetonitrile (99:1:1)	1.90	2.20	1.15	1.51	3475
Hexane–ethanol–methyl-*tert.*-butyl ether (99:1:1)	2.90	3.63	1.25	1.30	1189
Hexane–ethanol–ethyl acetate (99:1:1)	2.37	2.83	1.19	1.18	1575

[a] Plate number of second enantiomer.

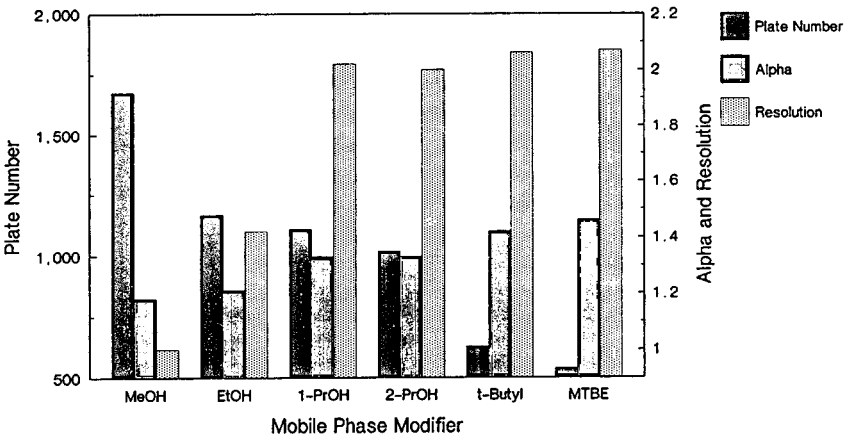

Fig. 8. Effect of mobile phase modifier on chromatography of carbamate drug. Column: 50 × 4.6 mm I.D. Chiralcel OD; solute, carbamate drug of Fig. 1; mobile phases, 5% (v/v) modifier, except 50% methyl-*tert.*-butyl ether; flow-rate, 0.5 ml/min; temperature, ambient; UV detector, 220 nm.

modified hexane is recommended as the starting mobile phase. The suggested initial ethanol level (10%) should be adjusted to obtained the desired retention ($k' = 1$–10) for all compounds. If inadequate resolution is obtained, bulkier (larger) alcohols are substituted as modifiers, again keeping retention in the desired range by adjusting alcohol concentration. If inadequate resolution again is obtained, an aprotic solvent modifier such as methyl-*tert.*-butyl ether, acetonitrile, or methylene chloride should be substituted. If no or partial resolution is obtained, column temperature or column type must be changed.

4. Conclusions

Aprotic solvent modifiers are useful for resolving drug enantiomers on derivatized cellulose carbamate HPLC stationary phases. Optimization of chiral separations on the Chiralcel OD column can usually be achieved with a limited number of mobile-phase combinations and short (5-cm) columns. Normally-used alcohol modifiers often can be replaced by certain aprotic solvents for superior separations. Based on these results, improvement in enantiomer resolution with aprotic solvents largely occurs when hydrogen bonding is the major source of chiral inter-

Table 2
Summary of chromatographic data on candidate amino-tetralin drug on Chiralcel OD

Mobile phase (v/v)	k_1'	k_2'	Selectivity, α	Resolution, R_s	Plate number[a]
Hexane–ethanol (98:2)	8.98	9.75	1.09	0.6	N/A[b]
Hexane–ethanol–acetonitrile (98:2:2)	6.74	7.42	1.10	0.7	N/A
Hexane–methanol (98:2)	9.53	11.27	1.18	2.37	1647

[a] Plate number of second enantiomer.
[b] Not available; peaks badly overlap.

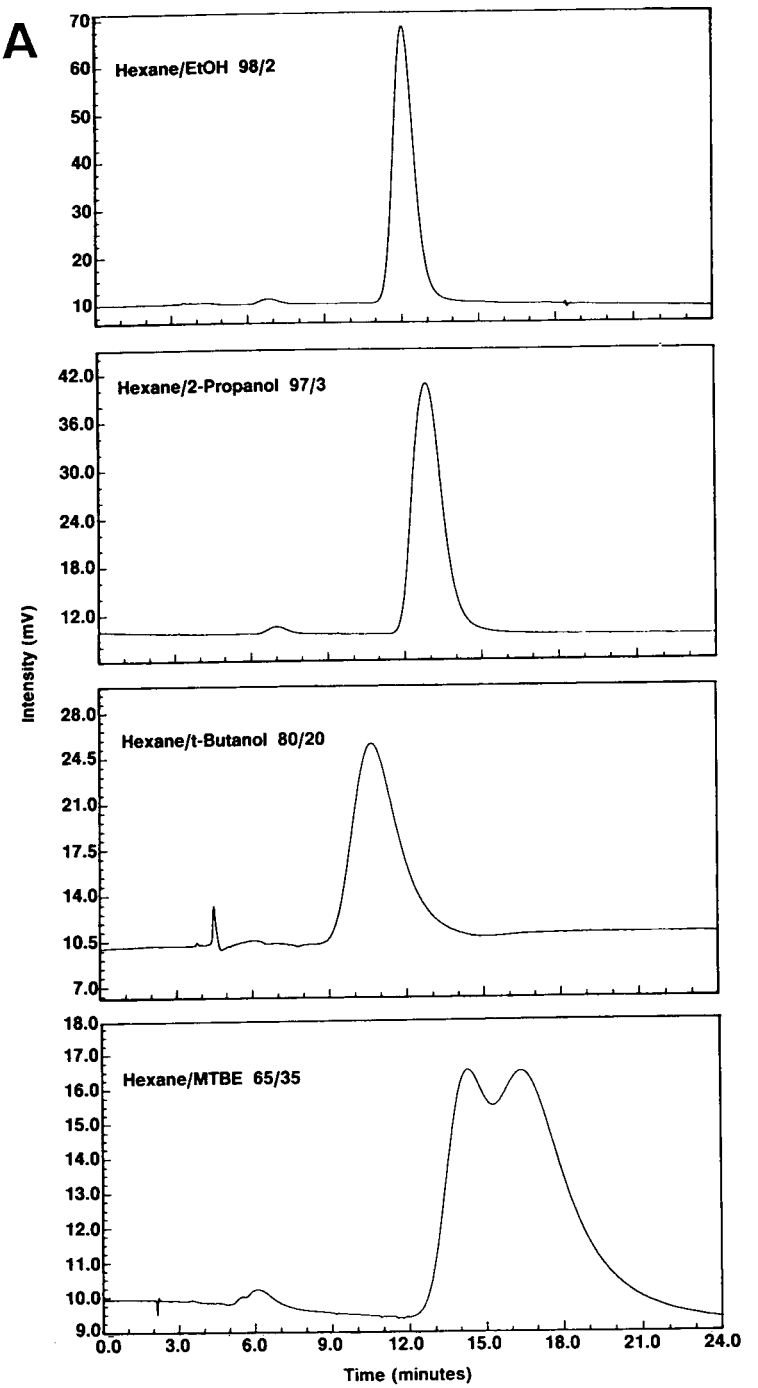

Fig. 9. Effect of stationary phase functionality and organic solvents on the separation of chiral "ester" enantiomers. Columns: 250 × 4.6 mm I.D.; temperature, ambient; UV detector, 230 nm; mobile phases as shown; flow-rate, 1.0 ml/min. (A) Chiralcel OC; (B) Chiralcel OG; (C) Chiralcel OF.

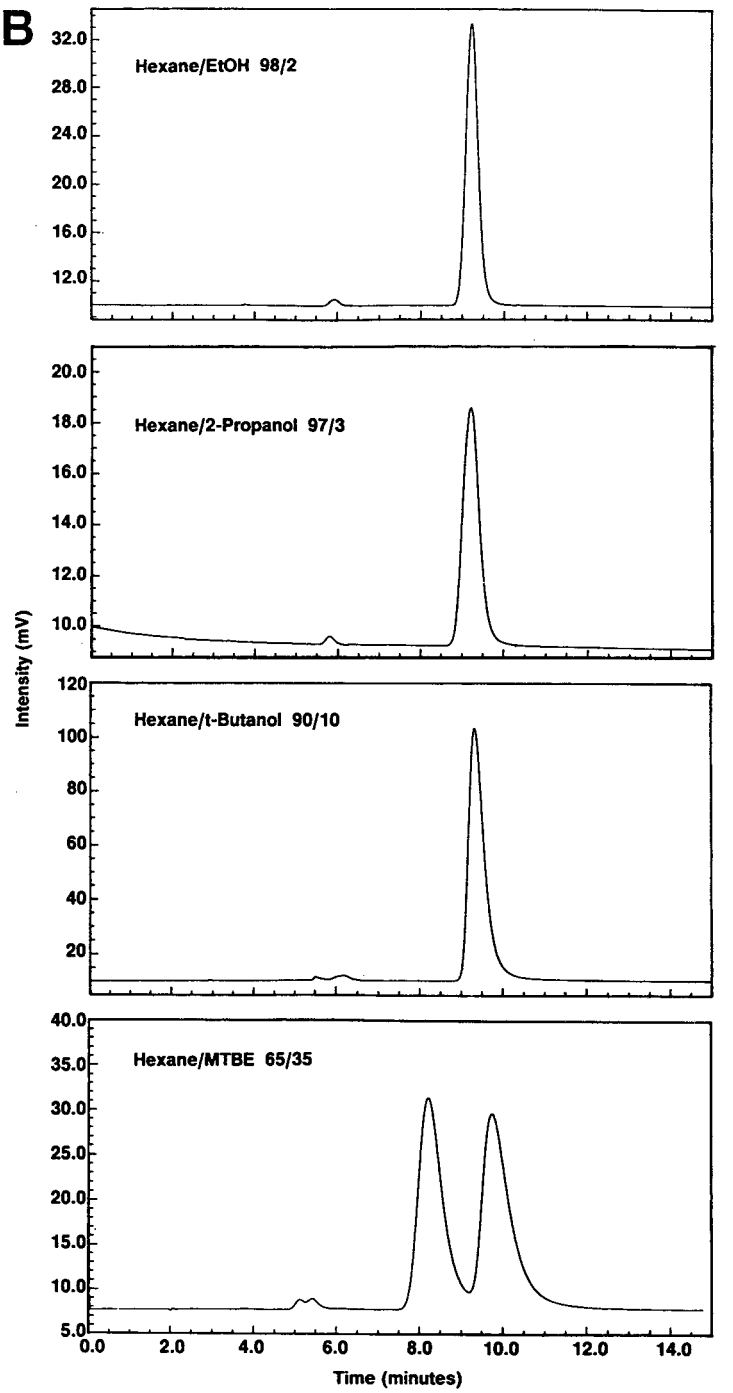

Fig. 9. (*continued*)

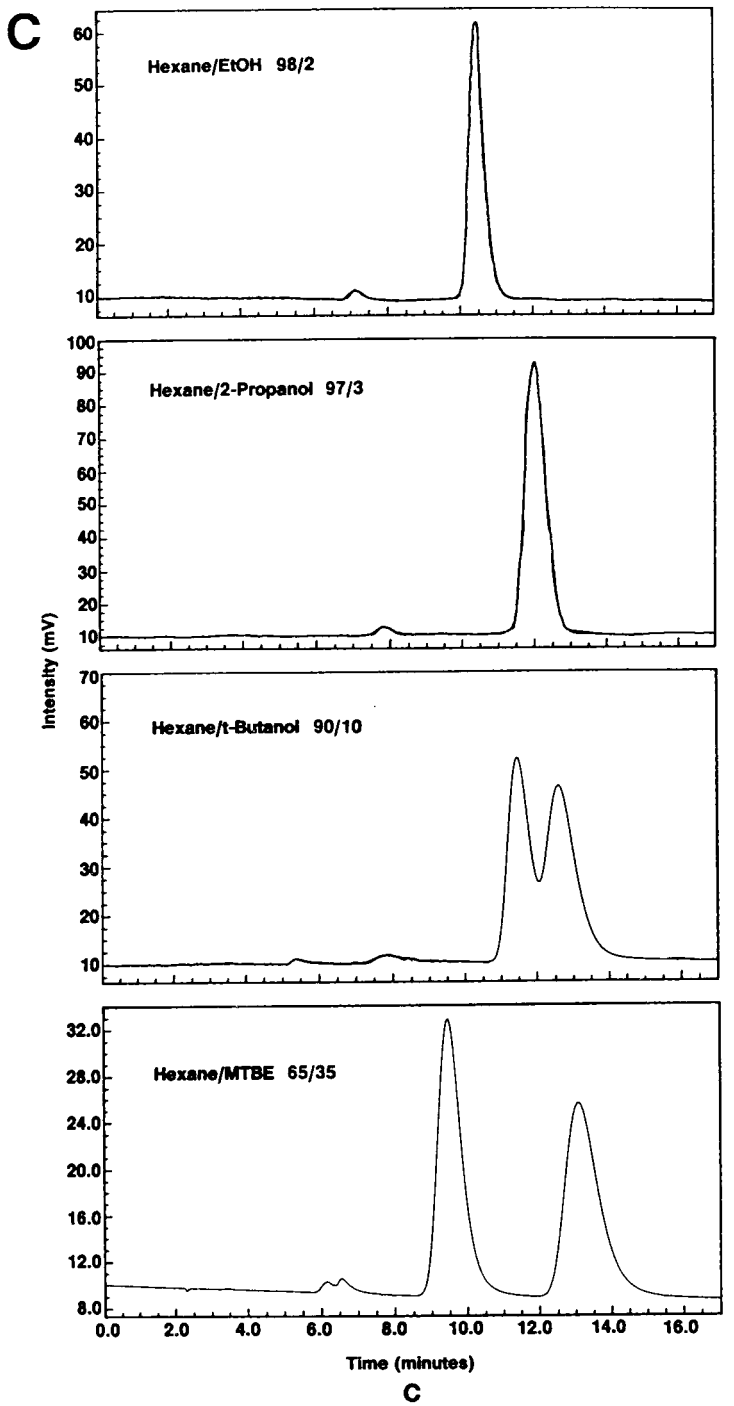

Fig. 9. (*continued*)

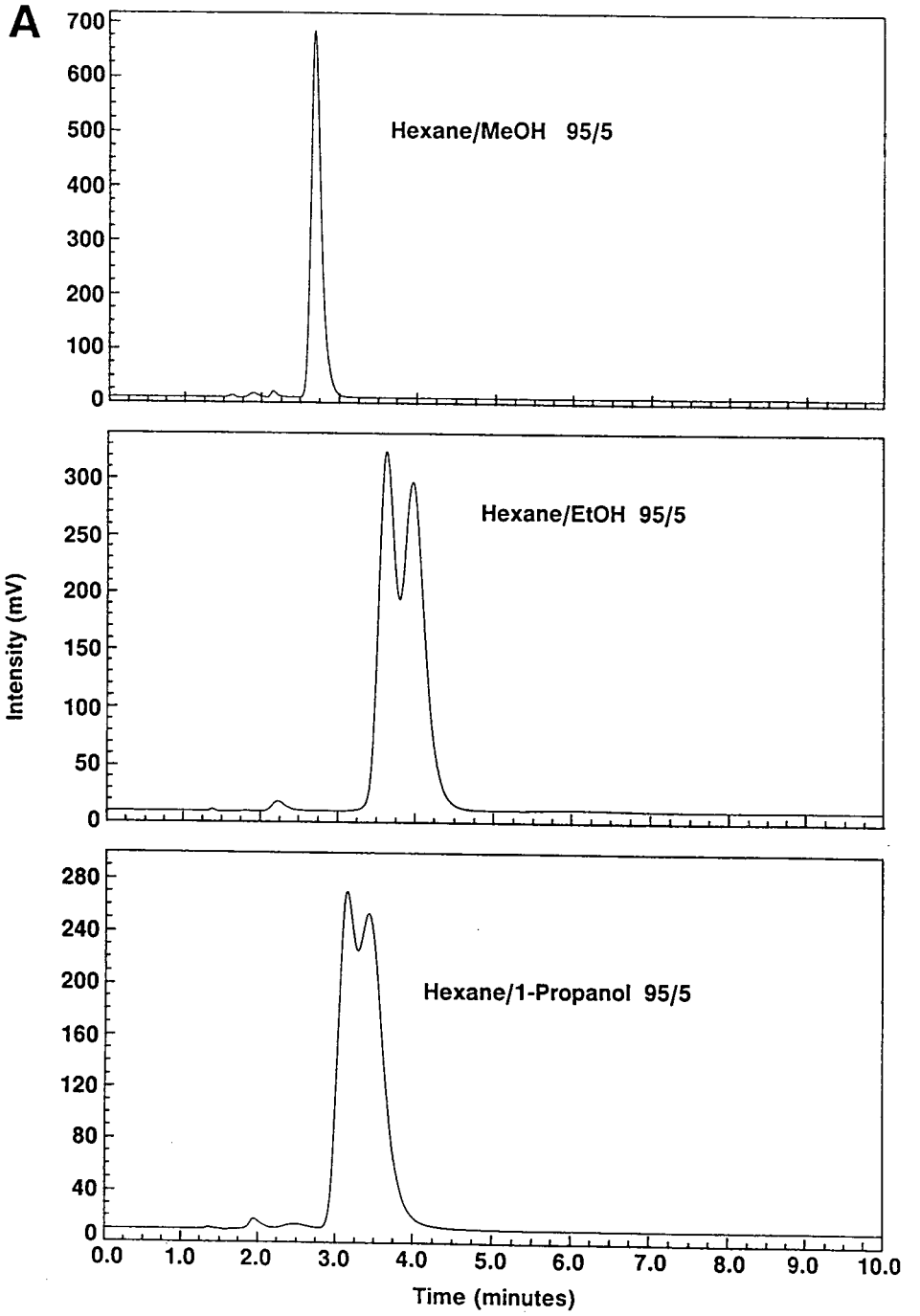

Fig. 10. Effect of protic modifiers on selectivity with the Chiralcel OJ column. Column: 50 × 4.6 mm I.D. Chiralcel OJ; solute, chiral "ester" of Fig. 1; flow-rate, 0.5 ml/min; temperature, ambient; UV detector, 230 nm. (A) Hexane–methanol, ethanol, 1-propanol; (B) hexane–2-propanol, *tert.*-butanol, methyl-*tert.*-butyl ether.

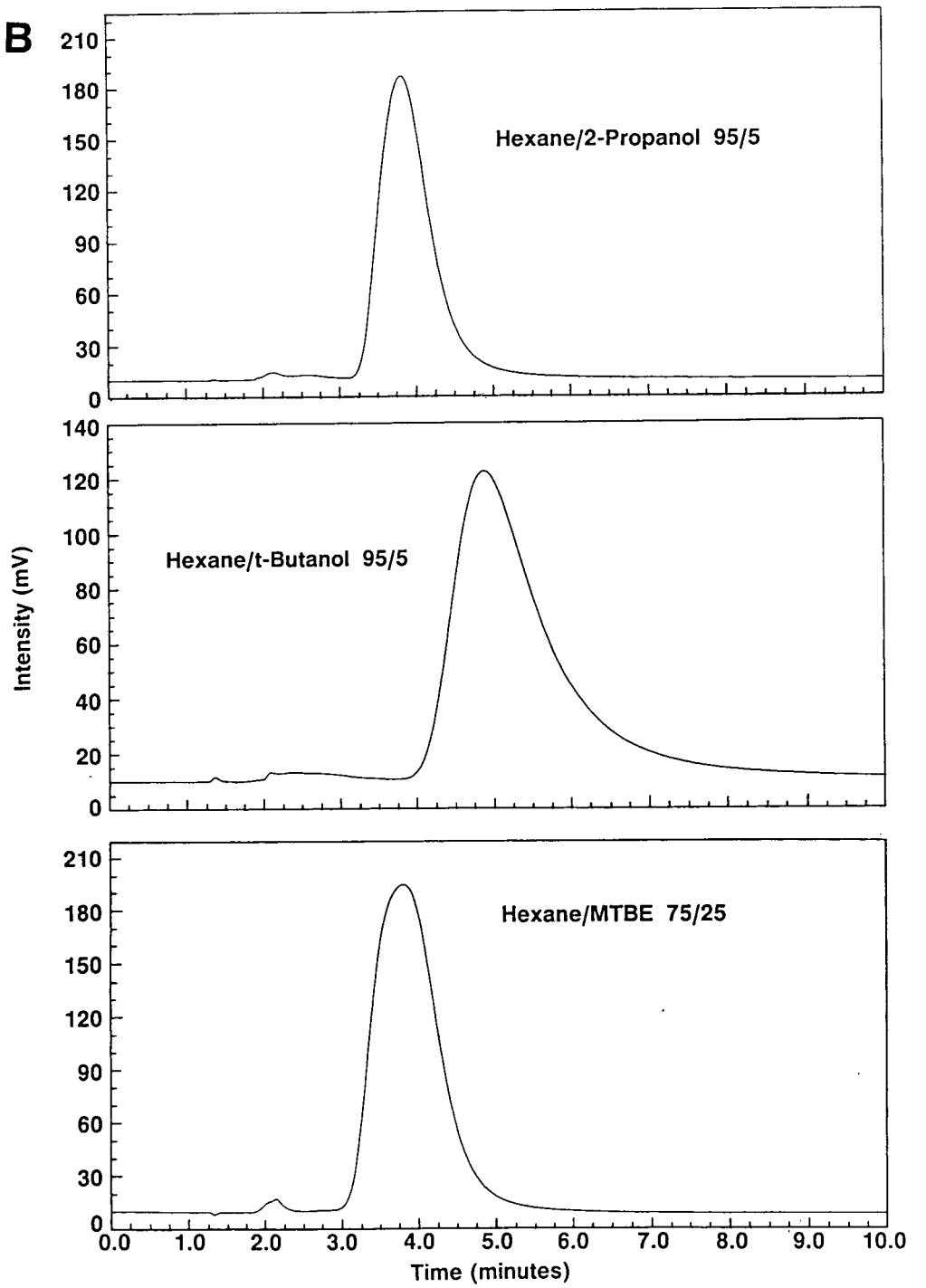

Fig. 10. (*continued*)

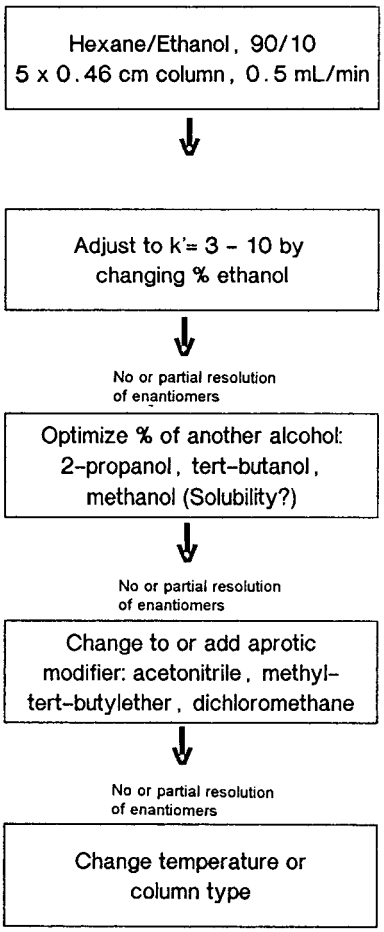

Fig. 11. Suggested strategy for optimizing separations on Chiralcel OD.

action. The Chiracel OD column appears stable to relatively high concentrations of certain aprotic solvent modifiers. Use of short Chiralcel OD columns with aprotic solvents expedites method development and is a cost-effective alternative to conventional approaches.

Acknowledgement

Appreciation is expressed to D.A. McCombs who assisted in the experiments.

References

[1] J.T. Ward and D.W. Armstrong, in M. Zief and L.J. Crane (Editors), Chromatographic Chiral Separations, Marcel Dekker, New York, NY, 1988, p. 131.
[2] S.G. Allenmark, Chromatographic Enantioseparation: Methods and Applications, John Wiley and Sons, New York, NY, 1988, Ch. 7.
[3] W.J. Lough and I.W. Wainer, in W.J. Lough (Editor), Chiral Liquid Chromatography, Chapman and Hall, New York, NY, 1989, p. 139.
[4] T. Shibata, K. Mori and Y. Okamoto, in A.M. Krstulovic (Editor), Chiral Separations by HPLC, John Wiley and Sons, New York, NY, 1989, p. 336.
[5] S.R. Perrin and W.H. Pirkle, in S. Ahuja (Editor), Chiral Separations by Liquid Chromatography, American Chemical Society, Washington, DC, 1991, p. 43.
[6] K.M. Kirkland, K.L. Neilson and D.A. McCombs, J. Chromatogr., 545 (1991) 43.
[7] K.M. Kirkland, K.L. Neilson, D.A. McCombs and J.J. DeStefano, LC·GC, 10 (1992) 322.
[8] K.M. Kirkland and D.A. McCombs, J. Chromatogr. A, 666 (1994) 211.
[9] Application Guide for Chiral Column Selection, 2nd ed., Chiral Technologies, Exton, PA, 1994.
[10] Y. Okamoto, Y. Kaida, R. Aburatani and K. Hatada, in S. Ahuja (Editor), Chiral Separations by Liquid Chromatography, American Chemical Society, Washington, DC, 1991, Ch. 5.
[11] I.M. Wainer, M.C. Alembik and E. Smith, J. Chromatogr., 388 (1987) 65.
[12] Chiral Technologies, Exton, PA, Operations Guide for Diacel Chiral Columns, First Edition.
[13] Y. Okamoto and Y. Kaida, J. Chromatogr. A, 666 (1994) 403.
[14] Chiral Technologies, Exton, PA, personal communication, January 1994.
[15] T. Shibata, I. Okamoto and K. Ishii, J. Liq. Chromatogr., 9 (1986) 313.
[16] Y. Okamoto, R. Aburatani, K. Hatano and K. Hatada, J. Liq. Chromatogr., 11 (1988) 2147.
[17] I.W. Wainer, R.M. Stiffin and T. Shibata, J. Chromatogr., 411 (1987) 139.
[18] L.R. Snyder, J. Chromatogr. Sci., 16 (1978) 223.
[19] L.R. Snyder, Principles of Adsorption Chromatography, Marcel Dekker, New York, NY, 1976, Ch. 8.
[20] L.R. Snyder, J.L. Glajch and J.J. Kirkland, Practical HPLC Method Development, John Wiley, New York, NY, 1988, Ch. 4.
[21] L.R. Snyder and T.C. Schunk, Anal. Chem., 54 (1982) 1764.

ELSEVIER

Journal of Chromatography A, 718 (1995) 27–34

JOURNAL OF CHROMATOGRAPHY A

Preparation of a hydrophobic porous membrane containing phenyl groups and its protein adsorption performance

Noboru Kubota[a], Minoru Kounosu[a], Kyoichi Saito[a,*], Kazuyuki Sugita[a], Kohei Watanabe[b], Takanobu Sugo[c]

[a]*Department of Specialty Materials, Faculty of Engineering, Chiba University, Chiba 263, Japan*
[b]*Industrial Membranes Development Department, Asahi Chemical Industry Co., Ltd., Fuji 416, Japan*
[c]*Takasaki Radiation Chemistry Research Establishment, Japan Atomic Energy Research Institute, Takasaki 370-12, Japan*

First received 23 January 1995; revised manuscript received 30 May 1995; accepted 7 June 1995

Abstract

A novel porous membrane was prepared by radiation-induced graft polymerization of an epoxy-group-containing vinyl monomer, glycidyl methacrylate, and subsequent addition of phenol and water. A phenyl group was appended to the polymer chain grafted on to a porous polyethylene hollow-fibre membrane. The presence of a diol group together with the phenyl group was required to reduce non-selective adsorption of the protein. A bovine serum albumin (BSA) phosphate buffer solution containing 2 *M* ammonium sulfate was forced to permeate through the resultant hydrophobic porous membrane, 0.36 mm thick with a phenyl-group density of 1.3 mmol/g. The breakthrough curves of BSA overlapped independent of the residence time in the range 12–1.2 s because of negligible diffusional mass-transfer resistance. A lower phenyl-group density resulted in a higher recovery of BSA after a series of adsorption and elution steps.

1. Introduction

Hydrophobic interaction chromatography (HIC) is recognized as a powerful technique for protein purification, along with affinity and ion-exchange chromatography [1]. HIC initially involved the use of charged beads, i.e., beads containing both a hydrophobic ligand and a charged group [2–6]. Later, uncharged beads were prepared to improve the performance of HIC [7–9].

To overcome the processing rate limitation caused by protein diffusion into the bead interior in conventional bead-packed column chromatography, the use of porous membranes [10–12], non-porous beads [13] and a continuous bed [14,15] has been suggested. Of these, a porous membrane, which has on its surface affinity ligands such as protein A [10,16], dye [17] and immobilized metal [18], and ion-exchange groups such as diethylamino [19,20] and sulfonic acid groups [21], is promising because of its high binding capacity for proteins and suitability for scale-up.

Tennikova and Svec [22] prepared a flat-sheet membrane consisting of a cross-linked terpolymer of glycidyl methacrylate–octyl methacrylate–ethylene dimethacrylate, in which the octyl group was directly bound to the matrix without a spacer and functioned as a hydro-

* Corresponding author.

0021-9673/95/$09.50
SSDI 0021-9673(95)00641-9

phobic ligand. The spacing between the matrix and ligand is effective in improving accessibility of the protein to the ligand [23]. For example, HIC which utilized beads containing a phenyl group as the hydrophobic ligand with a 2-hydroxypropane group as a spacer exhibited a higher resolution than that without a spacer [24].

Radiation-induced graft polymerization (RIGP) is a powerful modification technique in that a flexible polymer chain can be grafted on to various forms of trunk polymers. We have prepared functionalized porous membranes containing affinity ligands [18] and ion-exchange groups [21,25] by RIGP of glycidyl methacrylate and subsequent ring-opening reactions of the epoxy group produced. The functional moiety was immobilized on the graft chain of submicrometre length. The flexible graft chain may provide a favourable binding space for the protein because it can also function as a spacer.

The objective of this study was twofold: (1) to prepare an uncharged porous membrane for HIC by RIGP and (2) to evaluate the adsorption and elution characteristics of the protein during permeation through the resultant membrane. We adopted a phenyl group and a porous polyethylene hollow-fibre membrane as hydrophobic group and feasible matrix, respectively.

2. Experimental

2.1. Materials

A porous membrane of hollow-fibre form was used as a trunk polymer for grafting. This membrane, which was made of polyethylene (PE), had inner and outer diameters of 0.07 and 0.12 cm, respectively, with a nominal pore diameter of 0.2 μm and a porosity of 0.67. Technical-grade glycidyl methacrylate (GMA) ($CH_2=CCH_3COOCH_2CHOCH_2$) was purchased from Tokyo Kasei and used without further purification. Bovine serum albumin (BSA) was obtained from Sigma. Phosphate buffer (0.07 *M*, pH 7.4) was prepared by dissolving phosphate buffer powder (Wako) in deionized water. BSA was dissolved in phosphate buffer solution containing 2 *M* ammonium sulfate. Other reagents were of analytical-reagent grade or higher.

2.2. Introduction of phenyl group on to porous membrane

Ring opening of a poly-GMA chain was adopted to introduce a ligand on to a porous membrane [26,27]. Fig. 1 shows a schematic diagram of the procedure used to append a hydrophobic phenyl group to a PE membrane. This procedure consists of the following three steps. (1) Grafting of GMA on to the original membrane: the PE membrane irradiated with an electron beam is immersed in 10% (v/v) GMA–methanol solution solution at 313 K for 12 min [28]. (2) Introduction of the phenyl group for enhancement of HIC: the GMA-grafted membrane is immersed in 9.4% (w/w) aqueous phenol solution, the pH of which is adjusted to 9, at 353 K for 1–24 h. (3) Blocking of the

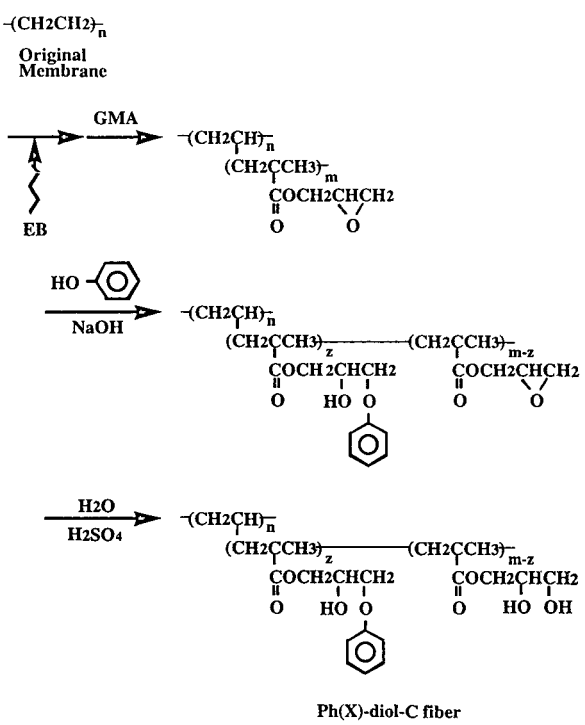

Fig. 1. Schematic diagram of procedure used to append phenyl and hydroxyl groups to polyethylene porous membrane.

remaining epoxy group for reduction of non-selective adsorption: the membrane is immersed in 0.5 *M* H_2SO_4 at 353 K for 2 h [25,29].

The degree of GMA grafting, defined as

$$d_g = 100[(W_1 - W_0)/W_0] \quad (1)$$

where W_0 and W_1 are the masses of the original and GMA-grafted membranes, respectively, was set to 150%.

The molar conversion of the epoxy group to the phenyl group, X, and phenyl-group density were calculated from the mass gain as follows [26,27]:

$$X = 100[142(W_2 - W_0)/(W_1 - W_0) - (142 + 18)]/(94 - 18) \quad (2)$$

phenyl-group density =

$$[(W_1 - W_0)/142](X/100)/W_2 \quad (3)$$

where W_2 is the mass of the resulting membrane and 142, 94 and 18 are the molecular masses of GMA, phenol and water, respectively. The membrane containing both phenyl and diol groups is referred to as a Ph(X)-diol-C fiber, where Ph, (X) and C denote phenyl group, conversion and capillary, respectively. For comparison, a Ph(0)-diol-C fibre, i.e., exclusively containing the diol group, was obtainable by reacting the GMA-grafted membrane with water.

2.3. Properties of the Ph-diol-C fibre

The inner and outer diameters and length of the hollow-fibre membrane in a wet state were measured with a scale. The porosity of the membrane was determined from measurement of its water content. After the membrane had been dried under reduced pressure, the specific surface area was determined using Quantasorb (Yuasa Ionics) according to the nitrogen adsorption method.

Determination of the permeation flux in a dead-end mode has been described elsewhere [26,27]. Briefly, a Ph(X)-diol-C fibre about 15 cm long was positioned in a U-configuration and the liquid was forced to permeate outwards through the hollow fibre at a constant permeation pressure of 0.1 MPa. Four kinds of liquids were permeated: pure water, phosphate buffer (0.07 *M*, pH 7.4) and phosphate buffers containing 1 *M* and 2 *M* ammonium sulfate. The permeation rate of the effluent penetrating the outside surface of the hollow fibre was determined. The permeation flux of the liquid through the hollow fibre was calculated by dividing the permeation rate by the inside surface area. For comparison, the permeation flux of the original hollow-fibre membrane was also determined. The relative viscosity of the liquid to water was determined with an Ostwald viscometer at 298 K.

2.4. Adsorption and elution of BSA during permeation through the Ph-diol-C fibre

The protein was adsorbed during permeation of the protein solution and subsequently eluted by permeation of an eluent through the Ph-diol-C fibre in a dead-end mode, using a procedure similar to that described above. First, a 0.2 mg/ml BSA phosphate buffer solution containing 2 *M* $(NH_4)_2SO_4$ was forced to permeate through the hollow fibre until adsorption equilibrium was attained. Second, phosphate buffer containing 2 *M* $(NH_4)_2SO_4$ was permeated to wash the pores. Third, the adsorbed BSA was eluted by permeating $(NH_4)_2SO_4$-free phosphate buffer. The permeation pressure ranged from 0.01 to 0.1 MPa. All the experiments were performed at 298 K.

3. Results and discussion

3.1. Introduction of phenyl and hydroxyl groups on to porous membrane

The epoxy groups of poly(glycidyl methacrylate) (GMA) grafted on to hollow fibres were converted into phenyl groups by the addition of phenol, and the conversion is shown in Fig. 2 as a function of reaction time. A conversion of 0–44% corresponded to a phenyl (Ph)-group density of 0–1.6 mmol/g. The phenyl-group density of this Ph-diol-C fibre was compared with

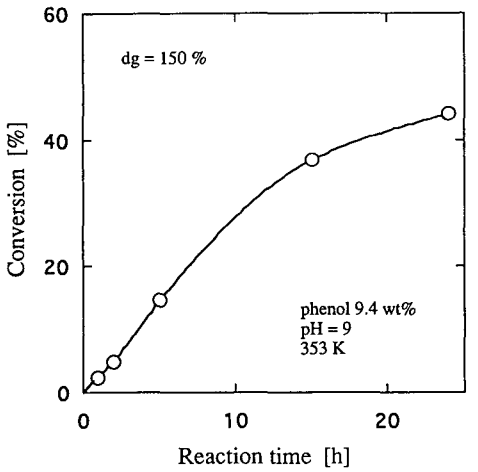

Fig. 2. Conversion of epoxy groups into phenyl groups as a function of reaction time.

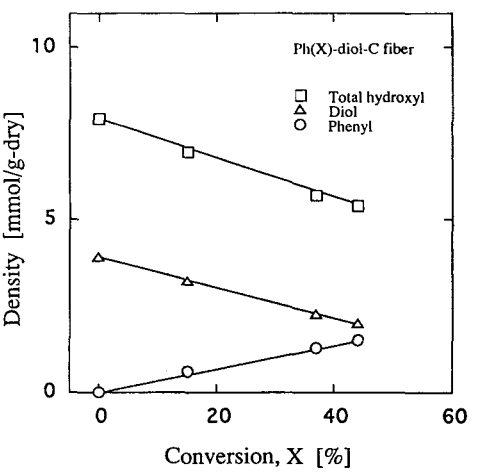

Fig. 3. Densities of phenyl, diol and total hydroxyl groups of the Ph(X)-diol-C fibre.

that of commercially available HIC gel beads: 0.1 mmol/ml of TSK gel Phenyl-5PW (Tosoh) [30] and 0.4 mmol/g of phenyl Sepharose FF (Pharmacia Biotech) [31] were equivalent to the phenyl-group densities of the Ph(5)-diol-C and Ph(10)-diol-C fibres, respectively.

The residual epoxy group was quantitatively converted into two adjacent hydroxyl (diol) groups via reaction with water. The density balance of the functional moieties on the graft chain, the units of which are represented mmol/g of the dry membrane, is shown in Fig. 3 as a function of the conversion. The total hydroxyl-group density was calculated as the sum of the density of monool groups produced by ring opening of the expoxy group with phenol and twice the density of diol groups produced by that of the residual epoxy groups with water. Kim et al. [29] reported that the critical density of the hydroxyl groups on the graft chain required for minimizing non-selective, i.e., irreversible, adsorption of the protein on to a porous polyethylene membrane was 14 mmol/g of original polyethylene membrane. This critical density corresponded to a total hydroxyl-group density of 4.3 mmol/g of Ph(67)-diol-C fibre. Therefore, the Ph-diol-C fibres below a conversion of 67% satisfy the requirement for hydrophilization, and will reduce non-selective adsorption of the protein.

3.2. Permeability of the Ph-diol-C fibre

Four kinds of liquids were permeated through the Ph-diol-C fibre with various conversions at a constant permeation pressure of 0.1 MPa: pure water, phosphate buffer and phosphate buffers containing 1 M and 2 M $(NH_4)_2SO_4$. Fig. 4 shows the permeation flux of the liquid as a function of the conversion. The permeation flux of each liquid of the Ph-diol-C fibre was independent of the conversion, i.e., phenyl-group density, and constant at 90% of the original hollow fibre. In contrast, the permeation flux of an ion-exchange porous hollow-fibre membrane is reported to decrease with increasing ion-exchange group density because mutual electrostatic repulsion of the graft chains induced stretching of the graft chains from the pore surface toward the pore interior [32,33]. The stability of the conformation of the polymer chains grafted on to the pore surface of the Ph-diol-C fibre towards the liquid is due to electrostatic neutrality of the graft chain, which is favourable for practical applications.

The permeation flux ratios of the phosphate

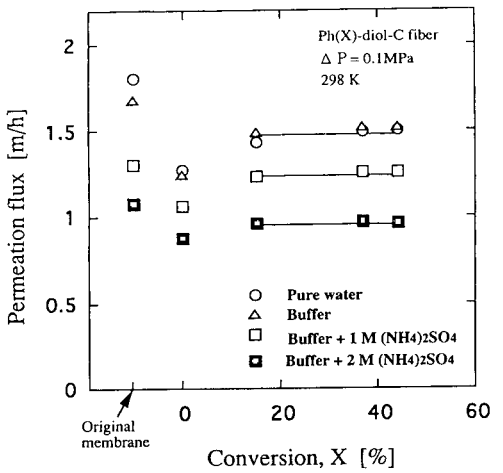

Fig. 4. Permeation flux of the Ph(X)-diol-C fibre as a function of conversion.

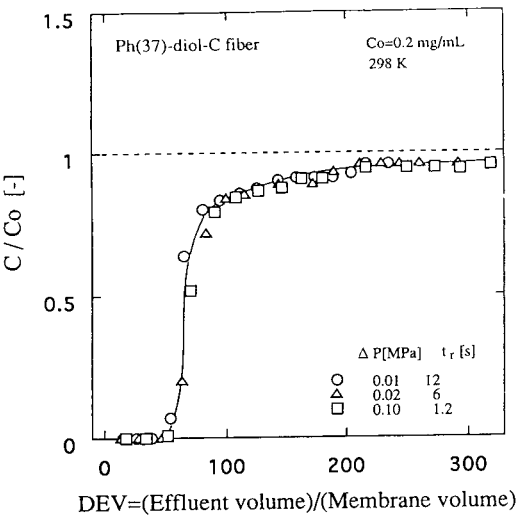

Fig. 5. Breakthrough curve of BSA across the Ph(37)-diol-C fibre with various permeation pressures.

buffer and phosphate buffers containing 1 M and 2 M $(NH_4)_2SO_4$ to water, 1.0, 0.84 and 0.66, respectively, were well correlated with the reciprocals of the relative viscosity, 0.97, 0.86 and 0.71, respectively. Therefore, the decrease in the permeation flux with increasing salt concentration could be explained by the increase in liquid viscosity.

3.3. Adsorption characteristics of BSA during permeation

A 0.2 mg/ml bovine serum albumin (BSA) buffer solution was fed to the inside surface of the pH(37)-diol-C fibre at a constant permeation pressure ranging from 0.01 to 0.1 MPa, i.e., a residence time ranging from 12 to 1.2 s. The residence time, t_r, was calculated as follows:

$$t_r = \varepsilon[\pi(d_o^2 - d_i^2)L/4](\text{permeation rate}) \quad (4)$$

where ε, d_i, d_o and L are the porosity, inner and outer diameters and length of the Ph-diol-C fibre in a wet state, 0.54, 0.073, 0.145 and 14.5 cm, respectively. The permeation rate of the BSA buffer solution for each permeation pressure remained constant during adsorption of the protein, e.g., 0.0083 ml/s at 0.01 MPa and 0.083 ml/s at 0.1 MPa. The time course of the protein concentration of the effluent, i.e., the breakthrough (BT) curve, is shown in Fig. 5 as a function of the dimensionless effluent volume (DEV), defined as effluent volume divided by the membrane volume. The BT curves overlapped independent of the permeation pressure, i.e., residence time. This indicates a negligible diffusional mass-transfer resistance of BSA to the phenyl group. Thus, a faster HIC of the protein can be realized using the Ph-diol-C fibre because the residence time of the protein solution across the membrane is much shorter (about $1/10^3$) than that across the conventional bead-packed column [10]. The advantage of using the porous membrane instead of beads has been demonstrated for HIC and also for pseudo-affinity [10,16–18,26,27] and ion-exchange [19–21,25] chromatography.

The amount of BSA adsorbed in equilibrium with the feed concentration, q_0, can be calculated by the following integration of the BT curve:

$$q_0 = \int_0^{V_s} (C_0 - C)\, dV/W_2 \quad (5)$$

where C_0(=0.2 mg/ml) and C are the concen-

trations of BSA in the feed and effluent, respectively, V is the effluent volume and V_s is the effluent volume when C reaches C_0. The q_0 values were compared with the theoretical saturation capacity, q_t, as shown in Fig. 6. The q_t of BSA on the Ph(X)-diol-C fibre can be calculated by assuming that BSA molecules cover the pore surface as a monolayer with end-on and side-on orientations, where the cross-sectional area, a, occupied by a BSA molecule is $1.4 \cdot 10^{-17}$ and $4.9 \cdot 10^{-17}$ m^2, respectively [34]:

$$q_t = a_v M_r / (a N_A) \quad (6)$$

where a_v, M_r and N_A are the specific surface area of the Ph(X)-diol-C fibre, molecular mass of BSA (66 300) and Avogadro's number, respectively. The a_v value was determined to be $6.7 \cdot 10^3$ m^2/kg irrespective of the conversion.

The amount of BSA adsorbed, i.e., the BSA binding capacity, was almost constant between two extreme orientations independent of the conversion, i.e., phenyl-group density.

The hollow-fibre membrane containing exclusively the diol group, i.e., the Ph(0)-diol-C fibre, had about 50% of the BSA binding capacity of the Ph(15)-diol-C fibre. The difference in BSA binding capacity between the Ph(0)-diol-C and Ph(15)-diol-C fibres is explained by the contribution of the phenyl group on the graft chain as a hydrophobic ligand. Poly(2-hydroxyethyl methacrylate) beads, which are analogues of the Ph(0)-diol-C fibre in terms of chemical structure, have been used as an HIC adsorbent [24]; the Ph(0)-diol-C fibre also exhibited hydrophobic interaction with the protein in the phosphate buffer containing 2 M $(NH_4)_2SO_4$.

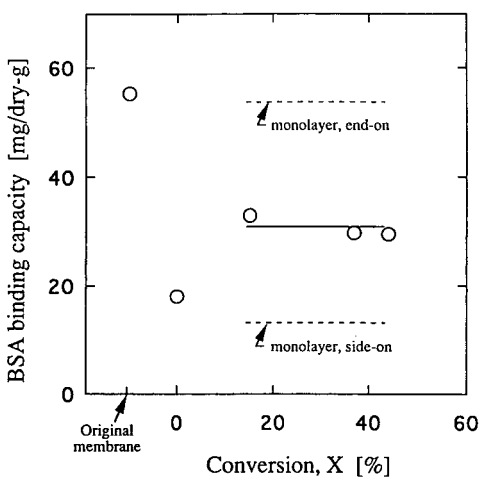

Fig. 6. BSA binding capacity of the Ph(X)-diol-C fibre.

3.4. Elution and recovery

A series of procedures for protein processing using the Ph-diol-C fibre in the conversion range 15–44% includes adsorption, washing and elution. Examples of breakthrough and elution curves of BSA are shown in Fig. 7, where the BSA solution and eluent were forced to permeate through the Ph(37)-diol-C fibre at a permeation pressure of 0.02 MPa. The recovery of the protein during permeation was defined as

$$\text{recovery (\%)} = 100\,[(\text{amount eluted})/(\text{amount adsorbed} - \text{amount washed})] \quad (7)$$

The recovery of BSA is shown in Fig. 8 as a function of the conversion. A higher density of the phenyl groups on the graft chain resulted in a lower recovery of BSA. This implies that BSA bound more strongly to the Ph-diol-C fibre which

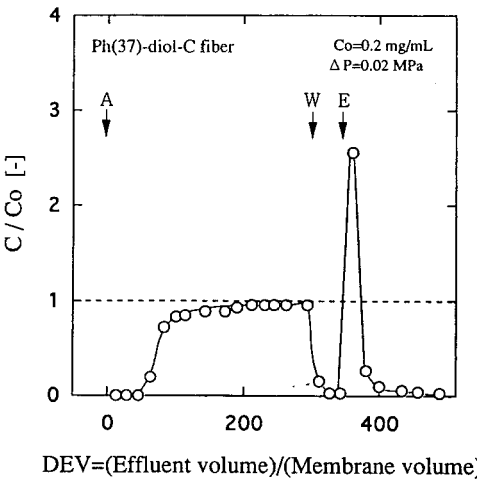

Fig. 7. Breakthrough and elution curves of BSA of the Ph(37)-diol-C fibre. A = adsorption; W = washing; E = elution.

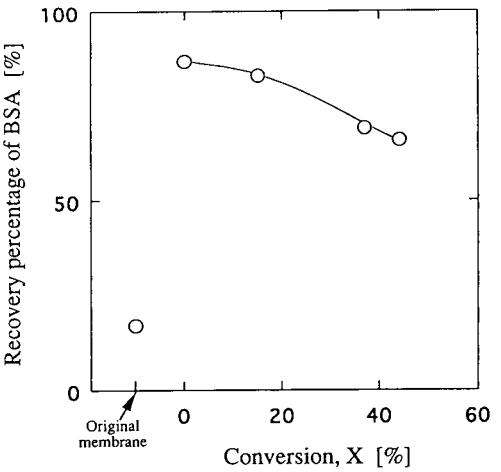

Fig. 8. Recovery of BSA with the Ph(X)-diol-C fibre as a function of conversion.

had a higher phenyl-group density. Rosengen et al. [35] have demonstrated that agarose-based beads with a higher density of hydrophobic groups such as octyl and phenyl groups exhibited a lower recovery of phycoerythrin as a model protein. The recovery of BSA with the Ph-diol-C fibre, 63–83%, was at the same level as that of commercially available HIC beads [TSK gel Phenyl-Toyopeal 650 (Tosoh) and Phenyl-Cellulofine S-type (Seikagaku Kogyo)] with an identical eluent, 53–92% [36,37].

The Ph(0)-diol-C fibre exhibited a recovery of 87% with a lower BSA binding capacity than the Ph(15–44)-diol-C fibre, whereas the original hollow-fibre membrane made of polyethylene exhibited a low recovery of 17%. This was due to non-selective adsorption, i.e., irreversible adsorption of BSA on to polyethylene.

4. Conclusion

A polymer chain containing both phenyl and diol groups as hydrophobic and hydrophilic groups, respectively, which was grafted on to the polyethylene hollow-fibre matrix, was demonstrated to provide adsorption space for hydrophobic interaction with a protein and to reduce the undesirable non-selective adsorption of the polyethylene matrix. The breakthrough curve was unchanged irrespective of the residence time of the bovine serum albumin (BSA) buffer solution containing 2 M $(NH_4)_2SO_4$ across the membrane in the dead-end mode because of negligible diffusional mass-transfer resistance. The membranes with a phenyl-group density of 0.6–1.6 mmol/g exhibited a BSA binding capacity of 30 mg/g, which indicated monolayer adsorption. The amount of BSA recovered by permeating an $(NH_4)_2SO_4$-free buffer through the membranes demonstrated that a higher density of phenyl groups decreased the recovery of BSA.

Symbols

a	cross-sectional area occupied by a BSA molecule (m^2)
a_v	specific surface area of the Ph-diol-C fibre (m^2/kg)
C	concentration of BSA in the effluent (mg/ml)
C_0	concentration of BSA in the feed (mg/ml)
d_g	degree of GMA grafting (%)
d_i	inner diameter of hollow-fibre membrane (cm)
d_o	outer diameter of hollow-fibre membrane (cm)
L	length of hollow-fibre membrane (cm)
M_r	molecular mass of BSA
N_A	Avogadro's number
Δp	permeation pressure (MPa)
q_0	amount of BSA adsorbed in equilibrium with C_0 (mg/g)
q_t	theoretical saturation capacity of BSA on the Ph-diol-C fibre (mg/g)
t_r	residence time (s)
V	effluent volume (ml)
V_s	effluent volume when C reaches C_0 (ml)
W_0	mass of the original membrane (g)
W_1	mass of the GMA-grafted membrane (g)
W_2	mass of the Ph(X)-diol-C fibre (g)
X	molar conversion of epoxy groups into phenyl groups (%)
ε	porosity of the Ph-diol-C fibre

References

[1] J.-C. Janson and L. Ryden (Editors), Protein Purification: Principles, High Resolution Methods, and Applications, VCH, New York, 1989, pp. 207–226.
[2] H. Weiss and T. Bucher, Eur. J. Biochem. 17 (1970) 561–567.
[3] L.A. Osterman, Anal. Biochem., 43 (1971) 254–258.
[4] R. Yon, Biochem. J., 126 (1972) 765–767.
[5] Z. Er-el, Y. Zaidenzaig and S. Shaltiel, Biochem. Biophys. Res. Commun., 49 (1972) 383–390
[6] S. Shaltiel and Z. Er-el, Proc. Natl. Acad. Sci. U.S.A., 70 (1973) 778–781.
[7] S. Hjerten, J. Chromatogr., 87 (1973) 325–331.
[8] J. Porath, L. Sundberg, N. Fornstedt and I. Olsson, Nature, 245 (1973) 465–466.
[9] S. Hjerten, J. Rosengren and S. Pahlman, J. Chromatogr., 101 (1974) 281–288.
[10] S. Brandt, R.A. Goffe, S.B. Kesser, J.L. O'Connor and S.E. Zale, Bio/Technology, 6 (1988) 779–782.
[11] Z.G. Su, G. Daun and C.K. Colton, in S. Furusaki, I. Endo and R. Matsumoto (Editors), Biochemical Engineering for 2001, Springer, Tokyo, 1991, p. 533.
[12] E. Klein, Affinity Membranes, Their Chemistry and Performance in Adsorptive Separation Processes, Wiley, New York, 1991.
[13] G. Jilge, R. Janzen, H. Giesche, K.K. Unger, J.N. Kinkel and M.T.W. Hearn, J. Chromatogr., 397 (1987) 71–80.
[14] J.L. Liao, R. Zhang and S. Hjerten, J. Chromatogr., 586 (1991) 21–26.
[15] S. Hjerten, Y.M. Li, J.L. Liao, J. Mohammad, K. Nakazato and G. Pettersson, Nature, 356 (1992) 810–811.
[16] P. Langlotz and K.H. Kroner, J. Chromatogr., 591 (1992) 107–113.
[17] B. Champluvier and M.-R. Kula, J. Chromatogr., 539 (1991) 315–325.
[18] H. Iwata, K. Saito, S. Furusaki, T. Sugo and J. Okamoto, Biotechnol. Prog., 7 (1991) 412–418.
[19] D. Josic, J. Rensch, K. Löster, O. Baum and W. Reuster, J. Chromatogr., 590 (1992) 59–76.
[20] J.A. Gerstner, R. Hamilton and S.M. Cramer, J. Chromatogr., 596 (1992) 173–180.
[21] H. Shinano, S. Tsuneda, K. Saito, S. Furusaki and T. Sugo, Biotechnol. Prog., 9 (1993) 193–198.
[22] T.B. Tennikova and F. Svec, J. Chromatogr., 646 (1993) 279–288.
[23] Affinity Chromatography: Principles and Methods, Pharmacia LKB Biotechnology/Pharmacia Biosystems, Tokyo, 2nd ed., 1988, p. 8.
[24] P. Smidol, I. Kleinmann, J. Plicka and V. Svoboda, J. Chromatogr., 523 (1990) 131–138.
[25] S. Tsuneda, H. Shinano, K. Saito, S. Furusaki and T. Sugo, Biotechnol. Prog., 10 (1994) 76–81.
[26] M. Kim, K. Saito, S. Furusaki, T. Sato, T. Sugo and I. Ishigaki, J. Chromatogr., 585 (1991) 45–51.
[27] M. Kim, K. Saito, S. Furusaki, T. Sugo and I. Ishigaki, J. Chromatogr., 586 (1991) 27–33.
[28] H. Yamagishi, K. Saito, S. Furusaki, T. Sugo and I. Ishigaki, Ind. Eng. Chem. Res., 30 (1991) 2234–2237.
[29] M. Kim, J. Kojima, K. Saito, S. Furusaki and T. Sugo, Biotechnol. Prog., 10 (1994) 114–120.
[30] Separation Report No. 031, Tosoh, Tokyo.
[31] B.-L. Johansson and I. Drevin, J. Chromatogr., 391 (1987) 448–451.
[32] S. Tsuneda, K. Saito, S. Furusaki, T. Sugo and I. Ishigaki, J. Membr. Sci., 71 (1992) 1–12.
[33] K. Kobayashi, S. Tsuneda, K. Saito, S. Furusaki and T. Sugo, J. Membr. Sci., 76 (1993) 209–218.
[34] P.G. Squire and M.E. Himmel, Arch. Biochem. Biophys., 196 (1979) 165–177.
[35] J. Rosengren, S. Pahlman, M. Glad and S. Hjerten, Biochim. Biophys. Acta, 412 (1975) 51–61.
[36] General Catalog for 1994/95, Tosoh, Tokyo, p. 184.
[37] Biochemicals Catalog for 1993/94, Seikagaku Kogyo, Tokyo, 1993, pp. 937–941.

ELSEVIER

Journal of Chromatography A, 718 (1995) 35–44

JOURNAL OF CHROMATOGRAPHY A

Biomimetic dye affinity chromatography for the purification of bovine heart lactate dehydrogenase

N.E. Labrou, Y.D. Clonis*

Enzyme Technology Laboratory, Department of Agricultural Biology and Biotechnology, Agricultural University of Athens, Iera Odos 75, 11855 Athens, Greece

First received 3 February 1995; revised manuscript received 6 June 1995; accepted 9 June 1995

Abstract

Three biomimetic dye ligands bearing as a triazine-linked terminal moiety a carboxylated structure, which mimics substrates and inhibitors of L-lactate dehydrogenase (LDH), were immobilized on cross-linked agarose Ultrogel A6R. These biomimetic dyes are purpose-designed analogues of commercial monochlorotriazine Cibacron Blue 3GA (CB3GA) and parent dichlorotriazine Vilmafix Blue A-R (VBAR). The corresponding biomimetic adsorbents, along with non-biomimetic adsorbents bearing CB3GA and VBAR, were evaluated for their ability to purify LDH from bovine heart crude extract. When compared with non-biomimetic adsorbents, all biomimetic adsorbents exhibited a higher purifying ability. Further, one immobilized biomimetic dye, bearing mercaptopyruvic acid as biomimetic moiety, displayed the highest purifying ability. The concentration of immobilized dye affected both the capacity and the purifying ability of the affinity column, exhibiting an optimum value 2.2 μmol dye/g moist gel. This affinity adsorbent was exploited for the purification of LDH from bovine heart in a two-step procedure. The procedure consisted in a biomimetic dye affinity chromatography step (NAD^+/sulphite elution, 25-fold purification, 64% step yield), followed by DEAE-agarose ion-exchange chromatography (1.4-fold purification, 78% step yield). The purified enzyme exhibited a specific activity of ca. 480 u/mg at 25°C (content of impurities: pyruvate kinase and glutamic–oxaloacetic transaminase were not detected; malate dehydrogenase, 0.01%), compared with ca. 250 u/mg of commercial bovine heart LDH (malate dehydrogenase, 0.05%) suitable for analytical purposes.

1. Introduction

Downstream processing is regarded as a key factor for the successful commercialization of high-purity proteins. Affinity chromatography [1–5], although a relatively expensive technique, is present in the production line of several high-purity products, e.g., therapeutic, molecular biology, analytical and diagnostic proteins. Reactive triazine dyes are robust affinity ligands promising for industrial-scale bioprocesses, and their immobilized forms are exploited in downstream processing [5–8]. Dyes offer clear advantages over biological ligands [4,5,7,8]; however, the main drawback of dye molecules appears to be their moderate, in general, selectivity for target proteins. Attempts to tackle this problem were realized through the biomimetic dye concept [9,10], according to which the presence of a purpose-designed biomimetic moiety on the parent dye can lead to a new dye mimicking natural ligands of the target protein. The purpose-de-

* Corresponding author.

0021-9673/95/$09.50
SSDI 0021-9673(95)00661-3

signed biomimetic dyes are expected to exhibit increased affinity and purifying ability for target proteins. Earlier studies confirmed the effectiveness of this approach both, in terms of measured K_D values of free biomimetic dyes with formate dehydrogenase [10], oxalate oxidase [11], oxalate decarboxylase [11] and oxaloacetate decarboxylase [12], and in the purification of alcohol dehydrogenase [9], trypsin [13], alkaline phosphatase [14,15] and formate dehydrogenase [16] on immobilized biomimetic dyes.

The present biomimetic dye ligands are analogues of commercial monochlorotriazine Cibacron Blue 3GA (CB3GA) and parent dichlorotriazine Vilmafix Blue A-R (VBAR), and exhibit as the biomimetic moiety, linked on the chlorotriazine ring, an α-keto acid structure. Therefore, the biomimetic moiety mimics natural substrates and inhibitors of L-lactate dehydrogenase (LDH), e.g., pyruvate, 2-oxobutyrate, oxamate and oxalate. The corresponding biomimetic affinity adsorbents (BM) are expected to show increased purifying ability for LDH. The target enzyme is a tetramer of $M_r \approx 140\,000$, with H_4 and H_3M being the dominant components of heart LDH [17]. Lactate dehydrogenase has attracted attention as an auxiliary or indicator enzyme in the determination of several metabolites and enzymes [17]. However, the enzyme from bovine heart has attracted considerably less attention. Therefore, a simple and effective method for the purification of bovine heart LDH, based on biomimetic dye affinity chromatography, would be both interesting and useful.

2. Experimental

2.1. Materials

Reduced β-nicotinamide adenine dinucleotide (NADH) (disodium salt, ca. 100%), NAD^+ (free acid, ca. 98%), pyruvate monosodium salt and crystalline bovine serum albumin (fraction V) were obtained from Boehringer (Mannheim, Germany). DEAE-Sepharose CL6B, lipophilic Sephadex LH-20, 4-morpholinepropanesulfonic acid (MOPS) and CB3GA were obtained from Sigma. The cross-linked beaded agarose gel Ultrogel A6R was a much appreciated gift from BioSepra.

2.2. Synthesis of biomimetic dye ligands and dye adsorbents

Biomimetic dyes (Table 1, structures 1–3) were synthesized following the method of Labrou and Clonis [10]. Dye purification was performed on a lipophilic Sephadex LH-20 column according to published procedures [10,18]. Immobilization of dye ligands on cross-linked agarose (adsorbents were stored as moist gels in 20% methanol at 4°C) and determination of immobilized dye concentrations by the acid hydrolysis method were performed as described previously [16].

2.3. Assay of enzyme activity and protein

LDH assays were performed at 25°C according to a published method [19] using a Hitachi U-2000 double-beam UV–Vis spectrophotometer equipped with a thermostated cell holder (10 mm path length). One unit of enzyme activity is defined as the amount that catalyses the conversion of 1 μmol of pyruvate to L-lactate per minute. Protein concentration was determined by the method of Bradford [20], using bovine serum albumin (fraction V) as standard.

2.4. Sodium dodecyl sulphate polyacrylamide gel electrophoresis (SDS-PAGE)

SDS-PAGE was performed according to Laemmli [21] on a 1.5 mm thick vertical slab gel (14×16 cm), containing 12.5% (w/v) polyacrylamide (running gel) and 2.5% (w/v) stacking gel. The samples, after appropriate incubation, were applied to the wells and run at a current of 30 mA per gel for 4 h. Protein bands were stained with Coomassie Blue R-250.

2.5. Preparation of bovine heart extract

The tissue was kept at −20°C for up to 6 months. Frozen tissue was cut into small pieces

and frozen again at −20°C (15 g), before potassium phosphate buffer [30 ml, 50 m*M*, pH 7.0, containing 0.2% (v/v) β-mercaptoethanol (β-MeSH)] was added (4°C). The tissue was disintegrated in a blender (total 2 min, breaking every 15 s), centrifuged (14 000 *g*, 30 min) and the supernatant (ca. 30 ml) was dialysed overnight against 150 volumes of MOPS–NaOH buffer (20 m*M*, pH 7.0), containing 0.2% (v/v) β-MeSH. The dialysate was filtered through a cellulose membrane filter (Millipore, 0.45 μm pore size) and contained, typically, 13.5 units LDH/mg protein (yield 300 units LDH/g tissue).

2.6. Evaluation procedure for dye adsorbents for LDH binding from bovine heart extract. Effect of immobilized dye concentration on protein binding

All procedures were performed at 4°C. Lactate dehydrogenase binding was assessed using analytical columns each packed with 0.6 ml of dye adsorbent. Columns were equilibrated with 20 m*M* MOPS–NaOH buffer (pH 7.0), containing 0.2% (v/v) β-MeSH. Bovine heart extract (1360 μl, 204 units LDH, 15.1 mg protein) was loaded on the dye adsorbent and the flow was stopped for 15 min. The column was then washed with equilibration buffer (10 ml) before bound LDH was eluted with 5 ml of buffer containing either KCl (1 *M*) or NADH (5 m*M*). Fractions (5 ml) were collected and assayed for LDH activity and protein (Bradford method [20]).

2.7. Purification of LDH from bovine heart extract on mercaptopyruvic-VBAR-Ultrogel A6R biomimetic adsorbent and DEAE-Sepharose CL6B anion exchanger

All procedures were performed at 4°C.

Step 1: affinity chromatography on mercaptopyruvic-VBAR-Ultrogel A6R biomimetic adsorbent

Dialysed tissue extract (2370 μl, 26.3 mg protein, 356 units LDH) was applied to a column of mercaptopyruvic-VBAR-Ultrogel A6R (1 ml, 2.2 μmol dye/g moist gel; Table 1, structure 1), which was previously equilibrated with 20 m*M* MOPS–NaOH buffer (pH 7.0) containing 0.2% (v/v) β-MeSH. Non-adsorbed protein was washed off with 23 ml of equilibration buffer followed by 2 × 16.5 ml of buffer containing 10 and 20 m*M* KCl, respectively. Bound LDH was eluted with equilibration buffer (3 ml) containing 0.1 m*M* NAD^+ and 1 m*M* sulfite. Collected fractions were assayed for LDH activity and protein (A_{280}, except for effluents containing NAD^+, where the protein was determined by the Bradford method [20]).

Step 2: ion-exchange chromatography on DEAE-Sepharose CL6B

The eluted LDH activity from the previous column (3 ml, 228 LDH units, 0.68 mg protein) was directly applied to a DEAE-Sepharose CL6B ion-exchanger column (1.6 × 1.5 cm I.D.) which was previously equilibrated with 20 m*M* MOPS–NaOH buffer (pH 7.0) containing 0.2% (v/v) β-MeSH. Non-adsorbed protein was washed off with 12 ml of equilibration buffer followed by 3 × 8 ml of buffer containing 50, 75 and 100 m*M* KCl, respectively. Bound LDH was finally eluted with equilibration buffer containing 200 m*M* KCl (5 ml). Collected fractions were assayed for LDH activity and protein (A_{280}).

2.8. Course of adsorption of bovine heart protein and LDH on mercaptopyruvic-VBAR-Ultrogel A6R biomimetic adsorbent

All procedures were performed at 4°C. Frontal analysis experiments were performed as follows: dialysed bovine heart extract [13.5 units LDH/mg protein, 150 units LDH/ml, 11.1 mg protein/ml in 20 m*M* MOPS–NaOH buffer (pH 7.0) containing 0.2% (v/v) β-MeSH] was continuously applied (2.0 cm/min) to the mercaptopyruvic-VBAR-Ultrogel A6R column (0.6 ml adsorbent, 2.2 μmol dye/g moist gel), which was previously equilibrated with the above buffer. The extract was applied until the LDH activity in the effluents had reached a constant maximum value.

Collected fractions (1 ml) were assayed for LDH activity and protein (A_{280}).

3. Results and discussion

The concept of purpose-designed biomimetic dye ligands was first introduced to solve problems associated with the moderate selectivity of commercial dyes and their adsorbents during protein binding [9,13–16]. Introducing an appropriate structural moiety on the parent dye molecule may lead to a new purpose-designed dye which mimics natural ligands of the target protein [9–12]. Therefore, the corresponding biomimetic affinity adsorbent is expected to show increased purifying ability for the target macromolecule [9,13–16].

In this work the biomimetic dye concept was realized by designing three biomimetic dyes, analogues of the well known Cibacron Blue 3GA, bearing terminal α-keto acid functions (Table 1, structures 1–3). The terminal biomimetic structures were chosen to mimic the LDH substrate pyruvate (structure 1) and inhibitor oxamate (structure 2). Further, a biomimetic dye bearing an aromatic keto acid moiety (structure 3), along with non-biomimetic CB3GA and parent VBAR (structures 4 and 5, respectively) were evaluated. The 4-aminophenyloxanilic acid substituent (structure 3) was considered because of its keto acid function and hydrophobic aromatic ring. To this end, it is known that the LDH-inactivating potency of N-alkylmaleimides increases with increasing hydrophobicity and chain length of the maleimide [22]. Biomimetic moieties, analogues of lactic acid, were not considered since the substrate lactate shows a 22-fold higher K_m than pyruvate [17,23].

All adsorbents were substituted with dye ligand at the same level (2.0–2.2 μmol/g) and fell in the range used by most workers [16,24–30]. When comparing affinity adsorbents, synthesis-effected equal ligand substitution (not adjusted afterwards by appropriate dilution with unsubstituted gel) is an important but often overlooked prerequisite [31–33]. Wide variations in immobilized ligand concentration are undesirable because the interpretation of results regarding adsorbent behaviour can be unreliable.

In order to reveal the most effective dye adsorbent for purifying LDH, all dye adsorbents were evaluated for their purifying ability. Dialysed crude extract [204 LDH units, 15.1 mg protein, in 20 m*M* MOPS–NaOH (pH 7.0), containing 0.2% (v/v) β-MeSH] was loaded on each dye adsorbent. The column was washed with buffer before eluted with either KCl (1 *M*) or NADH (5 m*M*). Salt elution leads to protein desorption, and therefore the technique reveals the adsorbent selectivity during adsorption [14,15,27,34,35]. On the other hand, elution with substrate/cofactor provides information on the ability of the bound enzyme to desorb biospecifically, leaving unwanted proteins on the column [14,15,27,28,30,35,36]. Table 1 shows the purifying ability of dyed adsorbents during adsorption (KCl) and biospecific elution (NADH) of LDH activity, and also their capacity (units LDH/μmol immobilized dye). All three biomimetic-dyes (adsorbents BM 1–3) exhibited higher purifying ability and capacity than non-biomimetic structures (adsorbents 4 and 5), Further, the biomimetic dye bearing a terminal mercaptopyruvate linked to the triazine ring (adsorbent BM 1), exhibited the highest purifying ability (tenfold) and capacity (144 units/μmol dye), followed closely by the aromatic keto acid-substituted analogue (adsorbent BM 3; 9.1-fold and 136 units/μmol dye, respectively). On the basis of the above observations, adsorbent BM 1 was studied further and was eventually integrated in the purification protocol for LDH.

Prior to designing the purification protocol, we investigated the following factors: concentration of immobilized dye, pH and elution conditions. High concentrations of immobilized affinity ligand may lead to no binding, owing to steric effects caused by the ligand molecules, or even to non-specific binding [24]. The concentration employed here fell within the range used commonly [16,24–30] and near to its low end. Table 2 summarizes the results obtained when studying the effect of dye concentration on the purifying ability and capacity of the BM 1 adsorbent. A concentration of 2.2 μmol/g was found to be the

Table 1
Evaluation of dye adsorbents for binding LDH from bovine heart extract

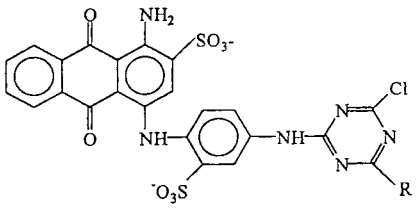

No.	Immobilized dye (-R)	Capacity (u/μmol dye)	SA[a] (u/mg)		Purification (-fold)		Recovery[b] (%)	
			KCl	NADH	KCl	NADH	KCl	NADH
1	$-SCH_2COCOO^-$	144	73	135	5.4	10	96	95
2	$-HN(CH_2)_2NHCOCOO^-$	130	65	107	4.8	7.9	99	90
3	$-p$-HNBenzNHCOCOO$^-$	136	69	123	5.1	9.1	95	94
4	$-o$-HNBenzSO_3^- (CB3GA)	122	62	103	4.6	7.6	95	90
5	–Cl (VBAR)	125	55	87	4.1	6.4	93	90

Dialysed extract [204 units LDH, 15.1 mg protein, 20 m*M* MOPS–NaOH buffer, pH 7.0, containing 0.2% (v/v) β-MeSH] was applied on each dye adsorbent (0.6 ml). The adsorbent was washed with equilibration buffer (10 ml) prior to eluting bound proteins with 5ml of 1 *M* KCl or 5 m*M* NADH.
[a] Specific activity.
[b] Calculated on the basis of bound LDH units (100%).

optimum, since it ensured the highest purification (5.4-fold) along with a good capacity (144 units/μmol). The observed pattern of increasing capacity with decreasing ligand substitution (Table 2) has been reported before [30] and is probably due to the fact that as the concentration of immobilized ligand decreases, a larger proportion of immobilized dye molecules becomes available for protein binding (i.e., a smaller fraction of dye molecules is sterically hindered by bound proteins) [24].

Table 3 summarizes the effect of pH (during adsorption) and elution conditions on LDH chromatography. At neutral to slightly acidic pH, BM 1 displayed the same purifying ability (tenfold) and similar capacity (144 and 153 units/μmol, respectively), whereas a dramatic fall was observed under alkaline conditions [Table 3(a)]. This behaviour is in agreement with previous findings that acidic conditions facilitate protein binding to dye adsorbents [14–16,29,37,38]. Between the two acceptable pH values of 6.0 and

Table 2
Effect of concentration of immobilized dye on the chromatography of bovine heart LDH on mercaptopyruvate-VBAR-Ultrogel A6R

[Dye] (μmol/g)	Capacity (u/μmol dye)	SA (u/mg)	Purification (-fold)	Recovery (%)
0.8	214	65	4.8	96
2.2	144	73	5.4	96
2.9	93	62	4.6	88

Dialysed extract [204 units LDH, 15.1 mg protein, 20 m*M* MOPS–NaOH buffer, pH 7, containing 0.2% (v/v) β-MeSH] was applied on each adsorbent (0.6 ml). The absorbent was washed with equilibration buffer (10 ml) prior to eluting bound LDH with 1 *M* KCl (5 ml).

Table 3
Effect of pH and elution medium on the chromatography of bovine heart LDH on mercaptopyruvate-VBAR-Ultrogel A6R

Method	Capacity (u/μmol dye)	Washed LDH[a] (%)	SA (u/mg)	Purification (-fold)	Recovery[a] (%)
(a) Adsorption at					
pH 6.0	153	–	140	10.4	85
pH 7.0	144	–	135	10.0	95
pH 8.5	13.6	–	59	4.3	100
(b) Elution sequentially with (pH 7.0)					
10 *mM* KCl	–	5.7	205	15.2	
and 20 m*M* KCl	–	16.7	342	25.3	
and 40 m*M* KCl	–	41.7	305	22.6	95

(a) Effect of pH on protein adsorption: dialyzed extract (220 units LDH, 16.3 mg protein) was applied on the affinity adsorbent (0.6 ml), which was previously equilibrated in 20 m*M* MOPS–NaOH buffer, pH 6 or 7, or 20 m*M* Tris–HCl, pH 8.5, containing 0.2% (v/v) β-MeSH (4°C). After the adsorbent had been washed with equilibration buffer (10 ml), bound LDH was eluted with 5 m*M* NADH (5 ml). (b) Effect of ionic strength (KCl) on the elution and purification of LDH: dialysed extract (220 units LDH, 16.3 mg protein) was applied on the affinity adsorbent (0.6 ml), which was previously equilibrated in 20 m*M* MOPS–NaOH buffer, pH 7, containing 0.2% (v/v) β-MeSH (4°C). Unbound proteins were washed off with equilibration buffer (15 ml) and the adsorbent was washed with 10 ml each of the media shown, prior to eluting LDH with 5 m*M* NADH (5 ml).
[a]Calculated on the basis of bound and non-washed LDH units (100%).

7.0, we finally chose pH 7.0 because at acidic pH the contaminating pyruvate kinase activity starts binding the dye column [29,30].

The conditions adopted for LDH elution from the BM 1 adsorbent were of particular importance. Prior to eluting LDH biospecifically with NADH, the column was washed with steps of increasing salt concentration (10–40 m*M* KCl) to remove unwanted bound proteins. During salt washing, increasing amounts of LDH were co-eluted, and the specific activity of the final product exhibited a maximum value [Table 3(b)]. Step washing with 10 m*M* KCl followed by 20 m*M* KCl was adopted as the optimum conditions, since it led to the highest purification (342 u/mg, after NADH elution) and a moderate loss of LDH in the washings. Although NADH was used as biospecific eluent (5 m*M*) during preliminary experiments for adsorbent evaluation (Tables 1 and 3), in the final purification protocol elution with a much more economical agent, NAD^+ (0.1 m*M*) and sulphite (1.0 m*M*), was preferred and it led to the same purification and recovery as with NADH.

Based on the above results, we designed a simple two-step purification protocol for bovine heart LDH. Non-pretreated dialysed tissue extract was applied directly on a BM 1 adsorbent (2.2 μmol/g). Unbound proteins were removed with equilibration buffer (20 m*M* MOPS–NaOH, pH 7.0), the column was washed with 10 and 20 m*M* KCl, prior to LDH activity being eluted with three-column volumes of 0.1 m*M* NAD^+ and 1 m*M* sulphite (Fig. 1). The eluted enzyme activity was then directly applied to a DEAE-Sepharose CL6B anion-exchange column. The column was washed with irrigating buffer followed by a low KCl concentration to remove some proteins, prior to the bound LDH activity being desorbed with 0.2 *M* potassium chloride.

The results obtained from a typical purification run are summarized in Table 4. We attempted to improve the purity of the final product by introducing inexpensive techniques used routinely by enzyme manufacturers (e.g., ammonium sulfate fractionation and anion-exchange chromatography) prior to affinity chromatography. Pretreatment of the starting tissue extract with 30–65% (w/v) $(NH_4)_2SO_4$ led to 2.5-fold step

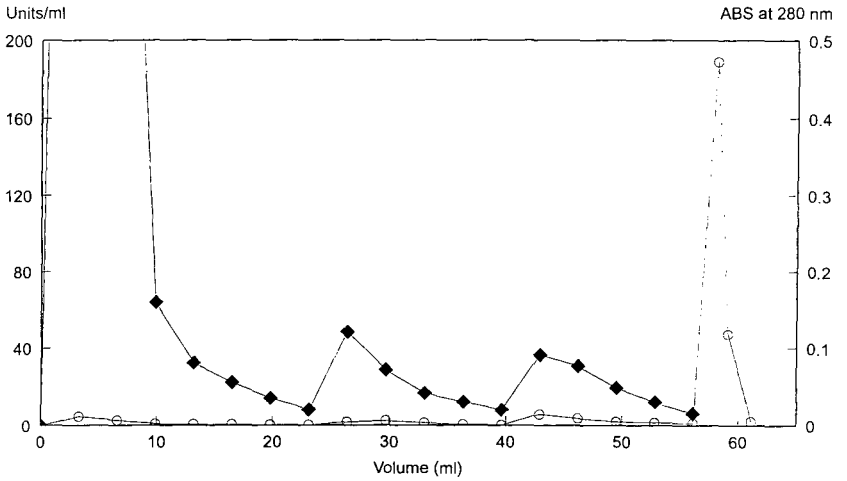

Fig. 1. Affinity chromatography of bovine heart extract on mercaptopyruvic-VBAR-Ultrogel A6R biomimetic adsorbent and the purification of LDH. Procedures were performed at 4°C. Dialysed cell-free extract (2370 μl, 26.3 mg protein, 356 units LDH) was applied at the biomimetic adsorbent (1 ml). Non-adsorbed protein was washed off with 23 ml of buffer followed by 2 × 16.5 ml of buffer containing 10 and 20 m*M* KCl. Bound LDH was eluted with equilibration buffer containing 0.1 m*M* NAD^+ and 1 m*M* sulfite (3 ml). Collected fractions were assayed for LDH (○) and protein (◆, A_{280} except for the fraction with NAD^+).

purification and 75% step recovery. However, when the pretreated extract was subsequently chromatographed on the BM 1 affinity adsorbent, the step purification on the affinity column remained unchanged (25-fold). Pretreatment of the starting extract by means of DEAE-cellulose anion-exchange chromatography (20 m*M* Tris–HCl, pH 7.4; desorption of bound LDH with 0.2 *M* KCl) led to 2.9-fold step purification and 71% step recovery. However, after the pretreated extract was chromatographed on a BM 1 adsorbent, the capacity of the affinity adsorbent was increased by 40% but the step purification remained approximately the same (≤26-fold). Therefore, since the purity of the final product could not be improved further, there was no need to perform any changes to the original protocol. Further, in order to demonstrate the superiority of biomimetic adsorbent BM 1 over the commercial dye, CB3GA bovine heart LDH was purified on immobilized CB3GA under the same conditions as for BM 1 (see legend to Fig. 1

Table 4
Summary of LDH purification from bovine heart extract

Step	Volume (ml)	Units (u)	Protein (mg)	SA (u/mg)	Purification (-fold)	Yield (%)
Crude extract	2.37	356	26.3	13.5	1	–
Step 1: Biomimetic dye chromatography (NAD^+–sulfite elution)	3.0	228	0.68	335	24.8	64
Step 2: Anion-exchange chromatography (KCl elution)	5.0	178	0.37	481	35.6	50

Procedures were performed at 4°C. The affinity adsorbent (1 ml) consisted of the ligand biomimetic mercaptopyruvate-VBAR immobilized on Ultrogel A6R (2.2 μmol dye/g moist gel). The agarose gel DEAE-Sepharose CL6B (1.6 × 1.5 cm I.D.) was employed as an anion exchanger. For experimental conditions, see text.

and Experimental). In this case both the specific activity and recovery of LDH were lower by 30% and 10%, respectively. Although such differences in adsorbent performance may numerically be regarded as undramatic, in practice, however, when the product purity approaches homogeneity, the above differences may prove to be significant and could mean an additional, third, step in the protocol had the biomimetic adsorbent not been used.

Upon protein chromatography with biomimetic adsorbent BM 1, we observed protein–protein competition phenomena, as became evident by frontal analysis experiments (Fig. 2). In an early phase (up to 4 ml of eluate), both total protein and LDH bound the adsorbent, although the former saturated the column faster. In the subsequent phase (4–8 ml of eluate), whereas adsorption of the total protein was accomplished, LDH kept binding the column. This observation indicates that protein–protein displacing phenomena operate during the binding process. Such phenomena have been observed before with dye ligand adsorbents [13,14,16,29].

The specific activity of our affinity-purified LDH, 335 u/mg (25°C) (step 1, Table 4), is substantially higher than for the respective commercial product suitable for analytical purposes (ca. 250 u/mg). However, in order to free LDH from remaining contaminating activity of malate dehydrogenase (MDH), it was necessary to add a second step to the purification protocol (step 2, Table 4), that of anion-exchange chromatography. Such a step does not affect significantly the speed and cost effectiveness of the total procedure, because the sample requires no dialysis prior to loading the adsorbent, and hence the LDH fraction obtained from the affinity adsorbent is applied directly to the anion exchanger. It is known that MDH, a nicotinamide nucleotide-dependent oxidoreductase, recognizes and binds anthraquinone dye ligands [6,39,40]. Further, the enzyme (mixture of mitochondrial and cytoplasmic activities) is present in

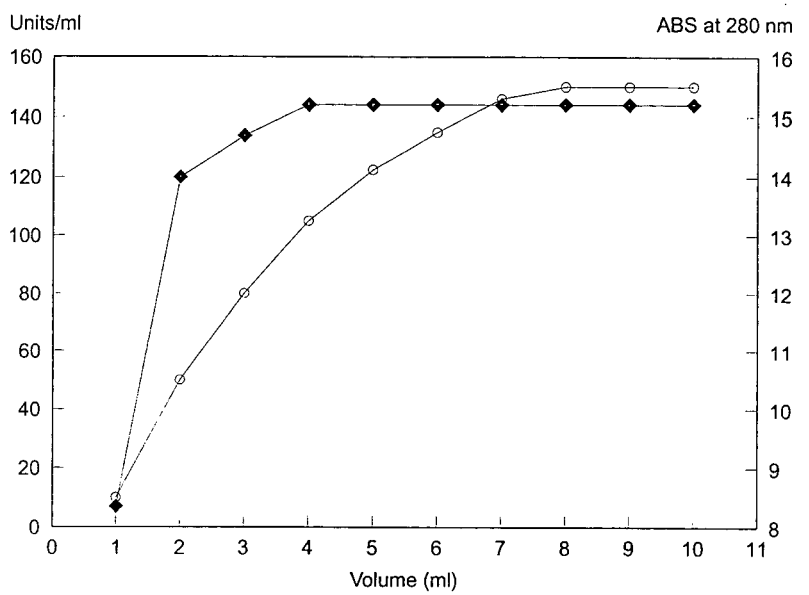

Fig. 2. Course of adsorption of bovine heart protein and LDH on mercaptopyruvic-VBAR-Ultrogel A6R biomimetic adsorbent. Procedures were performed at 4°C. A crude bovine heart extract [150 u LDH/ml, 11.1 mg protein/ml, in MOPS–NaOH buffer, 20 m*M*, pH 7.0, containing 0.2% (v/v) β-MeSH] was applied continuously to the biomimetic adsorbent (0.6 ml, 2.2 μmol/g wet gel) which was previously equilibrated in the same buffer. The application was stopped when the effluents had reached a constant activity of LDH. Collected fractions were assayed for LDH (○) and protein (◆, A_{280}).

the heart tissue at 420–350% over that of LDH activity (assayed in our laboratory). We found that it was impossible to separate completely the LDH and MDH activities on the affinity adsorbent BM 1. Applying the affinity-purified fraction with LDH activity on the anion exchanger, the contaminating mitochondrial MDH passed through, whereas cytoplasmic MDH bound the adsorbent and was removed with 100 m*M* KCl, prior to adsorbed LDH being eluted with 200 m*M* KCl.

Quality-control tests on L-lactate dehydrogenase purified by the above two-step procedure showed a specific activity 490 u/mg (25°C) and the following contaminating activities: MDH, 0.01%; pyruvate kinase and glutamic–oxaloacetic transaminase, not detectable. The purified enzyme showed one major band on SDS-PAGE (Fig. 3). The specific activity and contaminating activities of commercial bovine heart LDH, suitable for analytical purposes, have been quoted as follows: 250 u/mg (25°C); MDH, less than 0.05%; and pyruvate kinase, less than 0.01%. Further, our procedure compares favourably with that employing the triazine dye Procion Scarlet MX-G immobilized on a cellulose support via a diaminohexyl spacer [41,42]. The latter approach led to enzyme of specific activity 200 u/mg [41]. Consequently, the present method provides a simple and effective way for preparing, in two steps and with a good yield, L-lactate dehydrogenase suitable for analytical purposes.

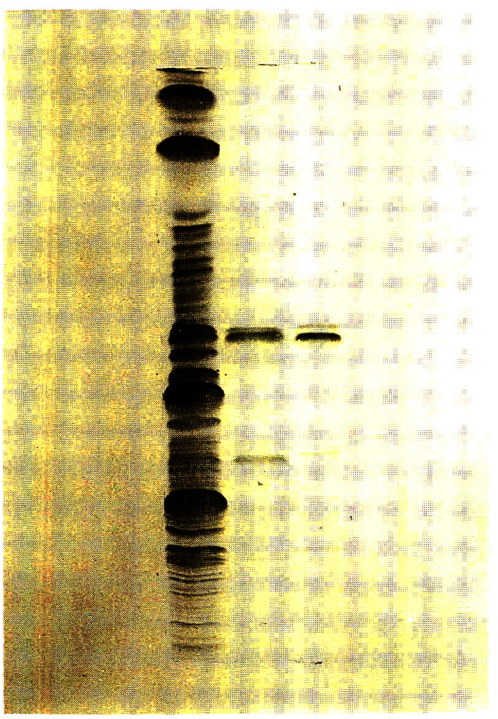

Fig. 3. SDS-PAGE of LDH. SDS-PAGE was performed on a 1.5 mm thick vertical slab gel (14 × 16 cm) containing 12.5% (w/v) polyacrylamide (running gel) and 2.5% (w/v) stacking gel. The protein bands were stained with Coomassie Bue R-250. Left lane, bovine heart extract; middle lane, LDH purified from the biomimetic dye affinity column (after step 1, Table 4); right lane, LDH purified from the anion-exchange column (after steps 1 and 2, Table 4).

Acknowledgements

The authors thank the Hellenic General Secretariat for Research and Technology for the financial assistance provided. This work was performed within the framework of the EUREKA EU-384 research contract. Biomimetic dyes, their immobilized forms and enzyme purification methods based on these materials are the property of the partners as specified in the above contract. Commercial exploitation of these materials and methods is prohibited without the written consent of the partners.

References

[1] P. Cuatrecasas and C.B. Anfinsen, Methods Enzymol., 22 (1971) 345.
[2] C.R. Lowe, in T.S. Work and E. Work (Editors), Laboratory Techniques in Biochemistry and Molecular Biology, Vol. 7(II), Elsevier, Amsterdam, 1979, p. 269.
[3] Y.D. Clonis, Biotechnology, 5 (1987) 1290.
[4] Y.D. Clonis, in J. Asenjo (Editor), Separation Processes in Biotechnology, Marcel Dekker, New York, 1990, p. 401.
[5] N.E. Labrou and Y.D. Clonis, J. Biotechnol., 36 (1994) 95.

[6] M.D. Scawen and A. Atkinson, in Y.D. Clonis, A. Atkinson, C. Bruton and C.R. Lowe (Editors), Triazine Dyes in Protein and Enzyme Technology, Macmillan, Basingstoke, 1994, p. 51.
[7] Y.D. Clonis, CRC Crit. Rev. Biotechnol., 7 (1988) 263.
[8] Y.D. Clonis, in M.T.W. Hearn (Editor), HPLC of Protein, Peptides and Polynucleotides, VCH, New York, 1991, p. 453.
[9] C.R. Lowe, S.J. Burton, J. Pearson, Y.D. Clonis and C.V. Stead, J. Chromatogr., 376 (1986) 121.
[10] N.E. Labrou and Y.D. Clonis, Arch. Biochem. Biophys., 316 (1995) 169.
[11] N.E. Labrou and Y.D. Clonis, J. Biotechnol., 40 (1995) 59.
[12] N.E. Labrou and Y.D. Clonis, Arch. Biochem. Biophys., 321 (1995) 61.
[13] Y.D. Clonis, C.V. Stead and C.R. Lowe, Biotechnol. Bioeng., 30 (1987) 621.
[14] N. Lindner, R. Jeffcoat and C.R. Lowe, J. Chromatogr., 473 (1989) 227.
[15] Y.D. Clonis and C.R. Lowe, J. Chromatogr., 540 (1991) 103.
[16] N.E. Labrou, A. Karagouni and Y.D. Clonis, Biotechnol. Bioeng., 48 (1995) in press.
[17] J. Keesey, Biochemica Information, Boehringer Mannheim, Indianapolis, IN, 1987, p. 46.
[18] J. Pearson, S.J. Burton and C.R. Lowe, Anal. Biochem., 158 (1986) 382.
[19] Boehringer Mannheim, Biochemica Information, Vol. I, 1975, pp. 124–125.
[20] M. Bradford, Anal. Biochem., 72 (1976) 248.
[21] U.K. Laemmli, Nature, 227 (1970) 680.
[22] B.M. Anderson, S.V. Vercellotti and T.L. Fisher, Biochim. Biophys. Acta, 350 (1974) 135.
[23] A.D. Winer and G.W. Schwert, J. Biol. Chem., 231 (1958) 1065.
[24] M.D. Scawen, J. Darbyshire, M.J. Harvey and T. Atkinson, Biochem. J., 203 (1982) 699.
[25] A. Ashton and G. Polya, Biochem. J., 175 (1978) 501.
[26] R. Beissner and F. Rudolph, Arch. Biochem. Biophys., 189 (1979) 76.
[27] Y.D. Clonis and C.R. Lowe, Biochim. Biophys. Acta, 659 (1981) 86.
[28] S.J. Burton, C.V. Stead and C.R. Lowe, J. Chromatogr., 455 (1988) 201.
[29] T. Makriyannis and Y.D. Clonis, Process Biochem., 28 (1993) 179.
[30] L.A. Huff and E. Easterday, in P.V. Sundaram and F. Eckstein (Editors), Theory and Practice in Affinity Techniques, Academic Press, New York, 1978, p. 23.
[31] C.R. Lowe, M.J. Harvey, D.B. Craven and P.D.G. Dean, Eur. J. Biochem., 133 (1973) 499.
[32] M.J. Harvey, C.R. Lowe, D.B. Craven and P.D.G. Dean, Eur. J. Biochem., 41 (1974) 335.
[33] Y.D. Clonis, J. Chromatogr., 407 (1987) 179.
[34] C.R. Lowe, M. Hans, N. Spibey and W.T. Drabble, Anal. Biochem., 104 (1980) 23.
[35] R.K. Scopes, V. Testolin, A. Stoter, K. Griffiths-Smith and E.M. Algar, Biochem. J., 228 (1985) 627.
[36] C.J. Burton and T. Atkinson, Nucleic Acids Res., 7 (1979) 1579.
[37] R.K. Scopes, J. Chromatogr., 376 (1986) 131.
[38] S.J. Burton, in A. Kenney and S. Fowell (Editors), Practical Protein Chromatography, Humana Press, Totowa, 1992, Ch. 7, p. 91.
[39] C.S. Ramadoss, J. Steczko, J.W. Uhlig and B. Axelrod, Anal. Biochem., 130 (1983) 481.
[40] P. Konecny, M. Smrz and S. Slovakova, J. Chromatogr., 398 (1987) 387.
[41] M. Naumann, R. Reuter, P. Metz and J. Kopperschläger, J. Chromatogr., 466 (1989) 319.
[42] R. Reuter, M. Naumann and G. Kopperschläger, J. Chromatogr., 510 (1990) 189.

ELSEVIER

Journal of Chromatography A, 718 (1995) 45–51

JOURNAL OF CHROMATOGRAPHY A

High-performance liquid chromatographic separation and detection of phenols using 2-(9-anthrylethyl) chloroformate as a fluorophoric derivatizing reagent

Walter J. Landzettel[a], Kelly J. Hargis[a], Jason B. Caboot[a], Kent L. Adkins[a], Timothy G. Strein[a], Hans Veening[a,*], Hans-Dieter Becker[b]

[a]*Department of Chemistry, Bucknell University, Lewisburg, PA 17837, USA*

[b]*Department of Organic Chemistry, Chalmers University of Technology and University of Gothenburg, S-412 96 Gothenburg, Sweden*

First received 20 December 1994; revised manuscript received 11 May 1995; accepted 12 June 1995

Abstract

This paper describes the use of 2-(9-anthrylethyl) chloroformate (AEOC) as a sensitive and convenient pre-column, fluorophoric derivatizing reagent for the separation and detection of phenol (P), *p*-methylphenol (PMP), 3,4-dimethylphenol (DMP), and 4-*tert.*-butylphenol (BP) using reversed-phase high-performance liquid chromatography (HPLC) with fluorescence detection. Experiments were carried out to determine maximum fluorescence excitation and emission wavelengths, optimum derivatization pH, efficient gradient programming, calibration curves, minimum detection limits, and stabilities for AEOC-derivatized phenols. The method was applied to several industrial waste water samples from Central Pennsylvania. The minimum detection limits for injected phenol samples ranged from 7 to 10 n*M*, or 9, 10, 12 and 11 pg for P, PMP, DMP and BP, respectively. This corresponded to concentrations of phenols in the original waste water samples of 56 to 80 n*M*.

1. Introduction

Analytical procedures for phenols are used in a wide range of applications. Phenols may occur in domestic and industrial waste waters, natural waters, and municipal water supplies [1]. Phenols are also used as starting material for several food preservatives (butylated hydroxytoluene and hydroxyanisole), herbicides, antiseptics (hexachlorophene), explosives, and polymers [2]. Phenols, such as vinylphenol, vinylguaiacol, ethylphenol, and ethylguaiacol, are important components in wines [3]. Phenol and *p*-cresol have also been found to be present in uremic serum samples collected from patients suffering from renal dysfunction [4]. Previous high-performance liquid chromatography (HPLC) detection methods for phenols have included UV absorption and photodiode-array techniques [5], fluorescence [4] and electrochemical methods [6,7]. Li and Kemp [8] developed a reductive, amperometric HPLC method to determine phenols between concentrations of 10^{-7} and 10^{-4} *M* in aqueous samples using pre-column derivatization with 4-aminoantipyrine. While the method is selective for phenols, it also requires

* Corresponding author.

0021-9673/95/$09.50
SSDI 0021-9673(95)00663-X

an extraction step during derivatization. Imai et al. [9] reported a pre-column derivatizing reagent, 4-(N-chloroformylmethyl-N-methyl)-amino-7-N,N-dimethylaminosulfonyl-2,1,3-benzoxadiazole, to determine phenols, alcohols, amines, and thiols in the fmol range. The derivatization step did require a catalyst. Zheng et al. [10] have described an HPLC method to detect 80 to 160 fmol of phenols by pre-column derivatization with 4-(2-phthalimidyl)benzoyl chloride and fluorescence detection. A pre-column HPLC derivatization procedure for phenols with dansyl chloride and imidazole (catalyst) leading to chemiluminescence detection was reported by Fu [11]. The detection limits were 1.2 to 2.2 pg for phenol and several alkyl phenols.

Fluorophoric chloroformates, such as 9-fluorenylmethyl chloroformate (FMOC), 2-(9-anthryl)ethyl chloroformate (AEOC), and 2-(1-pyrenylethyl) chloroformate (PEOC) have been used successfully as pre-column derivatizing agents in HPLC for the determination of analytes containing primary amine groups. The chloroformate functionality reacts with primary and secondary amines to form fluorescent carbamates. This reaction has been utilized successfully in pre-column HPLC derivatization procedures for the determination and detection of amino acids [12–14] and polyamines [15]. Recently, we reported AEOC and PEOC to be effective fluorophoric, pre-column HPLC reagents for the determination of biogenic polyamines [16,17]. We now report the use of AEOC as an HPLC pre-column derivatizing reagent for phenol (P), *p*-methylphenol (PMP), 3,4-dimethyl-phenol (DMP), and 4-*tert.*-butylphenol (BP). AEOC, like other chloroformates, reacts with phenols to form fluorescent, aromatic carbonates. Excess AEOC undergoes hydrolysis in aqueous media to form 2-(9-anthryl)ethanol (AEOH) which may react further with AEOC to give bis(2-(9-anthryl)ethyl) carbonate (BAEC), as shown in Fig. 1, reactions 1–3. The method reported here utilizes a newly synthesized fluorophoric chloroformate (AEOC), which we previously used successfully for pre-column derivatization of polyamines determined by HPLC [16]. In this investigation we have demonstrated the utility of AEOC, a as a versatile, fluorophoric, pre-column HPLC derivatizing reagent for determining traces of phenols contained in environmentally significant samples, such as industrial waste water.

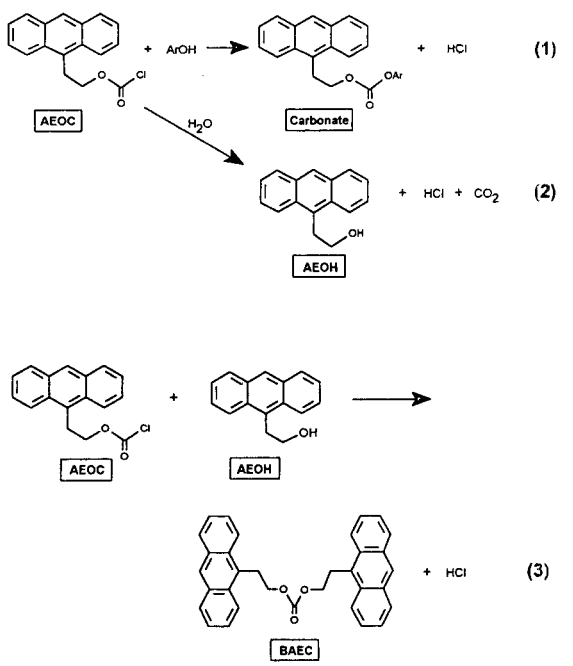

Fig. 1. Reaction of AEOC with phenols to form fluorescent carbonates (reaction 1) and hydrolysis of AEOC in aqueous media to form AEOH (reaction 2), which may react with AEOC to give BAEC (reaction 3).

2. Experimental

2.1. Apparatus

The chromatographic system was a Spectra-Physics SP-8800 ternary solvent delivery system (Spectra-Physics, San Jose, CA, USA) equipped with a Model 7010 Rheodyne injection valve and a 10-μl sample loop. Fluorescence detection was achieved with a Model 750 BX McPherson instrument (McPherson, Acton, MA, USA). An excitation wavelength of 256 nm (5 nm bandwidth) and a 418-nm low-end cutoff emission filter were used. The sensitivity range was set at 0.003 μA with a time constant of 0.5 s and low

suppression background. Fluorescence spectra were obtained using a Perkin-Elmer LS-50 Luminescence Spectrometer (Perkin Elmer, Oak Brook, IL, USA). A Hewlett-Packard 3396A integrator (Hewlett-Packard, Wilmington, DE, USA) was used for peak integration and for recording all chromatograms.

The analytical LC column was a Hewlett-Packard LiChrospher 100 RP-18, 125 × 4.0 mm I.D., packed with 5-μm particles. Separations were carried out at a flow-rate of 0.75 ml/min using a binary gradient of 70% acetonitrile, 30% deionized water (pH 6.1) programmed to 100% acetonitrile in 10 min and an isocratic post-time of 10 min. The column inlet pressure was 480 p.s.i. (3309.48 kPa). The column temperature was ambient.

2.2. Chemicals and reagents

Phenol (P), *p*-methylphenol (PMP), 3,4-dimethylphenol (DMP), and 4-*tert.*-butylphenol (BP) were obtained from Aldrich Chemical (Milwaukee, WI, USA) and were used without further purification. HPLC-grade acetonitrile was obtained from Fisher Scientific (Fair Lawn, NJ, USA). HPLC-grade water was generated in-house using a water purification system manufactured by Industrial Water Technology (No. Attleboro, MA, USA). Reagent-grade hydrochloric acid, sodium hydroxide, and sodium borate were used to prepare buffer solutions and were obtained from Fisher Scientific. AEOC was synthesized as previously described [18–20]. Since AEOC solutions have been found to undergo reactions upon exposure to laboratory light [18–20], reagent stock solutions were kept in light-protected containers and stored under refrigeration when not in use.

2.3. Derivatization procedure

Derivatization of phenol standards was accomplished by adding 500 μl of 2.59 μM AEOC in HPLC-grade acetonitrile to 100 μl of a standard mixture containing P, PMP, DMP, and BP and 200 μl of pH 9.6 aqueous borate buffer (0.025 M). The derivatization solution was allowed to stand for 35 min at 43°C to permit completion of the reaction, and a 10-μl sample was then injected. Industrial waste water samples were obtained from Wilson Testing Laboratories (Shamokin, PA, USA) and were filtered through a 0.2-μm filter to remove particulate matter. The water sample (100 μl) was then derivatized for 35 min at 43°C after adding 500 μl of 2.59 μM AEOC (in acetonitrile) and 200 μl of pH 9.6 borate buffer.

3. Results and discussion

The fluorescence excitation and emission spectra for five collected fractions of AEOC-derivatized phenol in acetonitrile (1.0 μg of phenol with excess AEOC injected) are shown in Fig. 2. The emission spectrum was scanned at $\lambda_{exc} = 256$ nm and the excitation spectrum at $\lambda_{em} = 389$ nm. Prominent excitation and emission maxima were observed at 256, 389, 412, and 436 nm, respectively. Very weak excitation bands were observed

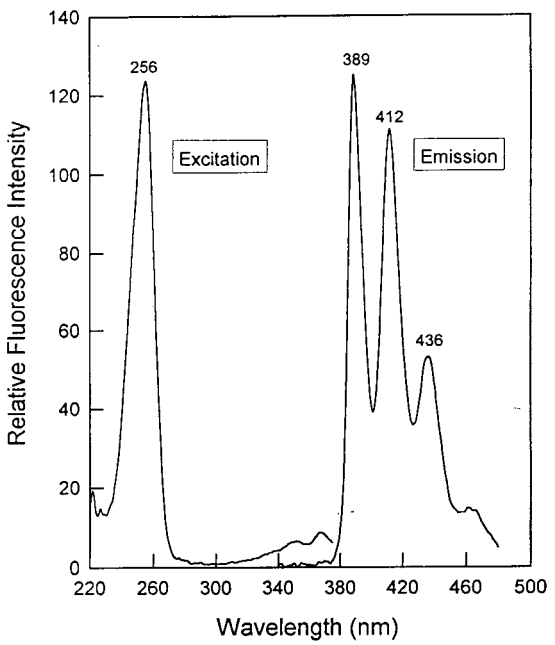

Fig. 2. Fluorescence excitation and emission spectra of eluted AEOC-derivatized phenol in CH_3CN (1.0 μg of phenol with excess AEOC injected).

at 352 and 367 nm, as shown in Fig. 2. (Scanning the excitation spectrum at $\lambda_{em} = 412$ nm yielded the same excitation spectrum.) The spectra obtained were very similar to those of other derivatized phenols and to the spectra reported previously for AEOC-, AEOH-, and AEOC-derivatized polyamines [16]. Based on the spectral data, HPLC detection of AEOC-derivatized phenols was optimized by using an excitation wavelength of 256 nm and a 418-nm low-cutoff emission filter. Use of a 390-nm low-end cutoff filter was investigated and found to be much less sensitive than the 418-nm filter.

Complete derivatization of phenols with AEOC was found to require 35 min at 43°C. The reaction of AEOC with phenols was found to be pH dependent. The optimum reaction pH was determined by derivatizing each of the four phenols at pH values ranging from 7.50 to 10.00 and measuring the fluorescence response ($\lambda_{exc} = 256$ nm; $\lambda_{em} > 418$ nm) for each eluted analyte as a function of pH. The results, shown in Fig. 3, indicate three maxima, at ca. pH 8.4, 8.9 and 9.6. It is clear that the pH dependence of the derivatization reaction is not straightforward; however, these results permitted the selection of an optimum derivatization pH of 9.60.

A chromatogram for the separation of a standard mixture of the four AEOC-derivatized phenols (P, PMP, DMP, and BP) is shown in Fig. 4. The identity of the BP peak at 12.32 min was confirmed by comparison of its retention time to that of an authentic sample of AEOC-derivatized 4-*tert.*-butylphenol, synthesized independently. The identity of the by-product peaks, AEOH and BAEC, was confirmed similarly. The reaction of AEOC with AEOH to form the carbonate (BAEC) is illustrated in Fig. 1, reac-

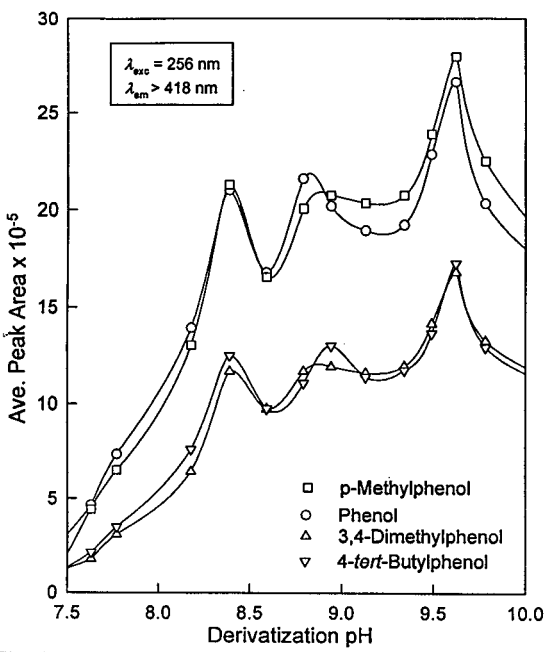

Fig. 3. Detector response versus derivatization pH for eluted AEOC–phenol derivatives.

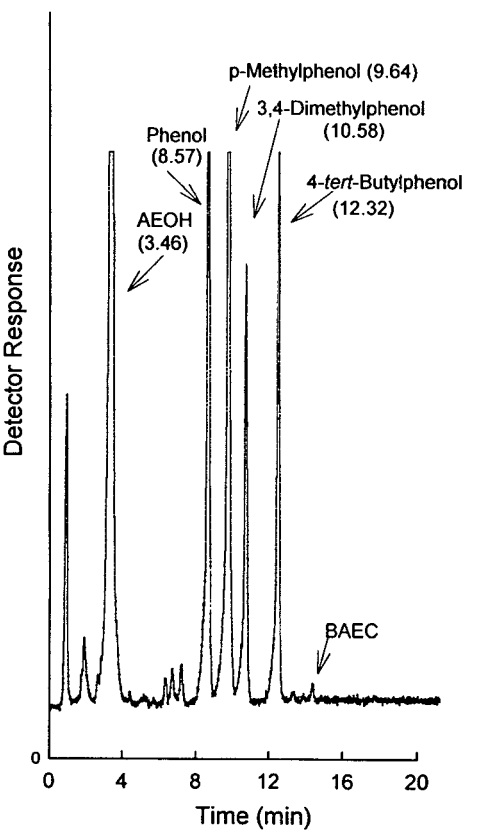

Fig. 4. Chromatogram for AEOC-derivatized phenol standards (0.2 ng of each phenol injected). Flow-rate: 1.0 ml/min, temperature: ambient, column: LiChrospher 100 RP-18, 100 × 10 mm, mobile phase: 70% CH_3CN–30% deionized H_2O (pH 6.1) to 100% CH_3CN in 10 min, isocratic post-time: 10 min, detection: fluorescence, $\lambda_{exc} = 256$ nm, $\lambda_{em} > 418$ nm.

tion 3. Neither of these by-products interfered in the separation; in fact, BAEC was found to be a useful relative retention time internal standard. Although, the retention times varied slightly from run to run, the retention times relative to BAEC were consistent. Under the gradient conditions used, the four derivatized phenols were completely resolved from each other and from reaction by-products.

A plot of corrected peak area versus nanograms of phenol injected is shown in Fig. 5. Data points were obtained by individually derivatizing solutions containing successively lower concentrations of each of the phenols prior to chromatography. The original plots exhibited significant curvature due to non-linear detector behavior at low concentrations. The data were re-plotted according to the method of Dorschel et al. [21] in order to show the actual response more clearly. In order to confirm completeness of derivatization, a second experiment was performed in which the calibration curve was determined by injecting increasingly smaller concentrations of already derivatized solutions of the phenols. The calibration curve obtained was identical to that shown in Fig. 5.

The limits of detection for this procedure were determined for each of the four phenols. This was accomplished by setting the detector sensitivity at the maximum range of 0.003 μA and individually derivatizing successively diminishing quantities of each of the diluted phenols prior to injection. Each detection limit was obtained by recording the smallest amount of phenol that still produced a peak at a signal-to-noise ratio of 3:1. The minimum detection limits for injected phenol samples ranged from 7 to 10 n*M*, or 9, 10, 12, and 11 pg for P, PMP, DMP, and BP, respectively. This corresponded to concentrations of phenols in the original waste water samples of 56 to 80 n*M*. A chromatogram illustrating the separation of a mixture of ca. 0.01 ng of each derivatized phenol injected (i.e., approximately the detection limit) is shown in Fig. 6.

In order to examine the stability of the AEOC–phenol derivatives, derivatized phenol solutions were allowed to stand at room tem-

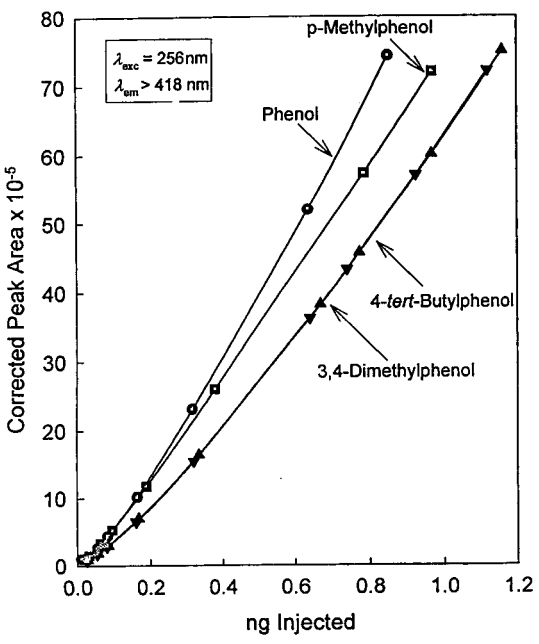

Fig. 5. Corrected peak area versus ng of analyte injected. (Experimental data replotted according to Ref. [21].)

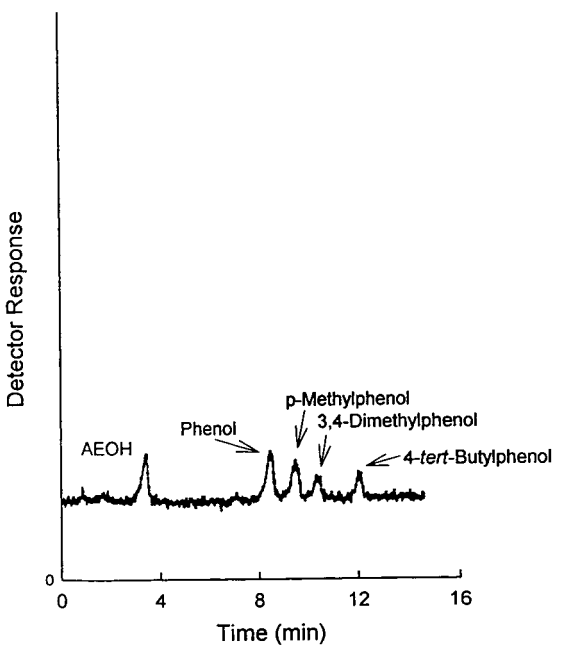

Fig. 6. Detection limits for AEOC-derivatized phenols (ca. 0.01 ng injected). Conditions the same as in Fig. 4.

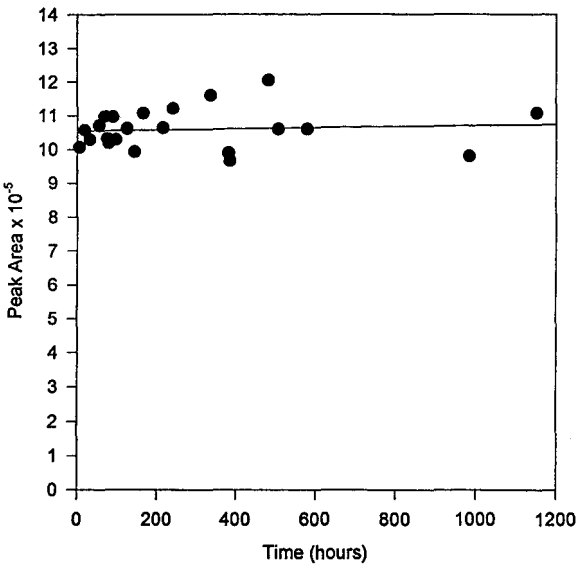

Fig. 7. Stability of AEOC-derivatized phenol as a function of time.

perature for various lengths of time prior to injection. The results of this study, shown in Fig. 7, indicate that the derivatives are very stable over at least several weeks.

The method was applied to several industrial waste water samples originating from Central Pennsylvania. While not all four of the standard phenols were detected in all of the samples, each sample was found to contain one or two of the four standard phenols. Chromatograms for two industrial waste water samples, A and B, are shown in Figs. 8A and 8B. Sample A (Fig. 8A) shows a phenol peak at 8.62 min corresponding to a level of 0.065 mg/100 ml. A peak at 10.60 min in Fig. 8B indicates the presence of DMP at a level of 0.0048 mg/100 ml in waste-water sample B. The average values obtained from three replicate analyses of waste-water samples A and B were 0.064 (0.065, 0.063, 0.064) and 0.0044 (0.0048, 0.0046, 0.0039) mg/100 ml of P and DMP, respectively. Independent analyses of

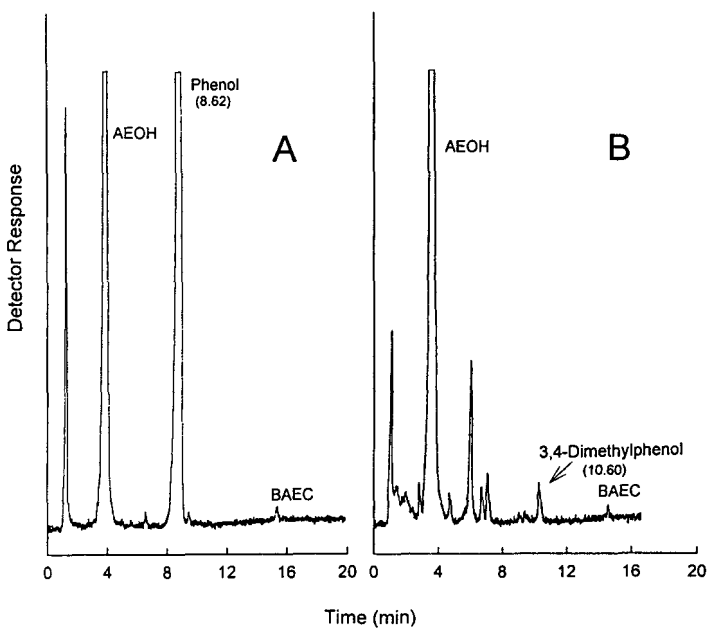

Fig. 8. Chromatograms for Central Pennsylvania waste water samples. (A) 0.07 mg phenol/100 ml. (B) 0.005 mg 3,4-dimethylphenol/100 ml. Conditions the same as in Fig. 4.

water samples A and B using gas chromatography (Wilson Testing Laboratories, Shamokin, PA, USA) yielded values of 0.07 and <0.005 mg/100 ml of P and DMP, respectively [22]. Peak identities were confirmed by comparing the retention times to those of the standards. Additional confirmation of peak identity was achieved by spiking the samples with small amounts of the known compounds resulting in the enlargement of existing peaks. A number of additional AEOC-reactive impurities were also observed.

4. Conclusion

It has been shown that 2-(9-anthrylethyl) chloroformate (AEOC) is a sensitive and convenient pre-column derivatizing reagent for the determination of phenols by HPLC with fluorescence detection. AEOC-derivatized phenols have been shown to be very stable and the detection limits are similar to those found previously for AEOC-derivatized polyamines. The derivatization procedure is rapid, simple, and reproducible, making the method attractive for environmental analyses such as the determination of phenols in industrial waste waters and municipal water supplies.

Acknowledgements

Acknowledgement is made to the Camille and Henry Dreyfus Foundation Scholar/Fellow Program for providing major financial support for this research. The authors are also grateful to the National Science Foundation (REU grant, CHE9100-538) and the Dow Chemical Company Foundation and for providing summer research fellowships for K.J.H. and J.B.C. Finally, the authors express their gratitude to Professor Brian W. Williams, Bucknell University, for running fluorescence spectra and to Mr. Harry Wilson, Wilson Testing Laboratories, Shamokin, PA, USA, for providing industrial waste water samples.

References

[1] A.E. Greenberg, L.A. Clesceri and A.D. Eaton (Editors), Standard Methods for the Examination of Water and Wastewater, 18th ed., American Public Health Association, Washington, DC, USA, 1992.
[2] J. McMurry, Organic Chemistry, Brooks/Cole Publishing, Pacific Grove, CA, USA, 1992, pp. 1012–1013.
[3] J. Siegrist, C. Salles and P. Etievant, Chromatographia, 35 (1993) 50–54.
[4] T. Niwa, Clin. Chem., 39 (1993) 108–111.
[5] G. Montedoro, M. Servilli, M. Baldioli and E. Miniati, J. Agric. Food Chem., 40 (1992) 1571–1576.
[6] M. Akasbi, D.W. Shoeman and A.S. Csallany, J. Am. Oil Chem. Soc., 70 (1993) 367–370.
[7] G. Achilli, G.P. Cellerino and P.H. Gamache, J. Chromatogr., 632 (1993) 111–117.
[8] C. Li and M.W. Kemp, J. Chromatogr., 455 (1988) 241–251.
[9] K. Imai, T. Fukushima and H. Yokosu, Biomed. Chromatogr., 8 (1994) 107–113.
[10] M. Zheng, H. Xu and C. Fu, Sepu, 12 (1994) 186–188; Chem. Abstr., 121 (1994) 194612.
[11] C. Fu, Hebei Daxue Xuebao, Ziran Kexueban, 14 (1994) 35–40; Chem. Abstr., 121 (1994) 148045.
[12] S. Einarsson, B. Josefsson and S. Lagerkvist, J. Chromatogr., 282 (1983) 609–618.
[13] S. Einarsson, S. Folestad, B. Josefsson and S. Lagerkvist, Anal. Chem., 58 (1986) 1638–1643.
[14] S. Einarsson, B. Josefsson, P. Möller and D. Sanchez, Anal. Chem., 59 (1987) 1191–1195.
[15] J.R. Price, P.A. Metz and H. Veening, Chromatographia, 24 (1987) 795–799.
[16] A.J. Faulkner, H. Veening and H.-D. Becker, Anal. Chem., 63 (1991) 292–296.
[17] M.A. Cichy, D.L. Stegmeier, H. Veening and H.-D. Becker, J. Chromatogr., 613 (1993) 15–21.
[18] H. Sörensen, Ph.D. Thesis, University of Göteborg, Sweden, 1989.
[19] B.M. Mikhailov, Izv. Akad. Nauk SSSR Ser. Khim., (1948) 420–423; Chem. Abstr., 43 (1949) 208g.
[20] H.-D. Becker, L. Hansen and K. Andersson, J. Org. Chem., 51 (1986) 2956–2961.
[21] C.A. Dorschel, J.L. Ekmanis, J.E. Oberholtzer, F.V. Warren, Jr. and B.A. Bidlingmeyer, Anal. Chem., 61 (1989) 951A–968A.
[22] Test Method 604, GC Determination of Phenol, U.S. Environmental Protection Agency, Cincinnati, OH, USA, 1982.

ELSEVIER

Journal of Chromatography A, 718 (1995) 53–58

JOURNAL OF CHROMATOGRAPHY A

Differences in the glycosylation of recombinant and native human milk bile salt-stimulated lipase revealed by peptide mapping ☆

Mats Strömqvist*, Kerstin Lindgren, Lennart Hansson, Kristina Juneblad

ASTRA HÄSSLE AB, Tvistevägen 48, S-907 36 Umeå, Sweden

First received 2 November 1994; revised manuscript received 25 May 1995; accepted 1 June 1995

Abstract

The milk of some mammals contains a bile salt-stimulated lipase (BSSL). Human milk BSSL is heavily glycosylated (30–40% carbohydrate) and present at a concentration of approximately 100–200 mg/l, thereby being one of the most abundant human whey proteins. BSSL has been shown to have an important role in the uptake of energy from human milk. The risk of HIV contamination has restricted the use of banked human milk for nutritional purposes. This has evoked an interest in the production of a recombinant form of the protein for supplementation of formula.

We have produced BSSL in mouse C127 and hamster CHO cells, and used chromatographic methods for the characterization of the products. This study was focused on study of the glycosylation of the protein by using peptide mapping and isolation of glycosylated fragments. The results show how human BSSLs from different sources differ both in extent of glycosylation, in glycan heterogeneity, and in lectin binding.

1. Introduction

Human milk contains a bile salt-stimulated lipase (BSSL) constituting approximately 0.5–1% of the total milk protein [1,2]. BSSL represents the major lipolytic activity in the milk and is therefore important for the uptake of energy from the milk [1]. The protein consists of 722 amino acids, carries one potential N-glycosylation site in the N-terminal part (Asn-187) and a repeat region of 16 segments of 11 amino acids each carrying several O-glycosylations close to the C-terminus (amino acids 536–711) [3,4]. By the study of mutants of the protein produced in C127 cells, non-glycosylated BSSL has been shown to have enzymatic activity similar to that of the glycosylated BSSL [5]. BSSL is sensitive to elevated temperatures and is inactivated by incubation at 40–50°C, thus pasteurization of the milk inactivates the enzyme [6]. As a major lipase in the human milk, BSSL might be interesting as a component of infant formula especially since pasteurization of donated human milk inactivates the enzymatic activity.

The aim of this study was to further characterize native and recombinant BSSL with emphasis on the glycosylation using high-performance liq-

* Corresponding author.

☆ Presented at the *14th International Symposium on the Separation and Analysis of Proteins, Peptides and Polynucleotides, Heidelberg, 2–4 November 1994.*

0021-9673/95/$09.50
SSDI 0021-9673(95)00632-X

uid chromatography. Additional information about the glycosylated repeat part of native as well as recombinant forms of BSSL produced in different cell lines could be obtained by purification of glycopeptides. Size-exclusion chromatography (SEC) gave information about the hydrodynamic size of the glycoproteins/glycopeptides and thereby the extent of glycosylation. Peptide mapping using reversed-phase liquid chromatography (RPLC) gave information on the heterogeneity of the glycan containing fragments. As a complement to these techniques, lectin affinity electroblotting was used to identify some of the glycan structures present in BSSL produced by the different cells.

2. Experimental

2.1. Purification of BSSL

Native BSSL

Human milk samples were collected from donors within the first three months of lactation. The donated milk was frozen until analyzed and purified. The milk was centrifuged at 30 000 *g* for 45 min. The fat layer and the pellet were removed and the remaining supernatant was filtered. To precipitate caseins, pH was adjusted to 4.3 with 1 *M* HCl and $CaCl_2$ was added to a final concentration of 60 m*M*. After incubation at room temperature for 1 h with stirring, the casein fraction was removed by centrifugation at 43 000 *g* for 90 min. The supernatant (whey) was dialyzed against 5 m*M* barbiturate-HCl, 50 m*M* NaCl, pH 7.4, applied to a Heparin-Sepharose column (Pharmacia Biotech., Uppsala, Sweden) and chromatographed as described previously [2]. Fractions were analyzed for presence of BSSL by ELISA and pooled for a second chromatography on Superdex 200 (Pharmacia Biotech.) equilibrated with 10 m*M* sodium phosphate, 0.5 *M* NaCl, pH 7.2.

Recombinant BSSL

Conditioned media harvested from roller-bottle cultures were filtered through a 0.22-μm sterile filter and thereafter chromatographed using the same two chromatographic steps as used for native BSSL. The purity, of both native and recombinant BSSL, was more than 95% according to densitometric scans of SDS-PAGE gels.

2.2. Enzymatic cleavage of BSSL

Carboxymethylation

Purified BSSL protein (5 mg) was dialyzed against distilled H_2O, lyophilized and dissolved in 1.5 ml 0.5 *M* ammonium acetate, 6 *M* guanidine-HCl. Dithiotreitol was added to a final concentration of 10 m*M* and the sample was incubated at room temperature under nitrogen for 1 h. Iodoacetic acid (0.5 *M*, freshly prepared) was added to a final concentration of 10 m*M* and the sample was incubated for another 2 h under nitrogen at room temperature in the dark. Finally the reaction was terminated by addition of 30 μl 2-mercaptoethanol and 525 μl glacial acetic acid.

Cleavage with trypsin

Carboxymethylated BSSL was dialyzed against 0.1 *M* NH_4HCO_3, pH 7.8. Trypsin [2% (w/w), sequencing grade, Boehringer-Mannheim Biochimica, Mannheim, Germany] was added and proteolytic cleavage was performed overnight (16–20 h) at 20–25°C. Digestions were conducted at a concentration of approximately 0.2–0.8 mg/ml of the carboxymethylated protein. The reaction was terminated by acidification to pH 3 with HCl and samples were stored on ice until analysis.

Cleavage with endoproteinase Lys-C

Carboxymethylated BSSL was dialyzed against 0.1 *M* NH_4HCO_3, pH 7.8 and cleaved with 1% (w/w) endoproteinase Lys-C (EndoLys-C, Boehringer-Mannheim) at 37°C. After 2 h of cleavage, another 1% EndoLys-C was added and the reaction was allowed to continue for 5 more hours. The reaction was conducted at approximately the same concentration as that with trypsin and was also terminated similarly. Total amino acid analysis was performed as described previously [7].

2.3. Chromatography

Chromatography was performed on a System Gold chromatographic system (Beckman Instruments, San Ramon, CA, USA) with a Model 126 pump and a Model 166 detector unit. Temperature control (for RPLC) was achieved by the use of a Waters TCM temperature control module (Millipore-Waters, Milford, MA, USA).

SEC

BSSL, digest as well as uncleaved protein, were applied on a TSK 3000 SW column (600 × 7 mm I.D., Beckman Instruments) equilibrated with 10 m*M* NaH_2PO_4, 0.3 *M* NaCl pH 7.2 at a flow-rate of 0.5 ml/min. As references for the molecular mass calculations, thyroglobulin (M_r 669), ferritin (M_r 440), IgG (M_r 150), bovine serum albumin (M_r 67) and ovalbumin (M_r 44) were used. Separations were carried out at 20°C.

RPLC

The protease digest was separated on a C_8 Ultrapore column (250 × 4.6 mm I.D., Beckman Instruments). The elution system consisted of two solvents: one consisting of 0.1% trifluoroacetic acid (TFA) in water and the second containing 90% acetonitrile and 0.089% TFA. The elution program was as follows: 0–5 min, 0% acetonitrile; 5–10 min, 0–12% acetonitrile; 10–55 min, 12–30% acetonitrile; 55–85 min, 30–60% acetonitrile. All gradients were linear, the flow-rate was 1 ml/min and the separations were made at 38°C.

2.4. Electroblotting and lectin staining

SDS-polyacrylamide gels were run according to Laemmli [8] using 4–15% precast polyacrylamide gels (Bio-Rad, Hercules, CA, USA). Proteins were transferred to Immobilon-P membranes (Millipore, Bedford, MA, USA) using semi-dry electroblotting as described previously [9]. Membranes were blocked with 2% ovine serum albumin in 20 m*M* Tris-HCl, 0.5 *M* NaCl, pH 8.2 over-night at 4°C and washed twice in 50 m*M* Tris-HCl, 150 m*M* NaCl, pH 7.5 (TBS). The membranes were thereafter incubated for 1 h at room temperature with the different digoxigenin labeled lectins (Boehringer-Mannheim) diluted from the 1 mg/ml stock solutions with TBS containing 1 m*M* $MnCl_2$, 1 m*M* $CaCl_2$ and 1 m*M* $MgCl_2$ as recommended by the manufacturer as follows:

Ricinus communis agglutinin (RCA)	1/100
Maackia amurensis agglutinin (MAA)	1/200
Aleuria aurantia agglutinin (AAA)	1/1000
Phytohemagglutinin-L (PHA-L)	1/200
Sambucus nigra agglutinin (SNA)	1/1000
Peanut agglutinin (PNA)	1/100
Concanavalin A (Con A)	1/100
Galantus nivalis agglutinin (GNA)	1/1000
Wheat germ agglutinin (WGA)	1/100
Datura stramonium agglutinin (DSA)	1/1000

After lectin incubations, membranes were washed 3 × 10 min in TBS and incubated 1 h at room temperature with alkaline phosphatase conjugated anti-digoxigenin Fab fragments (Boehringer-Mannheim) diluted 1/1000 in TBS. Membranes were washed 3 × 10 min in TBS and bound enzyme activity was detected as described [9].

3. Results and discussion

Cleavage of BSSL, enzymatically or chemically, results in a rather strange distribution of fragment sizes. Four different cleavage methods were tried; chemical cleavage with CNBr and enzymatic cleavages with endoproteinase Lys-C (EndoLys-C), trypsin and endoproteinase Glu-C (EndoGlu-C). Enzymatic cleavage with EndoGlu-C was not successful while the other three methods worked better. Cleavage with CNBr, trypsin or EndoLys-C resulted in the liberation of the repetitive sequence domain of 16 × 11 amino acids contained within a single fragment of approximately 200 residues. Cleavage of BSSL with EndoLys-C gives theoretically 38 peptide fragments (Fig. 1), 12 of which having only three or less amino acids and one being as long as 201 residues (EndoLys-C 37, amino acids 512–712 containing the 16 × 11 repeat region).

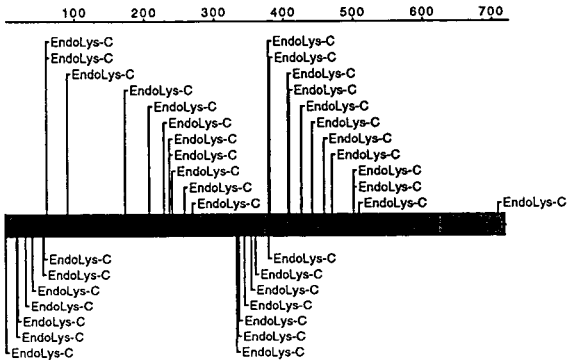

Fig. 1. Cleavage of BSSL with EndoLys-C. The positions of the cleavage sites are indicated by the vertical bars. The upper numbered horizontal bar represents the polypeptide backbone from N- to C-terminus.

The peptide maps obtained on reversed-phase chromatography of the three different forms of BSSL showed reasonably well separated peptides except for the peaks eluting at approximately 50–55 min (Fig. 2). The amino acid analysis of collected material in this region showed that the fragment containing all the repeats was present in these fractions. The origin of most of the other fragments could also be determined by

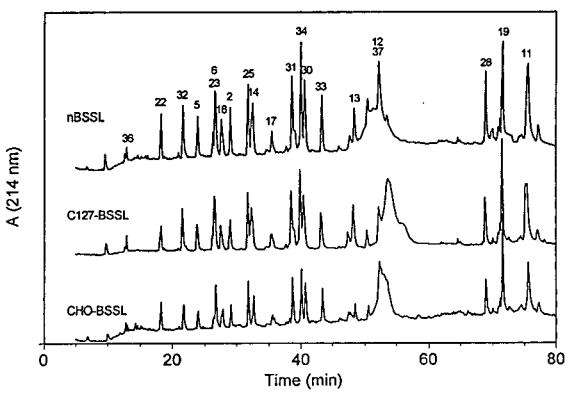

Fig. 2. Peptide map obtained on RPLC of the BSSL variants obtained after cleavage with EndoLys-C. The protein was cleaved as described under Experimental and applied to the column. In each run, 100 μl sample at a concentration close to 1 mg/ml was loaded on the column. Conditions for the chromatography are given in the Experimental section. The numbers represent the fragment number from N- to C-terminus. Abbreviations: nBSSL = native BSSL, C127-BSSL = BSSL produced in C127 cells, CHO-BSSL = BSSL produced in CHO cells.

amino acid analysis as indicated in Fig. 2. When uncleaved BSSL (native as well as recombinant) was analyzed by size-exclusion chromatography, the elution behavior of the protein indicated a large hydrodynamic molecular size of the protein ($>M_r$ 300, Table 1). Due to the presence of some arginines prior to the repeat part of this fragment, enzymatic cleavage with trypsin yields a somewhat shorter and more absolute repeat fragment (amino acids 521–712). For this reason, and also because trypsin is an economically better choice when cleavage is to be done for preparative purposes, trypsin instead of Endo-Lys-C was chosen for the further study of the O-glycosylation. Analysis of the tryptic digests of the proteins variants by SEC shows that the reason for the behavior as a very large protein on SEC resides in one fragment in the digest eluting early in the chromatogram (O-GF, Fig. 3). We could confirm that this fragment was the repeat fragment carrying the O-glycosylations. This fragment accounts for a molecular mass of approximately 18 when not considering the glycosylations. The elution position of the fragment in size-exclusion chromatography indicates a molecular mass above 200 (Fig. 3, Table 1). Thus, the behavior of the protein as being very large appears to be due to a large hydrodynamic size of this glycosylated fragment. This fragment could easily be prepared just by cleaving BSSL with trypsin. SEC could be used as a simple tool for comparison of the size of the fragment and thereby giving a hint on the extent of O-glycosylation of recombinant and native BSSL. Interestingly, the sizes obtained from SEC were very close when comparing the native

Table 1
Molecular masses of the intact BSSL variants and their O-glycosylated repeat fragments obtained by SEC

Type of BSSL	M_r intact protein	M_r glycopeptide
Native BSSL	321 ± 6	259 ± 5
C127-BSSL	331 ± 12	255 ± 7
CHO-BSSL	336 ± 7	260 ± 3

The figures represent the mean of three chromatographies.

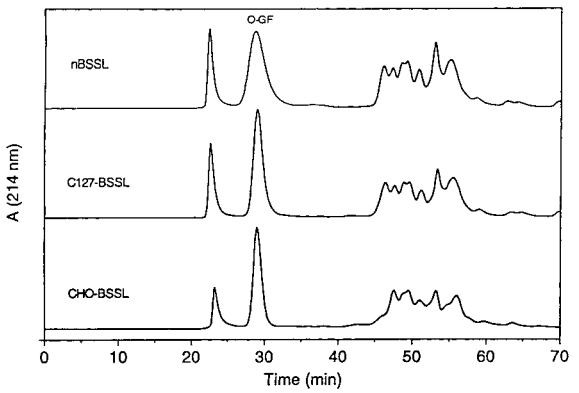

Fig. 3. Size-exclusion chromatography of BSSL cleaved with trypsin. The digest was applied to the column equilibrated with 10 m*M* NaH_2PO_4, 0.3 *M* NaCl pH 7.2. Abbreviations are as in Fig. 2. O-GF is the large O-glycosylated fragment. Approximately 40 μg of each protein digest in a volume of 100 μl was applied to the column. The peak at the void volume of the column (23 min) contains aggregated hydrophobic peptides. The material eluted after 45 min contains the "normal size" peptides. The calibrants eluted as follows under the same conditions: thyroglobulin (M_r 669) 22.6 min, ferritin (M_r 440) 26.1 min, IgG (M_r 150) 30.8 min, BSA (M_r 67) 34.1 min and ovalbumin (M_r 43) 37.9 min. Further details are given in the Experimental section.

and the two recombinant forms of BSSL (Fig. 3, Table 1). The uncleaved protein and the O-glycosylated fragment migrated as proteins larger than 300 and 200, respectively. From earlier data [5], it appears that C127 cell recombinant BSSL might be less heterogeneous than the native variants since it gives a more dense band upon SDS-PAGE. Later analysis has shown that BSSL produced by CHO cells is similar in this respect to BSSL produced by C127 cells; they comigrate and show the same band spreading (not shown). As an additional evidence for a more heterogeneous native protein, Fig. 3 shows that the peak representing the O-glycosylated fragment in native BSSL is wider than the corresponding peaks obtained with the two recombinant forms of BSSL. As a final step in the glycan analysis, the three variants of BSSL were subjected to electroblotting followed by staining with labeled lectins to obtain information on some specific glycan structures present on the glycoprotein. Also in this case, the reactions were similar; the two recombinant protein reacted exactly in the same

Table 2
Lectin binding properties of the different forms of BSSL

Lectin	Native BSSL	C127-BSSL	CHO-BSSL
Con A	no	weak	weak
RCA	strong	weak	weak
WGA	medium	medium	medium
SNA	weak	weak	weak
AAA	strong	weak	weak
MAA	weak	weak	weak
DSA	no	no	no
GNA	no	no	no
PNA	weak	weak	weak
PHA-L	no	no	no

Further details and abbreviations are given in the Experimental section. The interactions are classified as no, weak, medium and strong

way (Table 2). Some differences between the recombinant proteins and the native protein could however be detected (Table 2). The recombinant proteins reacted weakly with Con A and DSA, while native BSSL did not (Table 2). Native BSSL reacted more strongly with AAA and RCA indicating presence of more fucose and terminal β-galactose residues (Table 2). The reactivities with the lectins indicate that the N-glycosylation of both native and recombinant BSSL is of a complex type since Con A reacted weakly or not at all. The weak reaction of the recombinant variants with Con A was mediated through the N-glycosylation since a mutant lacking only the N-glycan did not react with this lectin (not shown). The degree of O-glycosylation is similar as judged by the chromatographic data. According to the lectin data, the native protein is certainly more fucosylated due to the very strong binding to AAA and contains also more terminal β-galactose due to the stronger binding to RCA. Similarities between the native and the recombinant forms of BSSL are that they contain no terminal mannose, they all contain α(2–3)- and α(2–6)-linked sialic acids, N-acetylgalactoseamine and that they most certainly all contain complex N-glycan structures. Another evidence for the presence of fucose-containing structures in native but not in recombinant BSSL was that the native protein reacted

with antibodies against the Lewis^b antigen while the recombinant forms did not react with these (not shown). In summary, we could, by quite simple standard chromatographic methods, show that recombinant BSSL proteins produced by C127 and CHO cells were glycosylated to a similar extent, but were less heterogeneous than the native protein. By the lectin binding study it was established that there were some differences in the specific glycans attached to the recombinant forms of BSSL compared to those attached to native BSSL. It was also shown that the two recombinant forms of BSSL were very similar in their glycosylation despite the fact that they were produced in cells from different species, i.e. mouse and hamster. The chromatographic techniques described here do not give any detailed characterization of the glycan structures but are suitable for preparing glycopeptides for further characterization. A follow-up on this study would be to release the glycans and analyze them by high-performance anion-exchange chromatography and mass spectrometry [10] to obtain a more detailed picture of the attached carbohydrates.

Acknowledgements

We thank Astra Hässle AB and Symbicom AB for generous financial support and Michael Edlund and Åsa Emanuelsson for production of recombinant BSSL.

References

[1] O. Hernell and T. Olivecrona, Biochim. Biophys. Acta, 369 (1974) 234.
[2] L. Bläckberg and O. Hernell, Eur. J. Biochem., 116 (1981) 221.
[3] J. Nilsson, L. Bläckberg, P. Carlsson, S. Enerbäck, O. Hernell and G. Bjursell, Eur. J. Biochem., 192 (1990) 543.
[4] T. Baba, D. Downs, K.W. Jackson, J. Tang and C.S. Wang, Biochemistry, 30 (1991) 500.
[5] L. Hansson, L. Bläckberg, M. Edlund, L. Lundberg, M. Strömqvist and O. Hernell, J. Biol. Chem., 268 (1993) 26692.
[6] O. Hernell, Eur. J. Clin. Invest., 5 (1975) 267.
[7] M. Strömqvist, J. Holgersoon and B. Samuelsson, J. Chromatogr., 548 (1991) 293.
[8] U.K. Laemmli, Nature, 27 (1970) 680.
[9] M. Strömqvist, J. Chromatogr., 621 (1993) 139.
[10] J.R. Barr, K.R. Anumula, M.B. Vettese, P.B. Taylor and S.A. Carr, Anal. Biochem., 192 (1991) 181.

ELSEVIER

Journal of Chromatography A, 718 (1995) 59–66

JOURNAL OF CHROMATOGRAPHY A

Elution of lipoprotein fractions containing apolipoproteins E and A-I in size exclusion on Superose 6 columns is sensitive to mobile phase pH and ionic strength

John Westerlund, Zemin Yao*

Lipid and Lipoprotein Research Group and Department of Biochemistry, University of Alberta, Edmonton, Alb., Canada

First received 22 February 1995; revised manuscript received 29 May 1995; accepted 7 June 1995

Abstract

Separation of lipoproteins secreted from McA-RH7777 (rat hepatoma) cells by Superose 6 column size-exclusion chromatography, using PBS buffer (NaCl 150 m*M*, sodium phosphate 10 m*M*, pH 7.5, EDTA 1 m*M*), produced apolipoprotein (apo) E or A-I profiles that did not correlate with lipoproteins separated by density ultracentrifugation. By density ultracentrifugation, apoE and apoA-I were mostly (>90%) confined to high-density lipoproteins (HDL, $d = 1.063–1.023$ g/ml), but by chromatography apoE and apoA-I were recovered in all lipoprotein classes, including low-density lipoproteins (LDL), HDL, and post-HDL. Moreover, the elution volume of phenol red on Superose 6 greatly exceeded the total column volume. These discrepancies were attributable to pH and ionic strength effects. In low ionic strength, high pH buffer (Tris 25 m*M*, pH 8.3), elution volumes of lipoproteins, albumin, and phenol red were minimized. Elution volumes increased 25–70% when buffer pH was lowered at constant ionic strength (Tris 25 m*M*, pH 7.4) or when ionic strength was increased at constant pH (Tris 25 m*M*, pH 8.3, NaCl 500 m*M*). Altered phase partition appeared to cause the altered elution volumes, since recovery (measured as analyte peak area), resolution (measured as peak width at half height), and column void volume varied little from buffer to buffer. In Superose 6 size-exclusion chromatography with PBS buffer, then, elution volumes vary with pH and ionic strength. We propose that TBE buffer (Tris-borate 89 m*M*, pH 8.3, EDTA 2 m*M*) may produce fewer artefacts than PBS. With TBE there were (i) better correlation between size-exclusion and ultracentrifugal fractions, (ii) lower elution volumes, and (iii) less "smearing" of McA-RH7777 apoE and apoA-I containing lipoprotein bands.

1. Introduction

The most prevalent classification scheme for plasma lipoproteins is based on their hydrated density. The categories of very low density lipoproteins (VLDL, $d < 1.006$ g/ml), low density lipoproteins (LDL, $1.019 < d < 1.063$ g/ml) and high density lipoproteins (HDL, $1.063 < d < 1.23$ g/ml) have proven useful both clinically and analytically. Size-exclusion chromatography is being used increasingly as a surrogate technique for analytical fractionation of lipoproteins from plasma and from other sources, both in the clinical laboratory [1] and research settings [2–9]. The increased use of size exclusion can be

* Corresponding author. Present correspondence address: Lipoprotein and Atherosclerosis Group, University of Ottawa Heart Institute, 1053 Carling Avenue, Ottawa, Ont. K1Y 4E9, Canada.

0021-9673/95/$09.50
SSDI 0021-9673(95)00640-0

attributed to improvements in size-exclusion technology, such as the introduction of the Superose 6 column for fast protein liquid chromatography. Plasma LDL and HDL isolated by the Superose 6 methods have lipid and apolipoprotein compositions comparable to those of the corresponding ultracentrifugal fractions [1,5], with the advantage of a 1-h separation time, compared to a day or longer for conventional size exclusion [10] or preparative ultracentrifugation [11].

The rat hepatoma cell line McA-RH7777 has been widely used to study metabolism of hepatic lipoproteins [12,13]. In the course of a study of McA-RH7777 lipoproteins, we undertook to characterize the profile of lipoproteins containing apolipoproteins E (apoE) and A-I (apoA-I) in McA-RH7777 conditioned medium by density gradient ultracentrifugation and by Superose 6 size exclusion (using phosphate buffered saline (PBS) running buffer), and observed a poor correlation between the two methods in regards to the distributions of apoE and apoA-I. When the discrepancy was investigated, we discovered that the distributions of McA-RH7777 lipoproteins containing apoE and apoA-I were highly sensitive to mobile phase pH and ionic strength during chromatography on the Superose 6 columns. We found that using Tris-borate-EDTA (TBE) buffer effectively minimized size-exclusion artefacts and generated McA-RH7777 LDL and HDL with apolipoprotein compositions which correlated well with the ultracentrifugal fractions. These observations emphasize the limitations of the size-exclusion technique as a surrogate for ultracentrifugation when analytes other than plasma are involved.

2. Methods

2.1. Cell culture

McA-RH7777 cells were grown to 60% confluence in 100-mm dishes, in Dulbecco's Modified Eagle's Medium (DMEM) supplemented with 10% fetal bovine serum and 10% horse serum (Life Technologies). Conditioned medium was obtained by washing the cells twice with 5 ml of serum-free DMEM, aspirating each wash, and then adding 12 ml of fresh DMEM. After 24-h incubation, the conditioned medium was decanted into chilled 15-ml polypropylene tubes, and stock solutions of protease inhibitors were added to give final concentrations of EDTA 5 m*M*, phenylmethylsulfonylfluoride 2 m*M*, benzamidine 2 m*M*, and sodium azide 0.05% (w/v). The McA-RH7777 lipoproteins were then separated by either ultracentrifugation or by size-exclusion chromatography on Superose 6 columns.

2.2. Ultracentrifugation

For ultracentrifugation, the lipoproteins were separated by sequential flotation in a TLA 100.3 rotor using a TLA-100 table-top centrifuge (Beckman). VLDL + LDL were collected by raising the density of the conditioned medium to $d = 1.063$ g/ml by addition of solid KBr, centrifuging at 99 000 rpm (540 000*g*), 4°C, for 4 h, and aspirating the top 240 μl of each 3-ml centrifuge tube. VLDL and LDL were isolated together because McA-RH7777 cells produce negligible VLDL ($d < 1.019$ g/ml lipoproteins) under serum-free conditions [13]. The bottom 1.5 ml infranate was adjusted to $d = 1.23$ g/ml by addition of solid KBr, and centrifuged for 5 h, 99 000 rpm, 4°C. The top 240-μl sample was collected as HDL ($d = 1.063$–1.23 g/ml), while the bottom 1.5 ml was recovered as the $d > 1.23$ g/ml fraction. After ultracentrifugal isolation, the lipoproteins in each fraction were adsorbed onto fumed silica (Cab-O-Sil, Sigma [14]), and apolipoproteins were separated on 3–18% gradient SDS-polyacrylamide gels [13].

2.3. Superose 6 column chromatography

Size exclusion was performed using phosphate buffered saline (PBS: sodium phosphate 10 m*M*, pH 7.5, NaCl 150 m*M*, EDTA 1 m*M*) with the following chromatographic parameters: flow-rate, 0.5 ml/min; back pressure, 1.1 MPa; monitor, mercury vapor lamp at 280 nm; recorder, analog chart. The elution volume of human

LDL or HDL standard, prepared by ultracentrifugation [11], was determined on the Superose 6 column and used for comparison with that of McA-RH7777 lipoproteins. A 12-ml volume of conditioned, serum-free McA-RH7777 medium was concentrated to 300 μl using Centricon-10 centrifugal concentrators (Amicon), 200 μl of the concentrate was loaded onto a Superose 6 column, and 30 fractions of 1 ml were collected. Apolipoproteins in each fraction were adsorbed onto fumed silica and visualized by SDS-polyacrylamide gel electrophoresis [13].

2.4. Immunoblot analysis

Proteins separated by SDS-polyacrylamide gel electrophoresis were transferred to nitrocellulose, and visualized by immunoblotting using rabbit antisera to rat apoE, apoB, or apoA-I followed by peroxidase-labelled goat anti-rabbit secondary antibodies and enhanced chemiluminescence detection (Amersham) [12]. All the antisera used were specific to each corresponding rat apolipoprotein.

3. Results and discussion

3.1. Discrepancies of apolipoprotein profiles separated by ultracentrifugation or Superose size exclusion using PBS running buffer

The distributions of McA-RH7777 apolipoproteins in ultracentrifugal density fractions are shown in Fig. 1A. The VLDL + LDL fraction contains most of the apoB100, plus traces of apoE and apoA-I. The HDL density fraction contains the bulk of the apoE, apoA-I, and apoB48. The $d > 1.23$ g/ml infranate density fraction contains negligible apoB, traces of apoE, and somewhat more apoA-I. The Superose 6 size-exclusion distribution of McA-RH7777 apolipoproteins was in sharp contrast to this ultracentrifugal density distribution. The size-ex-

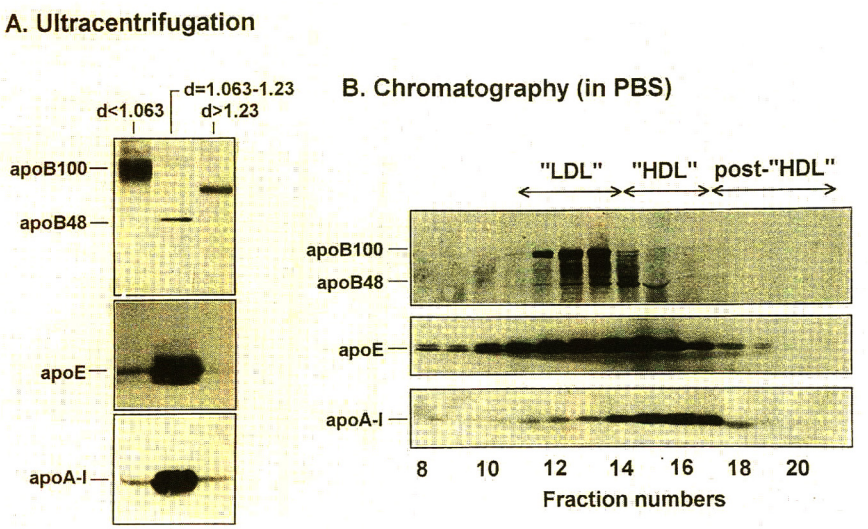

Fig. 1. Apolipoprotein composition of lipoproteins from McA-RH7777 conditioned medium isolated by density ultracentrifugation or by Superose 6 size-exclusion chromatography using PBS running buffer. (A) Distribution of apolipoprotein B (top), apoE (middle), and apoA-I (bottom) in VLDL/LDL ($d < 1.063$ g/ml), HDL ($d = 1.063$–1.23 g/ml), and $d > 1.23$ g/ml ("lipoprotein-free") infranate, isolated by sequential flotation. In the $d > 1.23$ g/ml infranate, a band which did not correspond to either apoB100 or apoB48 was observed to react with the rabbit polyclonal anti-rat-apoB antibody (top panel, right column). Its identity is unknown. (B) Distribution of apolipoproteins B, E, and A-I in Superose 6 size-exclusion chromatographic fractions. The labels "LDL" and "HDL" at the top indicate the fractions in which ultracentrifugally purified human LDL and HDL [11] eluted.

clusion distribution of McA-RH7777 apoE and apoA-I is shown in Fig. 1B. Although the peak distribution of apoE and apoA-I was in the "HDL" fractions, substantial amounts of each apolipoprotein were present in the "LDL" and the "post-HDL" fractions as well. In size exclusion apoE was particularly prominent in "LDL" and even in the early elution fractions, while apoA-I was more skewed into the "post-HDL" fractions. A manifest anomaly was also observed: phenol red (M_r 354), the dye from the McA-RH7777 medium, eluted from the Superose 6 column at a volume of 38 ml (see below), despite an absolute volume for the column of 24 ml (30×1 cm I.D.: $\pi r^2 h = 23.56$ cm^3). Thus, the apoE and apoA-I distributions were not consistent with centrifugal data, and the phenol red elution volume was clearly artifactual. However, the distributions of apoB100 and apoB48 after size exclusion were consistent with the ultracentrifugal data: apoB100 was confined to the "LDL" fractions, and apoB48 to the "HDL" fractions. There were no detectable degradation products of any of the medium apolipoproteins as determined by Coomassie blue staining and immunoblotting (data not shown).

3.2. Improved apolipoprotein profiles on Superose 6 columns using TBE running buffer

The discrepancies and artefacts observed led us to inquire whether non-ideal interactions were distorting the size-exclusion profile of McA-RH7777 apoE and apoA-I. We looked for buffer effects by repeating size exclusion using TBE buffer (Tris 89 m*M*, boric acid 89 m*M*, EDTA 2 m*M*, pH 8.3) in stead of PBS. TBE decreased the elution volume (V_e) of human LDL, human HDL, and the components of McA-RH7777 medium, as shown in Fig. 2. The V_e of purified LDL decreased from 11–13 ml in PBS to 8–10 ml in TBE (Fig. 2A), while V_e of HDL decreased from 15–17 ml to 10–12 ml (Fig. 2B). The decrease in V_e was a generalized effect of TBE buffer, since the components of McA-RH7777 medium were similarly affected, the V_e of the albumin peak shifted from 16.6 ml in PBS to 13.8 ml in TBE (Fig. 2C). These results were reproducible in each buffer; the V_e of any given analyte varied by less than 0.2 ml from run to run. The peak shapes of the analytes were not affected by the buffer change, nor were the peak areas altered, suggesting that recovery was identical. The column void volume (V_o) was essentially identical between the two buffers, suggesting that column architecture was also preserved. The V_e of phenol red (a marker of the approximate inclusion volume) decreased from 38 ml in PBS to 22.4 ml in TBE, which is appropriate for a column with a total volume of 24 ml.

When the TBE size-exclusion fractions of the medium lipoproteins were analyzed for apolipoprotein content, we found that, in contrast to our earlier results with PBS, the TBE-derived apolipoprotein distribution was consistent with the results of ultracentrifugation (Fig. 3). In TBE, the bulk of both apoE and apoA-I was confined to the "HDL" fractions, with apoE tailing into the "LDL" and apoA-I tailing more into the "post-HDL" fractions. ApoB100 and apoB48 elution profile, as before, was consistent regardless of buffer: apoB100 eluted almost exclusively in the "LDL" fractions, while apoB48 was mostly confined to the "HDL" fractions. Because McA-RH7777 apolipoproteins had improved correlation with ultracentrifugation fractions after TBE size exclusion (as compared to PBS), and because the manifestly artifactual V_e of phenol red in PBS resolved with the switch to TBE, we considered that TBE gave a more faithful representation of the distribution of analytes in McA-RH7777 medium than did PBS.

3.3. Mobile phase pH and ionic strength affects apolipoprotein profiles on Superose 6 columns

We next assessed the possible factors contributing to anomalous behavior on Superose 6 columns. We prepared a test solution of three standard analytes: blue dextran (marker of the void volume, V_o), bovine serum albumin, and phenol red, and adjusted their concentration in the solution so that each analyte gave an absorbance of 0.3. The V_e of these three analytes in

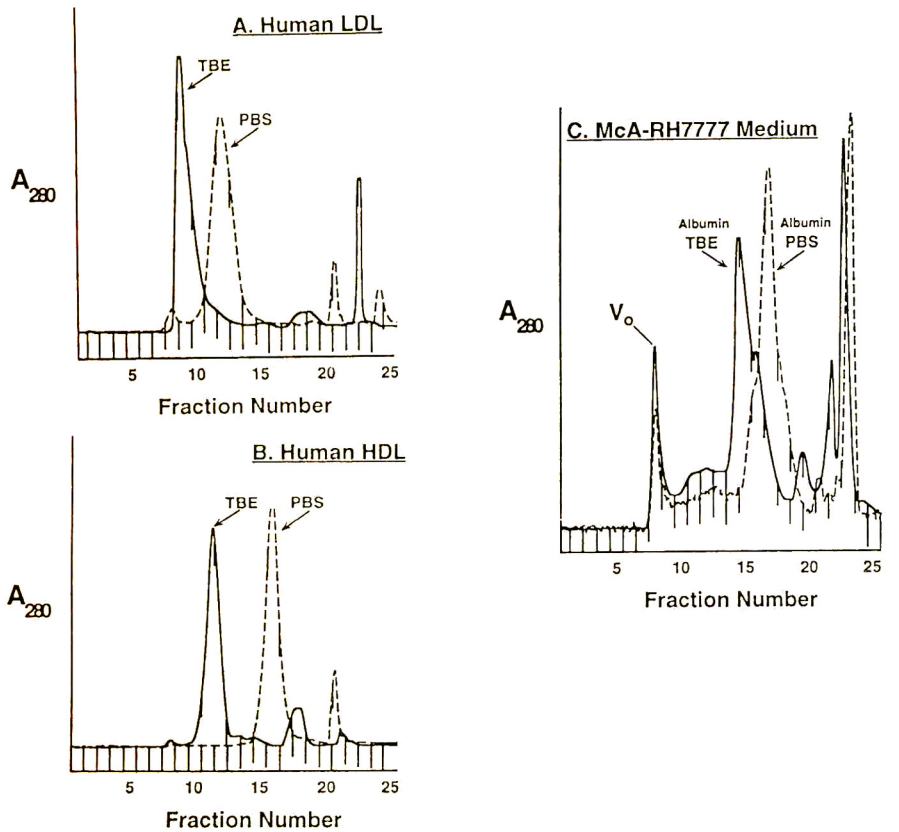

Fig. 2. Effect of PBS or TBE running buffer on Superose 6 size-exclusion profiles of control analytes. The V_e of control analytes shifted markedly when TBE running buffer (solid line) was used in place of PBS running buffer (dashed line), even though all other chromatographic parameters (see text) were held constant. The column was equilibrated with a minimum of 4 column volumes of buffer prior to chromatography, and each assay was done in duplicate. The coefficient of variance of V_o (void volume), V_e and peak height for any given analyte was less than 2% run to run. (A) Human LDL, 250 μg protein, (B) human HDL, 250 μg protein, (C) concentrated McA-RH7777 conditioned medium, 600–800 μg protein.

running buffers of varying pH and ionic strength was then assessed. The results are shown in Table 1 and can be summarized as follows: no buffer affected the V_o of the column to any marked degree, suggesting that column architecture (e.g. gel shrinkage, etc.) was not sensitive to buffer changes. However, the size exclusion of both albumin and phenol red were sensitive to both pH and ionic strength: at fixed ionic strength (Tris 25 m*M*), raising the pH from 7.4 to 8.3 reduced the V_e of albumin by 1.1 ml (7.4%). Likewise, at fixed pH (7.4), raising the ionic strength, from Tris 25 m*M* to Tris 25 m*M* + NaCl 500 m*M*, increased the V_e of albumin from 14.7 ml to 16.5 ml (12.2%). Phenol red was even more sensitive to pH and ionic strength than albumin; its V_e ranged from 22.8 ml in Tris 25 m*M*, pH 8.3 (cf. 22.4 ml in TBE) to 37.8 ml in Tris 25 m*M*, pH 7.4, NaCl 500 m*M* (cf. 38 ml in PBS). The addition of 100 m*M* urea had no effect on the V_e of albumin, suggesting that hydrogen bonding had little effect on the chromatographic behavior of albumin. For phenol red, though, a slight decrease in V_e was observed (Table 1). Thus Superose 6 gel filtration was remarkably sensitive to buffer conditions such as pH and ionic strength. The effect was generalized, affecting human lipoproteins, albumin, McA-RH7777 medium, and phenol red, and it could be minimized by certain buf-

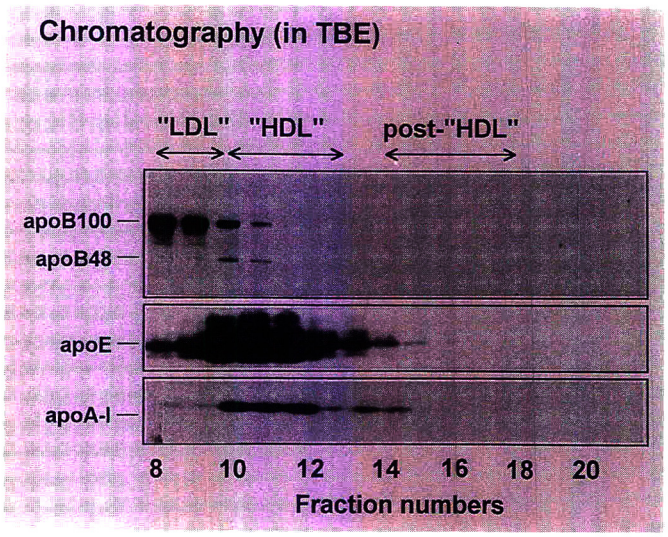

Fig. 3. Distribution of apolipoproteins from McA-RH7777 conditioned medium isolated by Superose 6 size-exclusion chromatography using TBE running buffer. This figure corresponds to Fig. 1B, with TBE used instead of PBS as running buffer. Observe the improved correlation with ultracentrifugal results (Fig. 1A).

fers. In TBE, or in Tris 25 m*M*, pH 8.3, the V_e of test analytes dropped to what appeared to be a minimum V_e value.

Our observations suggest that hydrophobic interactions artifactually increase the elution volumes of lipoproteins on Superose 6 in PBS buffer, while ion-exchange plays little role. Our data are comparable to those of Golovchenko et al. [15] who studied the non-size-exclusion interactions of the hydrophobic protein endoglucanase 1, and the hydrophilic proteins endoglucanase C and lysozyme, during chromatography on Superose 12 columns. Their data suggest that the artefacts induced by hydrophobic interactions require more careful buffer adjustment than the ion-exchange and ion-exclusion artefacts observed with hydrophilic proteins, which were readily avoided by addition of 100 m*M* $NaSO_4$ to their running buffer.

Our results demonstrate that the efficient separation of serum lipoproteins on Superose 6 columns using PBS running buffer [1,5] occurs in the presence of PBS-related elution artefacts. The efficiency of a chromatographic column, defined as the number of theoretical plates (N), is computed as: $N = 5.5\ (V_e/w_{1/2})^2$ [16], where $w_{1/2}$ is the peak width at half height. Since LDL, HDL, and albumin have an increased V_e in PBS compared to TBE, but a similar $w_{1/2}$, the number of theoretical plates is increased in PBS buffer, and column efficiency is improved. Column selectivity (α), which is related to a column's ability to resolve two analytes, is also improved by the increase in V_e for LDL and HDL. Selectivity is defined as: $\alpha = (V_{e1} - V_o)/(V_{e2} - V_o)$ [16]. Since LDL and HDL peaks tend to spread apart in PBS buffer, while V_o is unchanged, selectivity is improved. Thus the PBS buffer system has performed well for the analysis of lipoproteins in plasma, and the PBS-related Superose 6 column interactions actually improve the separation of plasma lipoproteins.

As compared to plasma lipoproteins, McA-RH7777 lipoproteins exhibit unfavorable non-size-exclusion interactions in PBS, presumably because of an altered protein conformation, a

Table 1
Effect of ionic strength, pH, and chaotrophic agent on the chromatographic profile of blue dextran, bovine serum albumin (BSA), and phenol red (Φ red) on Superose 6 columns

Test buffer	Expected effect	Elution volume (V_e)		
		Blue dextran	BSA	Φ Red
1. Tris 25 m*M*, pH 7.4	Low ionic strength buffer; reduced hydrophobic interaction between analyte and matrix.	6.7	14.7	29.1
2. Tris 25 m*M*, pH 7.4 Urea 100 m*M*	Low ionic strength with urea; decreased H-bond interaction (if any) of analyte with matrix.	6.8	14.7	28.4
3. Tris 25 m*M*, pH 8.3	Low ionic strength, high pH; to assess pH effects (cf. buffer 1).	6.7	13.6	22.8
4. Tris 25 m*M*, pH 8.3 NaCl 500 m*M*	High ionic strength, high pH; to assess effect of ionic effects on analyte–matrix interactions.	7.0	16.6	29.4
5. Tris 25 m*M*, pH 7.4 NaCl 500 m*M*	High ionic strength, lower pH than buffer 4; to assess effect of pH at higher ionic strength	6.8	16.5	37.8
TBE (Tris-borate 89 m*M*, EDTA 2 m*M*, pH 8.3)		6.6	13.8	22.4
PBS (NaCl 150 m*M*, Na Phosphate 10 m*M*, EDTA 1 m*M*, pH 7.4)		6.8	16.6	38.0

different lipid composition, or both. There are two apparent artefacts observed in PBS: excessive early elution of apoE and apoA-I (in the "LDL" fractions), and excessive late elution (in the "post-HDL" fractions). Although the late-eluting apoA-I and apoE peaks can probably be attributed to "tailing" due to non-ideal hydrophobic or ion-exchange interactions with the column matrix, the early elution artefact is more problematic. It may reflect ion-exclusion between the negatively-charged lipoproteins and the residual COOH and SO_4 groups on the matrix, or self association of apoA-I and apoE-containing lipoproteins in PBS, due to weak interactions which are eliminated by ultracentrifugation and by TBE buffer.

In summary, we have shown that non-ideal analyte–matrix interactions contribute significantly to the fractionation pattern of plasma or McA-RH7777 lipoproteins during size exclusion on Superose 6 columns in PBS running buffer. For the fractionation of plasma, the interactions actually enhance the chromatographic separation, improve the integrity of lipoprotein fractions, and thereby increase the correlation between size exclusion and ultracentrifugation fractions. For McA-RH7777 medium, the interactions introduce analytical discrepancies between size exclusion and ultracentrifugation, which can be avoided by using TBE running buffer. It is hoped that these observations will serve to increase the awareness of the limitations of the

size-exclusion technique as a surrogate for ultracentrifugation when analytes other than plasma are involved.

Acknowledgements

The authors thank Drs. Taira Ohnishi, Roger Davis, and Karl Weisgraber for providing antisera used in this study. Drs. Roger McLeod and Shinji Yokoyama made valuable comments and suggestions. This work was made possible by grants from the Medical Research Council of Canada, the Canadian Heart and Stroke Foundation, and the Alberta Heritage Foundation for Medical Research.

References

[1] W. Marz, R. Siekmeier, H. Scharnagl, U.B. Seiffert and W. Gross, Clin. Chem., 39 (1993) 2276.
[2] H.V. de Silva, S.J. Lauer, J. Wang, W.S. Simonet, K.H. Weisgraber, R.W. Mahley and J.M. Taylor, J. Biol. Chem., 269 (1994) 2324.
[3] C.H. Warden, C.C. Hedrick, J. Qiao, L.W. Castellani and A.J. Lusis, Science, 261 (1993) 469.
[4] M. Liu, F.R. Jirik, R.C. LeBoeuf, H. Henderson, L.W. Castellani, A.J. Lusis, Y. Ma, I.J. Forsythe, H. Zhang, E. Kirk, J.D. Brunzell and M.R. Hayden, J. Biol. Chem., 269 (1994) 11417.
[5] J.A. Westerlund and K.H. Weisgraber, J. Biol. Chem., 268 (1993) 15745.
[6] J.B. Hansen, N.E. Huseby, P.M. Sandset, B. Svensson, V. Lyngmo and A. Nordoy, Arterioscler. Thromb., 14 (1994) 223.
[7] N. Duverger, D. Rader, P. Duchateau, J.C. Fruchart, G. Castro and H.B. Brewer, Jr., Biochemistry, 32 (1993) 12372.
[8] E. Vilella, J. Joven, M. Fernandez, S. Vilaro, J.D. Brunzell, T. Olivecrona and G. Bengtsson-Olivecrona, J. Lipid Res., 34 (1993) 1555.
[9] M. Jauhiainen, J. Metso, R. Pahlman, S. Blomqvist, A. van Tol and C. Ehnholm, J. Biol. Chem., 268 (1993) 4032.
[10] L.L. Rudel, C.A. Marzetta and F.L. Johnson, Methods Enzymol., 129 (1986) 45.
[11] Manual of Laboratory Operations, Lipid Research Clinics Program, Vol. 1, Lipid and Lipoprotein Analysis, U.S. Department of Health, Education, and Welfare, Washington, DC, 1974, No. (NIH) 75–628.
[12] Z. Yao, S.J. Lauer, D.A. Sanan and S. Fazio, Arterioscler. Thromb., 13 (1993) 1476.
[13] R.S. McLeod, Y. Zhao, S.L. Selby, J. Westerlund and Z. Yao, J. Biol. Chem., 269 (1994) 8358.
[14] D.E. Vance, D.B. Weinstein and D. Steinberg, Biochim. Biophys. Acta, 792 (1984) 39.
[15] N.P. Golovchenko, I.A. Kataeva and V.K. Akimenko, J. Chomatogr., 591 (1992) 121.
[16] D.M. Ullman and C.A. Burtis, in N.W. Tietz. (Editor), Fundamentals of Clinical Chemistry, WB Saunders, Philadelphia, PA, 1986, pp. 159–172.

ELSEVIER

Journal of Chromatography A, 718 (1995) 67–79

JOURNAL OF CHROMATOGRAPHY A

Effects of salts and the surface hydrophobicity of proteins on partitioning in aqueous two-phase systems containing thermoseparating ethylene oxide–propylene oxide copolymers

Kristina Berggren, Hans-Olof Johansson, Folke Tjerneld*

Department of Biochemistry, Chemical Center, University of Lund, P.O. Box 124, S-221 00 Lund, Sweden

First received 17 February 1995; revised manuscript received 6 June 1995; accepted 9 June 1995

Abstract

The partitioning of five well-characterised model proteins, bovine serum albumin (BSA), lysozyme, β-lactoglobulin A, myoglobin and cytochrome c, in aqueous two-phase systems has been studied. As top phase polymers PEG (polyethylene glycol, 100% EO) and the thermoseparating ethylene oxide (EO)–propylene oxide (PO) random copolymers, Ucon 50-HB-5100 (50% EO, 50% PO) and $EO_{30}PO_{70}$ (30% EO, 70% PO), respectively, were used. The top phase polymers are increasing in hydrophobicity with increasing content of PO. Reppal PES 200 (hydroxypropyl starch) was used as the bottom phase polymer. Phase diagrams for Reppal PES 200–PEG and Reppal PES 200–$EO_{30}PO_{70}$ two-phase systems were determined. The partitioning of four salts with different hydrophobicity, and also the effect of the salts on protein partitioning in these systems, was studied. It was found that the partitioning of the salts followed the Hofmeister series. The partitioning of proteins with low surface hydrophobicity, myoglobin and cytochrome c, was little affected by hydrophobic polymers and salts. However, the partitioning of a protein with higher surface hydrophobicity, lysozyme, was strongly affected when polymer hydrophobicity was increased and a hydrophobic counterion was used. A protein with a relatively hydrophobic surface can be partitioned to a phase containing a thermoseparating EO–PO copolymer by using a hydrophobic counterion. The partitioning of lysozyme and cytochrome c in the polymer–water system formed after temperature-induced phase separation was also examined. Both proteins partitioned exclusively to the water phase. A separation of the protein and polymer was obtained by temperature-induced phase separation on the isolated phase containing the EO–PO copolymer. The partitioning data also indicated that the hydroxypropyl starch polymer had a weak negative charge.

1. Introduction

An aqueous two-phase system consists of a mixture of two structurally different polymers which separate into two phases above a critical concentration. A protein or any other substance included in the system partitions between the two phases. The partitioning of a protein depends on its properties such as net charge, size and hydrophobicity. It can also be affected by including various salts in the system, changing the pH, changing polymers or polymer molecular mass [1]. Partitioning in an aqueous two-phase system is a mild method for the purification of a protein from a cell homogenate because of the

* Corresponding author.

0021-9673/95/$09.50
SSDI 0021-9673(95)00657-0

high content of water (75–90%) in the two phases.

Partitioning in aqueous two-phase systems can be combined with temperature-induced phase separation if one of the polymers is thermoseparating [2–4]. After separation in the primary phase system, the phase containing the thermoseparating polymer is isolated in a separate container and the temperature is raised above the cloud point (CP) of the polymer. This leads to a new phase separation where the new top phase consists mainly of water and the new bottom phase consists mainly of the polymer [2–4]. Proteins partition almost exclusively to the water phase in this step and a separation of the polymer and protein is obtained. The thermoseparating polymer can be recycled in the process. It is desirable in a purification process to partition the target protein to the top phase in the primary phase system and then separate the protein from the polymer with temperature-induced phase separation at a temperature as low as possible to avoid denaturation of the target protein. The CP of the thermoseparating polymer can be lowered by either adding a suitable salt, e.g. sodium sulphate, to the system [2] or by making the polymer more hydrophobic [4].

Aqueous two-phase systems containing the polymers PEG (polyethylene glycol) and dextran have been extensively studied. In the present studies we have used the low-cost polymer hydroxypropyl starch, Reppal PES 200 [5] as bottom phase polymer instead of dextran. Hydroxypropyl starch polymers have earlier been studied as a substitute for dextran and were found to have similar phase-forming properties [6]. We have used three different top phase polymers having nearly similar molecular masses, PEG (100% EO, EO_{100}) and the random copolymers of ethylene oxide (EO) and propylene oxide (PO), Ucon 50-HB-5100 (50% EO, 50% PO; $EO_{50}PO_{50}$) and $EO_{30}PO_{70}$ (30% EO, 70% PO). EO–PO random copolymers are thermoseparating [2–4,7], and the polymer hydrophobicity increases with increasing content of PO.

The partitioning of five model proteins, bovine serum albumin (BSA), lysozyme, β-lactoglobulin A, myoglobin and cytochrome c, was studied. The proteins are well characterised with respect to structure and properties. The partitioning of the proteins was studied at different pH values, pH 7.1 and pH 5.0. The partitioning of four salts with different hydrophobicity, sodium phosphate ($Na^+HPO_4^{2-}/H_2PO_4^-$) (NaP), NaCl, $NaClO_4$ and triethylammonium phosphate (Et_3NH^+ $H_2PO_4^-$) (Et_3NP), was studied. The effect of the salts on protein partition in phase systems with EO–PO random copolymers was investigated. Ions have different affinity for the two phases and can therefore create a potential difference between the phases which will affect protein partitioning [1,8].

For the application of temperature-induced phase separation in protein purification it is necessary to partition the target protein to the top phase containing the thermoseparating polymer in the primary phase system. The purpose of this study was to investigate how the hydrophobicity of the thermoseparating polymer, and added salts with varying hydrophobicities, affected the partitioning of the model proteins, and how the effects could be correlated to the surface hydrophobicity of the proteins. We have also investigated the partitioning of lysozyme and cytochrome c in the polymer–water system formed by the temperature-induced phase separation.

2. Materials and methods

2.1. Proteins

The following proteins were obtained from Sigma (St. Louis, MO, USA): serum albumin, bovine fatty acid free (nr. A-6003); β-lactoglobulin A, bovine milk (nr. L-7880); myoglobin, horse heart (nr. M-1882); cytochrome c, horse heart (nr. C-2506). Lysozyme: hen egg white (nr. 107255) was obtained from Boehringer (Mannheim, Germany).

2.2. Polymers and chemicals

Bottom phase polymer was Reppal PES 200 (hydroxypropyl starch), molecular mass 200 000, from Reppe AB (Växjö, Sweden). The respective top phase polymers were PEG 4000 (EO_{100})

from Merck (Münich, Germany), Ucon 50-HB-5100 ($EO_{50}PO_{50}$) from Union Carbide (New York, NY, USA) and $EO_{30}PO_{70}$ from Shearwater Polymers (Huntsville, AL, USA). PEG and Ucon had a molecular mass of 4000, $EO_{30}PO_{70}$ had a molecular mass of 3200. All chemicals were of analytical grade. Triethylammonium phosphate was obtained by mixing triethylamine with phosphoric acid to the desired pH.

2.3. Phase diagrams

The specific rotation $[a]_D^{25}$ of Reppal PES 200 was determined by polarimetry (as the slope of a standard curve) to 192° ml g^{-1} dm^{-1}. Systems of 10 g with different concentrations (percent w/w) of Reppal, PEG (or $EO_{30}PO_{70}$) and water were prepared. The systems were centrifuged for 10 min at 5700 rpm. The top- and bottom phases were isolated and diluted six times. First the concentration of Reppal was determined in both phases by polarimetry. The concentration of PEG and $EO_{30}PO_{70}$, respectively, was determined by measuring the refractive index and by subtracting the Reppal contribution to the refractive index readings. A few points in the phase diagram, around the critical point, were determined by titration of the two-phase system with water until the formation of a one-phase system [1].

2.4. Two-phase systems for the partitioning of proteins

The phase diagrams of the two-phase systems using different polymers differ and, hence, to be able to compare the partition coefficients comparable two-phase systems were chosen. $\Delta\text{Reppal} = C_{\text{Reppal bottom phase}} - C_{\text{Reppal top phase}}$ was chosen to be the same (14%) in each system. Systems of 5 g with the following concentrations were mixed: 13.8% Reppal–6.5% PEG, 11% Reppal–5% Ucon, 10.6% Reppal–6.8% $EO_{30}PO_{70}$. All polymer concentrations in this paper are given as percent w/w. The systems also contained 10 m*M* buffer (sodium phosphate buffer at pH 7.1, sodium acetate buffer at pH 5.0), 0.5 mg/ml protein, 100 m*M* salt (NaCl, $NaClO_4$ or Et_3NP). When no salt was included the buffer concentration was 100 m*M*.

The partition of a substance is described by the partition coefficient K, which is defined as $K = C_T/C_B$, where C_T is the concentration of the substance in the top phase and C_B is its concentration in the bottom phase. All partition coefficients are average values from at least two experiments. Experiments with different salts at pH equal to p*I* for the protein were done with one of the top phases (Ucon). The systems were equilibrated at room temperature and were left standing for one hour. The top- and bottom phases were isolated and diluted 7–15 times. The phases were analysed for their protein content. BSA and myoglobin were analysed according to Bradford [10] with Coomassie Brilliant Blue G at 595 nm and with the respective protein as standard. Lysozyme and β-lactoglobulin A were analysed with the BCA method [11] with the respective protein as standard. Cytochrome c was analysed by measuring the absorbance at 408 nm.

2.5. Temperature-induced phase separation

The cloud points for Ucon and $EO_{30}PO_{70}$ are approximately 50°C [7] and 35°C [12], respectively. To obtain a macroscopic separation of the polymer- and water phases in a reasonable time the temperature must be raised 5–10°C higher than the cloud point. Temperature-induced phase separation was studied in systems with $EO_{30}PO_{70}$. After separation and isolation of the top- and bottom phases from the primary two-phase system at room temperature, the top phase was heated in a water bath to 44°C and was left standing for one hour. The new top- and bottom phases were isolated and diluted. The protein content was determined in the same way as in the primary two-phase system.

2.6. Two-phase systems for the partitioning of salts

Systems with the polymer concentrations (percent w/w) of 20% Reppal–9% PEG, 15.3% Reppal–8.1% Ucon and 16% Reppal–9.1% $EO_{30}PO_{70}$, 100 m*M* of the salts (NaP, NaCl,

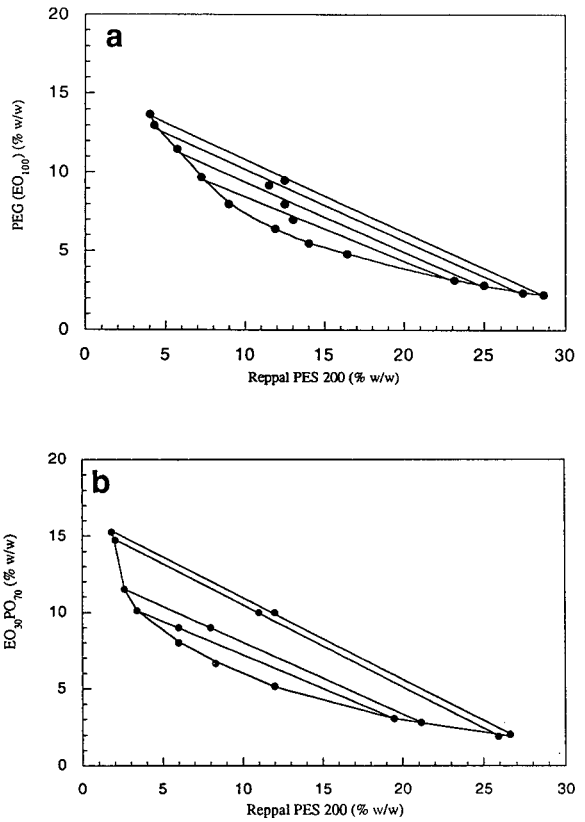

Fig. 1. (a) Phase diagram of Reppal PES 200–PEG 4000 (EO_{100})–water system at 20°C. (b) Phase diagram of Reppal PES 200–$EO_{30}PO_{70}$–water system at 20°C.

$NaClO_4$ or Et_3NP) and water to 5 g were prepared. The systems were equilibrated at room temperature and were left standing for one hour. The top- and bottom phases were then isolated and diluted 80 times. The partitioning of the salts was analysed by measuring the conductivity of the top and bottom phase, respectively.

3. Results and discussion

3.1. Phase diagrams

The phase diagram and the composition of the phases for the Reppal PES 200–PEG 4000–water system at 20°C are shown in Fig. 1a and Table 1. Table 2 shows the compositions of the phases for the Reppal PES 200–Ucon 50-HB-5100–water system at 20°C and the phase diagram can be found in Ref. [13]. The phase diagram and the composition of the phases for the Reppal PES 200–$EO_{30}PO_{70}$–water system at 20°C are shown in Fig. 1b and Table 3.

3.2. The partitioning of salts

The polymer concentrations that were used for the partitioning of the proteins showed very small difference in partition coefficients between different salts. Higher concentrations of the polymers are known to result in more extreme partition coefficients for a substance [1]. Hence we chose to partition the salts at higher polymer concentrations than that used for the proteins. In the three different systems Δ(top phase polymer) was kept constant (15%), where Δ(top phase polymer) is equal to the concentration of the dominating polymer in the top phase minus the

Table 1
Compositions of the phases in the Reppal PES 200–PEG 4000 (EO_{100})–water system at 20°C

Total system			Top phase			Bottom phase		
Reppal (% w/w)	PEG (% w/w)	H_2O (% w/w)	Reppal (% w/w)	PEG (% w/w)	H_2O (% w/w)	Reppal (% w/w)	PEG (% w/w)	H_2O (% w/w)
13.0	7.0	80.0	7.3	9.7	83.0	23.1	3.2	73.7
12.5	8.0	79.5	5.7	11.5	82.8	25.0	2.8	72.2
11.5	9.2	79.3	4.3	13.0	82.7	27.4	2.4	70.2
12.5	9.5	78.0	4.0	13.7	82.3	28.7	2.3	69.0

Table 2
Compositions of the phases in the Reppal PES 200–Ucon 50-HB-5100–water system at 20°C. The phase diagram is shown in Ref. [13]

Total system			Top phase			Bottom phase		
Reppal (% w/w)	Ucon (% w/w)	H_2O (% w/w)	Reppal (% w/w)	Ucon (% w/w)	H_2O (% w/w)	Reppal (% w/w)	Ucon (% w/w)	H_2O (% w/w)
6.9	7.5	85.6	3.9	8.8	87.3	18.8	1.5	79.7
7.5	8.0	84.5	3.3	10.1	86.6	19.7	1.7	78.6
10.0	8.0	82.0	2.8	11.5	85.7	24.4	0.6	75.0
9.2	10.0	80.8	2.1	13.9	84.0	25.8	0.8	73.4
11.6	12.5	75.9	1.2	18.5	80.3	31.9	0.5	67.6

Table 3
Compositions of the phases in the Reppal PES 200–$EO_{30}PO_{70}$–water system at 20°C

Total system			Top phase			Bottom phase		
Reppal (% w/w)	$EO_{30}PO_{70}$ (% w/w)	H_2O (% w/w)	Reppal (% w/w)	$EO_{30}PO_{70}$ (% w/w)	H_2O (% w/w)	Reppal (% w/w)	$EO_{30}PO_{70}$ (% w/w)	H_2O (% w/w)
6.0	9.0	85.0	3.4	10.1	86.5	19.5	3.0	77.5
8.0	9.0	83.0	2.6	11.5	85.9	21.2	2.8	76.0
11.0	10.0	79.0	2.0	14.8	83.2	25.9	1.9	72.2
12.0	10.0	78.0	1.8	15.3	82.9	26.6	2.0	71.4

concentration of this polymer in the bottom phase.

The well-known Hofmeister or lyotropic series describes the salting-out effects of ions on proteins, as well as the effect of ions on the surface tension of water [14]. The Hofmeister series can be used as a measure of the relative hydrophobicity of an ion. The hydrophobicity of the anions studied in this work is in the following order $ClO_4^- > Cl^- > CH_2COO^- > HPO_4^{2-}/H_2PO_4^-$, while the hydrophobicity of the cations is $Et_3NH^+ > Na^+$. Et_3NH^+ is an ion with hydrophobic groups and Na^+ is hydrophillic due to its high surface charge density. Fig. 2 shows that the partitioning of the salt to the relatively more hydrophobic top phase was enhanced with increase in hydrophobicity of the anion or cation, in accordance with Hofmeister series. The difference in hydrophobicity of the top phase polymer affected the partitioning of the salts very little.

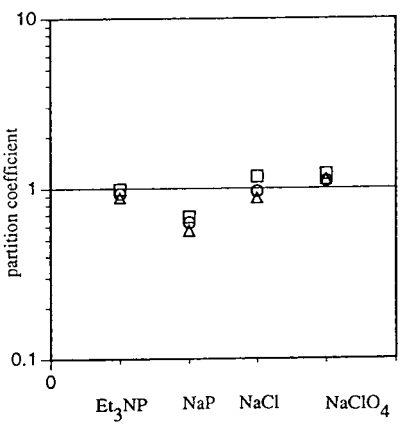

Fig. 2. The partitioning of the salts, at 100 m*M* concentration, triethylammonium phosphate (Et_3NP), sodium phosphate (NaP), sodium chloride (NaCl) and sodium perchlorate ($NaClO_4$) in the two-phase systems. The phase systems were 20% (w/w) Reppal–9% (w/w) EO_{100} (□), 15.3% (w/w) Reppal–8.1% (w/w) $EO_{50}PO_{50}$ (○) and 16% (w/w) Reppal–9.1% (w/w) $EO_{30}PO_{70}$ (△).

3.3. Protein properties

The hydrophobic interaction chromatography (HIC) of the proteins BSA, lysozyme, β-lactoglobulin A and myoglobin on butyl epoxy-Sepharose [18] has been studied earlier. Hydrophobic partitioning using fatty acids bound to PEG has been performed with BSA, β-lactoglobulin A and cytochrome c [19]. Studies in aqueous two-phase systems with hydrophobic groups, benzoyl and valeryl, bound to dextran have been made [20]. The influence of the average surface hydrophobicities on partitioning of the proteins BSA, lysozyme and β-lactoglobulin A in PEG–salt systems has been studied [21]. The partitioning in PEG–salt systems was better correlated with data from ammonium sulphate precipitation than with HIC data. Other studies in PEG–salt systems have shown that the content of the aromatic amino acid tryptophan (Trp) exposed on the surface is of importance in the partitioning of proteins [22]. Trp has also been found to partition very strongly to the hydrophobic Ucon phase in Ucon–water two-phase systems compared with other amino acids [23]. Literature data for the five model proteins on retention in HIC, ammonium sulphate precipitation, hydrophobic partitioning, the total content of Trp and Trp exposed on the surface are shown in Table 4, together with other properties of importance for partitioning: molecular mass, pI and the net charge at pH 7.1.

3.4. The partitioning of proteins

The logarithm of the partition coefficient ($\log K$) of a protein can be divided into contributions from different factors influencing the partitioning [1]:

$$\log K = \log K^0 + \log K_{el} + \log K_{hphob} + \log K_{size} + \cdots$$

where $\log K_{el}$ is the contribution from electrostatics, $\log K_{hphob}$ is the contribution from the surface hydrophobicity of the protein, $\log K_{size}$ depends on the size (molecular mass) of the protein and $\log K^0$ includes other factors. The $\log K_{el}$ is influenced by the partitioning of ions which creates an electrical potential difference between the phases. The partition of a protein with a positive or negative net charge is affected by this potential difference [8]. Log K_{el} can be shown to be linearly dependent on the protein net charge [1]. At pH equal to the pI of the protein there are no salt effects because the net

Table 4
Properties of the five model proteins

	Bovine serum albumin	Lysozyme	β-Lactoglobulin A	Myoglobin	Cytochrome c
Molecular mass	69 000 [28]	13 900 [27]	35 000 [28]	17 500 [28]	13 000 [27]
pI	5.0 [28]	11.0 [29]	5.1 [28]	7.1 [28]	9.4 [28]
Net charge at pH 7.1	−18 [25]	+7 [30]	−5 [24]	0 [28]	+6 [31]
Retention in HIC	10.33[a]	7.49[a]	4.41[a]	2.99[a]	– –
Hydrophobic partition	1.8[b]	– –	1.25[b]	– –	−0.1[b]
Precipitation	0.310[c]	0.416[c]	0.287[c]	– –	– –
Total content of Trp	0.3% [25]	4.6% [32]	1.1% [24]	1.3% [33]	0.9% [34]
Content of Trp exposed on the surface	0% [25]	4.0% [32]	0.6% [24]	– –	0% [34]

[a] Retention coefficient in hydrophobic interaction chromatography on butyl epoxy-Sepharose, determined in Ref. [18].
[b] Maximal Δ log K determined by hydrophobic partition using fatty acids bound to PEG, determined in Ref. [19]. Δ log K is the difference in log K of protein in a PEG–dextran system with and without fatty acid esterified groups. A high value indicates hydrophobic interaction with the polymer-bound ligand.
[c] The inverse of the concentration of ammonium sulphate needed for the precipitation of the protein, determined in Ref. [21]. A high value indicates a high protein surface hydrophobicity.

charge of the protein is zero, and the protein–polymer interaction will then mainly determine the partition [9]. In systems containing hydrophobic polymers the interaction will depend on the protein surface hydrophobicity. At pH values different from the p*I* a combination of protein–polymer interactions and charge effects will affect protein partitioning.

The model proteins were partitioned in phase systems with top phase polymers of increasing hydrophobicity. Comparable phase systems were used (see Material and Methods). The salts were included at a concentration of 100 m*M*; they were dominating over the buffer because the concentration of the salt was ten times higher than the concentration of the buffer [1]. The salts give rise to slightly different ionic strengths in the two-phase systems. It has been shown [8] in PEG–dextran systems that the partitioning of a protein at salt concentrations higher than 50 m*M* is independent of the ionic strength.

Bovine serum albumin

BSA has a negative net charge at pH 7.1 (Fig. 3a) and the tendency for the partition coefficients for BSA with different anions in the system were $K_{NaP} > K_{NaCl} > K_{NaClO_4}$. BSA was partitioned more to the top phase by the partitioning of the hydrophillic $HPO_4^{2-}/H_2PO_4^-$ to the bottom phase and the opposite effect was obtained with Cl^- and ClO_4^-. The hydrophobic triethylammonium ion has a strong tendency to partition to the top phase and the partition coefficients of BSA should, therefore, be higher when triethylammonium is the counterion compared to sodium, which is also seen in Fig. 3a. The top phase polymer change between $EO_{50}PO_{50}$ and $EO_{30}PO_{70}$ did not affect the partitioning as much as when $EO_{50}PO_{50}$ or $EO_{30}PO_{70}$ was exchanged with EO_{100}. The more hydrophillic top phase resulted in higher partition coefficients, especially when sodium phosphate was included in the system.

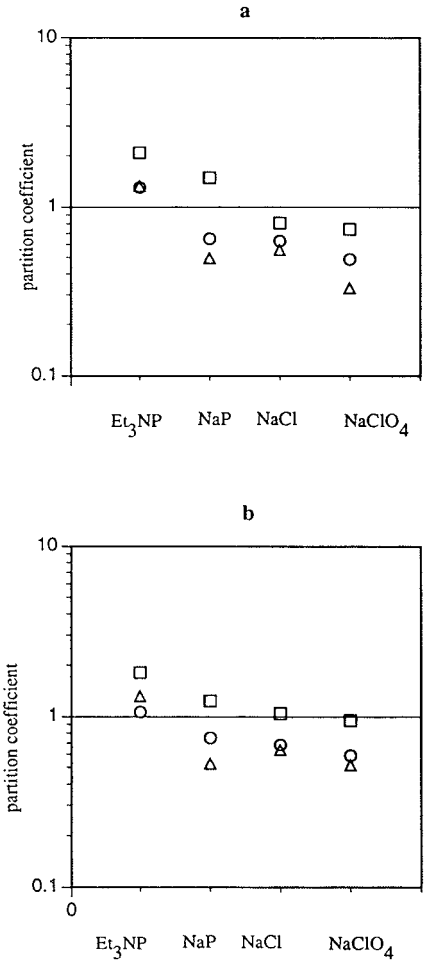

Fig. 3. (a) Partitioning of BSA at pH 7.1 (negatively charged) in two-phase systems. All systems were in 10 m*M* or 100 m*M* sodium phosphate buffer (100 m*M* when no salt other than NaP was included). NaCl, $NaClO_4$ and Et_3NP were at 100 m*M* concentration. The phase systems were 13.8% (w/w) Reppal–6.5% (w/w) EO_{100} (□), 11% (w/w) Reppal–5.0% (w/w) $EO_{50}PO_{50}$ (○) and 10.6% (w/w) Reppal–6.8% (w/w) $EO_{30}PO_{70}$ (△). Standard deviation 0.06. (b) Partitioning of β-lactoglobulin at pH 7.1 (negatively charged) in two-phase systems. All systems were in 10 m*M* or 100 m*M* sodium phosphate buffer (100 m*M* when no salt other than NaP was included). NaCl, $NaClO_4$ and Et_3NP were at 100 m*M* concentration. The phase systems were 13.8% (w/w) Reppal–6.5% (w/w) EO_{100} (□), 11% (w/w) Reppal–5.0% (w/w) $EO_{50}PO_{50}$ (○) and 10.6% (w/w) Reppal–6.8% (w/w) $EO_{30}PO_{70}$ (△). Standard deviation 0.11.

β-Lactoglobulin

The partitioning behaviour of the negatively charged β-lactoglobulin at pH 7.1 (Fig. 3b) was similar to the partitioning behaviour of BSA at the same pH (Fig. 3a). Similar effects of salt and polymer hydrophobicity were observed.

The partitioning behaviours of BSA and β-lactoglobulin were similar although the two proteins differ in molecular mass and net charge. However, β-lactoglobulin has a strong tendency to form dimers in the pH interval studied here [24], and β-lactoglobulin as dimer and BSA have relatively similar molecular masses and net charge at pH 7.1. Both proteins exhibited lower affinity for the top phase when the hydrophobicity of the top phase polymer increased and seem therefore to have relatively hydrophillic surfaces. Another indication of their relatively hydrophillic surfaces is that all partition coefficients at pH 5.0 (Fig. 4) were equal to or less than 1 for both proteins. Earlier results from HIC [18] and partitioning in aqueous two-phase systems with hydrophobic groups coupled to one of the polymers [19,20] indicated higher surface hydrophobicity for these proteins. Hydrophobic sites on the surface of the protein may give a high retention coefficient in HIC and may also interact with hydrophobic groups coupled to a polymer. BSA has a number of hydrophobic sites that can bind long-chain fatty acids [25], which can explain the HIC and hydrophobic partitioning results [18–20].

Lysozyme

The partitioning of the positively charged lysozyme at pH 7.1 (Fig. 5) was strongly affected by the hydrophobicity of the anions. Lysozyme could be transferred from the lower to the upper phase by the use of the relatively hydrophobic ClO_4^- instead of the hydrophillic phosphate ion. The partition coefficients were lowered when Et_3NH^+ was added to the system instead of Na^+. The partition coefficients were relatively independent of the difference in hydrophobicity of the top phase polymer, except when $NaClO_4$ was included in the system. With $NaClO_4$ the partition coefficients were highest for the most hydrophobic top phase polymer, $EO_{30}PO_{70}$. Partitioning at the p*I* for lysozyme could not be performed because of its low solubility at this pH.

Cytochrome c

The partitioning of the positively charged cytochrome c at pH 7.1 (Fig. 6) was also affected

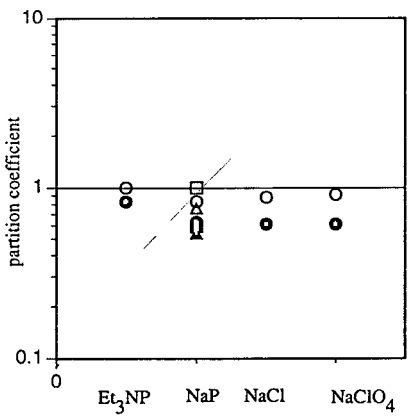

Fig. 4. Partitioning of BSA (filled symbols) and β-lactoglobulin (open symbols) at pH 5.0 (at the p*I*). All systems were in 10 m*M* or 100 m*M* sodium acetate buffer (100 m*M* when no salt other than NaAc was included). NaCl, $NaClO_4$ and Et_3NP were at 100 m*M* concentration. The phase systems were 13.8% (w/w) Reppal–6.5% (w/w) EO_{100} (■, □), 11% (w/w) Reppal–5.0% (w/w) $EO_{50}PO_{50}$ (●, ○) and 10.6% (w/w) Reppal–6.8% (w/w) $EO_{30}PO_{70}$ (▲, △). Standard deviation 0.08.

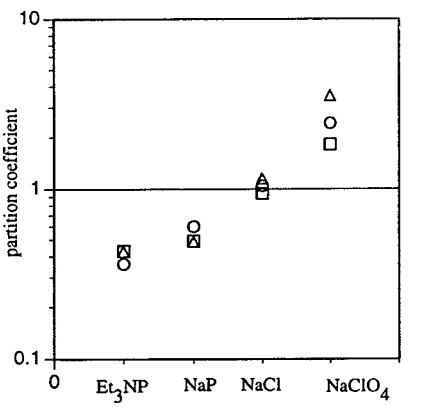

Fig. 5. Partitioning of lysozyme at pH 7.1 (positively charged). All systems were in 10 m*M* or 100 m*M* sodium phosphate buffer (100 m*M* when no salt other than NaP was included). NaCl, $NaClO_4$ and Et_3NP were at 100 m*M* concentration. The phase systems were 13.8% (w/w) Reppal–6.5% (w/w) EO_{100} (□), 11% (w/w) Reppal–5.0% (w/w) $EO_{50}PO_{50}$ (○) and 10.6% (w/w) Reppal–6.8% (w/w) $EO_{30}PO_{70}$ (△). Standard deviation 0.14.

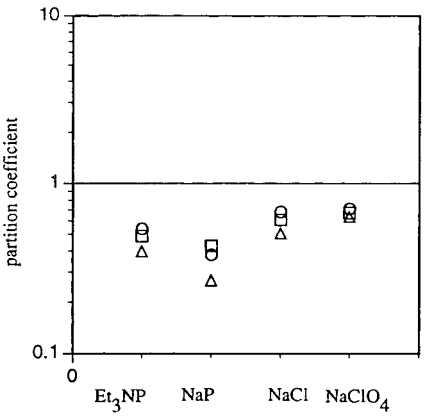

Fig. 6. Partitioning of cytochrome C at pH 7.1 (positively charged). All systems were in 10 m*M* or 100 m*M* sodium phosphate buffer (100 m*M* when no salt other than NaP was included). NaCl, $NaClO_4$ and Et_3NP were at 100 m*M* concentration. The phase systems were 13.8% (w/w) Reppal–6.5% (w/w) EO_{100} (□), 11% (w/w) Reppal–5.0% (w/w) $EO_{50}PO_{50}$ (○) and 10.6% (w/w) Reppal–6.8% (w/w) $EO_{30}PO_{70}$ (△). Standard deviation 0.04.

by the hydrophobicity of the anions but not to the same extent as lysozyme. The hydrophobicity of the cation had a small effect on the partitioning of cytochrome c, but in the opposite direction relative to lysozyme. The expected effect from the partitioning of the Et_3NH^+ ion was to lower the *K*-value, as in the case of lysozyme, but instead an increase was observed compared with the *K*-value for Na^+. A possible explanation can be that the hydrophobic Et_3NH^+ induces a conformational change in cytochrome c leading to exposure of hydrophobic residues. The partition coefficients varied very little with the hydrophobicity of the top phase polymer.

Cytochrome c and lysozyme have similar molecular mass and net charge (+6 and +7 at pH 7.1, Table 4) but they behaved differently in the two-phase systems, indicating a difference in surface hydrophobicity. Lysozyme has a relatively more hydrophobic surface than cytochrome c, which was also observed in studies with hydrophobically modified dextrans [20]. When ClO_4^- is added, the combined effect of a hydrophobic counterion and hydrophobic protein–polymer interaction directs lysozyme to the top phase. The effect is increased with increased polymer hydrophobicity (EO_{100} to $EO_{30}PO_{70}$). The hydrophobicity shown by lysozyme is in accordance with precipitation studies and the retention observed in HIC (Table 4). Cytochrome c, on the other hand, could not be partitioned to the top phase by ClO_4^- and in general the salt effects were small. This indicates that the protein has a low surface hydrophobicity, which is also in agreement with hydrophobic partitioning data [19,20] (Table 4).

Myoglobin

The partitioning of myoglobin at pH 5.0, positively charged, (Fig. 7b) was very little affected by salts and the difference in hydrophobicity of the top phase polymer. The protein was precipitated when $NaClO_4$ was included. Myoglobin could not be partitioned to the top phase with any of the top phase polymers or salts, which indicates a relatively hydrophillic surface. This is also in accordance with HIC [18] (Table 4) and partitioning with hydrophobically modified dextrans [20].

3.5. Salt effects on protein partitioning

At the p*I* of the proteins, when the protein had nearly zero net charge, the salts had little effect on their partitioning (Figs. 4 and 7a). At a pH different from the p*I* of the protein the partitioning followed Hofmeister series for almost all proteins and all top phase polymers. The partition coefficient for a positively charged protein increased with increasing anion hydrophobicity and for a negatively charged protein the partition coefficient decreased with increasing anion hydrophobicity. The only exception in this study was BSA and β-lactoglobulin with $EO_{30}PO_{70}$ as top phase polymer, where the partition coefficients were not lowered by the more hydrophobic Cl^- compared with phosphate.

Salts have a strong effect on the partitioning of a protein with a positive or negative net charge, which shows the importance of the term $\log K_{el}$. The $\log K_{el}$ is linearly dependent on the net charge of the protein, hence BSA (−18 at pH

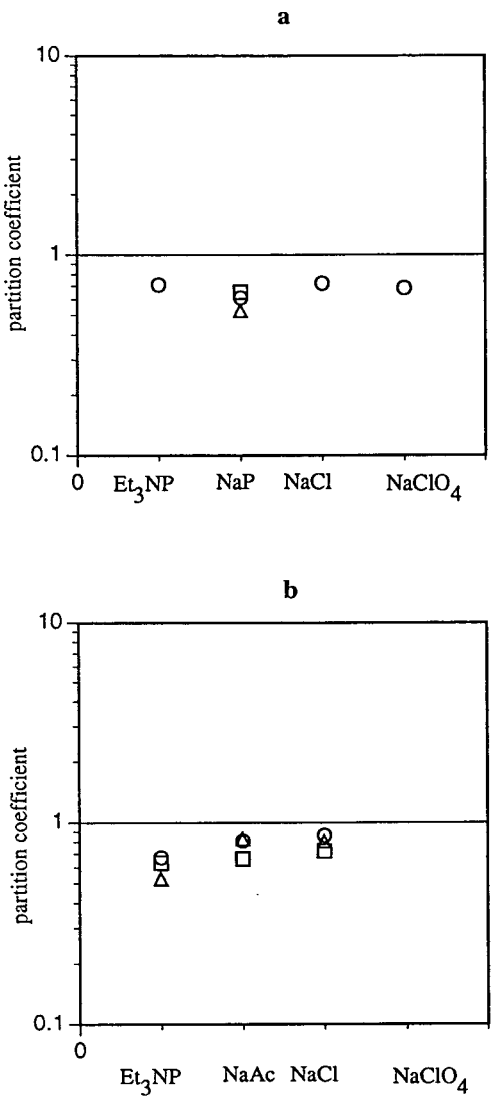

Fig. 7. (a) Partitioning of myoglobin at pH 7.1 (at the p*I*). All systems were in 10 m*M* or 100 m*M* sodium phosphate buffer (100 m*M* when no salt other than NaP was included). NaCl, $NaClO_4$ and Et_3NP were at 100 m*M* concentration. The phase systems were 13.8% (w/w) Reppal–6.5% (w/w) EO_{100} (□), 11% (w/w) Reppal–5.0% (w/w) $EO_{50}PO_{50}$ (○) and 10.6% (w/w) Reppal–6.8% (w/w) $EO_{30}PO_{70}$ (△). Standard deviation 0.02. (b) Partitioning of myoglobin at pH 5.0 (positively charged). All systems were in 10 m*M* or 100 m*M* sodium acetate buffer (100 m*M* when no salt other than NaAc was included). NaCl and Et_3NP were at 100 m*M* concentration. The phase systems were 13.8% (w/w) Reppal–6.5% (w/w) EO_{100} (□), 11% (w/w) Reppal–5.0% (w/w) $EO_{50}PO_{50}$ (○) and 10.6% (w/w) Reppal–6.8% (w/w) $EO_{30}PO_{70}$ (△). Standard deviation 0.04.

7.1) should be most affected among all the proteins studied here. However, this was not the case in our study; lysozyme is affected even stronger than BSA, so other factors such as hydrophobic interaction with the polymer are important in these systems. When the effects are in the same direction in the two-phase system the total effect is strong, lysozyme is strongly partitioned to the top phase with the hydrophobic top phase polymer $EO_{30}PO_{70}$ and the hydrophobic counterion ClO_4^- as compared with the relatively hydrophillic cytochrome c, which remains in the bottom phase in a similar system.

Our results indicate that lysozyme has the highest total surface hydrophobicity of the five proteins studied. BSA and β-lactoglobulin show similar and relatively low total surface hydrophobicity, which is also the case for myoglobin and cytochrome c. Partitioning of proteins in these kinds of systems seems to reflect the total surface hydrophobicity in the same way as precipitation studies do. Interestingly, the content of Trp exposed on the surface of the proteins (Table 4) corresponds well with the results obtained for partitioning in EO–PO copolymer systems. Lysozyme has the highest content of Trp (4.65%) and the residues are to a high degree (4.0%) exposed on the surface of the protein. On the contrary, cytochrome c has only 0.9% Trp, none of which is exposed on the surface of the protein. β-Lactoglobulin has one (0.6% of total) Trp exposed on the surface, and BSA has no exposed Trp's. This can explain the relatively low total surface hydrophobicity for cytochrome c, β-lactoglobulin and BSA shown in partitioning in EO–PO copolymer systems.

3.6. Temperature-induced phase separation

$EO_{30}PO_{70}$ was further subjected to temperature-induced phase separation, as it has the lowest CP of the three top phase polymers studied. Lysozyme was the model protein with the highest affinity for the thermoseparating polymers (see Fig. 5), and this protein was chosen in order to examine protein partitioning in temperature-induced phase separation. The purpose was to see if a protein with affinity for

the thermoseparating polymer would partition to the water phase in the polymer–water phase system formed after temperature-induced phase separation. $NaClO_4$ was added as this salt could direct the partitioning of lysozyme to the $EO_{30}PO_{70}$-containing phase in the primary phase system. For comparison the partitioning of cytochrome c in a similar system was studied because of the low affinity of cytochrome c for the thermoseparating polymers. The primary phase system was composed of 6.8% $EO_{30}PO_{70}$ and 10.6% Reppal. After phase separation, the top phase was isolated in a separate container and placed in a water bath at 44°C. A new top (water) and bottom (EO–PO copolymer) phase was formed. For both lysozyme and cytochrome c 100% of the protein content was obtained in the water phase after separation at 44°C. Thus a separation of the polymer and the protein was achieved with the hydrophillic cytochrome c as well as with the more hydrophobic lysozyme.

3.7. Partitioning with amino acids as buffers and the effect of salt concentration

Reppal, the bottom phase polymer, has been suggested to possess negative charges [15]. Experiments were carried out in order to study the effect of negative charges of Reppal on the partitioning of proteins. Partitioning experiments for BSA and lysozyme with the amino acids β-alanine (p*I* 6.9 [16]) and glycine (p*I* 6.1 [17]) as buffers without any other salt in the system were done (Table 5). The top phase polymer was Ucon and the bottom phase polymers were Reppal or dextran. The proteins were partitioned at the p*I* of the buffers. By use of zwitterionic buffers it is possible to have a buffered phase system with zero electrical potential difference between the phases. BSA is negatively charged and lysozyme is positively charged, both at pH 6.1 and 6.9. In the system with Reppal, BSA was partitioned to the top phase while lysozyme was partitioned strongly to the bottom phase. In the system containing dextran as bottom phase polymer the opposite partitioning behaviour for the two proteins was obtained, BSA was partitioned to the bottom phase while lysozyme to the top phase. For both proteins the *K*-values were close to unity in the dextran systems.

We also examined how the buffer concentration, 10 and 100 m*M* sodium phosphate or triethylammonium phosphate buffer at pH 7.1, influenced the partitioning of two of the proteins (BSA and cytochrome c) in PEG–Reppal systems (Table 6). The concentration of buffer had a significant effect on the partitioning of both BSA and cytochrome c. BSA, negatively charged at pH 7.1, was partitioned to the top phase while cytochrome c, positively charged, was partitioned to the bottom phase. The partition coefficients were more extreme for both proteins at 10 m*M* buffer concentrations than at 100 m*M* concentration.

The results shown in Table 5 and the observation that the partition coefficients were more extreme at 10 m*M* than at 100 m*M* of the salts (Table 6) support the conclusion that Reppal has a small negative charge. A concentration of 10 m*M* of the salt is not enough to screen the negative charges on Reppal. The negative charge

Table 5
Partition coefficients of BSA, negatively charged, and lysozyme, positively charged, at pH 6.1 and 6.9

	Reppal–Ucon system		Dextran–Ucon system	
	BSA	Lysozyme	BSA	Lysozyme
Glycine	3.13	0.11	0.76	1.13
β-Alanine	3.69	0.18	0.64	1.14

The phase systems were 11% (w/w) Reppal–5% (w/w) Ucon–100 m*M* glycine, pH 6.1, or 100 m*M* β-alanine, pH 6.9, and 5.1% (w/w) dextran–4.4% (w/w) Ucon–100 m*M* glycine or 100 m*M* β-alanine.

Table 6
Partition coefficients of BSA, negatively charged, and cytochrome C, positively charged, at pH 7.1. All systems were in 10 or 100 m*M* sodium phosphate (NaP), pH 7.1, and 10 or 100 m*M* triethylammonium phosphate (Et_3NP), pH 7.1. The phase systems were 13.8% (w/w) Reppal–6.5% (w/w) PEG

	10 m*M* salt		100 m*M* salt	
	BSA	Cytochrome C	BSA	Cytochrome C
NaP	3.16	0.18	1.49	0.43
Et_3NP	7.4	0.12	2.62	0.49

on Reppal must, however, be small, otherwise the phase separation with the uncharged PEG and EO–PO copolymers would be strongly salt dependent [26], which was not observed.

4. Conclusions

A protein with a relatively hydrophobic surface can be partitioned to a phase containing a thermoseparating EO–PO copolymer. The optimal partitioning is obtained by using a hydrophobic counterion. The increase of polymer hydrophobicity, e.g. by using polymers with a high content of propylene oxide, will then enhance the salt effects. The top phase polymer $EO_{30}PO_{70}$ used in this study is also advantageous because of the low cloud point, which reduces the risk for denaturation in the temperature-induced phase separation.

Acknowledgement

This research is supported by a grant from the Swedish Research Council for Engineering Sciences (TFR).

Abbreviations

BSA	bovine serum albumin
PEG	polyethylene glycol
EO	ethylene oxide
PO	propylene oxide
CP	cloud point
NaP	sodium phosphate
Et_3NP	triethylammonium phosphate
HIC	hydrophobic interaction chromatography
Trp	tryptophan

References

[1] P.-Å. Albertsson, Partition of Cell Particles and Macromolecules, Wiley, New York, 3rd ed., 1986.
[2] P.A. Harris, G. Karlström and F. Tjerneld, Bioseparations, 2 (1991) 237–246.
[3] P.A. Alred, F. Tjerneld, A. Kozlowski and J. Milton Harris, Bioseparation, 2 (1992) 363–373.
[4] P.A. Alred, A. Kozlowski, J. Milton Harris and F. Tjerneld, J. Chromatogr. A, 659 (1994) 289–298.
[5] F. Tjerneld, S. Berner, A. Cajarville and G. Johansson, Enz. Microbiol. Technol., 8 (1986) 417–423.
[6] S. Sturesson, F. Tjerneld and G. Johansson, Appl. Biochem. Biotechnol., 26 (1990) 281–295.
[7] H.-O. Johansson, G. Karlström and F. Tjerneld, Macromolecules, 26 (1993) 4478–4483.
[8] G. Johansson, Acta Chem. Scand. B, 28 (1974) 873–882.
[9] M. Carlsson, P. Linse and F. Tjerneld, Macromolecules, 26 (1993) 1546–1554.
[10] M.M. Bradford, Anal. Biochem., 72 (1976) 248–254.
[11] P.K. Smith, R.I. Krohn, G.T. Hermanson, A.K. Mallia, F.H. Gartner, M.D. Provenzano, E.K. Fujimoto, N.M. Goeke, B.J. Olson and D.C. Klenk, Anal. Biochem., 150 (1985) 76–85.
[12] F. Tjerneld, unpublished results.
[13] R.F. Modlin, P.A. Alred and F. Tjerneld, J. Chromatogr. A, 668 (1994) 229–236.
[14] W. Melander, C. Horvath, Arch. Biochem. Biophys., 183 (1993) 200–215.
[15] H. Walter and E.J. Krob, J. Chromatogr., 441 (1988) 261–273.
[16] R.M.C. Dawson, D.C. Elliot, W.H. Elliot and K.M. Jones, Data for Biochemical Research, Clarendon Press, Oxford, 3rd ed., 1986.

[17] CRC Handbook of Chemistry and Physics, CRC Press, Boca Raton, FL, 66th ed., 1985.
[18] E. Keshavarz and S. Nakai, Biochem. Biophys. Acta, 576 (1979) 269–279.
[19] V.P. Shanbhag and C.G. Axelsson, Eur. J. Biochem., 60 (1975) 17–22.
[20] Min Lu, P.-Å. Albertsson, G. Johansson and F. Tjerneld, J. Chromatogr. A, 668 (1994) 215–228.
[21] J.A. Asenjo, A.S. Schmidt, F. Hachem and B.A. Andrews, J. Chromatogr. A, 668 (1994) 47–54.
[22] C. Hassinen, K. Köhler and A. Veide, J. Chromatogr. A, 668 (1994) 121–128.
[23] H.-O. Johansson, G. Karlström, B. Mattiasson and F. Tjerneld, Bioseparation, (1995) in press.
[24] H.A. McKenzie, Milk Proteins: Chemistry and Molecular Biology, Academic Press, New York, 1971.
[25] T. Peters, Adv. Protein Chem., 37 (1985) 161–245.
[26] L. Piculell, S. Nilsson, L. Falck and F. Tjerneld, Polym. Comm., 32 (1991) 158–160.
[27] G. Zubay, Biochemistry, Macmillan Publishing Company, New York, 2nd ed., 1988, p. 88.
[28] P.G. Righetti and T. Caravaggio, J. Chromatogr., 127 (1976) 1–28.
[29] M. Wahlgren, Ph.D. Thesis, University of Lund, Lund, 1992.
[30] C. Tanford and M.L. Wagner, J. Am. Chem. Soc., 76 (1954) 3331–3336.
[31] H. Theorell and Å. Åkesson, J. Am. Chem. Soc., 63 (1941) 1818–1820.
[32] T. Imoto, L.N. Johnson, A.C. North, D.C. Phillips and J.A. Rupley, in P.D. Boyer (Editor), The Enzymes, Vol. 7, Academic Press, New York, 1972, pp. 665–868.
[33] M. Dautrevaux, Y. Bolonger, K. Han and G. Biserte, Eur. J. Biochem., 11 (1969) 267–277.
[34] R.E. Dickerson, T. Takano, D. Eisenberg, O.B. Kallai, L. Samson, A. Cooper and E. Margoliash, J. Biol. Chem., 246 (1971) 1511–1535.

ELSEVIER

Journal of Chromatography A, 718 (1995) 81–88

JOURNAL OF CHROMATOGRAPHY A

Separation of phenylurea pesticides by ion-interaction reversed-phase high-performance liquid chromatography Diuron determination in lagoon water

M.C. Gennaro[a,*], C. Abrigo[a], D. Giacosa[a], L. Rigotti[a], A. Liberatori[b]

[a]*Department of Analytical Chemistry, University of Turin, Via P. Giuria 5, 10125 Torino, Italy*

[b]*Water Research Institute, National Council of Research (CNR), Via Reno 1, 00198 Roma, Italy*

First received 22 March 1995; revised manuscript received 7 June 1995; accepted 9 June 1995

Abstract

An ion-interaction HPLC method is developed for the separation of the phenylurea herbicides asulam, diuron, isoproturon, linuron and monuron. C_{18} was used as stationary phase and octylammonium phosphate as ion-interaction reagent, in the presence of methanol or acetonitrile as organic modifier.

Detection limits lower than 9 μg/l can be obtained without preconcentration steps. The method was applied to the analysis of diuron in a sample of lagoon water. Using liquid–liquid extraction, a diuron concentration of 42 μg/l was found.

1. Introduction

A reversed-phase ion-interaction chromatographic method is presented for the separation of the phenylurea herbicides asulam, diuron, fenuron, isoproturon, linuron and monuron.

Phenylurea derivatives, used as soil sterilants, find their main utilization in weed control. Linuron is preferentially used as a pre-emergence selective herbicide for cereals, vegetables and small fruit crops; fenuron and monuron are mainly used for general weed control in noncrop land, while diuron is principally recommended for the control of aquatic weeds and algae in farm ponds, dugouts, irrigation banks, ditches and canals [1,2].

Phenylurea herbicides are photochemically unstable [3,4] and little information is available about their long-term toxic effects and mutagenicity [5]. Only monuron has been implicated for possible carcinogenity.

These herbicides are water soluble and from the soil they can easily migrate to crops and enter the food chain. Depending on the particular rainfall conditions and soil properties, the herbicides can also reach ground waters where, due to the absence of microbial activity, degradation processes are very slow and accumulation phenomena can easily lead to toxic levels [6].

The Commission of the European Community, Drinking Water Directive 80/778 (CEC-DWD) indicates a maximum amount of 0.5 μg/l

*Corresponding author.

0021-9673/95/$09.50
SSDI 0021-9673(95)00659-1

of total herbicide and 0.1 μg/l for each constituent. No concentration is given for other surface waters.

In the literature HPLC and GC methods have been described for the determination of phenylurea herbicides in surface waters as well as in crops and vegetables [7–11].

The sensitivity required for drinking water analysis is generally reached through preconcentration steps. A variety of adsorbents–such as C_8, C_{18}, cyclohexyl, bonded-silica or styrene–divinyl–benzene based size-exclusion phases [11–20]–are used for solid-phase extraction (SPE) often in combination with on-line enrichment or column switching [11,21–29]. Graphitized carbon-black Carbopack cartridges are also employed [30]. Liquid–liquid extraction [31] and post-column derivatization with *o*-phthalaldehyde–2-mercaptoethanol [32] have been used and examples can be found of HPLC with particle-beam [14,16,33] and thermospray mass spectrometric detection [7,27].

An ion-interaction method described for the determination of asulam in apples makes use of sodium cholate as the ion-interaction reagent in the presence of tetramethylammonium hydrogensulfate, triethylamine, acetic acid and methanol [34].

This paper presents the development and the optimization of a new and sensitive ion-interaction HPLC chromatographic method for the separation and determination of asulam, monuron, diuron, fenuron, linuron and isoproturon. The separation of thiourea, phenylurea and ethylenethiourea, which can be regarded as their base-structures, is also studied.

2. Experimental

2.1. Apparatus

The chromatographic analyses were carried out with a Merck-Hitachi Lichrograph chromatograph Model L-6200 (Tokyo, Japan), equipped with a two-channel D-2500 Chromato-integrator, interfaced with a UV–Vis detector L-4200 and a L-3720 conductivity detector with a temperature control unit from the same firm.

Spectrophotometric determinations were performed with a UV–Vis Hitachi (Tokyo, Japan) Model 150-20 spectrophotometer.

pH measurements were performed with a Metrohm (Herisau, Switzerland) 654 pH meter equipped with a combined glass-calomel electrode.

2.2. Chemicals and reagents

Ultrapure water from Millipore (Milford, MA, USA) Milli-Q was used for the preparation of solutions. Methanol and acetonitrile LiChrosolv gradient grade solvents and thiourea were Merck (Darmstadt, Germany) reagents. Octylamine, ethylenethiourea, phenylurea and orthophosphoric acid were Fluka (Buchs, Switzerland) analytical grade chemicals. Asulam, diuron, fenuron, isoproturon, linuron, monuron were analytical grade LabService Analytica (Anzola dell Emilia, Bologna, Italy) chemicals. All other chemicals were Carlo Erba (Milano, Italy) analytical reagents.

2.3. Chromatographic analysis

Reversed-phase ion-interaction HPLC was employed according to methods already used in this laboratory for separations of anions and amines [35,36].

A 5-μm ODS-2 Spherisorb (Phase Separation, Deeside, UK) column was used, equipped with an RP-18 (5 μm) guard column (Lichrospher, Merck, Darmstadt, Germany). The mobile phase was an aqueous or an aqueous-organic solution of *n*-octylammonium–*o*-phosphate. It was prepared by adding the organic solvent to the amount of octylamine weighted to prepare a 5.0 m*M* solution. Orthophosphoric acid was added to obtain a pH of 6.4 ± 0.2. The pH thus obtained for the aqueous-organic solution was also reported as an "operational" pH value [37].

The chromatographic system was conditioned by passing the eluent through the column until a stable baseline signal was obtained; a minimum

of 1 h was necessary at flow-rate of 1.0 ml/min. After use, the column was washed and regenerated with flowing water (0.50 ml/min for 15 min), water–methanol (50:50, v/v) or water–acetonitrile (50:50, v/v) (0.50 ml/min for 1 h), and then with 100% methanol or acetonitrile (0.50 ml/min for 5 min).

Zero retention time (t_0) was evaluated through injection of sodium nitrate solutions (15.0 mg/l) and the conductometric detection of the unretained sodium ion.

Spectrophotometric detection at 240 nm was employed for herbicide analysis.

Our results fit the model according to which the ion-interaction reagent contained in the mobile phase is bound onto the surface of the stationary phase through adsorption and electrostatic forces, giving rise to an electrical double layer. The interaction properties of the original reversed-phase packing material are therefore modified. The modified surface is able to simultaneously retain anions and cations [35,38].

2.4. Preparation of the real sample

The lagoon sample was collected in 2.0-l pyrex glass bottles previously washed with 0.2 *M* hydrochloric acid and repeatedly rinsed with ultrapure water. During sampling bottles were rinsed twice with the lagoon water, then filled and tightly capped. The entire sample was filtered through Millipore 0.45-μm filters and stored at 4°C. Analysis was performed within three days after sampling.

A 1500-ml volume of sample was brought to pH 2.50 with hydrochloric acid and filtered through a 0.22-μm nylon 66 membrane filter. A 100-g amount of $NaClO_4$ was added, and then the sample was extracted three times with 40.0-ml aliquots of dichloromethane. The combined extracts were dehydrated with sodium sulfate, concentrated on a Rotovapor at 25°C under vacuum, evaporated to dryness under a stream of nitrogen, and subsequently diluted to a final volume of 1.5 ml with the mobile phase.

3. Results and discussion

Separation of thiourea, phenylurea and ethylenethiourea was achieved (see Table 1) using a 5.0 mmol/l aqueous solution of octylammonium phosphate as the mobile phase. The separation of the phenylurea pesticides required the addition of organic modifier to perform the elution within reasonable analysis times (without modifier elution times longer than 100 min were obtained). Two series of experiments were carried out with different amounts of methanol or acetonitrile, respectively. The capacity factors obtained are reported in Table 1 and Fig. 1 shows the ln k' values [$k' = (t_R - t_0)/t_0$, where k' is the capacity factor, t_R and t_0 the retention time and zero retention time, respectively] as a function of methanol concentration. The plots can be fitted by straight lines, the slopes of which are very close for all analytes considered. This result suggests that the dependence of retention time on methanol concentration does not seem to be predominantly correlated to the chemical structures of the analytes. This is in agreement with results previously found [39] and will be later discussed.

The results collected in Table 1 show that the optimal concentration of organic modifier which assures a good resolution together with short analysis time is 55% of methanol (at flow-rate of

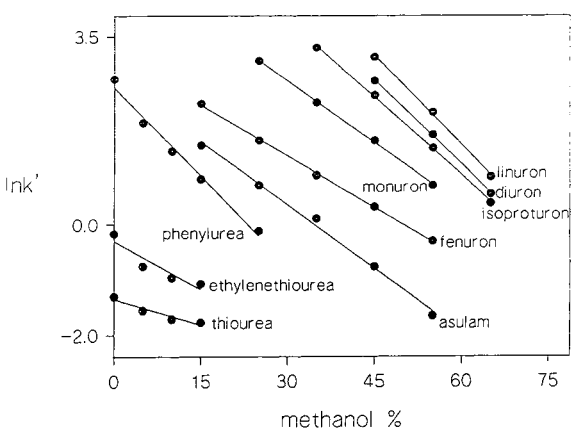

Fig. 1. Plots of ln k' vs. methanol percentages in the mobile phase.

Table 1
Capacity factors of the analytes as function of the organic modifier

Analyte	Mobile phase															
	Water–acetonitrile (65:35) (flow-rate 0.8 ml/min)	Water–methanol (45:55) (flow-rate 1.5 ml/min)	Aqueous 5.0 m*M* *n*-octylammonium–*o*-phosphate (flow-rate 0.7 ml/min)	5.0 m*M* *n*-Octylammonium–*o*-phosphate and acetonitrile at different percentages (flow-rate 0.8 ml/min)					5.0 m*M* *n*-Octylammonium–*o*-phosphate and methanol at different percentages (flow-rate 1.5 ml/min)							
				5	10	15	25	35	5	10	15	25	35	45	55	65
Diuron	11.34	7.70	–[b]	–[b]	–[b]	–[b]	–[b]	5.82	–[b]	–[b]	–[b]	–[b]	–[b]	14.30	5.20	1.76
Monuron	5.44	3.34	–[b]	–[b]	–[b]	–[b]	5.72	2.42	–[b]	–[b]	–[b]	20.84	9.62	4.66	2.03	*[a]
Linuron	21.15	11.16	–[b]	–[b]	–[b]	–[b]	–[b]	11.34	–[b]	–[b]	–[b]	–[b]	–[b]	22.49	7.97	2.38
Isoproturon	10.79	6.48	–[b]	–[b]	–[b]	–[b]	–[b]	5.26	–[b]	–[b]	–[b]	–[b]	26.83	10.87	4.04	1.48
Fenuron	1.19	1.52	–[b]	–[b]	–[b]	4.29	1.74	0.94	–[b]	–[b]	9.43	4.71	2.47	1.38	0.73	*[a]
Asulam	*[a]	*[a]	–[b]	–[b]	–[b]	1.83	0.52	0.23	–[b]	–[b]	4.31	2.06	1.12	0.46	0.19	*[a]
Thiourea	*[a]	*[a]	0.27	0.21	0.18	0.17	*[a]	*[a]	0.25	0.22	0.19	0.16	0.14	*[a]	*[a]	*[a]
Ethylenethiourea	*[a]	*[a]	0.84	0.47	0.38	0.34	*[a]	*[a]	0.58	0.43	0.38	0.25	0.21	*[a]	*[a]	*[a]
Phenylurea	*[a]	*[a]	14.88	6.58	3.85	2.30	0.89	*[a]	10.02	6.24	4.27	2.40	1.38	*[a]	*[a]	*[a]

[a] $k' = 0$.
[b] $k' > 30$.

1.5 ml/min) or 35% of acetonitrile (at flow-rate of 0.8 ml/min). Based on the absorbance/wavelength spectra recorded for the investigated analytes a detection wavelength of 240 nm was chosen.

Fig. 2 shows typical separations obtained for a mixture of the analytes (0.10 mg/l each) with *n*-octylammonium–*o*-phosphate as the interaction reagent in the presence of methanol (Fig. 2A) and acetonitrile (Fig. 2B).

Some suggestions can be made concerning the retention mechanism. As mentioned, ethylenethiourea, thiourea and phenylurea are separated (Table 1) with a mobile phase of an aqueous solution of *n*-octylammonium–*o*-phosphate. In such conditions, retention is likely due to ion-interaction mechanisms, based on the dynamic modification that the octylammonium–*o*-phosphate induces onto the surface of the stationary phase. On the other hand, in the separation of phenylurea pesticides, the addition of organic modifier was necessary in order to obtain analysis times of the order of 30 min. In these conditions, in order to distinguish if the retention process of phenylurea pesticides is really due to ion-interaction mechanisms and not to a conventional reversed-phase partition, chromatographic runs were performed in reversed-phase mode, i.e. by using a mobile phase of the same composition of methanol (55%) or acetoni-

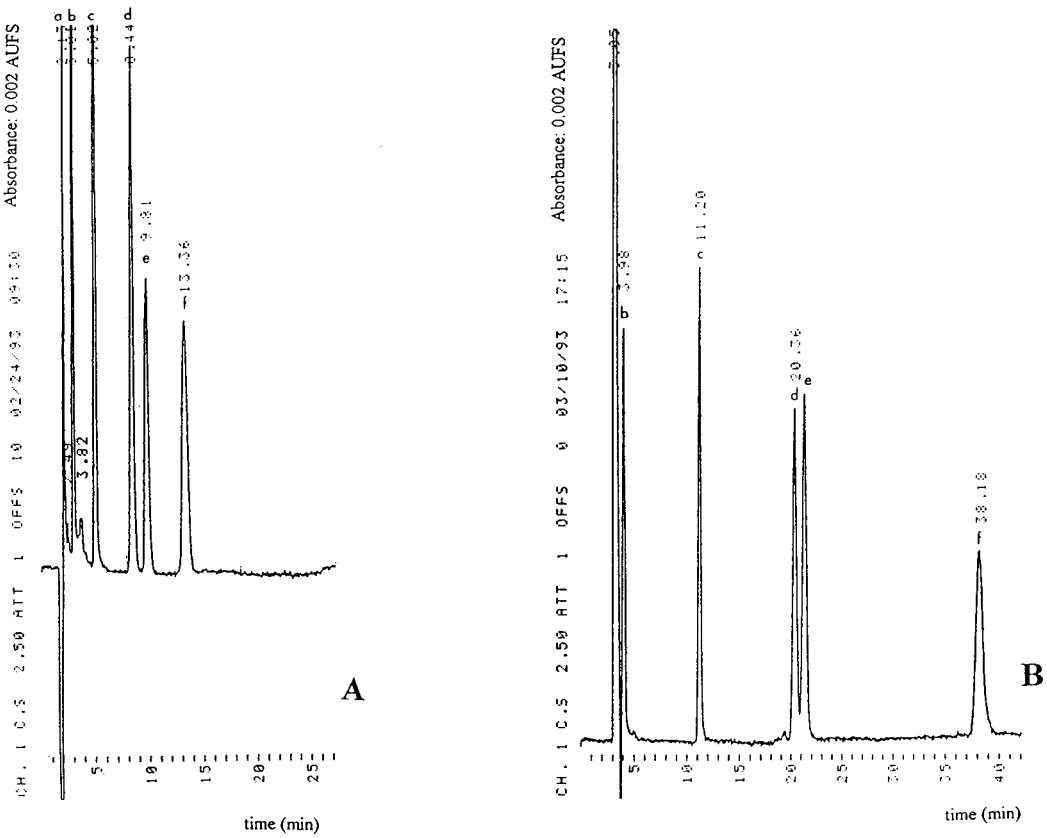

Fig. 2. Elution of the standards under optimized conditions. Stationary phase: Phase Separation ODS-2 Spherisorb, 250 × 4.6 mm I.D., 5 μm, endcapped. Spectrophotometric detection at 240 nm. Mobile phase: (A) 5.0 mmol/l octylammonium phosphate in water–methanol (45:55, v/v), pH 6.4, flow-rate: 1.5 ml/min; (B) 5.0 mmol/l octylammonium phosphate in water–acetonitrile (65:35, v/v), pH 6.4, flow-rate 0.8 ml/min. Peaks: a = asulam, b = fenuron, c = monuron, d = isoproturon, e = diuron, f = linuron.

trile (35%) as in the optimized separations presented in Fig. 2A and 2B, but without the presence of octylammonium–*o*-phosphate. As expected on the basis of their molecular structures, the analytes considered are also separated in reversed-phase mode, but retention times are different (Table 1) and resolution and sensitivity are generally poorer with respect to the elution with the mobile phase containing the ion-interaction reagent.

The result confirms that ion-interaction mechanisms are indeed taking place and the similar slopes of the $\ln k'$ vs. methanol concentration plots (Fig. 1) obtained for the different analytes can be ascribed to the predominant effect that the organic solvent exerts on the moiety adsorbed onto the surface of the stationary phase (and which affects all the analytes in the same way) rather than on the single structure of each analyte.

Calibration plots obtained in the concentration range 1.0–100.0 μg/l indicate a good linearity. From sensitivity data (S, expressed as the peak area given by the integrator for a 1.0 μg/l solution) and evaluation in the chromatogram of a peak area (a) corresponding to an average signal-to-noise ratio of 3, the limits of detection (LOD = a/S μg/l) for each analyte were evaluated. Detection limits were found to be lower than 9.0 μg/l for all analytes investigated. These concentrations are higher than those required for drinking water but are of the same order or lower than those generally reported for surface water, which range between 0.1 and 30 μg/l [16].

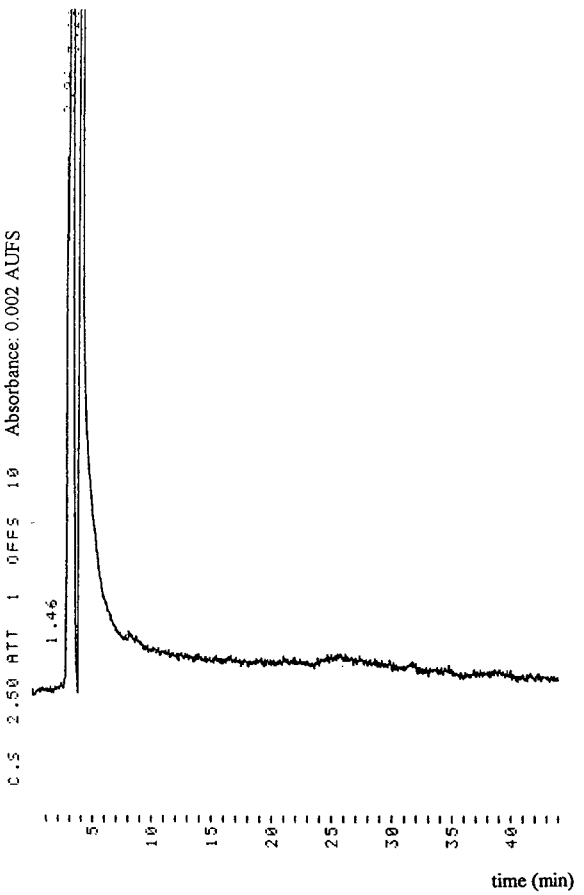

Fig. 3. Chromatographic analysis of a sample of lagoon water. Experimental conditions: Phase Separation ODS-2 Spherisorb column, 250 × 4.6 mm I.D., 5 μm; mobile phase: 5.0 mmol/l octylammonium phosphate in water–acetonitrile (65:35, v/v), pH 6.4, flow-rate 0.8 ml/min; spectrophotometric detection at 240 nm.

3.1. Application to real sample

The method was applied to the analysis of a sample of lagoon water collected in the tidal marsh of Palude di Cona (in the north-east of Venice lagoon) suspected to contain diuron, which is largely employed in river and sea waters for control of algal growth. A preliminary chromatographic run performed on a filtered sample of water under the optimized chromatographic conditions (Fig. 3) permits us to exclude the presence of diuron at a concentration close to or higher than the detection limit of the method (7 μg/l for diuron) and at the same time shows a very low matrix interference in the time window of the herbicide considered. It must in fact be considered that the ion-interaction technique is characterized by selective properties towards non-ionizable or high-molecular-mass species, properties which are particularly advantageous when dealing with complex matrices.

A preconcentration step was then performed for the lagoon water sample. Taking into account

the high boiling temperature of diuron, a preconcentration factor of 1000 was gained with the liquid–liquid extraction technique as described in the Experimental section. Preliminary experiments in triplicate, performed for standard solutions prepared by addition of 0.01 μg in 1000 ml of ultrapure water, gave a recovery of $87 \pm 2\%$. The limit of determination was determined by standard addition method and was found to be 10 μg/l.

Fig. 4A shows the chromatogram obtained for the 1000-fold preconcentrated sample of lagoon water. It can be seen that also in the concentrated sample the time window corresponding to the herbicide retention is interference free. By the standard addition method (an example is shown in Fig. 4B for the addition of 50 μg/l) a concentration of diuron of 42 ± 6 μg/l was estimated in the concentrated sample. This corresponds to an amount of at least 42 ng/l in the native sample.

As a conclusion, the method developed for the separation and determination of phenylurea herbicides is very suitable–also without preconcentration steps–for the analysis of surface waters with detection limits lower than 9 μg/l. The results obtained for a lagoon water sample show that with a preconcentration step, the method could be advantageously employed in the analysis of drinking water, taking also into account its much lower matrix interference with respect to sea water.

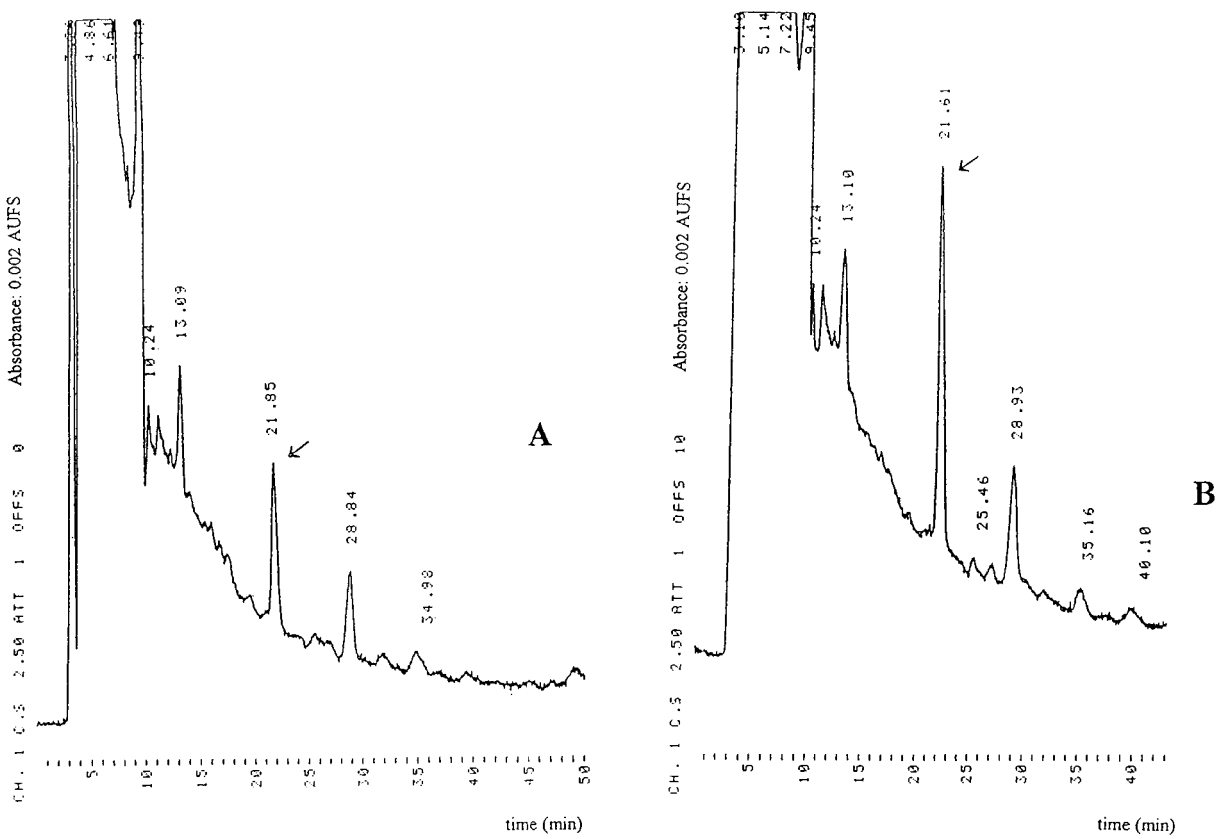

Fig. 4. Chromatographic analysis of the lagoon water sample after 1000-fold preconcentration. Experimental conditions as in Fig. 3. The arrows indicate the diuron peak before (A) and after (B) spiking with 50.0 μg/l of diuron.

Acknowledgement

This work was supported by the Consiglio Nazionale delle Ricerche (CNR), Roma, Comitato Nazionale Scienze e Tecnologie Ambiente e Habitat.

References

[1] Herbicide Handbook, 4th ed., Weed Science Society of America, Champaign, IL, 1979.
[2] J.D. Fryer and R.J. Makepeace (Editors), Weed Control Handbook, Vol. 1, 6th ed., Blackwell, Oxford, 1977.
[3] G.D. Hill, J.W. McGahen, H.M. Baker, D.W. Finnerty and C.W. Bingeman, Agron. J., 47 (1955) 93.
[4] D.G. Crosby, in P.C. Kearney, D.D. Kaufman (Editors), Herbicides, Chemistry, Degradation, and Mode of Action, Vol. 2, 2nd ed., Marcel Dekker, New York, NY, 1975, Ch. 18.
[5] M. Muccinelli, Prontuario dei Fitofarmaci, 6th ed., Edizioni Agricole, Bologna (Italy), 1990.
[6] R. Grover, A.E. Smith and H.C. Korven, Can. J. Plant Sci., 60 (1980) 185.
[7] C.H. Liu, G.C. Mattern, X. Yu, R.T. Rosen and J.D. Rosen, J. Agric. Food Chem., 39 (1991) 718.
[8] G.C. Mattern, C.H. Liu, J.B. Louis and J.D. Rosen, J. Agric. Food Chem., 39 (1991) 700.
[9] A. D'Amato, I. Semeraro and C. Bicchi, J. Assoc. Off. Anal. Chem. Int., 76 (1993) 657.
[10] G.E. Miliadis, P.A. Siskos and G.S. Vasilikiotis, J. Assoc. Off. Anal. Chem., 73 (1990) 435.
[11] A.J. Cessna, J. Liq. Chromatogr., 11 (1988) 725.
[12] G. Henze, A. Meyer and J. Hausen, Fresenius J. Anal. Chem., 346 (1993) 761.
[13] C. Schlett, Fresenius J. Anal. Chem., 339 (1991) 344.
[14] M.J. Incorvia Mattina, J. Chromatogr., 549 (1991) 237.
[15] A. Laganà, G. Fago, A. Marino and B. Pardo-Martinez, Chromatographia, 38 (1994) 88.
[16] A. Cappiello, G. Famiglini and F. Bruner, Anal. Chem., 66 (1994) 1416.
[17] A. Balinova, J. Chromatogr., 643 (1993) 203.
[18] D. Barceló, S. Chiron, S. Lacorte, E. Martinez, J.S. Salau and M.C. Hennion, Trends Anal. Chem., 13 (1994) 352.
[19] W. Dedek, K.D. Wenzel, F. Luft, H. Oberländer and B. Mothes, Fresenius Z. Anal. Chem., 328 (1987) 484.
[20] D. Puig and D. Barceló, J. Chromatogr. A, 673 (1994) 55.
[21] F.A. Maris, R.B. Geerdink, R.W. Frei and U.A.Th. Brinkman, J. Chromatogr., 323 (1985) 113.
[22] T. Suzuki, K. Yaguchi and I. Kano, J. Chromatogr., 643 (1993) 173.
[23] U.A.Th. Brinkman, J. Slobodnik and J.J. Vreuls, Trends Anal. Chem., 13 (1994) 373.
[24] C.E. Goewie, P. Kwakman, R.W. Frei, U.A.Th. Brinkman, W. Maasfeld, T. Seshadri and A. Kettrup, J. Chromatogr., 284 (1984) 73.
[25] S. Chiron and D. Barceló, J. Chromatogr., 645 (1993) 125.
[26] C.E. Goewie and E.A. Hogendoorn, J. Chromatogr., 410 (1987) 211.
[27] S. Chiron, S. Dupas, P. Scribe and D. Barceló, J. Chromatogr. A, 665 (1994) 295.
[28] E.A. Hogendoorn, C.E. Goewie and P. van Zoonen, Fresenius J. Anal. Chem., 339 (1991) 348.
[29] E.A. Hogendoorn, U.A. Th. Brinkman and P. van Zoonen, J. Chromatogr., 644 (1993) 307.
[30] A. Di Corcia and M. Marchetti, Anal. Chem., 63 (1991) 580.
[31] W. Schüssler, Chromatographia, 27 (1989) 431.
[32] C.J. Miles and H. Anson Moye, Anal. Chem., 60 (1988) 220.
[33] D.R. Doerge and C.J. Miles, Anal. Chem., 63 (1991) 1999.
[34] F. Garcia Sanchez, A. Navas Diaz and A. Garcia Pareja, J. Chromatogr. A, 676 (1994) 347.
[35] E. Marengo, M.C. Gennaro and C. Abrigo, Anal. Chem., 64 (1992) 1885.
[36] M.C. Gennaro, C. Abrigo and E. Marengo, J. Liq. Chromatogr., 17 (1994) 1231.
[37] R.M. Lopes-Marques and P.J. Schoenmakers, J. Chromatogr., 592 (1992) 157.
[38] M.C. Gennaro and P.L. Bertolo, J. Chromatogr., 509 (1990) 147.
[39] M.C. Gennaro, C. Abrigo, E. Pobozy and E. Marengo, J. Liq. Chromatogr., 18 (1994) 311.

ELSEVIER

Journal of Chromatography A, 718 (1995) 89–97

JOURNAL OF CHROMATOGRAPHY A

Identification of nonvolatile components in lemon peel by high-performance liquid chromatography with confirmation by mass spectrometry and diode-array detection

Alessandro Baldi[a], Robert T. Rosen[b], Elaine K. Fukuda[b], Chi-Tang Ho[a,*]

[a]*Department of Food Science, Cook College, New Jersey Agricultural Experimental Station, Rutgers University, New Brunswick, NJ 08903, USA*

[b]*Center for Advanced Food Technology, Cook College, New Jersey Agricultural Experimental Station, Rutgers University, New Brunswick, NJ 08903, USA*

First received 14 November 1994; revised manuscript received 13 June 1995; accepted 13 June 1995

Abstract

High-performance liquid chromatography (HPLC) with diode-array detection and thermospray mass spectrometry (LC–TSP-MS) were used to identify nonvolatile compounds in a lemon peel extract. In this way, the retention time characteristics, the UV–Vis spectra and the mass spectra provide structural information without the necessity of isolating the individual compounds. The lemon peel extract was separated into petroleum ether, chloroform, ethyl acetate and butanol fractions. The chloroform fraction was found to contain mainly the limonoids; the petroleum ether fraction contained coumarins, phenyl propanoid glycosides and flavones-C-glucosides; and the ethyl acetate fraction which had the best antioxidant activity, was found to contain flavonols, flavones-O-glycosides and flavonones.

1. Introduction

The chemical components of *Citrus* have an important role in the human diet and in human health. Their effectiveness in decreasing erythrocyte aggregation and blood coagulation in vitro [1] and, for some of them, the anticarcinogenic activity in vitro and in vivo are well known [2]. In the genus *Citrus*, the lemon (*Citrus limon* Burm. *f.*) is one of the most important crops. The flavonoid content of lemon peel has been studied since 1936 when Szent-Gyorgy [3] extracted "citrin", a mixture of lemon flavonoids formerly regarded as a vitamin. Since then, many studies have been conducted on this subject. The lemon peel bioflavonoids are characterized by the presence of four groups of flavonoids: flavones-O-glycosides, flavones-C-glycosides, flavonols, flavanones. The first group is very common among fruits, and in the lemon peel luteolin-7-rutinoside and diosmetin-7-rutinoside (diosmin) have been found [4].

* Corresponding author.

0021-9673/95/$09.50
SSDI 0021-9673(95)00676-1

Flavones-C-glycosides are broadly distributed in the plant kingdom [5]. Park et al. [6] found four flavones-di-C-glycosides in the lemon peel: 6,8-di-C-glucosyl-luteolin; 6,8-di-C-glucosyl-apigenin; 6,8-di-C-glycosyl-chrisoeriol; 6,8-di-C-glucosyl-diosmetin. The flavonol group in lemon peel is characterized by the presence of rutin (quercetin-3-O-rutinoside) and three polymethoxylated compounds: 3,5,7,4′-tetrahydroxy-6,8,3′-trimethoxy-flavone (limocitrol); 3,5,7,4′-tetrahydroxy-8,3′-dimethoxy-flavone (limocitrin); 3,5,7,3′-tetrahydroxy-6,8,4′-trimethoxy-flavone (isolimocitrol). These are less polar compounds compared to the other lemon bioflavonoids. Polymethoxylated flavones are present especially in the genus *Citrus* and are located in the flavedo [7]. These latter compounds are extremely interesting because of their physiological effects on animal and man. They have effect on high blood viscosity syndrome and, in addition, they possess antimicrobial and antiviral activity [8]. The last group is that of the flavanones. These compounds are very important in the genus *Citrus* because of their chemotaxonomic properties [9] and also because of their relation to taste and bitterness. The compounds present in lemon peel are the following three glycosides: hesperitin-7-rutinoside (hesperidin), naringenin-7-rutinoside and eriodictyol-7-rutinoside (eriocitrin) [10,11]. Several other groups of polyphenols are known to be present in lemon peel. Among those, phenolic acids and phenyl propanoids (coumarins, phenyl propanoid glycosides) have been reported [7]. The objective of this study was to develop a fast and reliable method to determine the presence and distribution of the various components in a lemon peel extract. High-performance liquid chromatography (HPLC) with diode-array detection (DAD) and thermospray mass spectrometry (LC–TSP-MS) were used to identify several compounds. In this way, the retention time characteristics, the UV–Vis spectra and the mass spectra provide structural information without the necessity of isolating the individual compounds. The methodology included a series of liquid–liquid extractions and optimization of the chromatographic conditions for HPLC–DAD and HPLC–MS analysis for each extract. Finally, the antioxidant activity of each extract was evaluated.

2. Experimental

2.1. Sample preparation

A dried lemon peel bioflavonoid extract (M. Phil Yen, New York, NY, USA) was used as raw material to analyze the flavonoid content. An amount of 2 g of lemon peel was extracted three times with 50 ml of 80% ethanol containing 0.1% HCl. The extracts were filtered with Whatman No. 1 filter paper and the ethanol was removed with a rotary evaporator at 30°C under vacuum. The residue was dissolved in 50 ml of water and extracted three times with 50 ml of petroleum ether, chloroform, ethyl acetate and water-saturated butanol, respectively (see Fig. 1). Solvents from all fractions were removed with a rotary evaporator at 30°C under vacuum to obtain the petroleum ether extract, chloroform extract, ethyl acetate extract and butanol extract. The residues were dissolved in 2 ml of water–methanol (1:1) for HPLC analysis, utilizing diode-array detection (DAD) and thermospray mass spectrometry (LC–TSP-MS).

2.2. HPLC–DAD analysis

The equipment used for the HPLC–DAD analysis consisted of a HPLC HP 1090A (Hewlett-Packard, Palo Alto, CA, USA) with a diode-array detector HP 1040 managed by a Workstation HP Series 9000. A Waters-Millipore Novapak C_{18} column (Waters, Milford, USA), 150×4.6 mm, 5 μm, supplied with a 10-mm precolumn packed with the same material, was used. The eluents were: 0.16% formic acid–0.20% triethylamine in water and methanol (Optima grade). The flow-rate was adjusted to 0.9 ml/min and the injected volume of each extract was 20 μl. The effluent was monitored at 254, 280 and 360 nm and scanned between 190 and 400 nm by the diode-array detector.

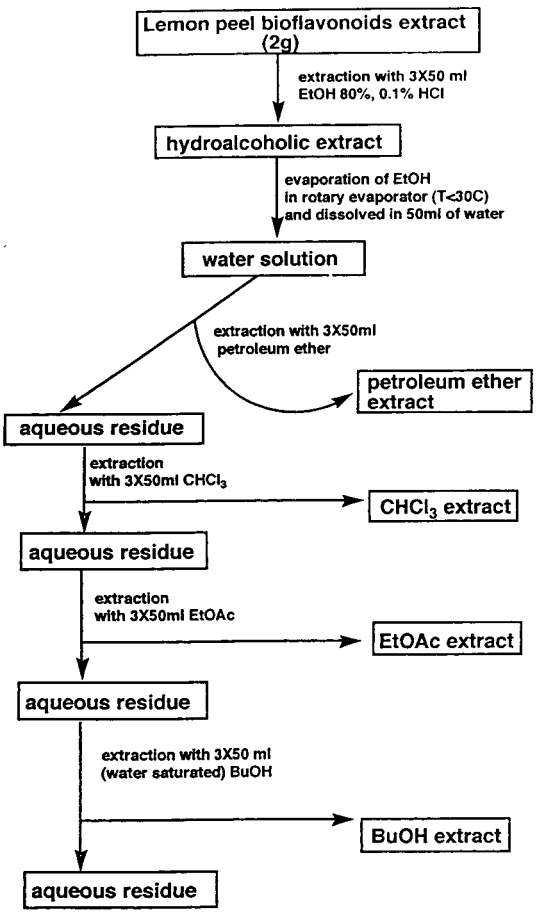

Fig. 1. Extraction and fractionation method.

2.3. HPLC–MS analysis

A HPLC Varian 9010 (Walnut Creek, CA, USA) with ABI Spectroflow 783 UV–Vis detector coupled with a Vestec Model 201 mass spectrometer was used for the HPLC–MS analysis. The interface was of the thermospray type and the mass spectrometer operated in the negative-ion thermospray discharge ionization mode. Sensitivity was enhanced using a triethylammonium formate buffer at the concentration described above for the HPLC–DAD analysis [12]. Methanol was used as organic modifier. The ion source temperature was 250°C and negative-ion spectra between 200 and 700 u were recorded at 3.2 s per scan.

2.4. Hydrolysis conditions

Acidic hydrolysis on the EtOAc extract was performed. The EtOAc extract (2 ml) was evaporated, dissolved in 6 *M* HCl solution and heated for 1 h at 105°C. Further extraction with EtOAc gave an extract that was analyzed by HPLC–DAD.

2.5. Antioxidative activity test

Pure lard (Hatfield Quality Meats, Hatfield, PA, USA) without any additives was used as substrate to evaluate the antioxidant activities of lemon peel extracts. The test samples were prepared by mixing the extracts with lard in 0.02% concentration on weight basis. A 670 Rancimat (Metrohm, Herisau, Switzerland) was used. A portion of 2.5 g of each test sample was loaded into the reaction vessel cylinder. Six different samples were examined in one batch: the four extracts, a sample added with BHT (butylated hydroxytoluene) and the control (only lard). The air supply was maintained at 20 ml/min and the heating temperature was kept at 100°C throughout the experiment.

3. Results and discussion

Good separation of the compounds present in the different extracts was obtained using several linear solvent gradients. Fig. 2 shows a representative chromatogram acquired using HPLC–DAD analysis. UV–Vis spectra of each peak were acquired, some of them showing the typical absorbance of the described groups of flavonoids. Both DAD and MS spectra were obtained for each compound. In this way the data obtained from the different analytical systems were compared and combined. The compounds were identified by their retention time characteristics, UV–Vis and mass spectra, specifically the structure of the aglycons was determined by HPLC–DAD.

Several flavanones, flavonols and flavones were found in the EtOAc extract of lemon peel by LC–TSP-MS. Peaks at *m/z* 596, 450 and 288

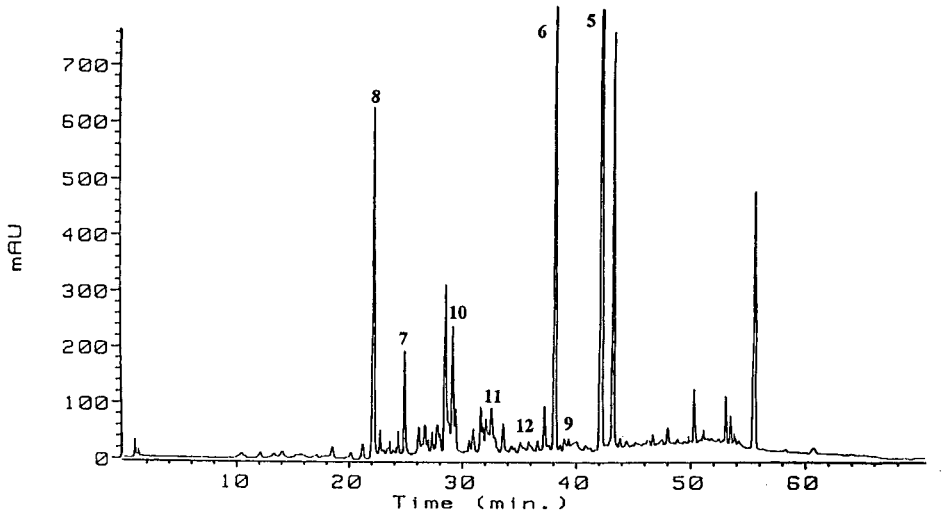

Fig. 2. Analytical HPLC separation of petroleum ether extract (254 nm).

corresponding respectively to the molecular ion $[M]^-$, the fragment resulting from the loss of a rhamnosyl moiety $[M-146]^-$ and the fragment resulting from the loss of a further glucose moiety, another 162, were observed in the mass spectrum of the compound identified as eriodictyol-7-rutinoside (Fig. 3). The mass spectra of the two other flavanones identified (hesperitin-7-rutinoside, naringenin-7-rutinoside) had similar patterns (Table 1). These three compounds showed UV–Vis spectra with a strong absorbance at 286 nm and a secondary absorbance at 328 nm, confirming the structure of the aglycones. Rutin, quercitin-3-rutinoside,

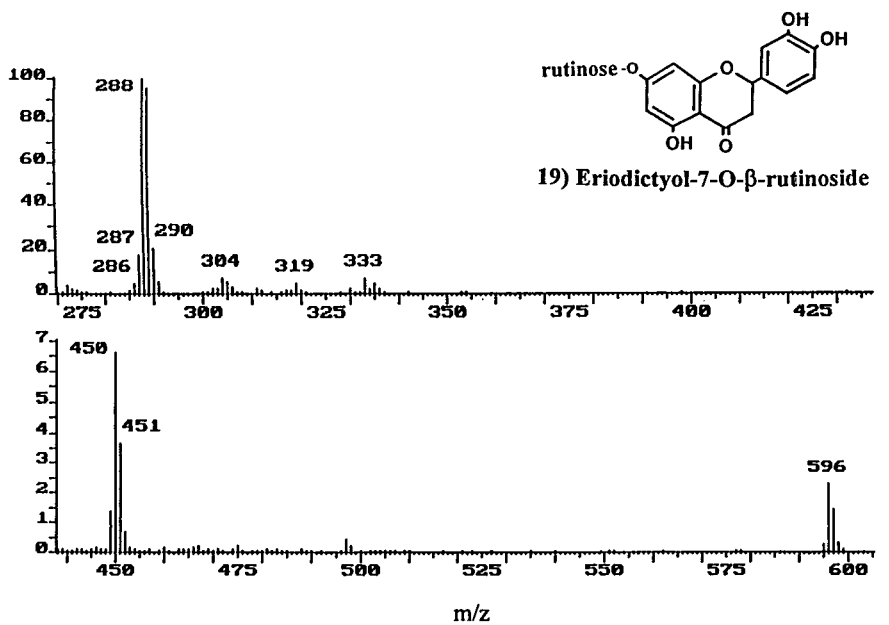

Fig. 3. Mass spectrum of eriodictyol-7-rutinoside.

Table 1
List of identified compounds and MS fragments

Compounds	Observed masses	UV maxima	Extract
Limonoids			
(1) Nomilinic acid	$[M-1]^-$ = 531		$CHCl_3$ extract
(2) Limonin	$[M]^-$ = 470	285	$CHCl_3$ extract
(3) Limonoic acid	$[M-1]^-$ = 487		$CHCl_3$ extract
(4) Limonin 17-β-D-glucoside	$[M-1]^-$ = 649		$CHCl_3$ extract
Phenyl propanoids			
Coumarin			
(5) Isoimperatorin	$[M]^-$ = 282	312–267–250–244	petroleum ether extract
(6) Bergamottin	$[M]^-$ = 328	299–263–249–243	petroleum ether extract
(7) Bergaptol	$[M]^-$ = 196	313–269	petroleum ether extract
(8) Limettin derivative a	$[M]^-$ = 260		petroleum ether extract
(9) Limettin derivative b	$[M]^-$ = 328	324–250–247–222	petroleum ether extract
Phenyl propanoids glycosides			
(10) Citrusin A	$[M]^-$ = 520; $[M-162]^-$ = 358		petroleum ether extract
Flavonoids			
Flavones-C-glucosides			
(11) 6,8-di-C-glucopyranosyl-luteolin	$[M]^-$ = 642	344–274–257	petroleum ether extract
(12) 6,8-di-C-glucopyranosyl-apigenin	$[M]^-$ = 626	335–274	
Flavonols			
(13) Limocitrol	$[M]^-$ = 376; $[M-30]^-$ = 346; $[M-60]^-$ = 316	377–350sh–275–260	EtOAc extract
(14) Isolimocitrol	$[M]^-$ = 376; $[M-30]^-$ = 346; $[M-60]^-$ = 316	375–350sh–276–260	EtOAc extract
(15) Limocitrin	$[M]^-$ = 346; $[M-30]^-$ = 316	378–340sh–273sh–259	EtOAc extract
(16) Rutin	$[M]^-$ = 610; $[M-146]^-$ = 464; $[M-308]^-$ = 302	361–258	EtOAc extract
Flavones-O-glucosides			
(17) Diosmetin-7-rutinoside	$[M]^-$ = 608; $[M-308]^-$ = 300	344–268–253	EtOAc extract
Flavanones			
(18) Hesperitin-7-rutinoside (hesperidin)	$[M]^-$ = 610; $[M-146]^-$ = 464; $[M-308]^-$ = 302	330–286	EtOAc extract
(19) Eriodictyol-7-rutinoside (eriocitrin)	$[M]^-$ = 596; $[M-146]^-$ = 450; $[M-308]^-$ = 288	330–286	EtOAc extract
(20) Naringenin-7-rutinoside	$[M]^-$ = 580; $[M-146]^-$ = 434; $[M-308]^-$ = 272	328–284	EtOAc extract

was also present in the EtOAc extract. This flavonol showed a mass spectrum similar to hesperitin-7-rutinoside with signals at m/z 610, 464 and 302, but the UV–Vis spectrum is totally different, showing maxima at 361 and 258 nm.

Methoxylated flavonols were also found in the EtOAc extract. Signals at m/z 376 $[M]^-$, 346 $[M-30]^-$, and 316 $[M-60]^-$ corresponding to the molecular ion and to one and two losses of methoxy groups were observed in the mass spectrum of the compound identified as limocitrol (Fig. 4). The isomer isolimocitrol, whose mass spectrum showed the same signals as above, was identified using UV–Vis spectra data [11]. Limocitrin, another polymethoxylated flavonol, showed a mass spectrum with signals at m/z 346 $[M]^-$ and 316 $[M-30]^-$. These last three compounds are the only polymethoxylated flavonols present in the lemon peel, while other citrus species show flavones with a higher number of methoxylations.

The only flavone we found in the lemon peel EtOAc extract was diosmetin-7-rutinoside, showing a mass spectrum with signals at m/z 608 and 300 corresponding respectively to the molecular ion $[M]^-$ and to the fragment resulting from

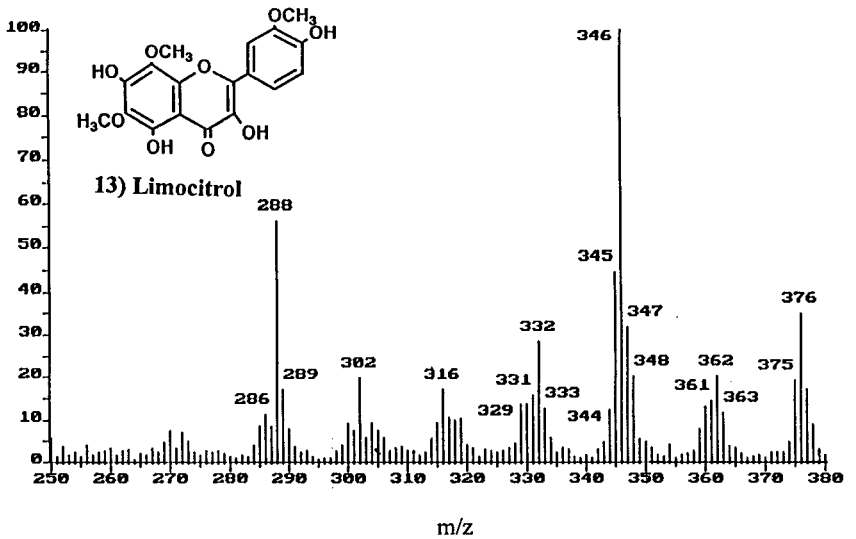

Fig. 4. Mass spectrum of limocitrol.

the loss of a rutinose moiety $[M-308]^{-}$. The three polymethoxylated flavonols together with quercitin, diosmetin, eriodictyol, hesperitin and naringenin, were found in the hydrolyzed EtOAc extract. Retention time characteristics, the comparison with several standards injected under the same conditions and the acquired UV–Vis spectra, allowed the confirmation of the presence of the above aglycons. Finally, the presence of two flavones-C-glucosides was presumed from the interpretation of the mass spectral data of two peaks present in the petroleum ether extract.

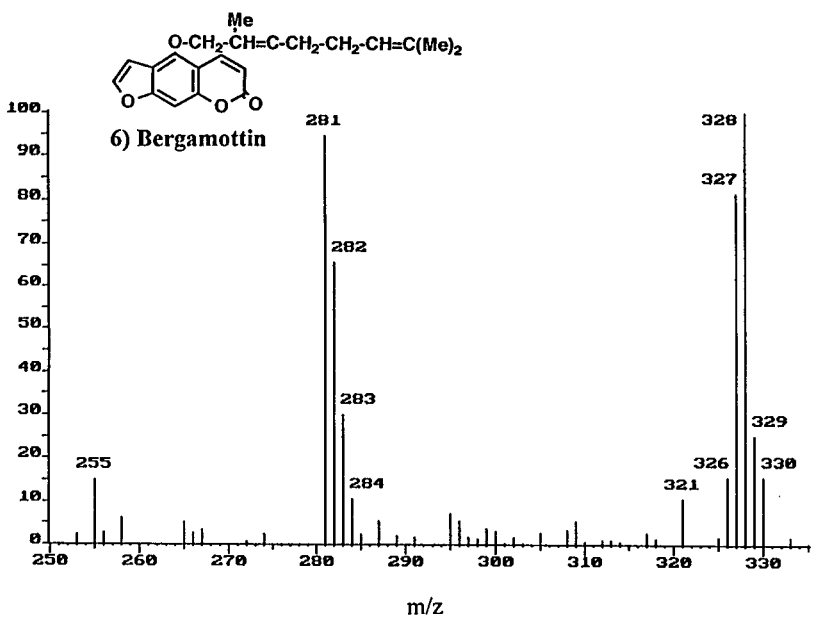

Fig. 5. Mass spectrum of bergamottin.

They show respectively a signal at m/z 642 and 626, corresponding to the molecular ions of 6,8-di-C-glucopyranosyl-luteolin and 6,8-di-C-glucopyranosyl-apigenin. The acquired UV–Vis spectra are consistent with data from the literature [11].

As shown in Table 1, flavonoids were found mainly in the EtOAc extract. The analysis of petroleum ether, chloroform and butanol extracts allowed to identify several components belonging to other groups of compounds. Particularly in the petroleum ether extract several coumarins were found according to the data in the literature [13]. These oxygen heterocyclic compounds have been investigated extensively and are useful taxonomic markers [14]. As for flavonoids, data from UV–Vis and mass spectra were used to identify the structure of each compound. Mass spectra showed the molecular ion of isoimperatorin, bergamottin, bergaptol and two limettin derivatives (Fig. 5 shows the mass spectrum of bergamottin). UV–Vis spectra were again consistent with data in the literature [13,14]. Citrusin A, a phenyl propanoid glucoside previously reported by Matsubara et al. [15], was found in the petroleum ether extract. The mass spectrum showed two main signals corresponding to the molecular ion $[M]^-$ (m/z 520) and to the loss of the glucose moiety $[M-162]^-$ (m/z 358), corresponding to the aglycon. The structures of these compounds are shown in Fig. 6.

Several limonoids were found to be present in the chloroform extract. Limonoids are triterpene derivatives found in the *Rutaceae* family and in particular in genus *Citrus*. They are important because some give a strong bitterness to citrus juices. Among those, limonin is the main bitter compound. A compound showing a mass spectrum consistent with the structure of limonin was found in the chloroform extract. The mass spectrum showed the molecular ion $[M]^-$ (m/z 470) (Fig. 7). Limonoic acid A ring lactone, which is the equilibrium form of limonin in the fruit tissues [16], showed an $[M-1]^-$ at m/z 487. Limonin 17-β-glucoside was also present and showed a mass spectrum with a signal at m/z 650 corresponding to the molecular ion and a weak

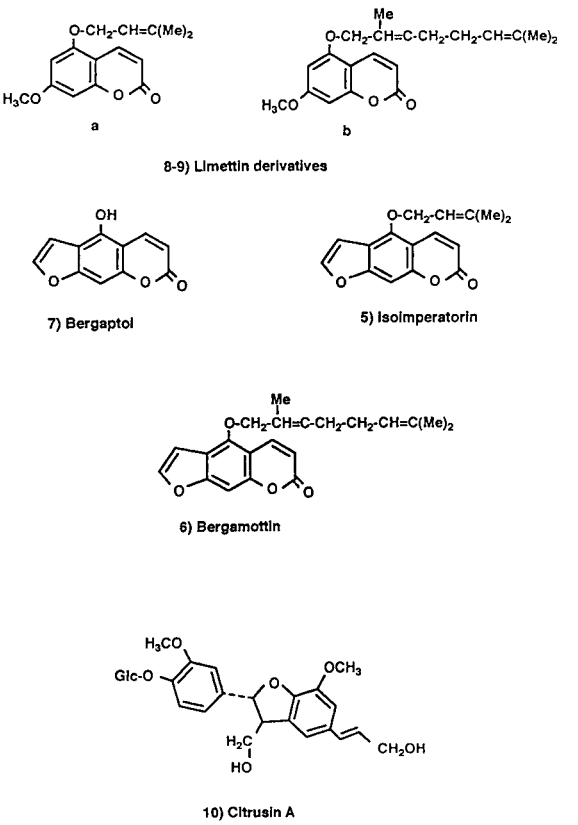

Fig. 6. Structures of identified phenyl-propanoids in the lemon peel.

signal at $[M-162]^-$ (m/z 488) corresponding to the loss of a sugar moiety. Finally, nomilic acid gave a mass spectrum with an $[M-1]^-$ ion at m/z 531. This data is consistent with that in the literature [16,17].

3.1. Results of antioxidant activities test

The antioxidant activities of lemon bioflavonoid extracts were measured by the Rancimat method. The induction times of lard with the extracts are shown in Table 2. Longer induction times suggest stronger antioxidant activities. Only the ethyl acetate fraction showed antioxidant activity, although the induction time is lower than that of the control sample with BHT. All other fractions did not show any antioxidant

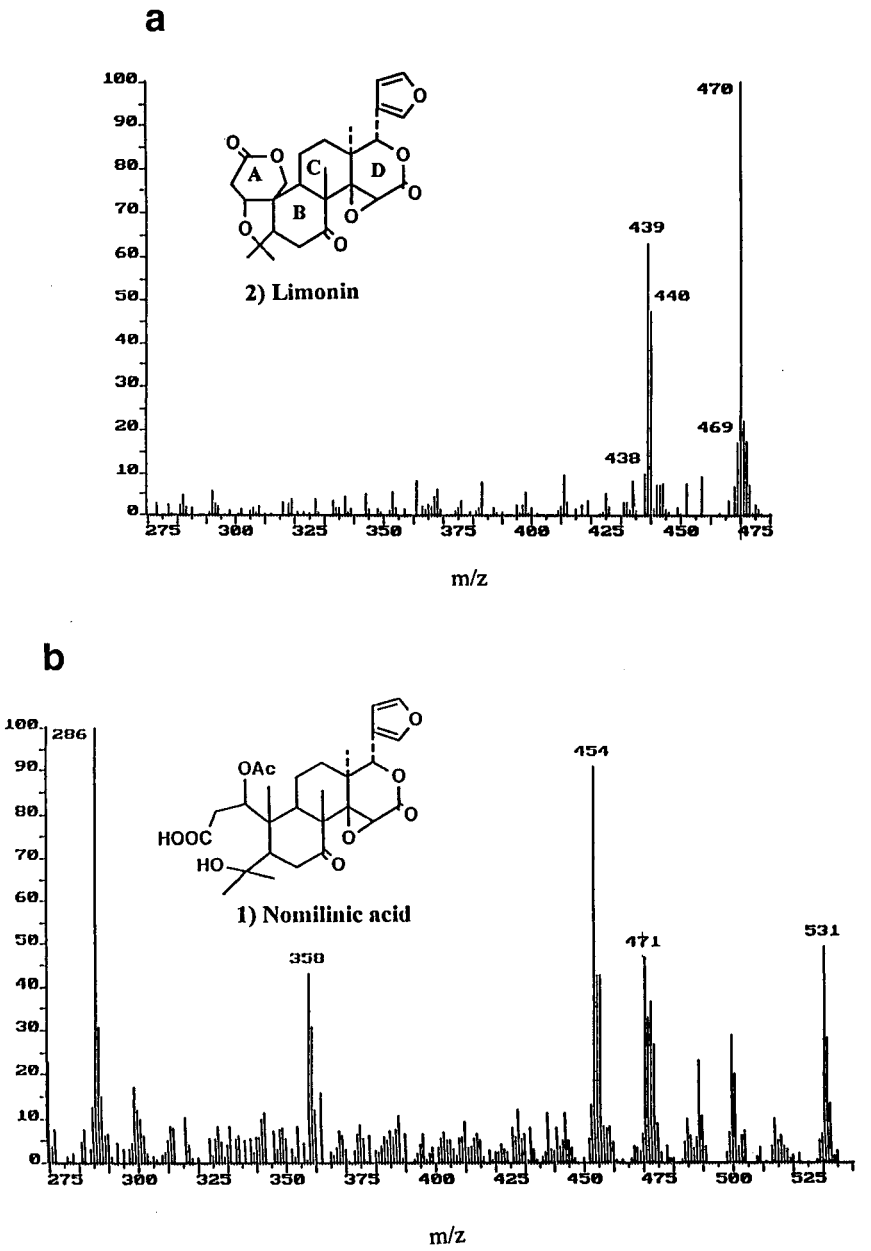

Fig. 7. Mass spectra of limonin (a) and nomilinic acid (b).

activity. Flavanols, flavones and flavanones inhibit lipid oxidation while coumarins and limonoids do not seem to show any antioxidant activity.

4. Conclusion

The application of thermospray mass spectrometry and diode-array detection coupled with

Table 2
Induction times of lemon peel extracts measured by Rancimat

Solvent fraction	Induction time (h)
Petroleum ether fraction	3.6
Chloroform fraction	3.1
Ethyl acetate fraction	4.8
Butanol fraction	3.7
BHT	7.8
Control	4.1

HPLC has proved very useful in the analysis of lemon peel extract. In particular, the use of two detectors (diode-array detector and mass spectrometer) allowed us to obtain the UV–Vis spectrum and the mass spectrum of each compound. Thermospray mass spectrometry is suitable for the analysis of flavonoids because of the observation of ions that correspond to the quasi-molecular or molecular ion of the compound and of the aglycon. Therefore, it was possible to identify several glycosides present in the lemon peel together with other compounds of different structure. Lemon peel extracts were found to be characterized by the presence of several compounds belonging to four different groups of flavonoids: flavones-O-glycosides, flavones-C-glycosides, flavonols and flavanones, according to published data. Furthermore, several coumarins, a phenyl propanoid glucoside and some limonoids were found. These last compounds are of particular interest because they are related to the bitterness of the extracts and juices. A test on the antioxidant activities of the extracts was performed using a Rancimat apparatus. Comparison of the induction times of the different samples showed that only the EtOAc extract possessed antioxidant activities while the others did not.

Acknowledgement

New Jersey Agricultural Experiment Station Project No. D-10205-2-94 supported by State Funds and Regional Project NE-116.

References

[1] J.B. Harborne, T.J. Mabry and H. Mabry (Editors), The Flavonoids, Academic Press, New York, 1975.
[2] A.K. Verma, in M.-T. Huang, C.-T. Ho and C.Y. Lee (Editors), Phenolic Compounds in Food and their Effects on Health II, ACS Symp. Ser. Vol. 507, American Chemical Society, Washington, DC, 1992, p. 250.
[3] A. Szent-Gyorgy, Z. Phys. Chem., 225 (1938) 126.
[4] O.R. Gottlieb, in J.B. Harborne, T.J. Mabry and H. Mabry (Editors), The Flavonoids, Academic Press, New York, 1975, p. 296.
[5] J. Chopin, H.L. Bouillant and E. Besson, in J.B. Harborne and T.J. Mabry (Editors), The Flavonoids: Advances in Research, Chapman and Hall, London, 1982, p. 449.
[6] G.L. Park, S.M. Avery, J.L. Byers and D.B. Nelson, Food Technol., 37 (1983) 98.
[7] J.-J. Macheix, A. Fleuriet and J. Billot, Fruit Phenolics, CRC Press, Boca Raton, FL, USA, 1990.
[8] J.A. Attaway, in M.T. Huang, T. Osawa, C.-T. Ho and R.T. Rosen (Editors), Food Phytochemicals for Cancer Prevention I. Fruits and Vegetables (ACS Symp. Ser., Vol. 546), American Chemical Society, Washington, DC, 1994, pp. 240–248.
[9] R.F. Albach and G.H. Redman, Phytochem., 8 (1969) 127.
[10] R.J. Grayer, in J.B. Harborne (Editor), Methods in Plant Phenolics, Academic Press, London, 1989, pp. 283–323.
[11] R.M. Horowitz and B. Gentili, in S. Nagy, P.E. Shaw and M.K. Veldhuis (Editors), Citrus Science and Technology, AVI, Westport, CT, 1977, p. 397.
[12] S. Steffenrud, E. Dewey and G. Maylin, Rapid Commun. Mass Spectrom., 11 (1990) 463.
[13] A.I. Gray and P.G. Waterman, Phytochem., 17 (1978) 854.
[14] D. Mc Hale, P.P. Khopkar and J.B. Sheridan, Phytochem., 26 (1987) 2547.
[15] Y. Matsubara, T. Yusa, A. Sawabe, Y. Iizuka and K. Okamoto, Agric. Biol. Chem., 55 (1991) 647–650.
[16] V.P. Maier, R.D. Bennett and S. Hasegawa, in S. Nagy, P.E. Shaw and M.K. Veldhuis (Editors), Citrus Science and Technology, AVI, Westport, CT, 1977, p. 355.
[17] Y. Ozaki, C.H. Fong, Z. Herman, H. Maeda, M. Miyake, Y. Ifuku and S. Hasegawa, Agric. Biol. Chem., 55 (1991) 137.

ELSEVIER

Journal of Chromatography A, 718 (1995) 99–106

JOURNAL OF CHROMATOGRAPHY A

High-performance liquid chromatographic profiles of aloe constituents and determination of aloin in beverages, with reference to the EEC regulation for flavouring substances

Fabio Zonta[a,*], Paolo Bogoni[b], Paola Masotti[b], Giuseppe Micali[c]

[a]*Istituto di Statistica e Ricerca Operativa, Università di Trento, via Verdi 26, I-38100 Trento, Italy*

[b]*Dipartimento di Economia e Merceologia delle Risorse Naturali, Università di Trieste, via Valerio 6, I-34127 Trieste, Italy*

[c]*Dipartimento di Scienze Merceologiche, Università di Messina, p.zza Pugliatti, I-98100 Messina, Italy*

First received 7 February 1995; revised manuscript received 11 May 1995; accepted 6 June 1995

Abstract

Characteristic HPLC profiles of fresh and aged aloe solutions, detected at 360 and 220 nm, are presented and compared. Several aloe constituents (aloesin, aloeresin A, hydroxyaloin, aloin A and B and aloinoside A and B) were simultaneously separated and identified. The determination of aloin is described (detection limit 0.15 ppm) and discussed. In aloe-based alcoholic beverages, the aloins could not be detected, owing to their instability and degradation in solution; this is discussed in relation to the EEC Council Directive 88/388, which fixed the values of maximum allowable concentrations for aloin in food and beverages. Instead of aloin, other aloe compounds (e.g., aloeresin A or aloesin) should perhaps be used as an index of the presence of aloe in alcoholic beverages.

1. Introduction

The term aloe refers to the dried latex extracted from the leaves of several species of Liliaceae, plants which grow mainly in South and East Africa (Cape aloes from *Aloe ferox* or *A. arborescens* Mill., Socotrine aloes from *A. perryi* Bak.) and in the Caribbean region (Barbados or Curacao aloes from *A. vera* Linn.).

Aloe is widely used for manufacturing food products and beverages, pharmaceuticals and cosmetics because of its aromatic properties, bitter taste, the cathartic activity of anthraquinones and other pharmacological activities (such as emolliency, reduction of inflammation and acceleration of wound healing; it is not yet well understood which activity may be related to which component) [1].

Aloin, a mixture of two diastereoisomers, aloin A (configuration at C_{10}, $C_{1'}$: *S,S*) and aloin B (*R,S*) [2], is an anthrone C-glucoside component of aloes (it is also present in extracts from cascara bark, *Rhamnus purshiana* DC, and from other vegetable sources); the other main aloe components are aloesin (formerly named aloeresin B) [3] and aloeresin A [4]. Several other constituents of commercial aloes have also been described: aloe-emodin [5], homonataloin and nataloe-emodin [6], aloinoside A and B [7],

* Corresponding author.

0021-9673/95/$09.50
SSDI 0021-9673(95)00637-0

aloenin A and B [8], 4-hydroxyaloin [9] and 5-hydroxyaloin [10].

Table 1 summarizes the names and absorbance spectral data as obtained from the cited references, and Fig. 1 depicts some of the corresponding structural formulae.

Aloin was included in the list of twelve restricted compounds for which, owing to their pharmacological activity, the EEC Council Directive 88/388 fixed the maximum allowable concentrations (MAC) in food products [11,12]. In Italy, the EEC Directive was enforced by a law [13] which established the MAC values but did not (as yet) publish the official method of analysis.

As far as analytical methods for aloin are concerned, the AOAC method [14] is not applicable to aloes; the pharmacopoeial methods [15,16] for drug preparations are based on TLC and are not suitable for food analysis. In fact, the Council of Europe [17], in 1981, reported the lack of methods for determining aloin in foods. Meanwhile, two papers have described HPLC methods for the analysis of food products and beverages for aloin: Yamamoto et al. [18] found aloin in Japanese candies with concentrations exceeding 1000 times the EEC MAC, whereas Zonta et al. [19] did not find aloin in any of the samples of bitter alcoholic beverages analysed.

Whereas TLC has often been used for aloe analysis [3,7,15,16], only a few papers have presented HPLC results for aloe constituents. Rauwald and Beil [20] recently reported the HPLC separation [with methanol–water (1:1) as isocratic mobile phase] of five anthraquinone derivatives from aloes: aloins (A and B), aloinosides (A and B) and 5-hydroxyaloin A, detected at 360 nm.

This paper describes and compares the HPLC profiles, detected at 220 and 360 nm, of fresh

Table 1
Some components of aloe, with names, absorbance spectral data (with corresponding ε or log ε values) and references

Name	Absorbance maxima (nm)[a]	Solvent	Ref.
Aloin (A and B)	208 (4.41), 255sh (3.77), 270 (3.91), 297 (3.96), 363 (4.05),		[6]
(formerly barbaloin)	261 (3.85), 269 (3.92), 297 (3.98), 362 (4.08)	MeOH	[8]
	269, 302, 379	KOH–MeOH	[8]
	260 (3.80), 269 (3.95), 298 (4.00), 360 (4.03)	MeOH	[21]
Aloesin	216 (4.31), 248 (4.21), 254 (4.23), 297 (3.96),	EtOH	[3]
(formerly aloeresin b)	212 (4.27), 244 (4.14), 252 (4.18), 296 (3.90)		[3]
Aloeresin A	228 (34 250), 243sh (25 900), 252 (25 000), 300 (37 960)	MeOH	[4]
Aloinoside (A and B)	269 (3.865), 296 (3.941), 360 (4.002)	MeOH	[7]
Aloenin B	205 (4.75), 224sh (4.48), 298 (4.44), 308 (4.45)	MeOH	[8]
5-Hydroxyaloin	Absorbance data not available		[10,20]
4-Hydroxyaloin	The absorbance spectrum is reported; the values of the absorbance maxima are not given and are difficult to be read from the figure. This substance was reported to be the main degradation product of aloin		[9]
Aloe-emodin	492, 510 (approximate values as deduced from the reported spectrum shape; aloemodin is the main product derived from aloin oxidation)	At pH 11	[5]
Homonataloin	222 (4.38), 250sh (3.85), 273sh (3.85), 294 (4.12), 347 (3.85)		[6]
Nataloe-emodin	232 (4.3), 260 (4.3), 290sh (4.0), 434 (3.89)		[6]

[a] Values in parentheses are ε or log ε.

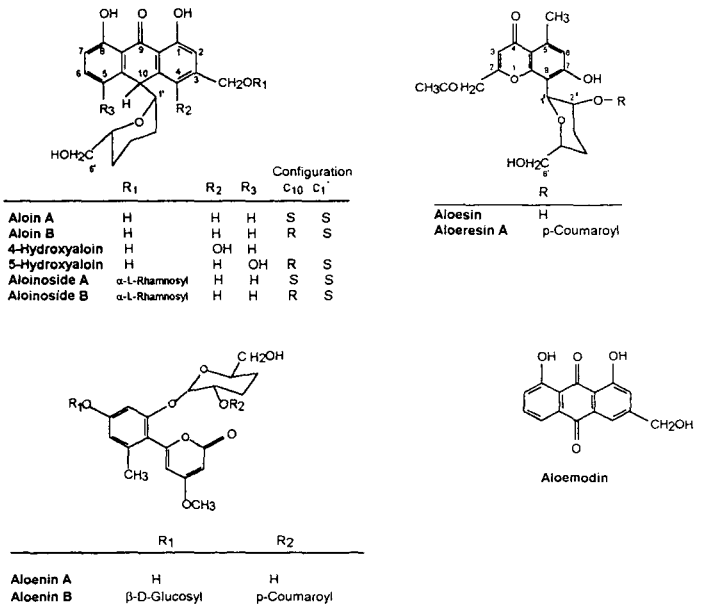

Fig. 1. Structural formulae of some aloe components.

and aged aloe solutions. In addition to the diastereoisomeric aloins A and B, many other peaks were simultaneously separated and the main components identified. The very short lifetime of aloin in aqueous–alcoholic solutions explains why aloin was not previously detected in beverages. As will be pointed out in the Discussion section, although the results presented here are satisfactory from the analytical point of view, they nonetheless lead to questions on the regulatory aspects.

2. Experimental

2.1. Apparatus

The chromatographic apparatus consisted of a pump module (Series 3 liquid chromatograph), a column oven (LC 100) and a variable-wavelength spectrophotometric detector (LC 55B) connected to a digital scanner (LC 55S) and a pen recorder (Model 56) (all from Perkin-Elmer, Norwalk, CT, USA). All chromatographic data were recorded and processed by means of Chromstar software (Bruker, Bremen, Germany).

The analytical column was a Supelcosil LC18 (250 × 4.6 mm I.D.) filled with a 5-μm body-porous stationary phase (Supelco, Bellefonte, PA, USA). The elution programme was isocratic [acetonitrile–water (18:82, v/v)] for 12 min, followed by a linear gradient to 35% acetonitrile in 20 min and isocratic again for 8 min; the run was then continued with a second linear gradient from 35% to 60% acetonitrile in 10 min. This was followed by a purge (95% acetonitrile for 10 min) and a re-equilibration step (to 18% acetonitrile) for 15 min before the next injection. The column was thermostated at 45°C, and the corresponding initial pressure drop was 9.2 MPa with a flow-rate of 1 ml/min. The spectrophotometric detector was set as required at either 360 or 220 nm.

2.2. Materials and methods

All solvents were of HPLC grade (Merck, Darmstadt, Germany). A crystalline sample of aloe (without specification of origin or purity) was a gift kindly supplied by Janousek (Trieste, Italy).

The powdered aloe (1 g) was mixed with water (100 ml) [15,16] or with aqueous–alcoholic mix-

tures (30%, v/v) or with absolute ethanol; the suspensions obtained were then centrifuged and diluted as required (e.g., 1:4). The solutions were kept in the dark at room temperature (about 20°C) or at 4°C for several weeks, to test their stability and changes; before the injection (injection volume 2 μl) they were filtered using HV 0.45-μm filters (Millipore).

Commercial samples of aloin of purity ca. 70% by TLC (Sigma, St. Louis, MO, USA) and >50% by TLC (Fluka, Buchs, Switzerland) were also used.

Commercial samples of alcoholic beverages (bitter and fernet) were purchased at random in grocery stores. They were filtered and injected directly for analysis (injection volume 3 μl).

3. Results and discussion

3.1. Qualitative analysis

This paper describes a reversed-phase gradient elution system (based on a water–acetonitrile mixture) which allows the simultaneous separation of many components of aloe. Characteristic HPLC profiles, detected at 220 nm, of fresh and aged aqueous solutions of aloe are shown in Fig. 2. Table 2 lists peak numbers, the corresponding spectral absorbance maxima and, where possible, their identification or tentative assignment, since some suggestions require further confirmation that could be obtained by preparative HPLC (which is planned as a continuation of this research).

Fig. 3 shows the shapes of the absorbance spectra of the eluting compounds, as recorded by means of the stop-flow method.

Aloins (peaks 14 and 17) were identified by using the available commercial standard (although impure and containing several other peaks characteristic of aloe chromatograms, which reveals it to be a natural, non-synthetic product).

The other main aloe constituents were known (from previous analytical results [3,4]) to be aloesin and aloeresin A, and these were found to correspond to the other two main peaks (3 and 11, respectively) on the chromatogram. Their elution order, also compared with aloins, was

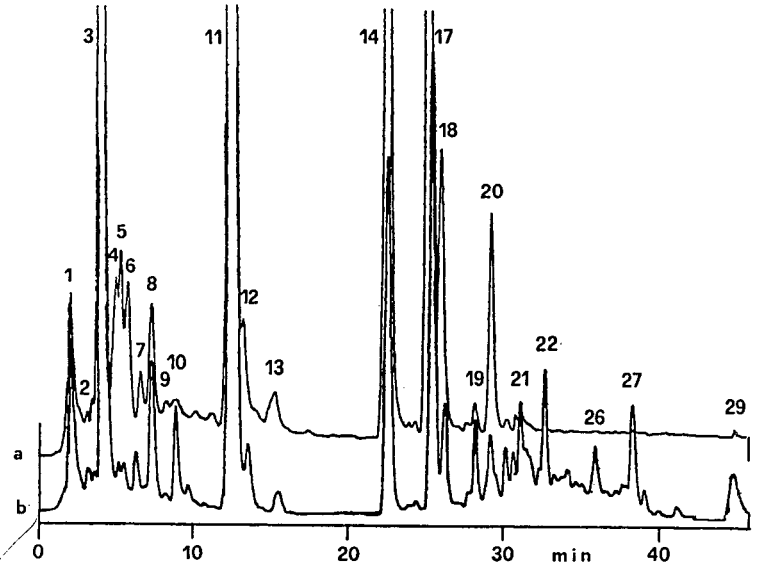

Fig. 2. HPLC profiles of aloe: (a) freshly prepared aqueous solution (superimposed above); (b) the same sample injected after 3 weeks (superimposed below). Detection wavelength, 220 nm; injection volume, 2 μl; recorder setting to 0.05 A.U.F.S. Other chromatographic conditions are described under Experimental. For peak identification, see Table 2.

Table 2
List of the main peaks of the chromatograms from aloe

Peak No.	Absorbance maxima (nm)										Peak identification
1	213,			253sh,			300,				
2	214,		245,	253,			298,				Aloesin
5	212,	228,		253,			304,				
6			246sh,	254,			303,				
10	211,		245sh,	254,			300				
11	212,	228sh,	243sh,	252,			303,				Aloeresin A
13	210,			253sh,	260sh,	269,	298,		359,		Hydroxyaloin (?)
14	210,			254sh,	262sh,	270,	300,		360,		Aloin B
17	210,			254,	262sh,	270,	299,		359		Aloin A
18				253,	261sh,	268,	298,		359,		Aloinoside B (?)
19				255,	265,	274,	290,	308,		365,	
20				255,	262sh,	269,	298,		359,		Aloinoside A (?)
21					265,	274,		308,		365,	
22	212,			255,		275,		305,		365,	
27	214,	228,			266,	275sh,	290sh,	306,		365,	

The absorption spectra of the peaks were recorded in the eluent solvent system (i.e., CH_3CN–H_2O) in the range 210–380 nm. Some data at the extremities of the explored wavelength range (210–220 and 370–380 nm) may be missing or uncertain owing to instrumental limitations.

consistent with that obtained by TLC [3]. Further, the absorbance spectral data corresponded with those in the literature. Although the spectral shapes of aloesin and aloeresin are remarkably similar, they show very different molar absorptivities, since the bands near 250 nm of

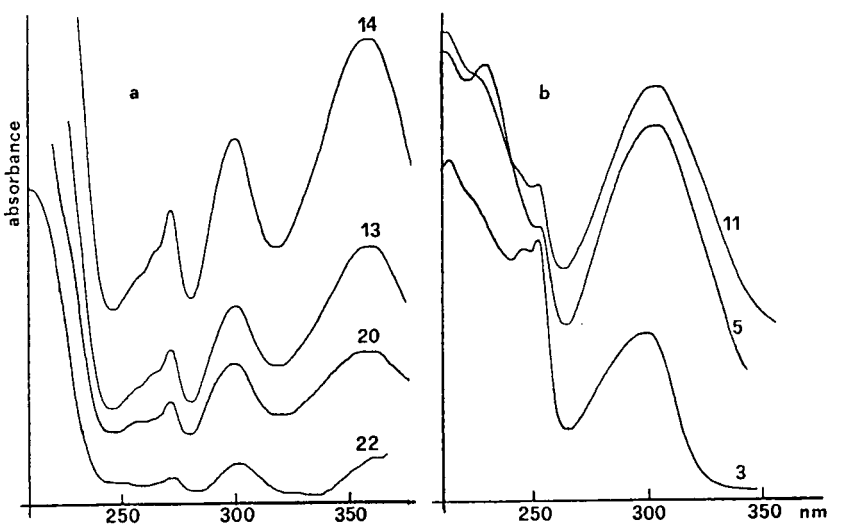

Fig. 3. Absorption spectra of some of the eluted peaks as recorded by means of the stop-flow method. Absorbances of the different spectra are not to scale. Spectral identification numbers refer to the peak numbers on the chromatograms. (a) "Aloin type" spectra with three major bands, around 270, 300 and 360 nm; (b) other spectra, lacking the band around 360 nm, with an absorbance and (benzenoid) around 300 nm. Detailed values of absorbance maxima are given in Table 2.

aloesin are higher than that near 300 nm; the opposite applies to aloeresin (compare the absorbance spectral data in Tables 1 and 2 and the spectral shapes in Fig. 3b).

Peak 18 (which is incompletely resolved and not pure) has an absorption spectrum similar to but not identical with that of peak 20. These two peaks should be the aloinoside A and B, respectively (and their heights decrease with time). Their tentative assignment is mostly based on the fact that when we reproduced a solvent system similar to that used by Rauwald and Beil [20] [CH_3OH–H_2O (1:1), but with a flow-rate reduced to 0.7 ml/min] and used the same detection wavelength (360 nm), a chromatogram of aloe very similar to theirs was obtained (and the pair of peaks 17 and 18 was much better separated). Further, the absorbance maxima of peak 20 correspond to those reported for the aloinoside [7].

The chromatogram of the aged (3 weeks) aloe solution is reported superimposed (profile b) in Fig. 2. Several changes were evident on comparing the two chromatograms: there was a large decrease, due to degradation, of the aloins (A and B, peaks 17 and 14, respectively) and of the supposed aloinosides (peaks 18 and 20); a corresponding increase in peaks 10, 21, 22, 26, 27 and 29, which should correspond to degradation products, was observed. Graf and Alexa [9] reported 4-hydroxyaloin (eluting before aloin) to be the main decomposition product of aloin, but this could not be clearly confirmed here. Rauwald and Beil [20] reported 5-hydroxyaloin (a component to which taxonomic significance was attributed) as another peak eluting before aloins and characteristic of aloe samples. The spectral shape and the elution position of peak 13 in the chromatogram suggest that it could perhaps be a hydroxyaloin, but this is a highly uncertain speculation.

At 360 nm, since many components of the mixture absorb very weakly, the chromatogram is simplified and fewer peaks are detectable; in fact, this is a selective wavelength for aloins (and other anthraquinone derivatives), but important information about other components is missing, as shown in Fig. 4,where the heights of the peaks

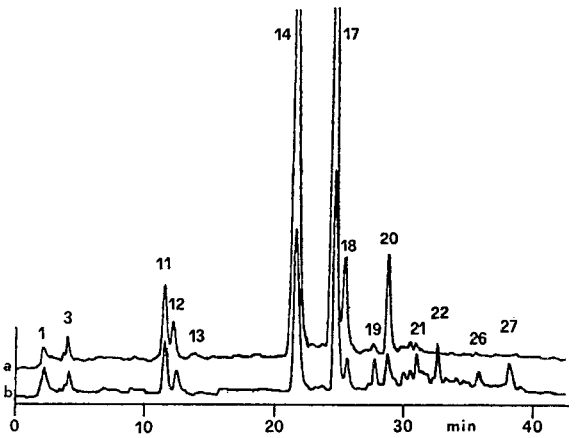

Fig. 4. Superimposed chromatograms of fresh (profile a, above) and aged (profile b, below) aloe solutions as detected at 360 nm. Chromatographic conditions and peak numbers as in Fig. 2.

attributable to aloesin and aloeresin are greatly reduced. Fig. 4 also shows, superimposed for comparison, the chromatograms obtained at 360 nm by using a fresh and an aged (3 weeks) aloe solution (profiles a and b, respectively).

3.2. Quantitative analysis

The HPLC determination of aloin has been described previously [19]. At 360 nm, which corresponds to an absorbance maximum of aloin, the log ε value (4.03) reported in the literature [21] was used for obtaining the concentration of a standard solution of pure aloin (obtained by preparative HPLC). The linearity of the calibration graph was verified within the range 0.15–60 ppm. The detection limit was 0.15 ppm for each of the two aloin diastereoisomers (with a signal-to-noise ratio of 3) [19].

The commercial standard (Sigma) was then analysed and the aloin concentration was found to be $73.1 \pm 0.7\%$ ($n = 7$), a value close to that declared on the label by the manufacturer (ca. 70% by TLC). The commercial unavailability (as far as we know) of highly pure aloin standards may lead to controversial results when official analytical controls of aloin concentration in food and beverages are required.

3.3. Aloin degradation

As shown above, the aloins (A and B) undergo rapid decomposition in solution; the decomposition is known to be most rapid at basic pH values [14] but also in neutral or acidic solutions the degradation occurs in a short time.

Aqueous, aqueous–alcoholic (30%, v/v) and ethanolic (absolute) solutions of aloe were prepared, and an aloe solution was also added to different bitter beverage samples. From these samples, the degradation kinetics of aloin were obtained by plotting the decrease in the aloin peak area as a function of time. The results obtained are depicted in Fig. 5: after 10 days only 40% of the aloin added to the sample of alcoholic bitter beverage (pH 3.4) remains detectable by HPLC. It follows that, after a brief shelf-life of any aloe-containing solution, it will be impossible to detect the presence of aloin any longer.

3.4. Regulatory aspects

Aloin was included in the EEC list of twelve restricted compounds because of its possible adverse pharmacological effects on consumers, but comparable or even worse effects are attributable to other components of aloe [22,23]. The cathartic effects of aloe in humans were studied by Mapp and McCarthy [22] who stated that "it would appear preferable to replace aloes with aloin for human oral use, thus avoiding the use of resins, aloesin and other variable constituents which differed tremendously in the nearly 100 aloe species examined". That statement was made with reference to pharmaceutical preparations, where it does indeed make sense. In contrast, it does not make any sense to limit in beverages (MAC value 50 ppm) the concentration of a substance (such as aloin) which cannot actually be detected by analysis because of its instability in solution (see above).

In aloe-based beverages, other marker substances with a longer lifetime than that of aloin should therefore be used for monitoring that the concentration of aloe used (which involves the presence of many other pharmacologically active substances) falls in the range of "good manufacturing practice" and is safe for consumers. Chromatograms obtained from a sample of fernet are reported in Fig. 6. Several peaks eluted with the same retention times as those from the aloe solutions (e.g., peaks 3, 11, 27). When recorded, the absorbance spectra of peaks 3 and 11 strongly suggested the presence of aloesin and aloeresin A in the beverage analysed, indicating, as expected, that the beverage was an aloe-based product in which aloin itself was by now absent. We therefore believe that, at least as far as

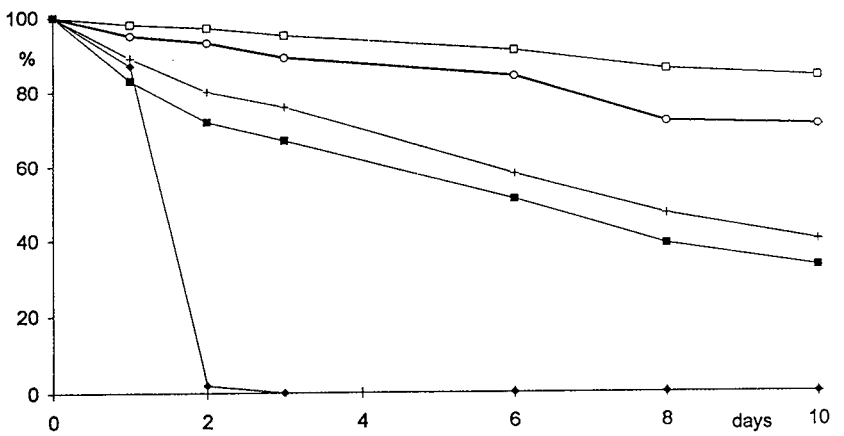

Fig. 5. Degradation kinetics of aloin solutions: percentages of aloin B peak area counts are reported versus shelf-life (days). □ = 100% ethanol at 20°C; ○ = 30% ethanol at 4°C; + = bitter sample at 20°C (pH 3.4); ■ = 30% ethanol at 20°C; ◆ = bitter sample at 20°C (pH 8.1).

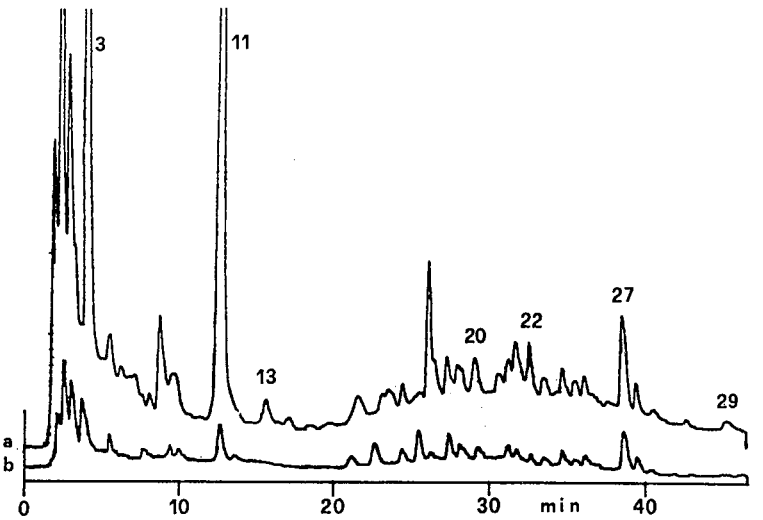

Fig. 6. Chromatograms of an aloe-based alcoholic beverage (fernet): (a) profile superimposed above, detection wavelength 220 nm; (b) profile below, detection wavelength 360 nm. Injection volume, 3 μl. Other chromatographic conditions and peak numbers as in Fig. 2.

beverages are concerned, the EEC list of restricted compounds should be revised and modified, excluding aloin and perhaps including aloeresin A and/or aloesin as aloe markers. Further research is needed, however, to confirm the identities of aloesin and aloeresin A, to improve their determination and to assess their lifetimes in beverages.

References

[1] R.P. Pelley, Y.T. Wang and T.A. Waller, Seifen Oele Fette Wachse, 119 (1993) 255.
[2] P. Manitto, D. Monti and G. Speranza, J. Chem. Soc., Perkin Trans 1, (1990) 1297.
[3] L.J. Haynes, D.K. Holdsworth and R. Russel, J. Chem. Soc. C, (1970) 2581.
[4] P. Gramatica, D. Monti, G. Speranza and P. Manitto, Tetrahedron Lett., 23 (1982) 2423.
[5] K.G. Stone and N. Howell Furman, J. Am. Chem. Soc., 68 (1946) 2742.
[6] L.J. Haynes, J.I. Henderson and J.M. Tyler, J. Chem. Soc., (1960) 4879.
[7] L. Horhammer, H. Wagner and G. Bittner, Z. Naturforsch., 19 (1964) 222.
[8] G. Speranza, G. Dadà, L. Lunazzi, P. Gramatica, P. Manitto, J. Nat. Prod., 49 (1986) 800.
[9] E. Graf and M. Alexa, Planta Med., 38 (1980) 121.
[10] H.W. Rauwald, Pharm. Weekbl., Sci. Ed., 9 (1987) 215.
[11] L.n. 184 of 15 July 1988, in Official Journal of the European Communities, p. 61 (EEC Council Directive 88/388, of 22 June 1988).
[12] P. Masotti and F. Zonta, Ind. Aliment., 31 (1992) 1135.
[13] D. Lgs. n.107 of 25 January 1992, in Gazzetta Ufficiale della Repubblica Italiana, Serie Generale, No. 39, 17 February 1992.
[14] K. Helrich (Editor), Official Methods of Analysis of the Association of Official Analytical Chemists, AOAC, Philadelphia, 15th ed., 1990, p. 602.
[15] Farmacopée Européenne, Conseil de l'Europe, 1984, Aloes Extractum Siccum Normatum, p. 259.
[16] Farmacopea Ufficiale della Repubblica Italiana, Droghe Vegetali e Preparazioni, Rome, 9th ed., 1991, p. 21.
[17] Flavouring Substances and Natural Sources of Flavourings. Appendix A. Methods for Determining Restricted Compounds, Council of Europe, Strasbourg, 1981, p. 33.
[18] M. Yamamoto, M. Ishikawa, T. Masui, H. Nakazawa and T. Kabasawa, J. Assoc. Off. Anal. Chem., 68 (1985) 493.
[19] F. Zonta, P. Masotti and P. Bogoni, Atti del XVI Congresso Nazionale di Merceologia, Pavia, 1–3 Settembre 1994, Vol. I, p. 392.
[20] H.W. Rauwald and A. Beil, J. Chromatogr., 639 (1993) 359.
[21] T. Hirata and T. Suga, Z. Naturforsch., Teil C, 32 (1977) 731.
[22] R.K. Mapp and T.J. McCarthy, Planta Med., 18 (1970) 361.
[23] A. Goodman Gilman, T.W. Rall, A.S. Nies and P. Taylor (Editors), Goodman and Gilman's the Pharmacological Basis of Therapeutics, Pergamon Press, New York, 1990, p. 921.

ELSEVIER

Journal of Chromatography A, 718 (1995) 107–118

JOURNAL OF CHROMATOGRAPHY A

Separation of planar organic contaminants by pyrenyl-silica high-performance liquid chromatography

D.E. Wells*, I. Echarri[1], C. McKenzie

Agriculture and Fisheries Department, The Scottish Office SOAFD, Marine Laboratory, P.O. Box 101, Aberdeen AB9 8DB, Scotland, UK

First received 7 February; revised manuscript received 6 June 1995; accepted 6 June 1995

Abstract

Planar organic contaminants are known to induce specific biological activity (e.g. aryl hydrocarbon hydrolase and ethoxy resorufin-*o*-deethylase). An unequivocal identification and accurate measurement is essential in order to correlate the potential biological effect to these compounds. Pyrenyl-silica high-performance liquid chromatography allows an effective separation of these planar compounds from most biological co-extractants and from each other. This group of planar compounds includes specific chlorobiphenyls, polycyclic aromatic hydrocarbons, polychlorodibenzo-*p*-dioxins, polychlorodibenzofurans and polychlorinated naphthalenes.

1. Introduction

The emphasis on the measurement of organic contaminants in marine environmental programmes in relation to observed biological effects has focused on those compounds which exhibit a relatively specific activity [1,2]. One such generic class of compounds is the toxic planar molecules which are known to induce liver microsomal enzyme activity. These compounds induce both aryl hydrocarbon hydrolase (AHH) and ethoxy resorufin-*o*-deethylase (EROD) and have a high affinity to the cytosolic receptor protein [3–6]. Both the toxic mechanism and the enzyme induction involve an initial binding of these contaminants to the same arylhydrocarbon (AH) receptor, and, not surprisingly, these compounds tend to have a similar spatial and structural chemistry [7].

The compound classes known to induce this type of biological activity are the polycyclic aromatic hydrocarbons (PAHs), the polychlorodibenzo-*p*-dioxins (PCDDs) and dibenzofurans (PCDFs), in particular the 2,3,7,8-substitution pattern, the non-*ortho* and mono-*ortho* chlorobiphenyls (CBs) and the polychlorinated naphthalenes (PCNs). Reports [8,9] on the determination of these compounds in environmental samples have tended to focus on the measurement of single compounds or compound classes while other materials present in the sample extract, including other planar compounds, are regarded as potential sources of interferences and are discarded.

When attempting to relate a specific biological effect, e.g. EROD, to a chemical insult, it is essential to measure all compounds that might have a significant contribution to the effect.

* Corresponding author.

[1] Present address: Departmento de Quimica Analytica, University of Zaragoza, Maria de Lina, Spain.

0021-9673/95/$09.50
SSDI 0021-9673(95)00635-4

When an accurate estimate of each individual compound is made, then it becomes possible to assess the relative toxic effect of each contaminant.

Although the final determination of each compound in each class must be specifically optimised, the isolation and separation of each group in a single sample is also necessary to obtain some assessment of the biological impact of these compounds as a whole. This holistic analysis may also be essential when the size of the sample, e.g. dab liver, is very limited and a separate analytical scheme is not an option. A low limit of detection ($1 \cdot 10^{-12}$ to 10^{-15}) is required for such measurements so that a reliable determination can be made on a single animal. Where this low detection limit is unattainable for a single sample, it may be necessary to resort to the analysis of pooled samples [8,10]. With, perhaps, the exception of some of the PAHs, which tend to occur at relatively higher concentrations, the errors caused by recording false positive values from other interfering materials at the ultra-trace level continues to be a problem. All of these groups of compounds occur as complex mixtures which require careful separation from each other prior to the final determination.

The separation techniques to isolate planar CBs from other contaminants have been fully reviewed by de Voogt et al. [8] and Wells [10]. The initial methods used carbon or granular charcoal in various grades and particles sizes [11,12]. The carbon was used in milligram quantities as a free powder or adsorbed onto foam to offer a greater surface area [13]. More recently, silica has been coated with graphite as the basis of the commercially available high-performance liquid chromatography (HPLC) Hypercarb columns [14,15]. The separation is based upon the retention of the planar, or near planar, molecules by the graphitic surface of the adsorbent. Non-planar molecules are either unretained or have a limited retention, whilst molecules with a "flat" structure similar to tetrachlorodibenzo-*p*-dioxin (TCDD) interlock with the graphite surface and are only removed by backflushing with a more polar solvent, like dichloromethane or toluene.

The development of the pyrenyl-silica HPLC column has made it possible to separate structurally similar molecules with different π-electron densities resulting from the spatial configuration of the aryl rings [16,17]. This stationary phase gives sufficient resolution between non-*ortho*, mono-*ortho* and the other *ortho*-chloro substituted CBs. Initially this type of column was developed to separate the toxic non-*ortho* CBs (CB 77, 126 and 169), which the carbon columns could achieve, and the mono-*ortho* CBs, which the carbon columns initially could not achieve. However, in addition to the separation of these toxic CBs, it is also possible to improve the resolution between other key CBs which may co-elute on the 5% phenylmethyl gas chromatography (GC) column. This technique, therefore, has the potential to remove a number of ambiguities that can exist in the final determination of CBs using GC [18,19]. Apart from the separation of different structural groups of CBs it is also possible to isolate the other planar contaminants which may co-elute or be compromised by other co-extracted materials.

In this paper we report on a number of key HPLC separations of CBs, and the extension of this technique to cover PCDDs, PCDFs, PCNs and PAHs using the pyrenyl-silica column prior to the final determination of these compounds by GC–electron capture detection (ECD) and GC–mass spectrometry (MS). The quantitative aspects of this technique and its application to the determination of specific CBs in biological matrices are given elsewhere [18,19].

2. Method

2.1. Chemicals

All solvents used were of the highest purity and were obtained as glass distilled grade from Rathburn Chemicals (Walkerburn, UK). The PAHs were obtained as individual pure, solid compounds from the European Union (EU)

Community Bureau of Reference, as were the CBs (CB 28, 52, 101, 105, 118, 128, 138, 149, 153, 156, 163, 170 and 180) [20], as either certified or well-characterised materials, which came also from Promochem (Wesel, Germany) (CB 44, 70, 77, 114, 126, 158, 169, 194). The PCDD and the PCDF standards were also obtained from Promochem via The Laboratory of the Government Chemist, London, UK. The PCN mixtures were obtained from the US Environmental Protection Agency. The internal standards (2,4-dichlorobenzyl alkyl ethers) were prepared and characterised in this laboratory [21]. All other materials used in the sample preparation have been reported elsewhere [22,23].

2.2. Liquid chromatography

The CBs were separated using a Cosmosil 5-PYE HPLC column [2-(1-pyrenyl)ethyldimethylsilylated silica gel], particle size 5 μm (Nacalai Tesque (Promochem)). The initial HPLC system used consisted of a Gilson 321 autosampler fitted with a 50-μl loop, a Gilson 302 pump and 401 diluter to dispense the sample into the loop. The fractions from the column were monitored with a Philips PU 4020 UV detector set at 254 nm and collected with a Gilson 202 fraction collector. The initial studies were conducted at room temperature (ca. 18–20°C) prior to using a column chiller. The injection and fraction cycle was controlled by the Gilson autosampler and the data collection was controlled by an Apple IIe microcomputer running Chromatochart software. This was superseded by a similar system using a Spectra Physics pump (P200) and autosampler (AS300). The temperature of the pyrenyl-silica column was regulated using a column chiller (Jones Chromatography 7955).

The cleaned-up samples from the alumina and silica [22,23] were concentrated to ca. 80 μl in Chromcol tapered vials and eluted with hexane at a flow-rate of 0.5 ml min^{-1}. Two internal standards, 2,4-dichlorobenzyl hexyl (D_6) and dodecahexyl (D_{16}) ether [24], were added (1 ml of 1 μg ml^{-1}) to each fraction, the sample was reconstituted in iso-octane and the CB content determined by capillary GC.

2.3. Gas chromatography

The Varian 3500 GC and 8200 autosampler was fitted with a 50 m × 0.22 mm I.D. CPSil 8 CB fused-silica column and a ^{63}Ni electron capture detector. The samples (100 μl) were injected (1 μl) into a splitless injector at 270°C and chromatographed at 80°C for 1 min and at 3°C/min to 280°C using hydrogen as carrier gas at a linear velocity of 40 cm/s. The chromatograph and data collection was controlled a by microcomputer operating Minichrom (VG Data Systems).

3. Results

The k'-values obtained for each of the planar compounds injected into the pyrenyl-silica HPLC column are given in Table 1 and plotted on a log scale for each of the five groups (Fig. 1). These data were obtained by injecting solutions of the initial individual compounds sequentially to obtain the retention volume. The variability of the k'-values were $< \pm 1\%$ over a six-month period for pure calibration solutions and for well-prepared and cleaned-up samples, provided that the column temperature is kept constant. A considerably higher variability occurs in the presence of co-extracted materials such as traces of lipids from sediment or biological tissue. The retention variability was monitored by injecting a series of compounds and comparing the measured and expected k'-values. The normal effect of contamination by lipophilic material was a reduction in k'-value and an increase in variability caused by a partial coating of the pyrenyl-bonded phase, thus reducing the selectivity of the column.

The column performance was restored by flushing with ethyl acetate for a minimum of two hours (normally overnight) at a flow-rate of 0.5 ml min^{-1} followed by 20–30 column volumes of

Table 1
Capacity factors (k') for planar molecules on the pyrenyl HPLC column

Compond	k'	Compound	k'
PAHs		*PCBs*	
Pyrene	0.61	CB 28	0.42
Benzo[*b*]naphtho(2,1-*d*)thiophene	0.82	CB 52	0.42
Benzo[*b*]naphtho(1,2-*d*)thiophene	0.82	CB 101	0.45
Benzo[*a*]anthracene	0.91	CB 149	0.48
Chrysene	0.97	CB 153	0.49
Triphenylene	1.09	CB 138	0.63
Benzo[*k*]fluoranthene	1.29	CB 180	0.63
Benzo[*b*]fluoranthene	1.44	CB 118	0.70
Benzo[*a*]pyrene	1.56	CB 163	0.72
Benzo[*e*]pyrene	1.66	CB 128	0.73
Perylene	1.79	CB 105	0.80
Indeno(1,2,3-*c*,*d*)fluoranthene	2.05	CB 170	0.81
Indeno(1,2,3-*c*,*d*)pyrene	2.30	CB 156	1.00
Benzo(*g*,*h*,*i*)perylene	2.65	CB 77	1.20
		CB 126	1.74
		CB 169	2.22
PCDDs		*Halonaphthalenes*	
1,3,6,8 TCDD	3.31	DiCNs	0.37
1,2,3,4 TCDD	3.44	TriCNs	0.62
1,3,7,9 TCDD	3.48	TriCNS	0.74
1,2,3,7 TCDD	3.54	TriCNs	0.93
1,3,7,8 TCDD	3.61	TriCNs/TetraCNs	1.24
1,2,7,8 TCDD	3.67	1,2,3,4 TCN	1.25
1,2,3,8 TCDD	3.73	TetraCNs	1.36
1,2,8,9 TCDD	3.94	TetraCNs	1.77
2,3,7,8 TCDD	4.29	PentaCNs	2.47
1,2,8,7 TCDD	5.00	PentaCNs	2.64
1,2,6,7 TCDD	5.00	PentaCNs	2.92
1,2,3,4,7 PCDD	8.20	HexaCNs	3.21
1,2,3,7,8 PCDD	9.02	HeptaCNs	3.35
1,2,3,4,7,8 HCDD	19.27	HeptaCNs	3.76
1,2,4,6,7,8 HCDD	21.01	1,2,3,4,6,7,8,9 OCN	4.32
1,2,3,7,8,9 HCDD	21.01	HeptaCNs	5.05
1,2,3,4,6,7,8,9 OCDD	172.46	HexaCNs	5.96
		HexaCNs	6.46
PCDFs		HexaCNs	7.54
1,2,7,8 TCDF	3.36	HexaCNs	8.68
2,3,4,8 TCDF	3.91	HeptaCNs	9.31
2,3,7,8 TDCF	4.50	1,2,3,4,6,7,8,9, OFN	17.36
1,2,3,8,9 PCDF	8.28	2 Bromonaphthalene	0.39
1,2,3,7,8 PCDF	8.29	2 Bromoanthracene	0.38
2,3,4,7,8 PCDF	13.64	2,9 Dibromoanthracene	1.16
1,2,3,7,8,9 HCDF	16.88		
1,2,3,4,8,9 HCDF	18.89		
1,2,3,4,7,8 HCDF	21.29		
1,2,3,6,7,8 HCDF	21.76		
1,2,3,4,6,7,8 H7CDF	64.62		
1,2,3,4,6,7,8,9 OCDF	145.62		

According to Wells and Echarri [18,19].
Conditions: 150 × 0.46 mm I.D. column; column eluent: hexane, 1 ml/min; temperature 20°C.

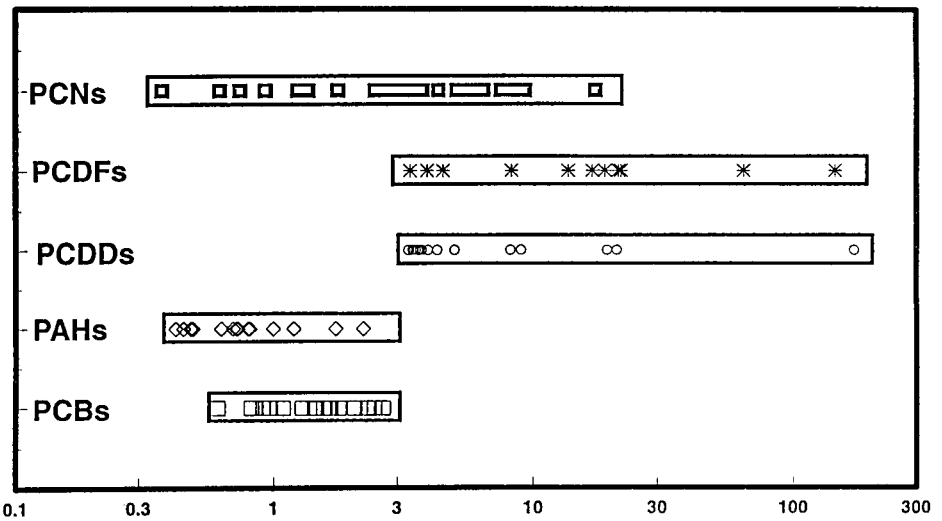

Fig. 1. Plot of $\log k'$ (capacity factor) for polychlorinated naphthalenes (PCNs), polychlorodibenzofurans (PCDFs), polychlorodibenzo-*p*-dioxins (PCDDs), polycyclic aromatic hydrocarbons (PAHs) and polychlorinated biphenyls (PCBs), obtained on the pyrenyl-silica PYE HPLC column, 150 × 0.46 mm I.D., using *n*-hexane as eluent at 1 ml min^{-1}.

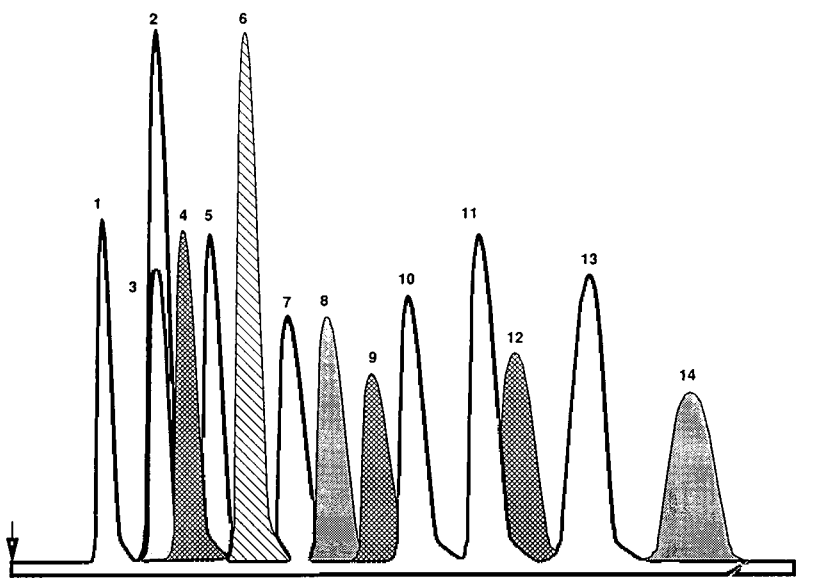

Fig. 2. Reconstructed chromatogram showing the separation of PAHs using the pyrenyl-silica PYE HPLC column, 150 × 0.46 mm I.D., with *n*-hexane as eluent at 1 ml min^{-1}. Peaks: 1 = pyrene, 2 = benzo[*b*]naphtho(2,1-*d*)thiophene, 3 = benzo[*b*]naphtho(1,2-*d*)thiophene, 4 = benzo[*a*]anthracene, 5 = chrysene, 6 = triphenylene, 7 = benzo[*k*]fluoranthene, 8 = benzo[*b*]fluoranthene, 9 = benzo[*a*]pyrene, 10 = benzo[*e*]pyrene, 11 = perylene, 12 = indeno(1,2,3-*c*,*d*)fluoranthene (internal standard), 13 = indeno(1,2,3-*c*,*d*)pyrene, 14 = benzo(*g*,*h*,*i*)perylene (see Table 1 for *k'*-values).

n-hexane to re-establish equilibrium. Using this method of periodic column restoration it has been possible to use the pyrenyl-silica column on a regular basis for some 3–4 years without replacement.

3.1. PAHs

The separation of planar and non-planar PAHs has been reported by Sanders et al. [25]. The PAHs included in this series of experiments were the less volatile >4 fused-ring compounds selected by the EC Measurement and Testing Programme (BCR) for the certification of environmental matrices. The pyrenyl-silica column is not only able to separate the aliphatic hydrocarbons from the PAHs, but also to isolate some specific PAHs which are each difficult to separate by capillary GC. Two such cases are the separation of chrysene and triphenylene, and benzo[*k*]- and benzo[*b*]fluoranthene (Fig. 2). The clean-up of sediment extracts for specific PAH measurement can be highly labour intensive, with a number of separate steps to remove co-extracted materials (Fig. 3). The time required for this method was substantially reduced by transferring the extract to the pyrenyl-silica column after preliminary treatment through an alumina (5 g, 1% w/w water)–silica (5 g 12% w/w water)–copper column. This alternative sample preparation eliminated two additional time-consuming steps using the Sephadex LH20 (20 g) and a further silica column. There was also a considerable improvement in the peak shape of the PAHs in the subsequent GC separation when the extract was passed through the pyrenyl-silica column as a result of the PAHs being separated from other

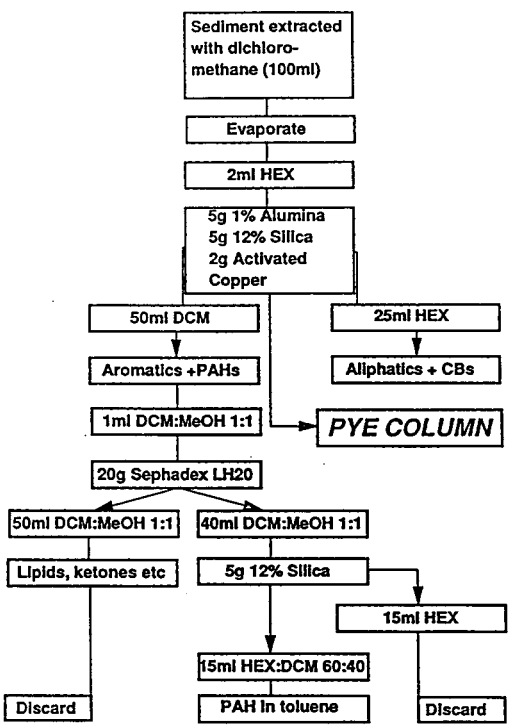

Fig. 3. Schematic diagram for the clean-up and isolation of PAHs from marine sediment. Scheme 1, on the left-hand side, shows the original method used in the SOAFD laboratory. Scheme 2, using the PYE column after alumina–silica clean-up is much more rapid and produces a cleaner extract for subsequent determination by GC or GC–MS.

Table 2
Capacity factors (k') for planar molecules on the pyrenyl HPLC column

Compound	k' at 0°C	k' at 25°C	Fraction (at 0°C)
CB3	1.44		I
CB52	1.58	0.53	I
CB101	1.66	0.59	I
CB149	1.68	0.53	I
CB153	1.77	0.69	I
CB70	1.79		I
CB180	1.87	0.88	I
CB138	2.02	0.84	I
CB128	2.11	0.96	I
CB118	2.16	0.96	I
CB163	2.18	0.96	II
CB114	2.20		II
CB170	2.30	1.10	II
CB105	2.39	1.17	II
CB156	2.78	1.41	II
CB157	2.88		II
CB77	3.28	1.74	III
HCB	3.62		III
CB126	4.76	2.52	III
CB169	5.65	3.24	III

Conditions: 250 × 0.46 mm I.D. column; column eluent: hexane, 1 ml/min.

co-extractants which affect the GC chromatography (Fig. 4). This highly selective separation, based on the spatial configuration of the determinands, is ideally suited to a method which subsequently uses a flame ionisation detector (FID) as the final method of detection.

The one disadvantage was that the performance of the pyrenyl-silica column was degraded after some 20–30 sediment samples, but this was readily restored with ethyl acetate as described earlier [18,19]. Even with this necessary LC restoration step the method was more rapid and produced a cleaner extract for the final GC analysis than the conventional column clean-up.

3.2. Chlorobiphenyls

The pyrenyl-silica column was initially used to separate the planar and non-planar CBs [16,17]. With some careful fractionation it was also possible to isolate the non-*ortho* CBs, the mono-*ortho* CBs and the di- and tri-*ortho* CBs from each other [18,19]. In addition some other useful separations have been possible, which further improve the subsequent GC determination of CB 138, which can be isolated from CB 163 [26,27]. This separation can be further enhanced by careful control of the column temperature (see later). Both of these CBs co-elute on most

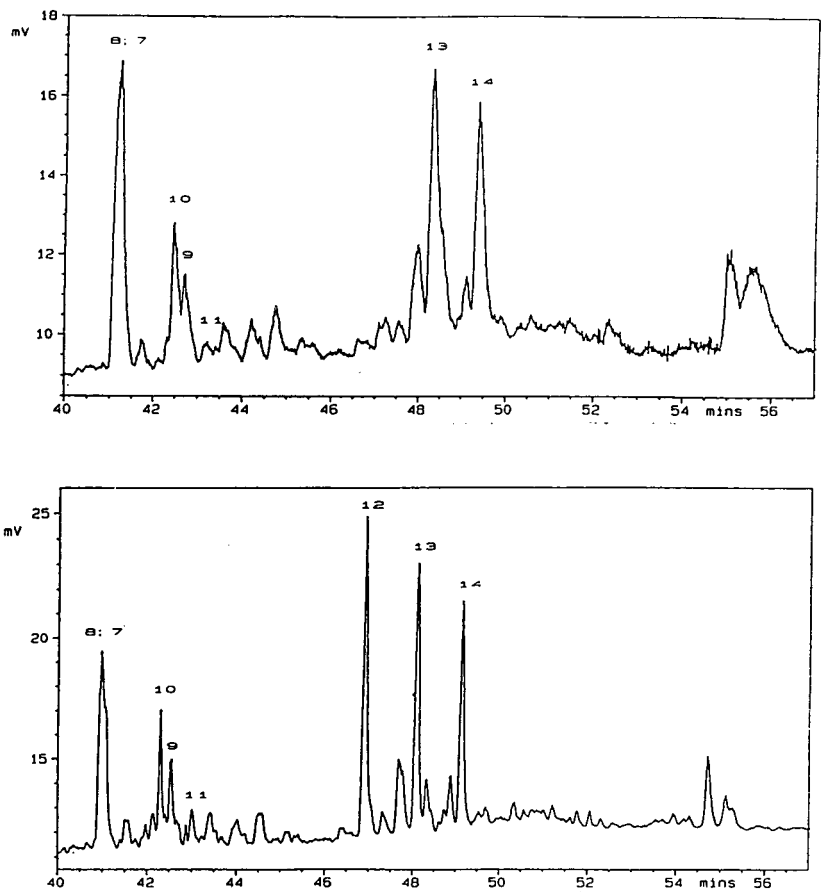

Fig. 4. Comparison of the GC–FID chromatograms for PAHs in Firth of Clyde marine sediment cleaned-up using Scheme 1 (top) and by Scheme 2 using the pyrenyl-silica column (bottom). See Fig. 3 for the clean-up scheme and Fig. 2 for identification of the peak numbers.

commonly used GC phases, with the exception of the HT5 phase. The mono-*ortho* CB 105 is also separated from CB 132, which is difficult to resolve on a 5% phenyl methyl silicone phase [10]. Clearly, there will be no cutoff volume which will isolate all congeners in one or the other of the fractions. CB 180, for example, is split between fractions I and II when using the 150 mm column (Table 2), but can be isolated in one fraction using the longer (250 mm) column and a lower column temperature of 0°C rather than ambient (ca. 25°C). However, it is possible to adjust the separation of selected CBs on the basis of their spatial configuration into three fractions. The major advantage of such a method is that it isolates the non-*ortho* chloro CBs, which are present at significantly lower concentrations in environmental samples. This allows the fractions to be concentrated in a small volume to obtain a higher level of sensitivity, particularly for biota where these toxic CBs are significantly metabolised [19]. In addition, some of the mono-*ortho* CBs are also difficult to determine using a single GC column [10]. In particular, CB 156 co-elutes with CB 171 and CB 202 on a 5% phenyl methyl silicone column and with other congeners if the GC column phase is changed. Ideally, it would be better if each of the key toxic CBs were separated on a single column, but, as yet, this seems unlikely. Currently there are two alternative methods. The first is multi-dimensional GC, which heart-cuts the unresolved peaks from one column onto a second column with a different phase which is then able to perform the more simple separations [28,29]. The second is an off-line separation using the pyrenyl-silica column or the PGC HPLC column [10]. In this study the CB

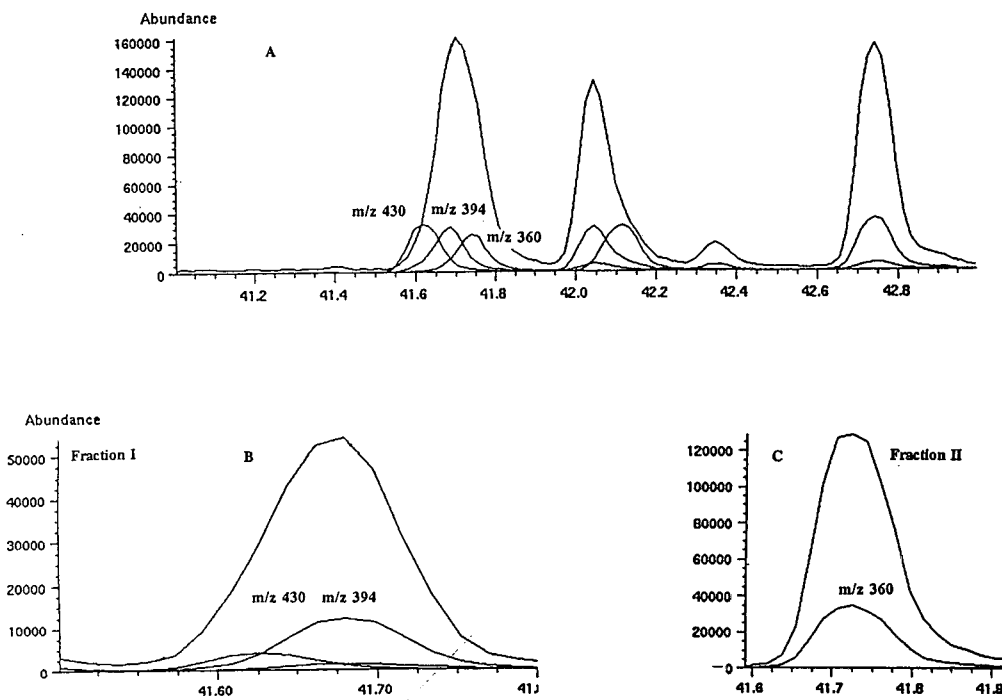

Fig. 5. (A) GC–MS total-ion and single-ion electron impact traces showing the separation of CB 156 (fraction II) from CB 171 and CB 202 (fraction I) using the pyrenyl-silica column. The upper GC–MS trace shows part of the composite mixture from the National Research Council of Canada (NRCC) with CB 156, CB 171 and CB 202 unresolved on a CP Sil 8 50 m column. The lower trace (B) for fraction I contains the CB 171 (*m/z* 394) and CB 202 (*m/z* 430) while the fraction II (C) only contains the CB 156 (*m/z* 360). (Time axis: min)

156 (fraction I) was separated from both CB 171 and CB 202 (fraction II) using the pyrenyl-silica column. This separation was confirmed using GC–MS in the single- and total-ion mode (Fig. 5). The three CBs were traced using m/z 360 for CB 156, m/z 394 for CB 171 and m/z 430 for CB 202. Care is required to fully separate these congeners, which are subsequently to be used to obtain the total burden of toxic CBs. False positive values from unresolved compounds can lead to a significant overestimation of those compounds and any subsequent calculation of toxic equivalent concentrations (TECs) [30].

3.3. PCDDs and PCDFs

Pyell and Garregues [31] have used the pyrenyl-silica column to separate some PCDDs by trapping on the column and backflushing. PCDDs and PCDFs (Cl > 4) can also be separated from both PAHs and CBs using the pyrenyl-silica column (Table 1, Fig. 6). The tetra CDDs and CDFs are isolated in a single fraction having a k' between 2.5 and 5.0. The remaining higher chlorinated PCDDs and PCDFs are eluted in hexane with a k' from 7.5 for the penta dioxins and furans up to k' 172 for the octachlorodibenzo-*p*-dioxin (OCDD). Some of the retention volumes are usually too excessive for normal isocratic analysis, both in terms of analytical time and the solvent volume of the final fraction. This may be overcome either by a stepwise or gradient elution using ethyl acetate or, less favourably, by backflushing the analytical columns following the elution of the tetrachloro dioxins and furans. Since most of the PCDDs and the PCDFs are subsequently determined by GC–MS in a single injection onto the chromatographic system, it is normally unnecessary to make a further group separation of these determinands. However, where additional group separation of the PCDDs and PCDFs is required, it is possible to obtain the necessary fractions from the pyrenyl-silica column.

3.4. PCNs

Polychlorinated naphthalenes (PCNs) are being used in industry and are present as planar environmental contaminants [32]. Many of these compounds exist as mixtures containing different degrees of chlorination, similar to the PCBs. One of the frequently used industrial formulations is the Halowax series with increasing degree of chlorination; HW 1010 (50% Cl), HW 1099 (52% Cl), HW 1013 (56% Cl) to HW 1014 (58% Cl). Mixtures of these PCNs were dissolved in iso-octane and chromatographed on the

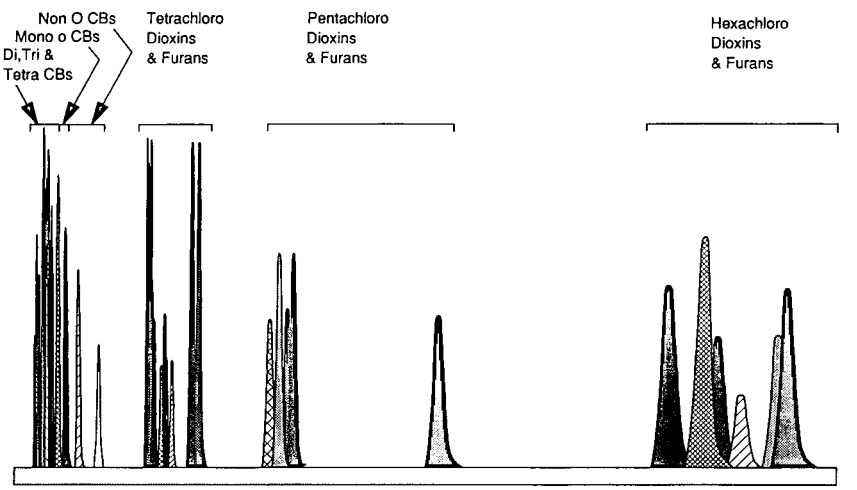

Fig. 6. Reconstructed chromatogram showing the separation of the PCDDs and PCDFs listed in Table 1 on the pyrenyl-silica pyrenyl-silica HPLC column, 150 × 0.46 mm I.D., using *n*-hexane as eluent at 1 ml min^{-1}. See Table 1 for k'-values.

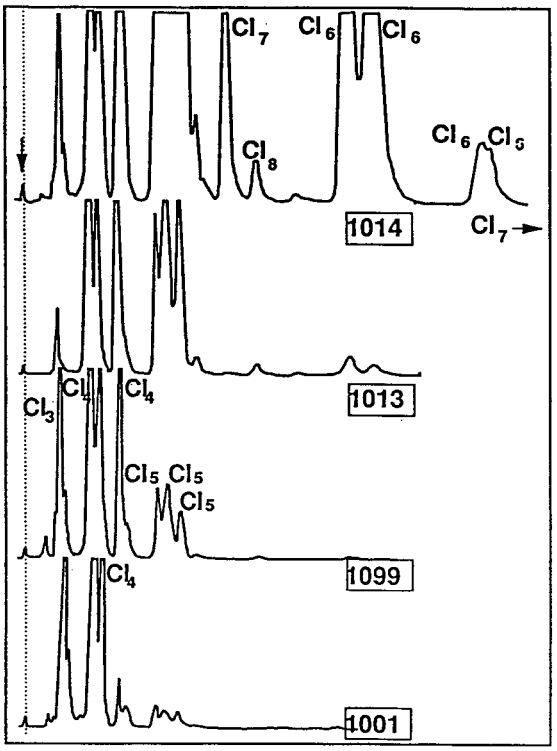

Fig. 7. HPLC chromatogram of the four Halowax (PCN) mixtures with increasing degree of chlorination: HW 1001 (50%), HW 1099 (52%), HW1013 (56%) and HW 1014 (56%). The level of chlorination found in each group was determined by collecting the fractions and re-examining by GC–MS. The separations were made using a 250 × 0.46 mm I.D. pyrenyl-silica HPLC column using *n*-hexane as eluent at 1 ml min^{-1}.

pyrenyl-silica column (Fig. 7). The *k'*-values for each of the major classes of chlorination are given in Table 1. It was clear from these chromatograms that the the penta- and hexachloronaphthalenes may co-elute in the same fraction as the non-*ortho* CBs (Fig. 1). A series of extracts including Halowax 1014 (Fig. 8, trace A), a cleaned-up extract of a cod liver (trace B) taken from the Firth of Clyde, West Scotland and a standard solution of the non-*ortho* CBs (trace C) were prepared to check these possible interferences. Each sample was injected onto the pyrenyl-silica column and the three fractions collected. Fraction III for each sample was analysed by GC and the chromatograms were compared (Fig. 8) using a 50 m × 0.22 mm CPSil 8 column, film thickness 0.25 μm. From these chromatograms it can be seen that all three non-*ortho* CBs were well separated from the penta- and hexa-CNs which eluted in this fraction.

3.5. Effect of column temperature

The *k'*-values for eluants in HPLC are generally temperature dependent. Most reports on the temperature effects of separation have been related to the elevation of the column temperature and the use of column heating ovens. However, the separation of the planar compounds on the pyrenyl-silica column can be improved by reducing the column temperature with a solid-state Peltier heat pump. The Peltier system operates by applying a d.c. voltage to the heat sink, and by reversing the polarity it is possible to obtain a stable cooling effect to ca. 25°C below ambient. Improved separation of CBs at lower column temperatures (0°C) has been observed by Sanders et al. [25].

One critical separation on the pyrenyl-silica column is between CB 138 and CB 163 [18,19,32]. It is difficult to resolve these congeners on most GC phases [24,25], so it is necessary to make this separation prior to the final chromatographic determination. At HPLC column temperatures of around 25°C there is a 5% overlap of these two congeners on the pyrenyl-silica column [19], but when the column temperature is reduced it is possible to improve the resolution and to obtain two completely separate compounds. The resolution increases to a maximum around 0°C, after which there is no further improvement in column performance (Fig. 9). The *k'*-value continues to increase as the temperature is reduced, but the peak width of the determinands also increases, so the overall resolution begins to decline. A comparison of the *k'*-values at 25°C and at 0°C is given in Table 2.

4. Conclusions

The pyrenyl-silica column is able to isolate a wide range of planar compounds both from each other and from co-extracted interfering compounds. It is particularly effective in separating

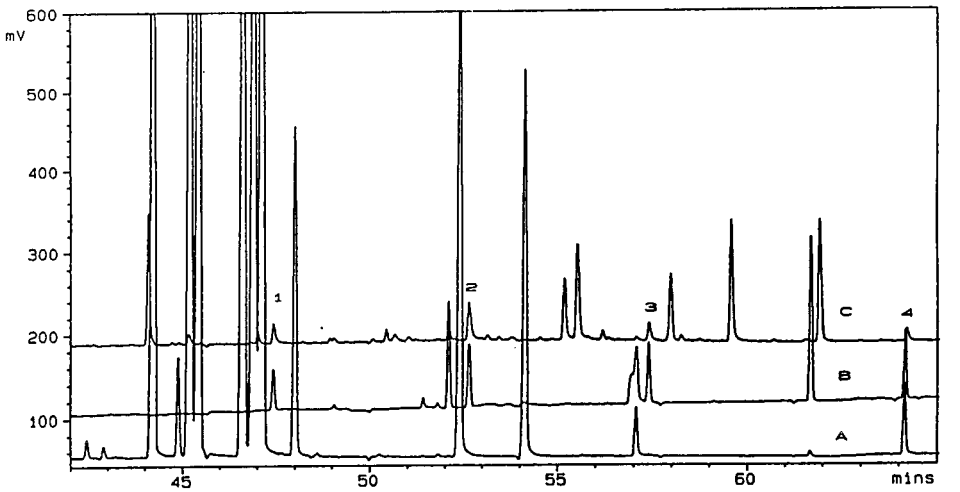

Fig. 8. GC–ECD chromatogram of fraction III from the pyrenyl-silica HPLC column containing pentachloronaphthalenes with Halowax 1014 (trace A), non-*ortho* CBs (trace B) and a cleaned-up extract of cod liver oil (trace C), showing the separation by CP Sil 8 50 m × 0.22 mm I.D., film thickness 0.22 μm. Peaks: 1 = CB 77, 2 = CB 126, 3 = CB 169 and 4 = internal standard.

groups of similar or different structural classes of planar compounds which are present in the samples at very different concentrations. The separation can be tailored to isolate compounds that may be unresolved by capillary GC with either ECD or MS (or both). Most of these separations are highly reproducible and readily automated. The columns are robust and stable over long periods of operation provided that the samples have been through a rigorous clean-up procedure. One of the main reasons for the longevity of the column is that it operates in the normal mode using simple non-polar solvents, as opposed to the reversed-phase mode where the water phase tends to dissolve the silica substrate. Where routine sample clean-up proves to be insufficient, the pyrenyl-silica column can be affected. Usually an incomplete clean-up, particularly involving lipids which have not been removed from biological tissue extract, will result in a decrease both in k' for each compound and a loss in resolution. Performance can be restored by flushing the column with ethyl acetate and then returning to the elution solvent, *n*-hexane. An improved stability and resolution is obtained for a number of separations, e.g. CB 138 and CB 163, if the pyrenyl-silica column is cooled to 0°C.

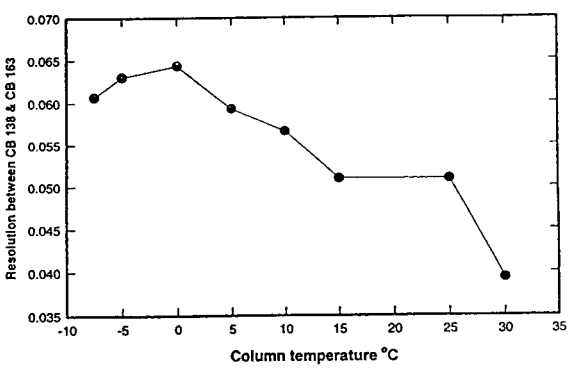

Fig. 9. Plot of the resolution between CB 138 and CB 163 on a pyrenyl-silica HPLC column, 250 × 0.46 mm I.D., as a function of the column temperature. The maximum resolution occurs around 0°C. The column cooling was controlled by a solid-state Peltier heat pump.

Acknowledgements

The authors would like to thank J.N. Robson for the chromatograms of the PAH analysis. I.E. would like to acknowledge the support of the EU Measurement and Testing Programme for part of the work undertaken in this paper. The authors acknowledge the gift of the pyrenyl-silica HPLC columns from Promochem.

References

[1] The Principles and Methodologies of the Joint Monitoring Programme of the Oslo and Paris Commissions, 48 Carey St., London WC2A 2JE, 1990.

[2] North Sea Task Force Monitoring Master Plan, Report No. 3, NSTF, 48 Carey St., London WC2A 2JE, 1990, ISBN 1 872349 02 1.

[3] A. Parkinson and S.H. Safe, in S. Safe (Editor), Mammalian Biologic and Toxic Effects of PCBs, Springer, Heidelberg, 1987, pp. 49–75.

[4] S. Safe, CRC Crit. Rev. Toxicol., 13 (1984) 319–393.

[5] S.S. Thorgeirsson and D.W. Nebert. Adv. Cancer Res., 25 (1977) 149.

[6] J.P. Boon, E. van Arnhem, S. Jansen, N. Kannan, G. Petrick, D. Schulz, J.C. Duinker, P.J.H. Reijnders and A. Goksoyr, Research Publication No. 29, Netherlands Institute for Sea Research (NIOZ), P.O. Box 59, Texel, Netherlands.

[7] J.A. Goldstein and S. Safe, in R.D. Kimbough and A.A. Jensen (Editors), Mechanism of Action and Structure–Activity Relationships for the Chlorinated Dibenzo-*p*-dioxins and Related Compounds, Elsevier, Amsterdam, 1989, pp. 239–293.

[8] P. de Voogt, D.E. Wells, L. Reutergardh and U.A.Th. Brinkman, Int. J. Environ. Anal. Chem., 40 (1990) 1–40.

[9] V.A. McFarland and J.U. Clarke, Environ. Health Perspect., 47 (1992) 75.

[10] D.E. Wells, in D. Barcelo (Editor), Environmental Analysis: Techniques, Applications and Quality Assurance, Elsevier, Amsterdam, 1993, Ch. 4, pp. 113–148.

[11] M.D. Erickson, Analytical Chemistry of PCBs, Butterworth, London, 1986.

[12] S. Safe, L. Safe and M. Mullins, in S. Safe (Editor), PCBs, Environmental Occurrence and Analysis, Springer, Berlin, 1987, pp. 1–13.

[13] N. Kannan, S. Tanabe, T. Wakimoto and R. Tatsukawa, J. Assoc. Off. Anal. Chem., 70 (1987) 451.

[14] J.H. Knox, K. Bulvinder and G.R. Milward, J. Chromatogr., 352 (1986) 3.

[15] C.S. Creasser and A. Al-Haddad, Anal. Chem., 14 (1989) 47.

[16] P. Haglund, L. Asplund, U. Jarnberg and B. Jenssen, J. Chromatogr., 507 (1990) 389–398.

[17] P. Haglund, L. Asplund, U. Jarnberg and B. Jenssen, Chemosphere, 20 (1990) 887.

[18] D.E. Wells and I. Echarri, Anal. Chim. Acta, 286 (1994) 431–449.

[19] D.E. Wells and I. Echarri, Int. J. Environ. Anal. Chem., 47 (1992) 75.

[20] K. Ballschmiter and M. Zell, Fresenius Z. Anal. Chem., 320 (1980) 20–31.

[21] D.E. Wells, M.J. Gillespie and A.E.A. Porter, J. High Res. Chromatogr. Chromatogr. Commun., 8 (1985) 443–449.

[22] D.E. Wells and S.J. Johnstone, J. Chromatogr., 140 (1977) 17–21.

[23] D.E. Wells, A.A. Cowan and A.E.G. Christie, J. Chromatogr., 328 (1985) 272–277.

[24] A.H. Roos, P.G.M. Kienhuis, W.A. Traag and L.G.M.Th. Tuinstra, J. Environ. Anal. Chem., 36 (1989) 155–161.

[25] B. Larsen and J. Riego, Int. J. Environ. Anal. Chem., 40 (1990) 59–68.

[26] J. de Boer and Q.T. Dao, Int. J. Environ. Anal. Chem., 43 (1991) 245–251.

[27] J. de Boer and Q.T. Dao, J. High Res. Chromatogr. Chromatogr. Commun., 12 (1989) 755–759.

[28] J. de Boer and U.A.Th. Brinkman, Anal. Chim. Acta, 289 (1994) 261.

[29] U. Pyell and P. Garregues, J. Chromatogr. A, 660 (1994) 223–229.

[30] A. de Kok, Ph.D. Thesis, Free University of Amsterdam, Netherlands, 1983.

[31] L.C. Sanders, R.M. Parris, S.A. Wise and P. Garrigues, Anal. Chem., 63 (1991) 2589–2597.

[32] I. Echarri, Thesis Doctoral, University of Zaragoza, Spain, 1994.

ELSEVIER

Journal of Chromatography A, 718 (1995) 119–129

JOURNAL OF CHROMATOGRAPHY A

Gas chromatography of petroleum-derived waxes and high-molecular-mass linear alcohols and acids

F.J. Ludwig Sr.*

Technology Department, Petrolite Corporation, 369 Marshall Avenue, St. Louis, MO 63119, USA

First received 13 March 1995; revised manuscript received 6 June 1995; accepted 7 June 1995

Abstract

Capillary gas chromatography procedures on a 15 m × 0.25 mm I.D. wall-coated open-tubular (WCOT) metal column have been developed to separate the components of microcrystalline waxes, paraffin waxes, Unilin® alcohols, or Unicid™ acids. For some microcrystalline waxes about 140 *n*-alkanes and non-normal, i.e., branched or cyclic, hydrocarbons with carbon numbers between 18 and 62 may be resolved. The peak-area percentages of the *n*-alkanes in microcrystalline or paraffin waxes are reproducible. In either underivatized Unilin® alcohols or Unicid™ acid methyl esters 20 to 24 homologs with carbon numbers between 14 and 60 are resolved from adjacent components and from *n*-alkane intermediates; their peak-area percentages are reproducible.

1. Introduction

Waxes of different compositions have been used for a variety of applications throughout the course of human civilization. Industrial waxes may be classified as natural waxes or synthetic waxes [1,2]. Waxes which are derived from petroleum may be subdivided into two classes on the basis of their physical properties and molecular masses: (1) paraffin waxes and (2) microcrystalline waxes. Paraffin waxes typically have average molecular masses ranging from about 360 to 420 and microcrystalline waxes have average molecular masses from about 580 to 700 [3]. Polywax® polyethylenes were introduced into the marketplace in 1970 by Petrolite (St. Louis, MO, USA), and are composed of polyethylene oligomers of molecular masses between about 350 and 2000. Within the past decade, Unilin® alcohols and Unicid™ acids have become commercially available. These products, which are based on the technology used to produce Polywax® polyethylenes, are used as reactive intermediates, e.g. for non-ionic surfactants, and in personal-care products, adhesives, emollients, defoamers, coatings, moldings, and pulp and paper products. The physical properties of petroleum-derived waxes depend on the relative amounts of *n*-alkanes and non-normal hydrocarbons and on the molecular mass distributions of these compounds. The physical properties and chemical reactivities of Unilin® alcohols and Unicid™ acids depend on the molecular mass distribution of the alcohols or acids and on total quantity of reactive components.

It is the objective of the work reported herein to measure the molecular mass distributions of Unilin® alcohols, Unicid™ acids, paraffin

* Corresponding author.

0021-9673/95/$09.50
SSDI 0021-9673(95)00639-7

waxes, and microcrystalline waxes using gas chromatography on a wall-coated open-tubular (WCOT) metal capillary column. The first chromatography of microcrystalline waxes on packed gas chromatography (GC) columns was reported many years ago [4]. About 40 *n*-alkane peaks of carbon numbers 20 to 70 in the urea-adducible fractions of four microcrystalline waxes with melting points from 60 to 80°C were resolved on a 2 ft. × 1/4 in. (0.61 m × 0.635 cm) O.D. stainless-steel column packed with 3% SE-52 on Chromosorb G [4]. Good resolution was also obtained for seven paraffin waxes. The unfractionated microcrystalline waxes, however, did not show satisfactory separation of normal alkanes from non-normal hydrocarbons on this short packed GC column. No well-defined peaks were seen for components with more than about 74 carbon atoms. This same column did give good resolution of about 40 *n*-alkanes in a Fisher–Tropsch wax [5].

When capillary GC columns were developed, much better resolution of *n*-alkanes from non-*n*-alkanes and elution of hydrocarbons of carbon numbers greater than 70 was achieved. For example, when aluminum-clad fused-silica WCOT capillary columns were introduced in 1986, there was a dramatic improvement in both resolution and the upper temperature limit of the column, thereby allowing peaks of at least 100 carbon atoms to be observed [6,7]. Since 1986, there have been numerous reports of high-temperature capillary gas chromatography of waxes and other compounds. Many of these results for petroleum-derived waxes and various synthetic waxes have been summarized recently by Philp [8] and Del Rio and Philp [9]. Barker [10,11] has published two excellent, very comprehensive, and thoughtful reviews of chromatographic analyses of refined and synthetic waxes. He clearly describes the problems of injection, column types, detection, and integration of gas chromatography peaks.

Another major improvement in capillary column technology took place about the start of this decade, namely the introduction of WCOT stainless-steel columns which were based on the work of Takayama and Takeichi [12] and Buyten et al. [13]. Using this technology, Chrompack developed the Ultimetal HT-SIMDIST-CB columns. Using a 15 m × 0.25 mm I.D. HT-SIMDIST-CB Ultimetal column in this laboratory, GC procedures which are reported below have been developed to detect batch-to-batch variations in microcrystalline waxes, paraffin waxes, Unilin® alcohols, or Unicid^{RM} acids and to provide some information about composition.

2. Experimental

2.1. Reagents and materials

Be Square® 195 Amber microcrystalline wax, Victory® Amber microcrystalline wax, Unilin® alcohols, and Unicid^{TM} acids are commercial products which are manufactured and sold by Petrolite Polymers Division (Tulsa, OK, USA). The fully refined paraffin wax of melting point 165°F (74°C) was obtained from another source.

The solvent 1,2-dichlorobenzene was purchased from Sigma–Aldrich (Milwaukee, WI, USA), catalog no. 27, 059-8, 99% HPLC grade.

To prepare known mixtures, the following chemicals, 98–99%, were purchased: *n*-tetracontane, *n*-pentacontane, and *n*-hexacontane from Fluka Chemika–Biochemika (Ronkonoma, NY, USA), and *n*-dotriacontane, *n*-tetracosane, *n*-C_{14}–C_{24} alcohols, and *n*-C_{14}–C_{24} fatty acid methyl esters from Alltech (Chicago, IL, USA).

Meth Prep II (5.3% *m*-trifluoromethylphenyl trimethyl ammonium hydroxide in methanol) is sold by Alltech (Chicago, IL, USA).

The 1-μl syringe with the sample contained in the needle was purchased from Hamilton (Reno, NV, USA), catalog no. 7001.

2.2. Instrumentation

The Model 8500 gas chromatograph with flame ionization detector and programmed temperature vaporizer (PTV) is produced by the Perkin-Elmer (Norwalk, CT, USA).

The Hewlett-Packard (Palo Alto, CA, USA) LDS with 5.24 software was used for peak-area integration and generation of the chromatograms

and figures. The horizontal baseline method, which is described by Barker [10], was used for peak integration of all waxes except Victory® Amber.

2.3. Procedure for microcrystalline wax

Column: 15 m × 0.25 mm I.D., WCOT Ultimetal, film thickness 0.15 μm, stationary phase HT-SIMDIST-CB, maximum operating temperature programmed 450°C, Chrompack International (Middelburg, Netherlands), catalog no. 99921 (custom made). This column still gives good separation after at least 250 injections. Carrier gas: helium (zero grade); flow-rate 41.3 ± 0.383 cm/s or 1.2 ml/min at initial oven temperature. Flow-rates combustion gases: hydrogen (zero grade), 40 ml/min; air (zero grade), 400 ml/min. Flame ionization detector (FID) temperature 430°C. Sensitivity: high. PTV events: −1.99 min: tempearture 50°C; 0.01 min: temperature 425°C. Oven temperature program: initial oven temperature 170°C, hold 2 min; ramp 1 rate, 13°C/min to 300°C; ramp 2 rate, 10°C/min to 430°C, hold 5 min. Depth of injection into PTV liner, 50 mm. Injection volume, 0.5 to 1.0 μl. Split ratio, 25:1. Sample concentration in *o*-dichlorobenzene at ca. 60°C: 0.5–0.7 wt.%.

2.4. Procedure for Unilin® alcohols

The same 15 m × 0.25 mm I.D. HT-SIMDIST-CB column as for microcrystalline waxes was used. Carrier gas, helium (zero grade); flow-rate, 1.2 ml/min. Flow-rates combustion gases: hydrogen 40 ml/min; air 400 ml/min. FID detector temperature 435°C. Sensitivity: high. PTV events: −1.99 min: temperature 50°C; 0.01 min: temperature 385°C. Oven temperature program: initial oven temperature 90°C, hold 2 min; ramp 1 rate, 21°C/min to 180°C; ramp 2 rate, 16°C/min to 250°C; ramp 3 rate, 10°C/min to 430°C, hold 1 min. Depth of injection into PTV liner, 50 mm. Injection volume: 0.5 to 1.0 μl. Split ratio, 25:1. Sample concentration in *o*-dichlorobenzene at ca. 60°C: 0.5–0.7 wt.%.

2.5. Procedure for Unicid™ acids

The same 15 m × 0.25 mm I.D. HT-SIMDIST-CB column as for microcrystalline waxes was used. Carrier gas: helium; flow-rate, 1.2 ml/min. Flow-rates combustion gases: hydrogen 40 ml/min; air 400 ml/min. FID detector temperature, 435°C. Sensitivity, high. PTV events: −1.99 min: temperature 50°C; 0.01 min: temperature 420°C. Oven temperature program: initial oven temperature 140°C, hold 2 min; ramp 1 rate, 21°C/min to 180°C; ramp 2 rate, 16°C/min to 250°C; ramp 3 rate, 10°C/min to 435°C. Depth of injection into PTV liner, 50 mm. Injection volume: 0.5 to 1.0 μl. Split ratio, 25:1. Esterification procedure: weigh about 35 mg of Unicid™ acid in a 5-ml round-bottom flask. Add 3.0 ml *o*-dichlorobenzene and attach to a condenser. Heat at ca. 60°C until solid has dissolved. Add 1.0 ml of Meth Prep II (Alltech, Deerfield, IL, USA) through the top of the condenser. Heat 3 to 5 min until solution is homogeneous. Quickly transfer the solution to a 5 ml vial. Inject an aliquot of the warm (ca. 60°C) solution into the PTV.

3. Results and discussion

3.1. Petroleum-derived waxes

The chromatogram of Be Square® 195 Amber, a microcrystalline wax of melting point 93°C, is shown in Fig. 1. Certain peaks which elute at the same retention time as pure *n*-alkanes are marked. Based on proton NMR peak areas of CH_2 and CH_3 groups, the major peaks are presumed to be mostly *n*-alkane homologs. Hence these components are designated "*n*-alkanes" in Figs. 2 and 4, Table 1, and the following text. Peaks which contain hydrocarbons with 21 to 74 carbon atoms are shown in Fig. 1. *n*-Alkanes and non-normal hydrocarbons, which probably include branched and cyclic alkanes, co-elute if they contain more than 62 carbon atoms. In Fig. 2, the area-percents of *n*-alkanes are plotted as a function of their carbon numbers. The total amount of *n*-alkanes

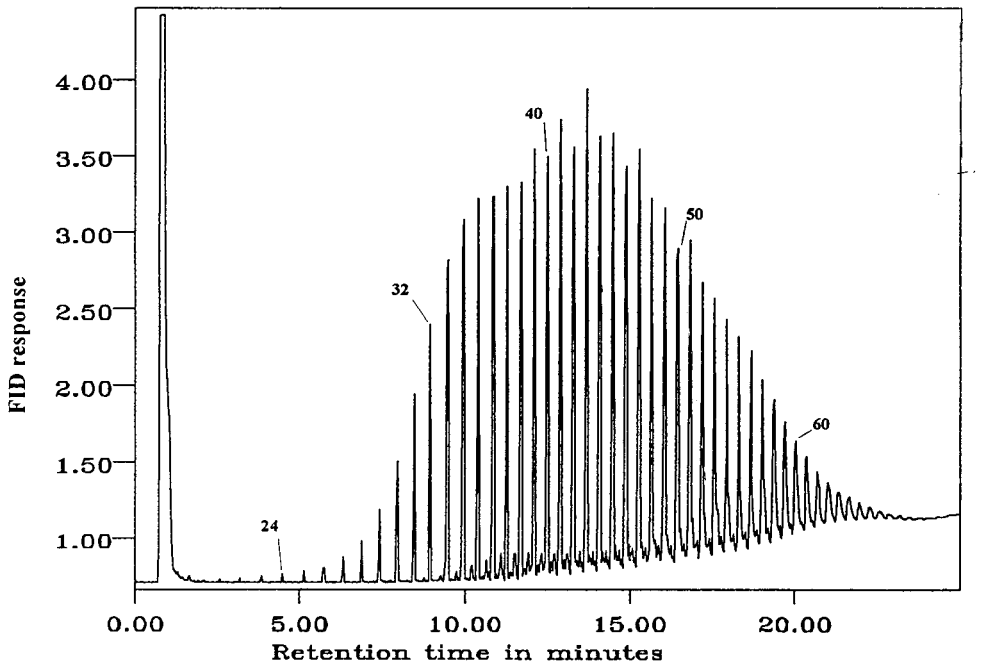

Fig. 1. Gas chromatogram of Be Square® 195 Amber microcrystalline wax.

with carbon numbers between C_{22} and C_{62} is 83 area-percent and the total amount of all hydrocarbons with carbon numbers between C_{63} and C_{73} is 4.2 area-percent. Hence this wax contains about 15% non-normal hydrocarbons. Barker [10] has reviewed the composition of petroleum-derived waxes. He describes their complexity in detail.

The area-percents of the *n*-alkanes in the Be Square® 195 Amber are probably a good approximation of their weight-percents, since for known mixtures of several pure *n*-alkanes with 24 to 60 carbon atoms the area-percents and weight-percents are about equal, e.g. differing by ca. 1–2%.

The mean values of five replicate GC runs and their standard deviations of selected *n*-alkanes with carbon numbers between 22 and 60 are given in Table 1. From these values of the standard deviations, it may be concluded that the reproducibility of this GC procedure is good.

The chromatogram of Victory® Amber, a microcrystalline wax of melting point 79°C, is shown in Fig. 3. The distribution of *n*-alkanes is shown in Fig. 4. For components with more than 57 carbon atoms the *n*-alkanes and non-normal alkanes co-elute. The rather large rising "background" starting at about 34 carbon atoms probably is caused by incomplete resolution of *n*-alkanes and non-normal hydrocarbons of similar

Table 1
Mean values and standard deviations of the area-percents of selected *n*-alkanes in Be Square® 195 Amber and Victory® Amber

Carbon number	Be Square 195 Amber Mean ± S.D. ($n = 5$)	Victory Amber Mean ± S.D. ($n = 5$)
22	0.0469 ± 0.0103	0.0488 ± 0.00294
26	0.151 ± 0.0147	0.232 ± 0.00705
30	0.976 ± 0.0182	0.616 ± 0.0166
34	2.18 ± 0.0517	1.63 ± 0.0358
38	2.68 ± 0.0568	2.26 ± 0.0612
42	3.48 ± 0.0418	2.03 ± 0.0763
46	3.31 ± 0.181	2.01 ± 0.119
50	3.03 ± 0.0202	1.60 ± 0.0857
54	2.57 ± 0.0243	1.11 ± 0.0564
58	2.06 ± 0.0213	1.18 ± 0.0342

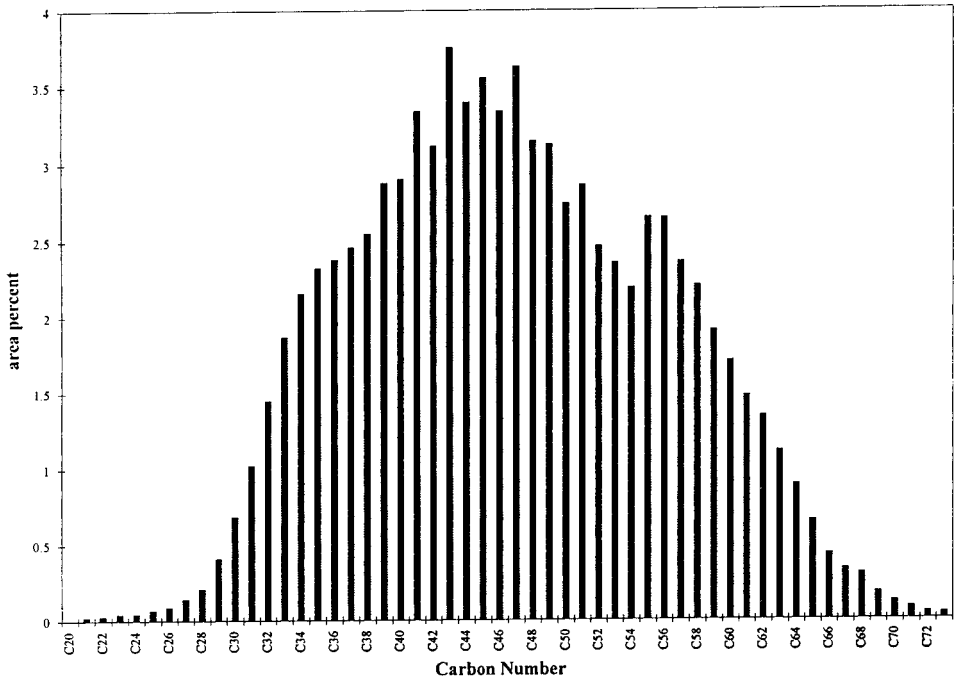

Fig. 2. Distribution of *n*-alkanes in Be Square® 195 Amber microcrystalline wax.

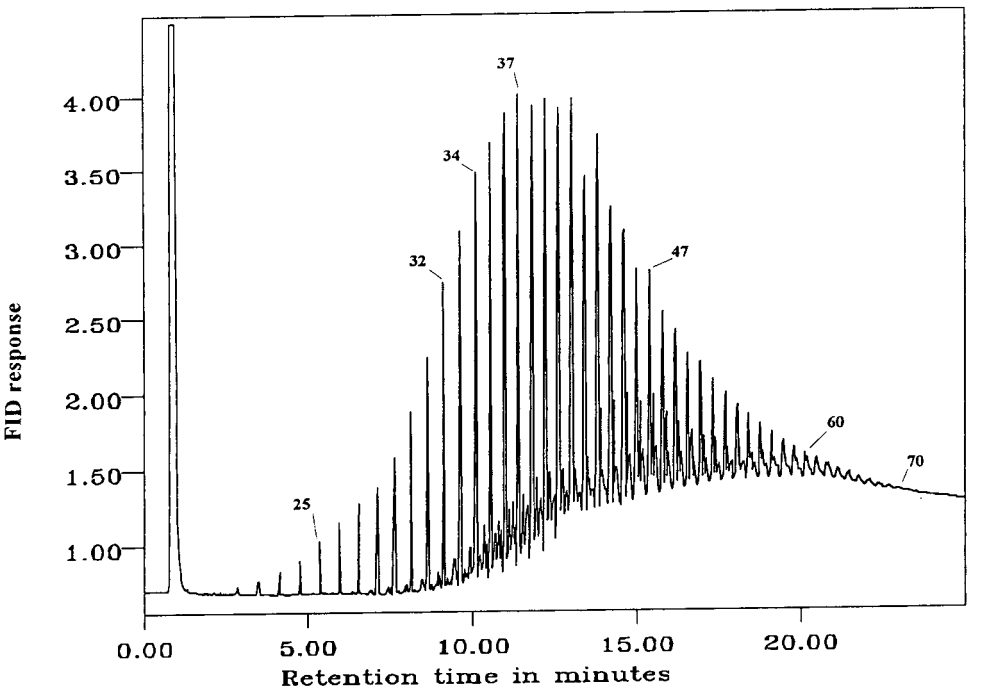

Fig. 3. Gas chromatogram of Victory® Amber microcrystalline wax.

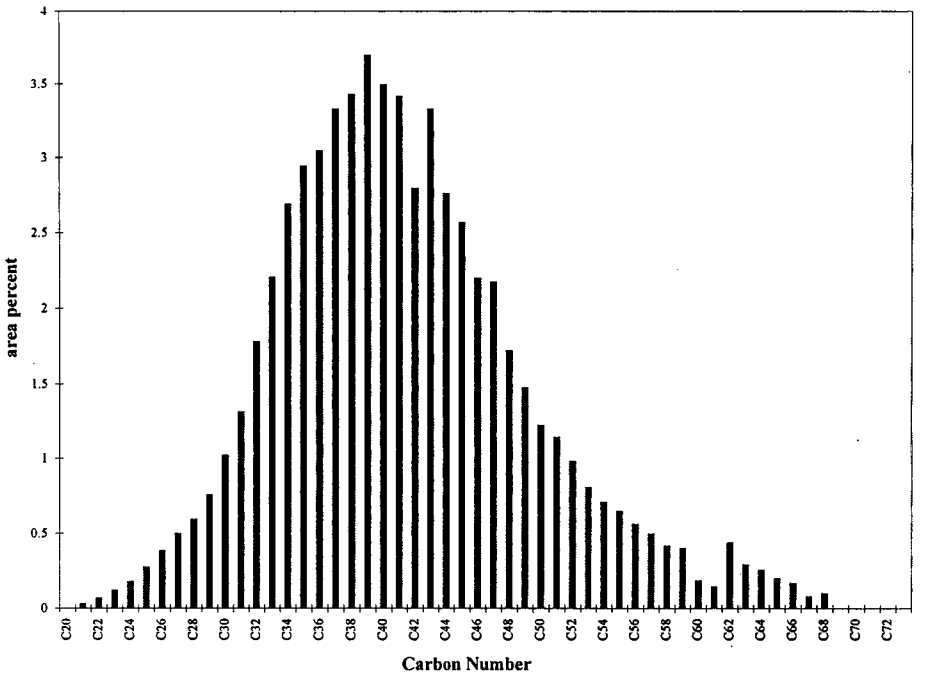

Fig. 4. Distribution of *n*-alkanes in Victory® Amber microcrystalline wax.

carbon numbers. The sum of the area-percents of the major peaks above the background using a modified horizontal background integration is 59% for components with 20 to 62 carbon atoms. The sum of the area-percents of peaks with 62 to 68 carbon atoms is only 1.1%. The mean values and standard deviations of the area-percents of selected *n*-alkane peaks between C_{22} and C_{60} are given in Table 1. Because of incomplete resolution and possible co-elution, the standard deviations tend to be larger than those of the major components of Be Square® 195 Amber. Nevertheless, gas chromatography appears to be a satisfactory means of detecting batch-to-batch variations in lower-melting-point microcrystalline waxes. Barker [10] has given a very thorough discussion of these problems of integration and resolution of components of microcrystalline waxes.

The GC procedure for microcrystalline waxes which is described in the Experimental section above for a 15-m long column, represents a compromise between two diametrically opposite goals: (1) maximum resolution of *n*-alkanes from non-normal hydrocarbons, particularly in the 20 to 50 carbon number range, and (2) elution of the highest-molecular-mass hydrocarbons in the wax near the maximum operating temperature of the column and thermal stability of the hydrocarbons. As noted above, C_{74}, which elutes at 430°C after a 2 min hold, appears to be the last peak that can be integrated accurately. Three or four non-normal hydrocarbon peak areas are measured between *n*-alkane pairs of carbon numbers 32 and 48, while only two non-normal hydrocarbons are resolved between *n*-alkane pairs of carbon numbers 49 an 57. A larger column, e.g. 30 m, would give better resolution of the C_{20}–C_{40} hydrocarbons, but then no components with more than possibly 55 carbon atoms would have peaks of reproducible areas or even be detected at all. Because microcrystalline waxes, particularly those with melting points less than about 85°C, probably contain at least sever-

al hundred chemical compounds, gas chromatography of the unfractionated waxes in a finite time to determine their exact compositions is not possible, but useful comparisons of waxes can still be made.

An appreciably different and much simpler chromatogram is obtained for a fully refined paraffin wax as is shown in Fig. 5. Here, the *n*-alkanes of carbon numbers C_{22} through C_{37} constitute 91% of the peaks which were integrated. The distribution of *n*-alkanes, i.e., area-percent versus carbon number, which is shown in Fig. 6, is much sharper than the distributions of the microcrystalline waxes, which are depicted in Figs. 2 and 4. For paraffin waxes it would be readily feasible to use a longer column to improve resolution of *n*-alkanes and non-normal hydrocarbons. The mean values and standard deviations of *n*-alkanes with 22 to 36 carbon atoms in this paraffin wax are presented in Table 2, demonstrating that the procedure has a very good reproducibility.

One key problem which must be addressed in high-temperature chromatography, is that of sample discrimination during the injection process, resulting in incomplete transfer of the higher-boiling-point compounds from the syringe into the injection part and onto the column. The use and optimization of the Perkin-Elmer programmed temperature vaporizer has been described [14–16]. Barker [10,11] has made extensive studies of injection techniques, especially PTV. Grob [17] recently has reviewed injection techniques in capillary GC. Although he concludes "today's injection techniques often provide satisfactory results" he laments the lack of progress in solving "severe problems". The results in Table 3 suggest that our PTV program is not causing discrimination of C_{50} or C_{60} in the mixture of pure *n*-alkanes–alkanes, since the theoretical weight-percents and measured area-percents differed by 2.3% and 1.3%, respectively. The author believes that use of the PTV injector and a syringe with sample in the needle

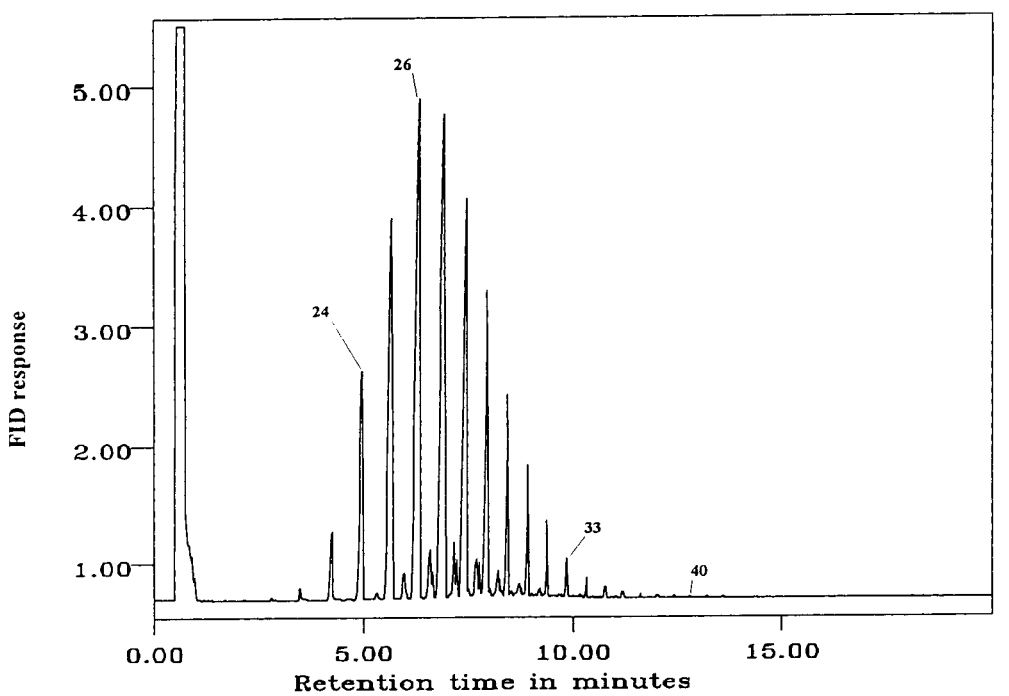

Fig. 5. Gas chromatogram of fully refined 165°F paraffin wax.

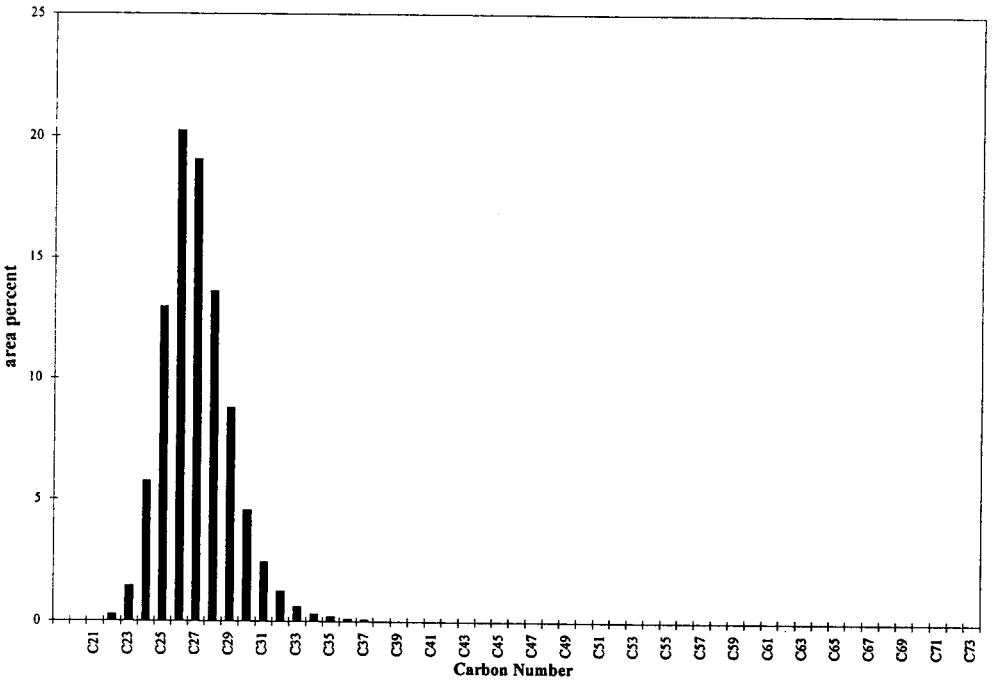

Fig. 6. Distribution of *n*-alkanes in fully refined 165°F paraffin wax.

is required for reproducible GC of microcrystalline waxes, Unilin® alcohols, and Unicid™ acids.

Table 2
Mean values and standard deviations of *n*-alkanes with 22 to 36 C atoms in a fully refined 165°F paraffin wax

Carbon number	Mean ± S.D. ($n = 5$)
22	0.248 ± 0.0175
23	1.46 ± 0.0693
24	5.81 ± 0.116
25	13.0 ± 0.0895
26	20.2 ± 0.144
27	18.9 ± 0.205
28	13.6 ± 0.243
29	8.67 ± 0.129
30	4.52 ± 0.0415
31	2.47 ± 0.0737
32	1.33 ± 0.0554
33	0.633 ± 0.0602
34	0.389 ± 0.0356
35	0.229 ± 0.0225
36	0.133 ± 0.0151

3.2. Unilin® alcohols

Unilin® alcohols of average molecular masses between 350 and 700 are commercially available. The chromatogram of one of these products, Unilin® 425, is shown in Fig. 7. About 55 components in all are resolved. The major peaks are *n*-alkanols of carbon numbers 14 to about 66,

Table 3
Comparison of weight-percents in a known mixture of *n*-alkanes with measured GC area-percents

Carbon no. of *n*-alkane	Weight-percent theory	Measured area-percent ± S.D. ($n = 10$)
24	11.7	10.0 ± 0.479
32	22.2	21.25 ± 0.854
40	14.4	13.4 ± 0.665
50	24.4	26.7 ± 0.666
60	27.2	28.5 ± 2.56[a]

[a]Peak is on slightly rising background and shows some tailing.

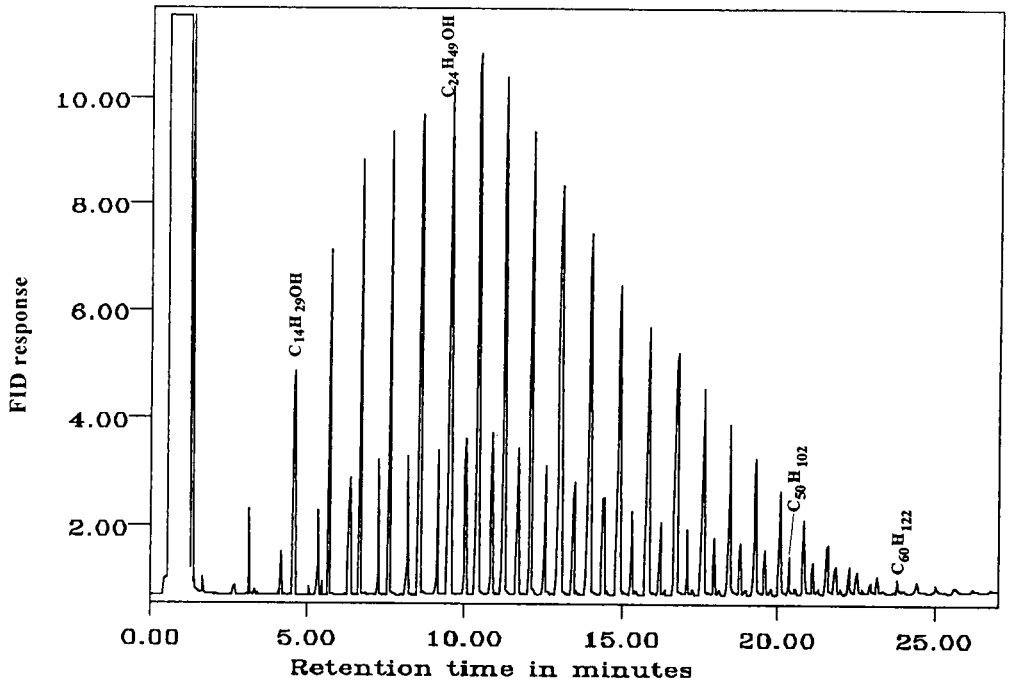

Fig. 7. Gas chromatogram of Unilin® 425 alcohol.

while the minor peaks are *n*-alkanes. After $C_{54}H_{109}OH$, the alcohols and alkanes co-elute. The sum of the area-percents of *n*-alkanols with carbon numbers 14 through 54 is 80.0 ± 0.163 (eight replicate runs). This value is consistent with the total *n*-alkanol content which is measured by the hydroxyl-number procedure. The mean values and standard deviations of the area-percents of selected *n*-alkanols in the carbon number range are presented in Table 4. These standard deviations show that the procedure is reproducible.

A known mixture of pure *n*-alkanols with 14, 16, 18, 20, 22, and 24 carbon atoms of weight-percents 19.7, 15.4, 20.5, 11.8, 16.2, and 16.4%, respectively, was prepared to determine retention times and to compare measured GC area-percents with these theoretical weight-percents. The weight-percents and area-percents of the *n*-alkanols in this mixture differed by less than 2%. *n*-$C_{24}H_{49}OH$ eluted without loss during injection or decomposition with PTV programs of either 50 to 285°C or 50 to 325°C. A source of

Table 4
Mean values and standard deviations of the area-percents of selected *n*-alkanols in Unilin® 425

Carbon number	Mean ± S.D. ($n = 8$)
14	1.25 ± 0.0458
16	2.10 ± 0.0747
18	3.02 ± 0.0601
20	3.92 ± 0.0553
22	4.77 ± 0.0851
24	5.62 ± 0.0699
26	6.51 ± 0.0476
28	7.02 ± 0.0770
30	7.17 ± 0.100
32	7.02 ± 0.116
34	6.47 ± 0.114
36	5.57 ± 0.129
38	4.61 ± 0.0734
40	3.87 ± 0.129
42	3.15 ± 0.151
44	2.44 ± 0.142
46	1.85 ± 0.130
48	1.34 ± 0.118
50	0.920 ± 0.0952
52	0.590 ± 0.0746

pure *n*-alkanols with carbon numbers in the 30 to 50 range was not found. If these were available, it would be desirable to measure response factors and verify thermal stability of the higher-molecular-mass alcohols under the PTV and column operating temperature.

The GC procedure is satisfactory for product quality comparisons and to aid process improvement studies. Supercritical fluid chromatography on packed columns may be an alternate approach, since it has been shown to give very good resolutions of Polywax® 665 and Polywax® 1000 polyethylenes, which are commercially available synthetic waxes [18]. This instrument, however, is not available in many research laboratories.

3.3. Unicid™ acids

Unicid™ acids of average molecular mass in the range of 350 to 700 are commercially available. The chromatogram of one of these products, Unicid™ 550, is shown in Fig. 8. About 55 components in all are resolved. A known mixture of fatty acid methyl esters with 14, 16, 18, 20, 22, and 24 carbon atoms was run to measure their retention times and also to compare measured area-percents with theoretical weight-percents. The area-percents were within 1 to 2% of the weight-percents. No pure carboxylic acids with 30 to 60 carbon atoms were available to measure response factors. In Fig. 8, two peaks of the same retention times as those of pure *n*-alkanes and those of two carboxylic acid methyl ester peaks are noted.

The sum of the area-percents of the methyl esters of carboxylic acids with 16 to 60 carbon atoms is 78.1 ± 0.632% for seven replicate runs. The mean values and standard deviations of the area-percents of selected carboxylic acid methyl esters are given in Table 5. The reproducibility of this procedure is very good. Evidently, the pyrolytic methylation procedure, for which a mechanism has been proposed [19], is satisfactory for aliphatic carboxylic acids with 30 to 60 carbon atoms.

This method is satisfactory for correlation of composition, e.g., total acid content and molecu-

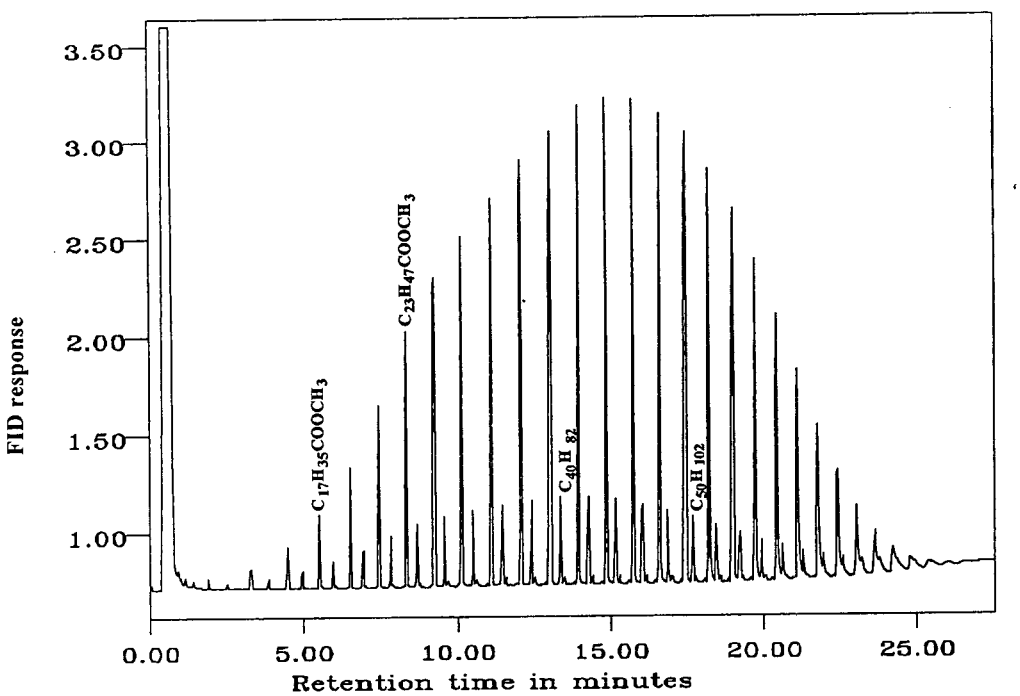

Fig. 8. Gas chromatogram of Unicid™ 550 methyl esters.

Table 5
Mean values and standard deviations of the area-percents of selected methyl esters of carboxylic acids in Unicid® 550

Carbon number	Mean ± S.D. ($n = 6$)
16	0.234 ± 0.0689
20	0.519 ± 0.0403
24	1.20 ± 0.0692
28	2.31 ± 0.0822
32	3.61 ± 0.0691
36	4.93 ± 0.00902
40	5.83 ± 0.109
44	5.98 ± 0.104
48	5.41 ± 0.108
52	4.36 ± 0.0985
56	3.14 ± 0.0906

lar mass distribution, with reactivity and physical properties of Unicid™ acids.

Acknowledgements

The author thanks J.E. Coovert of Petrolite for preparation of the figures, J.V. Hinshaw of Perkin-Elmer Corporation for helpful advice concerning operation of the PTV injector, and D. Redmore of Petrolite for permission to publish this paper and suggestions about the manuscript.

References

[1] H. Bennett, Industrial Waxes, Chemical Publishing, New York, 1975.
[2] R. Sayers, Wax an Introduction, European Wax Federation and Gentry Books, London, 1983.
[3] H. Bennett, Industrial Waxes, Chemical Publishing, New York, 1975, p. 98
[4] F.J. Ludwig, Sr., Anal. Chem., 37 (1965) 1732.
[5] F.J. Ludwig, Sr., Soap Chem. Spec., 43 (1966) 70.
[6] S.R. Lipsky and M.L. Duffy, J. High Resolut. Chromatogr. Chromatogr. Commun., 9 (1986) 376.
[7] S.R. Lipsky and M.L. Duffy, J. High Resolut. Chromatogr. Chromatogr. Commun., 9 (1986) 725.
[8] R.P. Philp, J. High Resolut. Chromatogr., 17 (1994) 398.
[9] J.C. Del Rio and R.P. Philp, Org. Geochem., 8, No. 4 (1992) 541.
[10] A. Barker, in E.R. Adlard (Editor), Chromatography in the Petroleum Industry, Journal of Chromatography Library Series Vol. 56, 1995, Elsevier, Amsterdam, Ch. 3.
[11] A. Barker, in G. B Crump (Editor), Petroanalysis '87, Wiley, New York, 1988, pp. 159–171.
[12] Y. Takayama and T. Takeichi, J. Chromatogr. A, 685 (1994), 61–78.
[13] J. Buyten, C. Duvekot, J. Peene, J. Lips and M. Mohnke, 11th Int. Symp. on Capillary Chromatography, Monterey, CA, 1990, p. 91.
[14] J.V. Hinshaw, Jr., J. Chromatogr. Sci., 25 (1987) 49.
[15] J.V. Hinshaw and L.S. Ettre, J. High Resolut. Chromatogr., 12 (1989) 251.
[16] A. Tipler and G. Johnson, J. High Resolut. Chromatogr., 13 (1990) 365.
[17] K. Grob, Anal. Chem., 66 (1994) 1009A.
[18] S.M. Shariff, T. Tong and K.D. Bartle, J. Chromatogr. Sci., 32 (1994) 541.
[19] W.C. Kossa, J. MacGee, S. Ramachondran and A.J. Webber, J. Chromatogr. Sci., 17 (1979) 177.

ELSEVIER

Journal of Chromatography A, 718 (1995) 131–139

JOURNAL OF CHROMATOGRAPHY A

Determination of pentachlorophenol in leather using supercritical fluid extraction with in situ derivatization

Anja Meyer, Wolfgang Kleiböhmer*

Institut für Chemo- und Biosensorik e.V., Lehrstuhl für Analytische Chemie, Westfälische Wilhelms-Universität Münster, Mendelstraße 7, D-48149 Münster, Germany

First received 17 February 1995; revised manuscript received 8 June 1995; accepted 9 June 1995

Abstract

An in situ supercritical fluid extraction (SFE) and derivatization procedure for the determination of pentachlorophenol (PCP) in leather is described. PCP was extracted from leather with supercritical carbon dioxide and in situ derivatized with acetic anhydride in the presence of a base (e.g., triethylamine). The influence of several extraction and derivatization parameters (e.g., pressure, temperature, extraction time in the static and dynamic extraction mode, amount of the base and of acetic anhydride) on the extraction efficiency has been investigated. Since the leather sample had no certified PCP content, the SFE results were compared with those obtained by Soxhlet extraction with methanol. With SFE instead of conventional Soxhlet extraction, the overall time required for sample preparation, extraction, derivatization, evaporation, clean-up and analysis steps can be reduced from about 2 days to approximately 3 h.

1. Introduction

Since its commercial introduction in 1936, pentachlorophenol (PCP) has found world-wide application, e.g., in commercial wood treatment (as a preservative, insecticide and microbiocide), for paper production (for reduction of slime), in leather industry (as a preservative and fungicide) and in agriculture (as an herbicide and insecticide) [1–3]. Therefore, human exposure to this chemical cannot be prevented. PCP is an environmental concern as it is toxic to fish and mammals [1]. However, because of its broad efficiency spectrum and the low cost of production, PCP is still in use.

In 1989, the German pentachlorophenol prohibition order has established an upper limit of 5 mg/kg for the PCP content in leather and other matrices [4,5].

Solvent extraction (e.g., Soxhlet extraction) or steam distillation techniques are widely used for extractions of PCP from leather [6], although these methods are time-consuming. In the case of solvent extractions, large amounts of organic solvents are required and several clean-up steps are necessary to remove coextractives. Both techniques require an additional derivatization step if PCP is to be analyzed by gas chromatography (GC) in the form of, e.g., an acetyl derivative. However, the risk of sample losses increases with each step in the process.

Therefore, the aim of this work was to develop

* Corresponding author.

0021-9673/95/$09.50
SSDI 0021-9673(95)00660-5

a simple, rapid and precise method for the determination of PCP in leather samples.

Supercritical fluid extraction (SFE) has been proved to be an efficient alternative to conventional methods for extractions of polychlorinated biphenyls, polynuclear aromatic hydrocarbons, dioxins and chlorobenzenes from soils, sediments and other solid matrices [7–13]. However, quantitative extractions of polar analytes (e.g., phenols) require the addition of a polar modifier (e.g., methanol) to the non-polar carbon dioxide. Recently, extractions of phenols from soils and sediments have been performed by in situ extraction and chemical derivatization under SFE conditions [14].

No extra step is required for derivatization of the analytes. In addition, the polarity of the analytes is usually decreased by derivatization, and therefore they are easier to extract, and they become more amenable to subsequent column clean-up than the free compounds.

In this study, a method for the determination of pentachlorophenol in leather being based upon SFE with in situ acetylation is presented. The influence of individual extraction and derivatization parameters on the extraction efficiency was investigated. The results of the SFE–derivatization procedure were compared with those obtained by conventional Soxhlet extraction.

2. Experimental

2.1. Samples and standards

Pentachlorophenol was obtained from Alltech (Unterhaching, Germany), 2,4,6-tribromophenol (TBP) from Aldrich (Steinheim, Germany) and 2-methyl-4-nitrophenol (2-M-4-NP) from Dr. Ehrenstorfer (Augsburg, Germany). Isopropylamine was purchased from Fluka (Neu-Ulm, Germany). All solvents as well as acetic anhydride, triethylamine (TEA) and potassium hydrogencarbonate were obtained from Merck (Darmstadt, Germany) in the highest purity available. The anhydride was triple-distilled and the fraction of b.p. 138–140°C was used. Carbon dioxide with a helium head pressure of 100 atm (1 atm = 101 325 Pa) was supplied by Westfalen Gas (Münster, Germany).

Stock solutions of PCP (8 mg/ml) and the internal standard 2,4,6-tribromophenol (18 mg/ml) have been prepared in toluene. For spiking purposes, acetone solutions containing 0.5 mg PCP/ml and 0.7 mg TBP/ml were prepared. Acetylated 2-methyl-4-nitrophenol ("2-M-4-NPAc") was used as an internal standard for GC analysis and it was prepared by aqueous derivatization according to an established procedure [15]. For calibration of the instrument, PCP and TBP also had to be derivatized. Stock solutions of acetylated PCP (9 μg/ml), TBP (70 μg/ml) and 2-M-4-NP (220 μg/ml) were prepared in toluene.

2.2. Extraction of PCP from leather

Soxhlet extractions

A 70-ml Soxhlet extractor with 100 × 25 mm I.D. extraction thimbles (Schleicher & Schüll, Dassel, Germany) and a 100-ml round-bottomed flask was used for all extractions. The extraction process was based upon a procedure described in [16]. Each extraction was carried out with 6 g of the leather sample and 80 ml of methanol for 8 h in the dark. The internal standard 2,4,6-tribromophenol was added to the extract in such an amount that the final concentration was the same as it had been in the calibration procedure of the GC–ECD system (0.2 μg/ml). After concentration and several liquid–liquid partitioning-steps, the extract was cleaned-up on silica gel. Finally, derivatization of PCP was performed in aqueous solution as described by Lee et al. [15]. To determine the amount of PCP being actually in the extract, a defined volume of the internal standard 2-M-4-NPAc was added to appropriate dilutions of the extracts in toluene for GC–ECD analysis.

Supercritical fluid extractions

All supercritical fluid extractions were performed with an in-house-built SFE system which consists of a syringe pump, a metal block (especially designed to the form of the extraction

cells) which was heated with water, a thermostat which controls the temperature of the water bath, several valves that allow extractions in the static and dynamic mode and a heated restrictor (PEEK-capillary; 10 cm × 125 μm I.D.).

For recovery experiments, the extraction cells (Dionex, Idstein, Germany; 3.5 ml; 5 cm × 9.4 mm I.D.) were filled with silanized glass-fibre wadding (Macherey-Nagel, Düren, Germany) and about 1.6 g of Chromabond C_{18} endcapped (Macherey-Nagel). The material was spiked with 50 μl of the PCP solution containing 473 μg/ml acetone and 40 μl of the internal standard TBP (710 μg/ml acetone). The solvent was allowed to evaporate. After addition of 100 μl of triethylamine, the loaded cell was heated in the metal block to 50°C for 5 min before 400 μl of acetic anhydride was added via an extra valve. At a pressure of 300 atm, the sample was then extracted for 10 min in the static and for about 15 min (corresponding to 20 ml of carbon dioxide, measured in its liquid state) in the dynamic extraction mode.

Analyte collection after off-line SFE was performed with chilled dual-chamber trapping vials [17] which were filled with light petroleum.

For extractions of PCP from leather, the extraction cells were filled with 1.8 g of the leather sample which was cut up (in the cm^2 range), and after addition of the internal standard TBP, extractions were carried out as described above (otherwise the parameters are mentioned in the text).

2.3. Clean-up

The extracts were partitioned with 3 ml of 2% potassium carbonate solution in a separation funnel for 1 min. This step was necessary for the removal of the excess acetic anhydride and the acetic acid formed in the derivatization step. Both of these can lead to chromatographic problems if the uncleaned extracts are analyzed [14].

Under a gentle stream of nitrogen, the solvent was evaporated to about 2 ml. A clean-up column [Pasteur pipette (23 × 0.5 cm I.D.) filled with silanized glass-fibre wadding, 0.55 g of silica gel (30–60 μm; J.T. Baker, Gross-Gerau, Germany) and 0.25 g of anhydrous sodium sulphate (Merck)] was rinsed with 5 ml of *n*-hexane. The light-petroleum extract was transferred to the clean-up column which was finally rinsed with 0.5 ml of *n*-hexane. This fraction was discarded. Elution of the acetylated chlorophenols was performed with 9 ml of toluene. In a volumetric flask the extract was filled up to 10 ml with toluene. For GC–ECD analysis a defined volume of 2-M-4-NPAc was added to appropriate dilutions of the extracts.

2.4. Gas chromatographic analysis

Gas chromatographic analysis was carried out with a Varian (Darmstadt, Germany) Series 3300 gas chromatograph equipped with a split/splitless injection port and an electron capture detector. Split (1:20) injection (1 μl) was performed with a Dynatech GC-411V autosampler. The 25 m × 0.32 mm I.D. Permabond SE-54-DF-0.25 capillary column (Macherey-Nagel, Düren, Germany) and the 2-m deactivated fused-silica precolumn (Macherey-Nagel) were initially heated to 80°C. Temperature was then increased to 130°C at 20°C/min, to 150°C at 5°C/min, to 200°C (held for 1 min) at 10°C/min and finally to 230°C (held for 5 min) at 30°C/min. Nitrogen was used as carrier gas with a column head pressure of 1.05 atm. Dionex AI-450 software was used for data acquisition and analysis. For instrument calibration, acetyl derivatives of PCP, TBP and 2-M-4-NP were prepared as described above. Quantification was performed according to the multilevel internal standard calibration method. Therefore, appropriate dilutions of acetylated PCP (0.03–0.36 μg/ml) were prepared in toluene, each containing 0.2 μg of acetylated TBP/ml and 0.8 μg of 2-M-4-NPAc/ml.

3. Results and discussion

SFE with in situ derivatization is an efficient alternative to conventional SFE techniques as this approach further reduces sample preparation

Table 1
Recovery of PCP from spiked C_{18}

	PCP added (μg)	PCP recovered $\bar{x} \pm \sigma$ (μg)	Recovery $\bar{x} \pm \sigma$ (%)
PCP, determined with TBP	23.6	24.3 ± 1.2	103 ± 5
PCP, determined with 2-M-4-NPAc	23.6	24.8 ± 1.3	105 ± 7

Abbreviations as in Fig. 1. Extractions were carried out as described in the text. $n = 10$.

time and at the same time enhances the extractability of polar analytes by reducing their polarity [14].

In order to evaluate the efficiency of the in situ SFE–derivatization method (especially of analyte collection and clean-up steps), the recovery of PCP from an inert matrix (C_{18}) being spiked at a known level has been determined, and the results are presented in Table 1.

As PCP was completely recovered from spiked C_{18}, no sample losses had occurred during sample preparation.

In naturally contaminated matrices, interactions between the analytes and the active sites of the matrix can be very strong. In order to investigate the influence of matrix effects on the PCP-recovery from leather, the described SFE procedure was applied to a "naturally" contaminated leather sample. Fig. 1 shows a chromatogram of a leather extract after SFE–derivatization and clean-up.

Since the leather sample used for this study had no certified PCP-content, conventional Soxhlet extraction with methanol (see above) was used to determine it. The presence of PCP has been proved by GC–MS (Fig. 2). 2,3,4,6-Tetrachlorophenol has also been detected in the leather sample. A comparison between the results obtained by Soxhlet extraction and SFE is presented in Fig. 3.

The two methods yielded comparable results. Despite the differences in extraction, derivatization and clean-up steps, determination of PCP with the internal standard TBP yielded higher recoveries than determination with 2-M-4-NPAc for both methods.

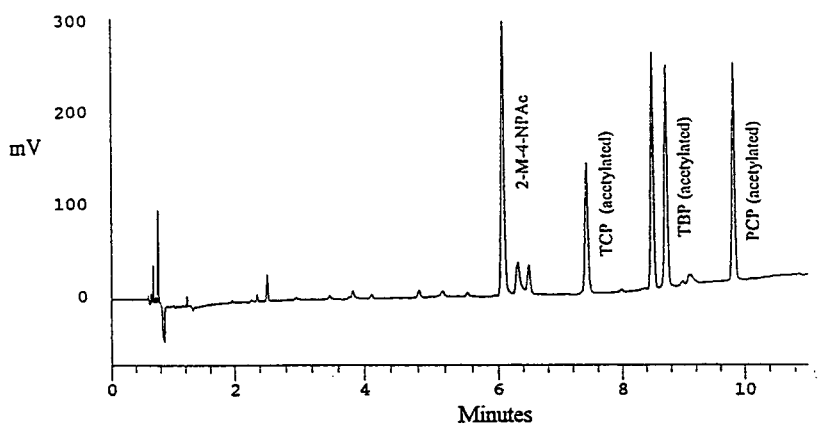

Fig. 1. GC–ECD chromatogram of a leather extract obtained by SFE with in situ acetylation. Chromatographic conditions are described in the text. 2-M-4-NPAc = acetylated 2-methyl-4-nitrophenol; TCP = 2,3,4,6-tetrachlorophenol; TBP = 2,4,6-tribromophenol; PCP = pentachlorophenol.

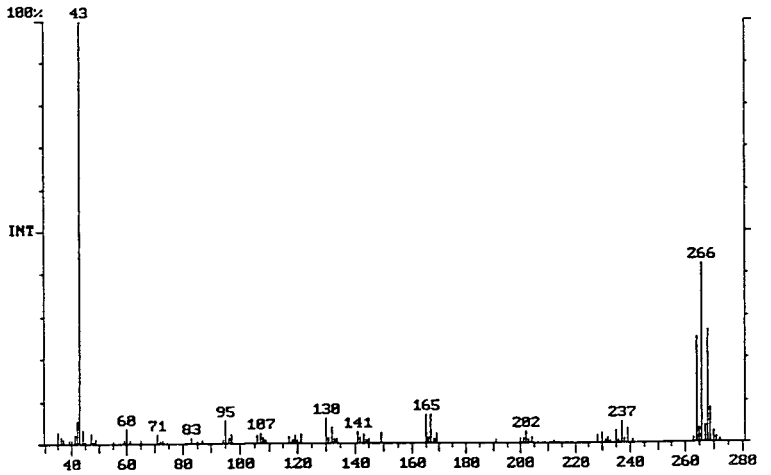

Fig. 2. Mass spectrum of acetylated PCP in a leather extract.

TBP has to be derivatized and extracted like PCP. Therefore, determination with TBP should compensate analyte losses due to incomplete derivatization and/or extraction while determination of PCP with 2-M-4-NPAc (which is added to the extract just before GC analysis) only indicates the amount of PCP being actually in the extract. Differences between these two methods must therefore be a consequence of analyte losses. It should be noted, that according to statistical tests, the results are really different (at least for SFE) although the error bars overlap.

Analyte collection is one of the most problematic steps in SFE, but in this case, quantitative recoveries have been observed for SFE of PCP from spiked C_{18} (note Table 1) using light-petroleum traps. Besides, these traps yielded the best results for PCP extractions from leather when being compared with other trapping methods [18].

Clean-up of the extracts, which is another problematical step in SFE, has been optimized in a previous study [18]. Hence, in the case of SFE, the discrepancy between the two determination methods must have been caused by incomplete extraction and/or derivatization of the analytes. This could be a consequence of matrix effects, since determination with both internal standards yielded comparable results for extractions of PCP from spiked C_{18} (note Table 1).

To optimize the SFE method, influences of individual extraction and derivatization parameters on the recovery of PCP have been investigated in this study.

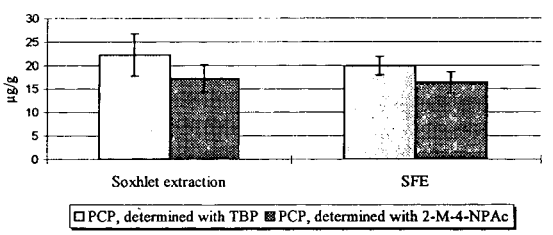

Fig. 3. Results obtained from Soxhlet extraction and SFE. Abbreviations as in Fig. 1. Soxhlet extractions were performed with methanol as described in the text; $n = 8$. SFEs were carried out as described in the text using 20 ml of liquid CO_2 for dynamic extractions; $n = 12$; note Table 3.

3.1. Influence of type and amount of the base and of the amount of acetic anhydride

In water samples, chlorophenols can easily be converted into stable acetyl derivatives using acetic anhydride and a base such as potassium hydrogencarbonate. Therefore, derivatization under SFE conditions was also carried out in the presence of potassium hydrogencarbonate, although quantitative recovery had already been achieved with triethylamine (note Table 1).

According to the water resistance of leather samples, the addition of potassium hydrogencarbonate was problematical. Isopropylamine has also been employed for SFE with in situ acetylation in this study. The results are presented in Fig. 4.

In the case of isopropylamine, determination with the internal standard TBP yielded very high but less reproducible results. This may be a consequence of incomplete recovery of TBP, and this assumption was confirmed by the chromatograms, in which the TBP peak was much smaller than expected. With potassium hydrogencarbonate the results were slightly better. In contrast to this, PCP recoveries being determined with 2-M-4-NPAc almost reached the expected value for these bases. The addition of triethylamine yielded the best results.

Reproducible results were obtained with 100 μl of TEA and 400 μl of acetic anhydride. In the case of PCP extractions from soils with in situ acetylation, the best results were achieved with small amounts of TEA and acetic anhydride (30 μl of each), while the application of a large excess of these chemicals (250 μl and more) deteriorated the results [14]. Hence the influence of the amounts of TEA and acetic anhydride used for derivatization of PCP in leather was investigated in this study.

The amount of the derivatization agents actually influences the efficiency of the method (Fig. 5). In contrast to extractions from soils (see above), addition of 100 μl of TEA and a large excess of acetic anhydride (400 μl) yielded the

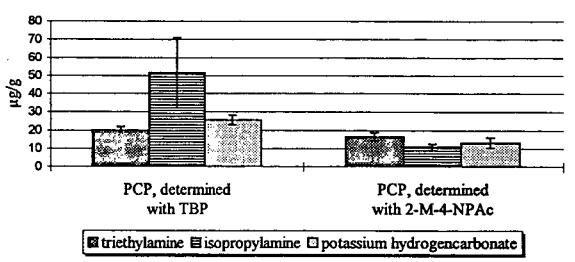

Fig. 4. In situ SFE–derivatization in the presence of different bases. SFE parameters: $p = 300$ atm, $T = 50$°C, $V_{base} = 100$ μl, $V_{acetic\ anhydride} = 400$ μl; extractions were carried out as described in the text; $n = 12$ for triethylamine, $n = 8$ for isopropylamine, $n = 6$ for potassium hydrogencarbonate. Abbreviations as in Fig. 1

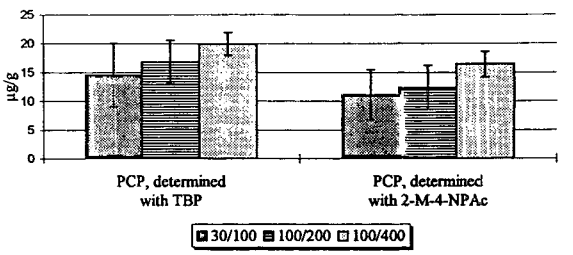

Fig. 5. Results of SFEs performed in the presence of different amounts of TEA and acetic anhydride. In the cases 30/100 and 100/200 amounts of 30 μl (100 μl) of TEA and 100 μl (200 μl) of acetic anhydride were added to the leather sample prior to thermostatization of the cells. Here $n = 6$ and 11, respectively. In the case 100/400 an amount of 100 μl of TEA was added prior to thermostatization of the cell while 400 μl of acetic anhydride was added afterwards (but prior to static extraction) via an extra valve. Here $n = 12$. Abbreviations as in Fig. 1. SFEs were carried out as described in the text.

best results. This might be a consequence of matrix effects since TEA and acetic anhydride may act as modifiers which can change the polarity of the supercritical CO_2 and increase the extraction efficiency by reducing the affinity of the analytes for sorptive sites of the matrix. Apart from this, fatty acids being present in leather samples will also be derivatized, whereby the acetic acid consumption is increased.

3.2. Influence of temperature and pressure on the extraction efficiency

The solvent strength of CO_2 strongly depends on the extraction parameters chosen. At a constant temperature, the density of supercritical fluids (which is related to the solvent strength) increases with pressure. In contrast to this, an elevation of temperature at a given pressure results in a decrease in fluid density, but thermal desorption effects, solute diffusivities and vapour pressures are enhanced at the same time.

The presence of acetic anhydride and TEA made it impossible to predict the optimum parameters for PCP extractions from leather. To determine the optimum pressure, extractions were performed at 200 and 300 atm while the temperature remained at 50°C. The syringe pump was not able to produce pressures above 300 atm, so that possible influences of higher

Table 2
Results of SFEs performed at different temperatures and pressures

	50°C, 200 atm[a] $\bar{x} \pm \sigma$ (μg)	50°C, 300 atm[b] $\bar{x} \pm \sigma$ (μg)	70°C, 300 atm[c] $\bar{x} \pm \sigma$ (μg)	90°C, 300 atm[d] $\bar{x} \pm \sigma$ (μg)
PCP, determined with TBP	20 ± 2	20 ± 2	23 ± 4	21 ± 3
PCP, determined with 2-M-4-NPAC	15 ± 2	16 ± 2	17 ± 3	14 ± 2

Abbreviations as in Fig. 1. Extractions were carried out as described in the text.
[a] $n = 10$. [b] $n = 12$. [c] $n = 6$. [d] $n = 6$.

pressures could not be evaluated in this study. The results are presented in Table 2 and they indicate that pressure had almost no effect on the extraction efficiency in this case.

The optimum temperature was determined by extracting the leather at 50, 70 and 90°C while the other extraction and derivatization parameters remained constant. Temperatures higher than 90°C could not be realized since heating of the extraction cells was carried out with hot water.

Temperature influences the extraction efficiency only to a small extent (Table 2). While at 70°C the results seemed to be slightly better than for the other temperatures, the best reproducibilities were obtained for extractions at 50°C. However, only extractions with good TBP recoveries were taken into consideration. Outliers mainly occurred at 70°C, so that reproducibility was actually even poorer for this temperature than indicated in Table 2. Hence the optimum temperature for PCP extractions from leather (at least for the leather sample used for this study) was 50°C.

However, the choice of the optimum temperature and pressure seemed to play a subordinate role for PCP extractions from leather using SFE with in situ acetylation. Thus, once derivatization has occurred, CO_2 seems to be responsible mainly for the elution of acetylated PCP from the leather sample.

3.3. Influence of the extraction time on the extraction efficiency

Quantitative recovery of PCP from C_{18} was observed for extractions being performed for 10 min in the static and for about 15 min (corresponding to 20 ml of liquid carbon dioxide) in the dynamic mode. In the case of soils, static and dynamic extractions for 5 min each were enough to recover PCP quantitatively [14].

Therefore, PCP extractions from leather were performed with various extraction times in the static mode (2, 5, 10 min) and different volumes of CO_2 in the dynamic mode (20 and 40 ml, measured in the liquid state of CO_2, corresponding to an extraction time of about 15 and 30 min).

Extractions with a static extraction step of 5 min seemed to yield the highest recovery of PCP, but only if determination was performed with TBP (Fig. 6). However, higher amounts of PCP being determined with this internal standard may be a consequence of incomplete recovery of the acetylated TBP. Determination with 2-M-4-NPAc yielded the lowest recoveries for SFEs with static extractions of 2 and 5 min. Hence static extraction times of 10 min were necessary for quantitative and reproducible recovery of PCP from leather samples.

The best results were obtained if static ex-

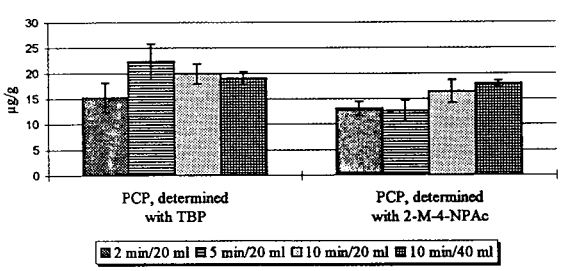

Fig. 6. Results of SFEs performed with various static extraction times and different amounts of liquid CO_2 used for dynamic extractions. Here $n = 5$ (2 min), 7 (5 min), 12 (10 min/20 ml), 3 (10 min/40 ml). Abbreviations as in Fig. 1. Extractions were carried out as described in the text.

Table 3
Comparison between Soxhlet extraction and SFE–derivatization

	Soxhlet extraction[a] $\bar{x} \pm \sigma$ (μg)	SFE (20 ml)[b] $\bar{x} \pm \sigma$ (μg)	SFE (40 ml)[b] $\bar{x} \pm \sigma$ (μg)
PCP determined with TBP	22 ± 5	20 ± 2	20 ± 1
PCP determined with 2-M-4-NPAC	17 ± 3	16 ± 2	17 ± 1

[a] Soxhlet extractions were performed with methanol as described in the text; $t = 8$ h; $n = 8$.
[b] SFE parameters: $p = 300$ atm, $T = 50$°C, $V_{TEA} = 100$ μl, $V_{acetic\ anhydride} = 400$ μl, $t_{static} = 10$ min. Extractions were carried out as described in the text; $n = 12$ (20 ml) or 9 (40 ml).
Abbreviations as in Fig. 1.

tractions of 10 min were followed by dynamic extractions with 40 ml of liquid CO_2. Even the correspondence between determination with TBP and 2-M-NPAc was slightly increased. Thus the differences between these two methods had partially been caused by incomplete extraction of the acetylated analytes. However, reliable determination was possible with less than 40 ml using TBP as an internal standard.

Table 3 shows a comparison between the results obtained by Soxhlet extraction and the optimized SFE–derivatization procedure.

The optimized SFE–derivatization procedure yielded even better results than the Soxhlet extraction with methanol. SFEs were performed at 50°C and 300 atm for 10 min in the static and for about 30 min (40 ml of liquid CO_2) in the dynamic mode. Amounts of 100 μl of triethylamine as well as 400 μl of acetic anhydride were necessary for quantitative and reproducible recovery of PCP from leather.

Since the procedure is very simple, it seems to be an efficient alternative to conventional Soxhlet extraction.

4. Conclusions

PCP was extracted from leather using SFE with in situ acetylation. The results are in good agreement with those obtained by Soxhlet extraction with methanol, while the organic solvent consumption is reduced from about 300 ml to less than 50 ml.

The efficiency of the method was poorly influenced by extraction parameters like temperature and pressure. Increases in extraction efficiency were only obtained by optimization of the extraction time in the static and dynamic mode, the type and amount of the base and the amount of acetic anhydride in this study.

With SFE–derivatization instead of conventional Soxhlet extraction, determination of PCP in leather becomes very simple and the complete time required for the entire analytical sequence (including sample preparation and gas chromatographic analysis) is reduced from about 2 days (Soxhlet) to 3 h.

Acknowledgements

The financial support of the Ministerium für Wissenschaft und Forschung des Landes Nordrhein-Westfalen is gratefully acknowledged. This study is part of a Ph.D. thesis.

References

[1] D.G. Crosby, K.I. Beynon, P.A. Greve, F. Korte, G.G. Still and J.W. Vonk, Pure Appl. Chem., 53 (1981) 1051–1080.
[2] M. Secchieri, C.A. Benassi, S. Pastore, A. Semenzato, A. Bettero, M. Levorato and A. Guerrato, J. Assoc. Off. Anal. Chem., 74 (1991) 674–678.
[3] L.L. Needham, R.E. Cline, S.L. Head and J.A. Liddle, J. Anal. Toxicol., 5 (1981) 283–286.
[4] Pentachlorphenolverbotsverordnung v. 12.12.1989, BGBI. 59, S. 2235

[5] Verordnung zum Schutz vor gefährlichen Stoffen (Gefahrstoffverordnung Gef-Stoff V) vom 26.10.1993.
[6] W. Fischer and G. Nickolaus, Leder, 41 (1990) 174–77.
[7] M.M. Schantz and S.N. Chesler, J. Chromatogr., 363 (1986) 397.
[9] S.B. Hawthorne and D.J. Miller, Anal. Chem., 59 (1987) 1705.
[10] A. Meyer, W. Kleiböhmer and K. Cammann, J. High Resolut. Chromatogr., 16 (1993) 491–494.
[11] A. Meyer and W. Kleiböhmer, J. Chromatogr. A, 657 (1993) 327–335.
[12] N. Alexandrou and J. Pawliszyn., Anal. Chem., 61 (1989) 2770.
[13] H.-B. Lee and T.E. Peart, J. Chromatogr. A, 663 (1994) 87–95.
[14] H.-B. Lee, T.E. Peart and R.L. Hong-You, J. Chromatogr., 605 (1992) 109–113.
[15] H.-B. Lee, Y.D. Stokker and A.S.Y. Chau, J. Assoc. Off. Anal. Chem., 70 (1987) 1003–1008.
[16] E. Verdú, D. Campello, M. Almela and F. Maldonado, AQEIC Bol. Tec., 44 (1993) 14–28.
[17] N.L. Porter, A.F. Rynaski, E.R. Campbell, M. Saunders, B.E. Richter, J.T. Swanson, R.B. Nielsen and B.J. Murphy, J. Chromatogr. Sci., 30 (1992) 367–373.
[18] A. Meyer and W. Kleiböhmer, 16th International Symposium on Capillary Chromatography, Riva del Garda, Italy, September 1994.

ELSEVIER

Journal of Chromatography A, 718 (1995) 141–146

JOURNAL OF CHROMATOGRAPHY A

Gas chromatography of 4,4′-diphenylmethane diisocyanate in the workplace atmosphere[1]

Gianvico Melzi D'Eril[a,*], Nino Cappuccia[b], Maurizio Colli[c], Vittorio Molina[c]

[a]*Dipartimento di Biochimica, Facoltá di Medicina e Chirurgia II, Universitá di Pavia, 27100 Pavia, Italy*

[b]*Servizio di Analisi Biochimico Cliniche, IRCCS, Fondazione C. Mondino, Pavia, Italy*

[c]*Centro Analisi, Monza, Italy*

First received 5 January 1995; revised manuscript received 6 June 1995; accepted 12 June 1995

Abstract

A sensitive gas chromatographic procedure for the determination of 4,4′-diphenylmethane diisocyanate concentration in air is described. Traps containing 20–40-mesh silica gel coated with phosphoric acid are used. After the aspiration of the air, the silica gel is eluted with sodium hydroxide in methanol. The amine formed is then separated with a gas chromatograph and measured with a nitrogen–phosphorus detector. This can be performed in 7 min. Virtually no breakthrough occurs if an air concentration of up to 128 nmol in 20 l is sampled. The detection limit based on a 20-l air sample is 0.7 $\mu g/m^3$. Complete analysis requires about 30 min. The method was used to determine the concentration of 4,4′-diphenylmethane diisocyanate in working environments during spraying operations.

1. Introduction

The aromatic diisocyanates, toluene diisocyanate (a mixture of the 2,4- and 2,6-isomers) and 4,4′-diphenylmethane diisocyanate (MDI) are widely used raw materials in the production of polyurethane foams and coatings. They are the essential building blocks for the manufacture of flexible and rigid polyurethane foams, respectively. They are also involved in the production of other industrial substances, such as synthetic rubbers and elastomers, moulded products for marine and automotive purposes and polyurethane resins for paint and varnish formulations [1]. In recent years, the demand for MDI has increased, mainly owing to its low vapour pressure, which decreases the likelihood of inhalation exposure in its various applications. However, exposure to MDI does occur during production and application processes. The symptoms resulting from inhalation of vapour aerosol or fine particles of isocyanate include eye and mucous membrane irritation, coughing fits and dyspnea [2,3]. Chronic exposure may lead to allergies such as asthma. Although sensitization does not occur in all individuals, exposure to very low concentrations can trigger this reaction.

The threshold limit value for MDI according to the American Conference of Governmental Industrial Hygienists as a time weighted average (TLV-TWA) is 51 $\mu g/m^3$ [4]. The National Institute for Occupational Safety and Health (NIOSH)-recommended exposure limit (REL) is

* Corresponding author.

[1] Originally submitted for the Thematic Issue on Chromatography and Electrophoresis in Environmental Analysis: Air Pollution (Vol. 710, No. 1).

0021-9673/95/$09.50
SSDI 0021-9673(95)00667-2

50 $\mu g/m^3$, with a 200 $\mu g/m^3$ ceiling (TLV-C) [5]. This represents the exposure level that should at no time be exceeded during the workday, not even instantaneously. The Occupational Safety and Health Administration (OSHA) only recommended a ceiling of 200 $\mu g/m^3$ [6]. Therefore, sensitive methods are required to determine this low threshold limit in the environment.

The most common sampling method involves bubbling of the air sample through an absorbing solution [7]. Impinger sampling, however, is cumbersome for workers. Because toluene or xylene is used as an absorbing solution [8], other drawbacks include possible spillage during sampling and the evaporation of organic solvents at high airflow sampling rates. Evaporation can be a limiting factor for the total air volume pumped and can present the risk of solvent exposure for workers.

The original procedure developed for the determination of the aromatic diisocyanates collected [9] has been modified in several studies [10–13]. Spectrophotometric methods are not specific: if mixtures of isocyanates are present, these methods only indicate the total concentration of the substances. Several chromatographic methods for determining isocyanates in air, including gas chromatography [14,15], thin-layer chromatography [16,17] and high-performance liquid chromatography [18–22], have been published. This paper describes the preliminary results of a promising method, which is quick and simple, for the determination of MDI in air. The isocyanate was collected by reaction in a solid acid medium, and the corresponding amine, after separation with gas chromatography, was measured with a nitrogen–phosphorus detector.

2. Experimental

2.1. Reagents and standards

MDI (97% pure) was purchased from Kodak (Rochester, NY, USA) and 4,4′-diaminodiphenylmethane (DAPM) (99% pure), a derivative of MDI hydrolysis, from Merck (Darmstadt, Germany). All other chemicals were of analytical-reagent grade.

Stock solutions of MDI were prepared at 10 mmol/l by diluting a known amount of the isocyanate with the appropriate amount of acetone, and stock solutions of DAPM were prepared at the same concentration by weighing a known amount of amine and dissolving in the appropriate amount of acetone. Working standard solutions of 0.3 μmol/l MDI and DAPM were prepared by serial dilution with acetone. MDI solution is not stable and must be prepared daily; DAPM solution is stable for 10 days when stored at 4°C.

2.2. Equipment

A Perkin-Elmer (Norwalk, CT, USA) Model 8500 gas chromatograph, equipped with a nitrogen–phosphorus detector (range 1×8) and an automatic on-column injector, was employed. After injection, the sample was routed through a 2 m × 4 mm I.D. glass column containing 1.5% OV-17 + 1.95 QF-1 on Chromosorb W HP (100–200 mesh) from Supelco (Bellefonte, PA, USA). Helium was used as the carrier gas at a flow-rate of 35 ml/min. The separation was performed with the injector at 250°C, the detector at 270°C and the oven at 220°C. Chromatograms were recorded and the peaks integrated on a Shimadzu (Kyoto, Japan) CR GA integrator (attenuation 3, speed 5 mm/min).

2.3. Procedure

Glass tubes (85 mm × 5 mm I.D.) used as traps were filled with 200 mg of H_3PO_4–silica gel prepared as described elsewhere [23]. These traps, closed at each end with glass-wool plugs, remain unaltered for at least 6 months if kept at room temperature [23]. Known concentrations of MDI were added to the trap using a microsyringe to prepare the calibration graph and to study the collection efficiency. This was done in accordance with the NIOSH evaluation of sampling parameters. Air samples were sucked through the trap using an MWG membrane pump (Neuberger, Freiburg, Germany). The

sampling rate was of the order of 0.5 l/min. The silica gel was then transferred from the trap into a glass test-tube and the DAPM was eluted with 600 μl of 1.7 mol/l sodium hydroxide in methanol. The mixture was first sonicated for 10 min and then centrifuged at 3300 *g* for 5 min. A vacuum centrifuge was used to concentrate the 600 μl of supernatant to 100 μl. Compared with a rotary evaporator, the vacuum centrifuge has two advantages: bumping is avoided and several samples can be handled at the same time. A 2-μl volume of the concentrated supernatant was then injected into the gas chromatograph.

2.4. Field studies

MDI values were obtained in a factory producing polyurethane-insulated pipes by the spray technique. Measurements were performed at various distances from the production machinery. The average temperature in the factory was 24°C and the relative humidity ranged between 40 and 50%. The flow-rate through the trap was maintained at 0.5 l/min. After 10 and 20 min of sampling the solid absorbers were analysed for MDI content. The experiment was repeated five times on the same day.

3. Results

3.1. Collection and recovery efficiency

The collection efficiency of the solid absorber medium for MDI was examined by using two traps in series. Increasing amounts of standard MDI were added to the first trap with a microsyringe while air at a flow-rate of 0.5 l/min was sucked through the traps. The air flow was continued for 40 min. After sampling, the absorbent medium in each trap was analysed for the MDI derivative using the reported method. The results are given in Table 1. There is 1.6% MDI breakthrough at the highest concentration studied. There is no breakthrough from the first trap at a concentration of 4 nmol, equivalent to 20 l of 50 $\mu g/m^3$ concentration (the current threshold limit value for MDI). This indicated that the trapping efficiency was essentially 100% and that only one trap is required for collection in the field. Tests performed with sampling tubes spiked with 3 μmol of MDI showed that virtually 100% of the DAMP was recovered using 600 μl of sodium hydroxide in methanol. Dharmarajan [24] has demonstrated that under normal operating conditions virtually all of the MDI in air is present as an aerosol and not in the gaseous form. The efficiency of MDI aerosol collection was studied by inserting a Teflon filter between the trapping system and the pump. After sampling, the filter was eluted with acidic methanol and the solution analysed for MDI content following our procedure. The concentration of MDI collected by the filter was less than 1.8% of the MDI collected by the trapping system in the workplace atmosphere. Our experimental procedure consisted of four runs, each repeated twice; the results ranged from 2.3 to 21.1 $\mu g/m^3$.

Table 1
Efficiency of the sampling procedure for the collection of MDI

Run[a]	MDI added (nmol)	MDI collected (nmol)	
		Trap 1	Trap 2
1	2.0	2.00	–
2	4.0	3.94	–
3	8.0	7.88	–
4	64.0	64.31	–
5	128.0	127.94	–
6	256.0	251.58	4.10

[a] Each run is the mean of three experiments.

3.2. Chromatographic analysis

Good separation of DAPM was achieved within 7 min under the experimental conditions described above. Typical chromatograms of a standard solution of MDI and of an air sample are shown in Fig. 1. Quantification of DAPM was performed using a calibration graph. The calibration graph was prepared by introducing 1.0, 3.0, 5.0, 7.0 and 10.0 μl of working standard solution (0.3 μmol/l MDI) with a microsyringe

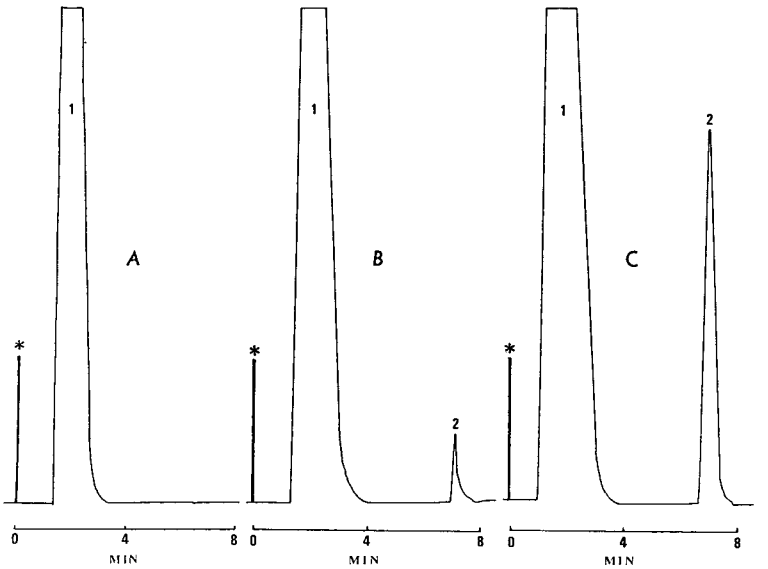

Fig. 1. Gas chromatogram of methanolic eluate of the absorber: (A) untreated, i.e. used as a blank, (B) with a standard solution of 0.3 nmol of MDI and (C) after air sampling of a concentration of 20.7 $\mu g/m^3$. Peaks: 1 = front; 2 = DAPM; * = injection.

into the traps, thereby obtaining standards of 3.75, 11.25, 18.75, 26.25 and 37.50 $\mu g/m^3$, respectively (for a 20-l air sample). Analysis of the standard gave a calibration graph $y = 4.5x$, where y is the amount of MDI and x is the peak area. The resulting function was used to calculate the amount of MDI in a sample. The calibration function was checked at regular intervals by injecting 1.0, 5.0 and 10.0 μl of working standard solution.

Fig. 2 shows a chromatogram of 0.6 nmol of MDI added to a trap and that of the same amount of DAPM added to another trap. The retention times and the areas of the peaks are identical, confirming the complete transformation of MDI into DAPM.

The absolute retention time was reproducible within 6%. Reproducibility was also determined for quantitative analyses via the calibration graph. Triplicate injections of standard sample at the five different concentrations gave an R.S.D. of less than 5%. The linearity of the assay was verified by determining increasing amounts of MDI standards (up to 3 nmol). The response was linear over the range investigated.

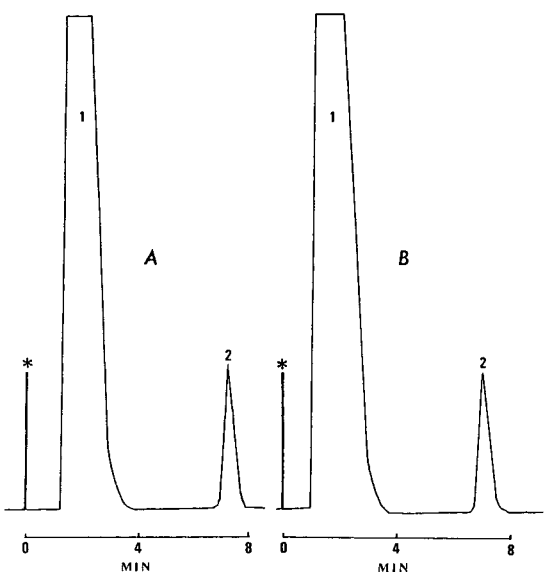

Fig. 2. Gas chromatogram of (A) 0.6 nmol of MDI standard solution added to the trap and (B) 0.6 nmol of DAPM standard solution injected directly into the column. Peaks: 1 = front; 2 = (A) MDI or (B) DAPM; * = injection.

3.3. Reproducibility

The precision of the method was evaluated with both within-run (twelve equal samples of a standard solution added to the traps and analysed on the same day) and between-run assays (samples of equal concentration to the traps and analysed on ten consecutive days). These results are reported in Table 2.

3.4. Detection limit

As is customary, the detection limit of the procedure was defined as the concentration derived from a signal three times the noise level. With an air sample of 20 l, the MDI derivative (DAPM) showed a detection limit of 0.7 $\mu g/m^3$, which was suitable for routine analytical work.

3.5. Storage stability

Stability permitting, it is often more practical to collect samples over a number of days and perform analysis subsequently. In the present case, storage studies indicated that samples should be desorbed within 10 days for maximum recovery when they are stored at 4°C in the dark. Losses of up to 7% can occur after 15 days. The recovery of DAPM was unchanged up to 10 days for refrigerated desorbed solutions.

3.6. Field studies

Table 3 summarizes the results of the analyses in the field. The MDI concentrations were found to vary between 2.1 and 21.4 $\mu g/m^3$. As expected, lower concentrations were observed at a greater distance from the machinery and the concentrations found with a longer collection time were the same as those found with a shorter collection time. The concentrations found are all below the threshold limit value for MDI according to ACGIH.

Table 2
Precision of the MDI assay

n	x (nmol)	S.D. (nmol)	R.S.D. (%)
Within-run precision			
12	0.85	0.02	2.3
12	18.15	0.85	4.6
Between-run precision			
10	0.89	0.04	4.4
10	17.91	1.05	5.8

Table 3
Workplace atmosphere concentrations of MDI at various distances from production machinery

Distance (m)	Volume of air sampled (l)	Concentration ± S.D. ($\mu g/m^3$)
2	10	19.8 ± 0.79
2	20	21.4 ± 0.91
6	10	7.0 ± 0.29
6	20	5.9 ± 0.30
10	10	1.8 ± 0.02
10	20	2.1 ± 0.02

4. Discussion

During the last few decades, considerable efforts have been channelled into developing increasingly sensitive chromatography-based methods for the determination of atmospheric isocyanate monomer concentrations. As a result, spectrophotometric methods have generally been discarded or overlooked. However, the principal advantage of this method is its considerably reduced sample handling prior to the chromatographic step. The simplicity of the method is the result of the very rapid and complete one-step sample preparation and the fact that unreacted H_3PO_4 does not interfere with the subsequent chromatography. The column remains unaltered over 1000 injections. Our method is linear up to at least 3 nmol, which is 100 times above the detection limit. Complete determination, including sample preparation and analysis, can be performed in less than 30 min. This procedure is a very efficient method of collecting MDI in industrial environments, even when measuring trace concentrations. The equipment required is

relatively inexpensive and readily available. This enables on-site analysis to be carried out by most factories.

Since DAPM is also present in the environment, it can be trapped in the silica gel and consequently simulate the presence of MDI. In order to determine the environmental level of MDI only, we took advantage of the fact that MDI does not collect on silica gel without acid. This was done by preparing two types of traps: one containing acid which collected both MDI and DAPM and another without acid which collected only DAPM.

Other amines (hexamethylendiamine, 2,4-toluendiamine, 2,6-toluendiamine) do not interfere since they have different retention times and 2,4-toluene diisocyanate and 2,6-toluene diisocyanate do not interfere since they cannot be determined by gas chromatography, probably because of their polymerization.

References

[1] M.M. Key, A.F. Henschel, J. Butler, R.N. Ligo and I.R. Talershaw, Occupational Diseases, Publication No. 77-181, US Department of Health, Education and Welfare, Public Health Service, Center of Disease Control, National Institute for Occupational Safety and Health, Cincinnati, OH, 1977.
[2] P.F. Wollrich, Am. Ind. Hyg. Assoc. J., 43 (1982) 89.
[3] Nordiska Expertgruppen for Gransvardesdokumentation. 9. Diisocyanater, Arbete och Halsa, 34 (1979) 1.
[4] American Conference of Governmental Industrial Hygienists, Threshold Limit Values and Biological Exposure Indices for 1991, American Conference of Governmental Industrial Hygienists, Cincinnati, OH, 1991, p. 26.
[5] M. Seymour and A.W. Teass, NIOSH Manual of Analytical Methods—Isocyanate Group, Method 5505, Revision No. 1, 3rd ed., Publication 84-100, 1985.
[6] OSHA, Chemical Information Manual, 1987.
[7] D.H. Chadwick and T.H. Cleveland, in M. Grayson and D. Eckroth (Editors), Encyclopedia of Chemical Technology, Vol. 13, Wiley-Interscience, New York, 1981.
[8] S. Patai (Editor), The Chemistry of Cyanates and Their Thio Derivatives, Parts 1 and 2, Wiley, Chichester, 1977.
[9] K. Marcali, Anal. Chem., 29 (1957) 552.
[10] K.E. Grim and A.L. Linch, Am. Ind. Hyg. Assoc. J., 25 (1964) 287.
[11] D.W. Meddle, D.W. Radford and R.A. Wood, Analyst, 94 (1969) 369.
[12] D.W. Meddle and R. Wood, Analyst, 95 (1970) 402.
[13] R.F. Walker and M.A. Pinches, Analyst, 104 (1979) 928.
[14] B.B. Wheals and J. Thomson, Chem. Ind. (London). (1967) 753.
[15] G. Skarping, C. Sango and B.E.F. Smith, J. Chromatogr., 208 (1981) 313.
[16] J. Keller, K.L. Dunlap and R.L. Sandridge, Anal. Chem., 46 (1974) 1845.
[17] J. Keller and R.L. Sandridge, Anal. Chem., 51 (1979) 1868.
[18] W.S. Wu, R.E. Stoyanoff, R.S. Szklar and V.S. Gaind, Analyst, 115 (1990) 801.
[19] F. Schmidtke and B. Seifert, Fresenius' J. Anal. Chem., 336 (1990) 647.
[20] D.C. Hakes, G.D. Johnson and J.S. Marhevka, Am. Ind. Hyg. Assoc. J., 47 (1986) 181.
[21] C. Sango and E. Zimerson, J. Liq. Chromatogr., 3 (1980) 971.
[22] C. Rosenberg and T. Tuomi, Am. Ind. Hyg. Assoc. J., 45 (1984) 117.
[23] M. Colli, L. Zabarini, G.V. Melzi d'Eril and R. Marchetti, J. Chromatogr., 643 (1993) 51.
[24] V. Dharmarajan, J. Environ. Pathol. Toxicol., 2 (1979) 1.

ELSEVIER

Journal of Chromatography A, 718 (1995) 147–152

JOURNAL OF CHROMATOGRAPHY A

Thermodynamic background of selectivity shifts in temperature-programmed, constant-density supercritical fluid chromatography

Michal Roth

Institute of Analytical Chemistry, Academy of Sciences of the Czech Republic, 61142 Brno, Czech Republic

Received 10 April 1995; accepted 17 May 1995

Abstract

Theoretical principles of the temperature-driven selectivity shifts in capillary supercritical fluid chromatography (SFC) at a constant density of the mobile phase fluid are outlined. Sensitivity of the separate thermodynamic properties involved in the shifts in the intensity of a particular pairwise interaction between components of the solute–stationary polymer–supercritical fluid system is discussed. Thermodynamic analysis confirms the expected significance of dissolution of the mobile phase fluid in the stationary polymer ("swelling") for this kind of selectivity shift. With a single exception, all the thermodynamic derivatives involved in the shifts are either directly related to or at least partly influenced by swelling. The selectivity shifts do not involve any property that would depend only on interaction between a solute and a pure stationary polymer. This finding shows that swelling of the stationary phase can hardly be ignored in the theoretical interpretation of selectivity in SFC.

1. Introduction

In an experimental study of temperature-programmed, capillary supercritical fluid chromatography (SFC) at a constant density of the mobile phase fluid (carbon dioxide), Chester and Innis [1] noted density- and temperature-dependent selectivity shifts for phenanthrene and anthracene with respect to alkanes. The selectivity shifts varied strongly with substituents on the siloxane backbone of the stationary polymer, increasing from poly(dimethylsiloxane) through biphenyl-substituted polysiloxane to cyanopropyl-substituted polysiloxane. Chester and Innis concluded that the selectivity shifts most likely arose because of swelling of the stationary phase by the absorbed mobile phase.

In capillary SFC, retention and/or selectivity have been correlated or predicted by employing diverse theoretical or semi-empirical treatments, e.g., those based on the mean-field lattice-gas models of statistical thermodynamics [2–4]. However, the predictions based on such treatments are always qualified and limited by the approximations embedded in the development of the particular model. Therefore, it might be useful to return to classical rather than statistical thermodynamics and, within a model-independent analysis, attempt to identify the well defined thermodynamic properties of the solute–stationary polymer–supercritical fluid system

0021-9673/95/$09.50
SSDI 0021-9673(95)00590-0

that are responsible for the selectivity shifts mentioned above.

2. Theory

The starting point is the expression for the change in the solute capacity factor with temperature at a constant density of the mobile phase fluid [4–6]. From that expression, one obtains the following relationship for the temperature derivative of the logarithm of the separation factor, α^{f}_{ab}, of solutes a and b on a stationary phase f at a constant density, ρ_m, of the mobile phase fluid m,

$$[\partial \ln \alpha^{f}_{ab}/\partial(1/T)]_{\rho_m} = [\Delta H^{m\to f}_{tb} - \Delta H^{m\to f}_{ta} - T\gamma_{mV}(\Delta V^{m\to f}_{tb} - \Delta V^{m\to f}_{ta})]/R + (T/R)[(\partial \mu^{\infty}_{af}/\partial w_{mf}) - (\partial \mu^{\infty}_{bf}/\partial w_{mf})] \times [(\partial w_{mf}/\partial T)_{P,\sigma} + \gamma_{mV}(\partial w_{mf}/\partial P)_{T,\sigma}] \quad (1)$$

where R is the molar gas constant, T the absolute temperature, P the pressure, γ_{mV} the thermal pressure coefficient of the mobile phase fluid, w_{mf} the mass fraction of the mobile phase fluid m in the stationary phase f and the subscript σ denotes saturation of the stationary phase with the absorbed mobile phase fluid. It has been assumed in Eq. 1 that bulk dissolution is the only mechanism of solute retention, that the solute concentrations in both phases are close to infinite dilution and that the temperature and pressure in the column are well removed from the mobile phase critical point so that the presence of a small amount of solute does not disturb the equilibrium mass fraction of the mobile phase fluid in the stationary phase. The derivatives of the infinite-dilution chemical potentials, μ^{∞}_{af} and μ^{∞}_{bf}, of the two solutes in the stationary phase with respect to w_{mf} are those at constant temperature, pressure and amount of the stationary polymer. The ΔHs and ΔVs denote the transfer properties of the indicated solute, e.g., $\Delta H^{m\to f}_{ta}$ is the molar enthalpy of transfer of solute a from the mobile phase m to the stationary phase f:

$$\Delta H^{m\to f}_{ta} = \bar{h}^{\infty}_{af} - \bar{h}^{\infty}_{am} \quad (2)$$

where $\bar{h}^{\infty}_{am}$ and $\bar{h}^{\infty}_{af}$ are the infinite-dilution partial molar enthalpies of the solute in the two phases, respectively. Throughout this paper, the term "stationary phase" includes the absorbed mobile phase fluid, e.g., the stationary phase f is an equilibrium mixture of a stationary polymer φ with the dissolved mobile phase fluid m. Employing general thermodynamic identities, one may recast the last bracketed term in Eq. 1 as

$$(\partial w_{mf}/\partial T)_{P,\sigma} + \gamma_{mV}(\partial w_{mf}/\partial P)_{T,\sigma} = [\gamma_{mV} - \Delta S^{m\to f}_{tm}/\Delta V^{m\to f}_{tm}](\partial w_{mf}/\partial P)_{T,\sigma} \quad (3)$$

where $\Delta S^{m\to f}_{tm}$ and $\Delta V^{m\to f}_{tm}$ denote, respectively, the molar entropy and molar volume of transfer of the mobile phase fluid m from the pure mobile phase into the stationary phase f, i.e.

$$\Delta S^{m\to f}_{tm} = \bar{s}_{mf} - s^{0}_{m} \quad (4)$$

$$\Delta V^{m\to f}_{tm} = \bar{v}_{mf} - v^{0}_{m} \quad (5)$$

where s^{0}_{m} and v^{0}_{m} are the molar entropy and molar volume of the pure mobile phase fluid and $\bar{s}_{mf}$ and $\bar{v}_{mf}$ are the partial molar entropy and partial molar volume of the mobile phase fluid dissolved in the stationary phase. The two terms in brackets on the right-hand side of Eq. 3 have the same physical dimension, since

$$\gamma_{mV} \equiv (\partial P/\partial T)_{\rho_m} = (\partial s^{0}_{m}/\partial v^{0}_{m})_{T} \quad (6)$$

For discussion of the selectivity shifts mentioned above [1], the relevant quantity is the difference between the rates of temperature change in selectivity for solutes a and b on stationary phases f and g at a constant density of the mobile phase fluid. It follows from Eqs. 1–3 that

$$[\partial \ln \alpha^{f}_{ab}/\partial(1/T)]_{\rho_m} - [\partial \ln \alpha^{g}_{ab}/\partial(1/T)]_{\rho_m} = [\Delta H^{f\to g}_{tb} - \Delta H^{f\to g}_{ta} - T\gamma_{mV}(\Delta V^{f\to g}_{tb} - \Delta V^{f\to g}_{ta}]/R + (T/R)\left[\left(\frac{\partial \mu^{\infty}_{af}}{\partial w_{mf}}\right) - \left(\frac{\partial \mu^{\infty}_{bf}}{\partial w_{mf}}\right)\right]\left[\gamma_{mV} - \frac{\Delta S^{m\to f}_{tm}}{\Delta V^{m\to f}_{tm}}\right] \times \left(\frac{\partial w_{mf}}{\partial P}\right)_{T,\sigma} - (T/R)\left[\left(\frac{\partial \mu^{\infty}_{ag}}{\partial w_{mg}}\right) - \left(\frac{\partial \mu^{\infty}_{bg}}{\partial w_{mg}}\right)\right]$$

$$\times\left[\gamma_{mV}-\frac{\Delta S_{tm}^{m\to g}}{\Delta V_{tm}^{m\to g}}\right]\left(\frac{\partial w_{mg}}{\partial P}\right)_{T,\sigma} \quad (7)$$

The mobile phase fluid and its density are the same for both stationary phases. Therefore, the solute properties in the mobile phase are absent from Eq. 7, and the ΔHs and ΔVs in the first bracket on the right-hand side refer to solute transfer from the stationary phase f to the stationary phase g. The molar volume of transfer of solute a, for example, is

$$\Delta V_{ta}^{f\to g}=\bar{v}_{ag}^{\infty}-\bar{v}_{af}^{\infty} \quad (8)$$

where $\bar{v}_{af}^{\infty}$ and $\bar{v}_{ag}^{\infty}$ are the infinite-dilution partial molar volumes of the solute a in the stationary phases f and g, respectively. The stationary phase g is an equilibrium mixture of a stationary polymer γ with the dissolved mobile phase fluid m.

The difference given by Eq. 7 exactly equals zero only in the trivial case when the two stationary phases are the same, $f=g$ ($\varphi=\gamma$). This situation is characterized by the following equalities in the types and/or intensities of the three kinds of pairwise interactions that occur within the system:

$a-\varphi = a-\gamma$
$b-\varphi = b-\gamma$ — solute–polymer;

$\varphi-m = \gamma-m$ — polymer–mobile phase fluid; and

$(a-m)_f = (a-m)_g$
$(b-m)_f = (b-m)_g$ — solute–mobile phase fluid interaction within the stationary phase.

Consequently, a temperature-driven selectivity shift between the stationary phases f and g results only if at least one equality within the three groups above has been broken. It is important to note that, because of generality of Eq. 7, the particular character of intermolecular interactions involved is immaterial; the interactions may range from ubiquitous dispersion, induction and orientation forces through specific interactions by hydrogen bonding or charge transfer to shape selectivity resulting from chiral discrimination or from effects of oriented mesophases (liquid crystals). In what follows, the terms in Eq. 7 that are affected by a particular pairwise interaction between components of the chromatographic system will be identified and discussed.

2.1. Solute–stationary polymer interaction ($a-\varphi$)

Among the three kinds of pairwise interactions underlying the selectivity shifts, this one is the easiest to interpret. In Eq. 7, the only quantities influenced by the $a-\varphi$ interaction are $\Delta H_{ta}^{f\to g}$, $\Delta V_{ta}^{f\to g}$ and $(\partial\mu_{af}^{\infty}/\partial w_{mf})$. The first two quantities relate to the transfer of solute a between swollen stationary phases f and g. In the two stationary phases, the polymers φ and γ are diluted with the absorbed mobile phase fluid. For this reason, the effects of the $a-\varphi$ interaction on $\Delta H_{ta}^{f\to g}$ and $\Delta V_{ta}^{f\to g}$ will be suppressed as compared with the transfer of solute a from the state of infinite dilution in the pure polymer φ to the state of infinite dilution in the pure polymer γ.

In effect, the quantity $(\partial\mu_{af}^{\infty}/\partial w_{mf})$ measures how the solute fugacity responds to the changing molecular environment in the stationary phase. This quantity results from a complex interplay of the enthalpic and entropic effects because

$$(\partial\mu_{af}^{\infty}/\partial w_{mf})=(\partial\bar{h}_{af}^{\infty}/\partial w_{mf})-T(\partial\bar{s}_{af}^{\infty}/\partial w_{mf}) \quad (9)$$

where $\bar{s}_{af}^{\infty}$ is the infinite-dilution partial molar entropy of the solute a in the stationary phase f. At a low pressure, $w_{mf}\to 0$, and a strong and/or specific $a-\varphi$ interaction will result in a value of $(\partial\mu_{af}^{\infty}/\partial w_{mf})$ that will be different from the values typical of systems dominated by dispersion forces. The trend in that value with increasing pressure and increasing w_{mf} will depend on the strength and specificity of both $a-m$ and $\varphi-m$ interactions. If these interactions are not specific, then the effect of a strong $a-\varphi$ interaction on $(\partial\mu_{af}^{\infty}/\partial w_{mf})$ will gradually be attenuated by an increasing amount of the mobile phase fluid dissolved in the stationary phase. In a model system dominated by dispersion forces, with a = naphthalene, φ = poly(dimethylsiloxane) and $m=CO_2$, previous statistical thermodynamic calculations [4] suggest that

$(\partial\mu^{\infty}_{af}/\partial w_{mf})$ is negative, ranging from −3 to −5, and that it makes an important contribution to the slope $\partial \ln k'_{af}/\partial(1/T)$ at a constant density of the mobile phase fluid. In a system with a specific a–φ interaction, the ratio $(\partial\mu^{\infty}_{af}/\partial w_{mf})$ would be even more important. This will result in amplification of the selectivity shift for the solutes a and b between the stationary phases f and g.

2.2. Stationary polymer–mobile phase fluid interaction (φ–m)

Among the three kinds of pairwise interactions within the solute–stationary polymer–mobile phase fluid system, the φ–m interaction concerns the largest number of thermodynamic properties appearing in Eq. 7. The quantities directly affected by the φ–m interaction are $(\partial w_{mf}/\partial P)_{T,\sigma}$ and $\Delta S^{m\to f}_{tm}/\Delta V^{m\to f}_{tm}$. In addition to these first-order effects, there are a number of second-order effects involving the ratios $(\partial\mu^{\infty}_{af}/\partial w_{mf})$ and $(\partial\mu^{\infty}_{bf}/\partial w_{mf})$ as well as all the transfer properties of the solutes, $\Delta H^{f\to g}_{ta}$, $\Delta H^{f\to g}_{tb}$, $\Delta V^{f\to g}_{ta}$ and $\Delta V^{f\to g}_{tb}$.

First-order effects

The ratio $(\partial w_{mf}/\partial P)_{T,\sigma}$ measures the isothermal rate of increase with pressure in the equilibrium mass fraction of the mobile phase fluid in the stationary phase. Among the polymer–supercritical fluid systems of interest in open-tubular capillary SFC, the largest amount of reliable data on swelling is available for the poly(dimethylsiloxane)–CO_2 system in the form of changes in volume [7–11] or composition [9–12] with pressure. Information on other systems is scarce [13–16]. The pressure courses of w_{mf} and of the swollen volume generally follow complex S-shaped patterns, and, in the poly(dimethylsiloxane)–CO_2 system, they have been correlated by employing diverse forms of the lattice-gas model of statistical thermodynamics [4,11,12,17,18]. A strong or specific φ–m interaction promotes both the solubility, w_{mf}, and the rate of its increase with pressure, $(\partial w_{mf}/\partial P)_{T,\sigma}$. For example, at a fixed temperature and pressure, the solubility of CO_2 in poly(methyltrifluoropropylsiloxane) [13,14] is larger than that in alkyl- or aryl-substituted polysiloxanes because of a specific interaction between an oxygen atom in CO_2 and the hydrogen atoms of the methylene group adjacent to the trifluoromethyl group in the side-chain of the polymer. It is apparent from Eq. 7 that an increase in $(\partial w_{mf}/\partial P)_{T,\sigma}$ enhances the selectivity shift between the stationary phases f and g.

The ratio $\Delta S^{m\to f}_{tm}/\Delta V^{m\to f}_{tm}$ reflects the changes in the molar entropy and molar volume of the mobile phase fluid upon its dissolution in the stationary phase. The contribution of the uptake of mobile phase fluid by the stationary polymer to the temperature-induced selectivity shifts (Eq. 7) is proportional to the difference between the thermal pressure coefficient, γ_{mV}, of the pure, supercritical, mobile phase fluid and the ratio $\Delta S^{m\to f}_{tm}/\Delta V^{m\to f}_{tm}$. Recalling Eq. 6, one finds that the difference $\gamma_{mV} - \Delta S^{m\to f}_{tm}/\Delta V^{m\to f}_{tm}$ measures how the ratio of changes in the molar entropy and molar volume of the mobile phase fluid upon its dissolution in the stationary polymer departs from the slope of an isochore of the pure mobile phase fluid. The transfer properties $\Delta S^{m\to f}_{tm}$ and $\Delta V^{m\to f}_{tm}$ will be correlated to some extent, and the correlation will tend to produce a levelling among the ratios $\Delta S^{m\to f}_{tm}/\Delta V^{m\to f}_{tm}$ in different polymer–fluid systems. However, the absolute difference $\gamma_{mV} - \Delta S^{m\to f}_{tm}/\Delta V^{m\to f}_{tm}$ will generally increase with increasing strength and/or specificity of the φ–m interactions. For example, at a given temperature and pressure, the difference is certainly larger in magnitude in the poly(methyltrifluoropropylsiloxane)–CO_2 system as compared with the poly(dimethylsiloxane)–CO_2 system, for the reasons mentioned above.

Second-order effects

The indirect effects of the φ–m interaction in Eq. 7 concern the differences between some properties of solutes a and b, namely $(\partial\mu^{\infty}_{af}/\partial w_{mf}) - (\partial\mu^{\infty}_{bf}/\partial w_{mf})$, $\Delta H^{f\to g}_{ta} - \Delta H^{f\to g}_{tb}$ and $\Delta V^{f\to g}_{ta} - \Delta V^{f\to g}_{tb}$. Therefore, if neither of the interactions a–φ, b–φ, a–γ, b–γ, a–m and b–m is specific or much stronger than the rest, the

effect of even a strong φ–m interaction on the three differences will be only minor because of a large degree of compensation.

2.3. Solute–mobile phase fluid interaction (a–m) within a stationary phase

In Eq. 7, the quantities directly affected by the title interaction are $(\partial\mu^{\infty}_{af}/\partial w_{mf})$ and $(\partial\mu^{\infty}_{ag}/\partial w_{mg})$. A strong and/or specific a–m interaction will shift both ratios from the values typical of non-polar systems. The two ratios appear in Eq. 7 with opposite signs although not as a plain difference. Therefore, the effects of the a–m interaction on $(\partial\mu^{\infty}_{af}/\partial w_{mf})$ and $(\partial\mu^{\infty}_{ag}/\partial w_{mg})$ will largely counterbalance each other, at least in systems where none of the a–φ, a–γ, φ–m and γ–m interactions is much stronger than the rest.

The a–m interaction also has indirect, second-order effects on the transfer properties $\Delta H^{f\rightarrow g}_{ta}$ and $\Delta V^{f\rightarrow g}_{ta}$. As both stationary phases f and g are swollen with the absorbed mobile phase fluid, the effects of the a–m interaction on $\Delta H^{f\rightarrow g}_{ta}$ and $\Delta V^{f\rightarrow g}_{ta}$ will be minor.

Finally, therefore, the most important effects of a particular pairwise interaction within a chromatographic system on the properties involved in temperature-driven selectivity shifts may be summarized as follows:

Interaction	Property
a–φ, solute–stationary polymer	$(\partial\mu^{\infty}_{af}/\partial w_{mf})$, $\Delta H^{f\rightarrow g}_{ta}$, $\Delta V^{f\rightarrow g}_{ta}$
φ–m, stationary polymer–mobile phase fluid	$\Delta S^{m\rightarrow f}_{tm}/\Delta V^{m\rightarrow f}_{tm}$, $(\partial w_{mf}/\partial P)_{T,\sigma}$
a–m, solute–mobile phase fluid	

These interaction–property correspondences confirm the importance of stationary phase swelling in the temperature-induced selectivity shifts at a constant density of the mobile phase fluid. The quantities $(\partial\mu^{\infty}_{af}/\partial w_{mf})$, $\Delta S^{m\rightarrow f}_{tm}/\Delta V^{m\rightarrow f}_{tm}$ and $(\partial w_{mf}/\partial P)_{T,\sigma}$ are direct reflections of the swelling. The effects of swelling on the transfer properties $\Delta H^{f\rightarrow g}_{ta}$ and $\Delta V^{f\rightarrow g}_{ta}$ are less direct but definite. Interestingly, none of the properties appearing in Eq. 7 depends solely on the interaction between a solute and a pure stationary polymer.

In the systems investigated by Chester and Innis [1], the observed shifts in selectivity most likely originate from variations in the ratios $(\partial\mu^{\infty}_{af}/\partial w_{mf})$ for different solutes in different polymer–fluid systems. Further, as $(\partial w_{mf}/\partial P)_{T,\sigma}$ and $\Delta S^{m\rightarrow f}_{tm}/\Delta V^{m\rightarrow f}_{tm}$ vary from one polymer–fluid system to another, the variations in these solute-independent quantities serve to amplify those in the composition derivatives of the solute chemical potential (cf., Eq. 7).

3. Conclusion

A model-independent treatment has been presented of selectivity in temperature-programmed, constant-density, capillary SFC. Thermodynamic analysis confirms the expected importance of stationary phase swelling in determining the temperature-driven selectivity shift for a pair of solutes between two stationary phases. It appears that the thermodynamic background of the shift does not involve any property that would depend only on the interaction between a solute and a stationary polymer. Instead, the selectivity shift involves properties that depend either on the interaction between the stationary polymer and the mobile phase fluid or on all the three possible pairwise interactions within the solute–stationary polymer–supercritical fluid system. The only other thermodynamic derivative that contributes to the selectivity shift is the thermal pressure coefficient of the pure mobile phase fluid. It follows from these findings that swelling of the stationary phase plays an essential role in determining the temperature-induced shifts in selectivity among different stationary phases at a constant density of the mobile phase fluid.

Acknowledgement

This contribution is based on work supported by the Grant Agency of the Academy of Sci-

ences of the Czech Republic under Grant No. A4031503, which the author gratefully acknowledges.

References

[1] T.L. Chester and D.P. Innis, J. Microcol. Sep., 5 (1993) 127.
[2] D.E. Martire and R.E. Boehm, J. Phys. Chem., 91 (1987) 2433.
[3] D.E. Martire, J. Liq. Chromatogr., 10 (1987) 1569.
[4] M. Roth, J. Phys. Chem., 96 (1992) 8552.
[5] M. Roth, J. Chromatogr., 543 (1991) 262.
[6] M. Roth, J. Chromatogr., 641 (1993) 329.
[7] J.-J. Shim and K.P. Johnston, AIChE J., 35 (1989) 1097.
[8] J.-J. Shim and K.P. Johnston, AIChE J., 37 (1991) 607.
[9] G.K. Fleming and W.J. Koros, Macromolecules, 19 (1986) 2285.
[10] B.J. Briscoe and S. Zakaria, J. Polym. Sci. B, Polym. Phys., 29 (1991) 989.
[11] D.S. Pope, I.C. Sanchez, W.J. Koros and G.K. Fleming, Macromolecules, 24 (1991) 1779.
[12] A. Garg, E. Gulari and C.W. Manke, Macromolecules, 27 (1994) 5643.
[13] G.D. Wedlake and D.B. Robinson, J. Chem. Eng. Data, 24 (1979) 305.
[14] V.M. Shah, B.J. Hardy and S.A. Stern, J. Polym. Sci. B, Polym. Phys., 24 (1986) 2033.
[15] V.M. Shah, B.J. Hardy and S.A. Stern, J. Polym. Sci. B, Polym. Phys., 31 (1993) 313.
[16] S.R. Springston, P. David, J. Steger and M. Novotny, Anal. Chem., 58 (1986) 997.
[17] S.K. Goel and E.J. Beckman, Polymer, 33 (1992) 5032.
[18] C. Panayiotou and I.C. Sanchez, Polymer, 33 (1992) 5090.

ELSEVIER

Journal of Chromatography A, 718 (1995) 153–165

JOURNAL OF CHROMATOGRAPHY A

Statistical evaluation of various qualitative parameters in capillary electrophoresis

C.P. Palmer[1], B.G.M. Vandeginste*

Unilever Research Laboratorium Vlaardingen, P.O. Box 114, 3130 AC Vlaardingen, Netherlands

First received 24 January 1995; revised manuscript received 6 June 1995; accepted 6 June 1995

Abstract

Various qualitative migration parameters for capillary electrophoresis have been evaluated. A theoretical discussion of the relative merits of the parameters is presented. The parameters were experimentally determined under a series of conditions to ascertain their dependence on such factors as the temperature and applied field. Statistical analysis of the results was used to elucidate the relative importance of the experimental conditions on the variance in the measured parameters. It was found that the relative parameters provide more reproducible results and are independent of experimental conditions, although they require the addition of at least one migration standard to the sample. Parameters which use the relative mobilities of the analyte and reference standard are most reproducible.

1. Introduction

The rate of migration for a given compound in capillary electrophoresis (CE) is determined by its effective molecular charge and hydrodynamic radius. Fast and highly efficient separations have been achieved over the past decade for a variety of water soluble compounds [1,2].

However, there still are several limitations to the approach. These include the need for reproducible, stable and reliable surface-coating technologies and the reproducibility of quantitative (amount) and qualitative (identity) information.

Solutions to many of these problems are the subject of intense study, and there have been several reports concerning qualitative reproducibility [3–11] and on-line monitoring of electroosmotic flow to improve qualitative repeatability [12]. Migration time remains the qualitative parameter most often reported (although occasionally relative migration times [8–10,13] or electrophoretic mobilities are used). As the separations performed with CE become more complex, and as the technique becomes more generally applied in regulatory environments, where the reliable transfer of methodology is essential, the need for a dependable and reproducible qualitative parameter will become more acute. Such a parameter would also be very helpful in the development of new methodology, especially when several instruments, laboratories, or conditions are employed.

An ideal qualitative parameter should depend only on the properties of the analyte and those conditions of analysis which are completely

* Corresponding author.

[1] Present address: Himeji Institute of Technology, Faculty of Chemistry, Kamigori, Hyogo 678, Japan.

0021-9673/95/$09.50
SSDI 0021-9673(95)00636-2

under the control of the analyst. Given these properties, and careful work by the analyst, such a parameter would also yield high reproducibility. The capacity factor in isothermal gas chromatography, for example, represents such a qualitative parameter. Capacity factors can be reproduced with different instruments and different laboratories with relative ease, provided that the same stationary phase and temperature are used.

In CE, even with state-of-the-art commercial instrumentation, the operator really only has complete control of the buffer composition and the applied field (or current). With most instruments the temperature can also be controlled, but the temperature control capabilities vary widely with manufacturer. Temperature has been shown to rise due to the effects of Joule heating even in thermostated systems [14–17]. Additionally, the portion of the capillary which is under temperature control varies between instruments, and with a given instrument the proportion of the total capillary length which is under temperature control varies with the length of the capillary itself. The variability between the temperature control capabilities of various instruments may also become apparent in their ability to offset the effects of Joule heating, resulting in different optimum field strengths for different instruments. Thus, it would be best if the parameter were also independent of the applied potential.

The capillary dimensions are not always completely under the control of the operator. Certainly, the inner diameter of the capillary, as reported by the manufacturer, is only a mean value and can vary significantly [18]. While the operator can in principle set the capillary length very accurately and precisely, in practice capillaries are often cut to length after they have been installed in a cartridge. Additionally, changes in capillary length, either large or small, are often part of the method development process.

Perhaps the most difficult factor to control is the electroosmotic flow. Electroosmotic flow directly affects the migration time of every analyte. The dependence of electroosmotic flow on the chemistry of the silica surface (zeta potential) makes it very difficult to control or reproduce. Potential solutions to this problem include the development of new capillary materials with more reproducible surfaces, or the development of reproducible and stable surface modification procedures for fused-silica surfaces which eliminate the problems associated with the zeta potential. In the meantime, however, a qualitative parameter should be independent of the zeta potential, so that it can be employed with present technology.

The result of the problems presented above is that the duplication of separation conditions, between different laboratories, or different instruments, or indeed different capillaries, is difficult. Previous reports of inter-laboratory validation studies [8,10] have shown excellent intra-laboratory results for relative migration time, but inter-laboratory results have shown 1.3 [8] to 4.5 [10] percent R.S.D. A qualitative parameter which is independent of the problematic factors discussed above is necessary to permit method development and transfer of methodology. The qualitative parameter should depend only on the buffer composition and the analyte properties, and should be independent of the temperature, the applied field, the capillary dimensions, and the electroosmotic flow.

Lee and Yeung [3] have reported the use of a migration index and adjusted migration index for improving qualitative precision, but this approach requires that the internal diameters of the capillaries be known to within 0.5%. This presents a significant problem in light of current capillary manufacture technology [19]. Vespalec et al. [5] have reported a method which permits the determination of the "actual effective mobility" of the unknown. This can be determined from its migration time and the migration times of two migration reference standards in the same electrophoretic run. The actual mobilities of the two reference standards, under a given set of conditions, must be known. This approach produces reproducible results under a variety of conditions, and is reported to be independent of temperature. The limitation of this approach is the requirement that the electrophoretic mobilities of the two standards be known. Others have

shown the utility of relative migration times, in which the migration time of the analytes is divided by the migration time of an internal standard, for improving the qualitative results [8–10,13]. Recently, the utility of a retention index [19,20] and migration indices [11] in micellar electrokinetic chromatography have been investigated.

In this work a comparative study of the migration time, relative migration time, electrophoretic mobility, actual mobility, and relative mobility has been performed for a series of test analytes. The repeatability, reproducibility and practicality of the various parameters are compared.

2. Theory

Capillary electrophoresis separates ions by differences in their electrophoretic mobility. The effective migration rate of a given analyte is determined by its mobility and the electroosmotic flow through the capillary.

The electrophoretic mobility of a given compound can be most simply expressed in terms of its radius, r, the charge on the molecule, q, and the viscosity of the separation medium, η, as follows:

$$\mu_{ep} = \frac{q}{6\pi r\eta} \tag{1}$$

This simple equation is limited to fully ionized species, and does not account for non-ideality. More complete treatments, which account for the effects of ionic strength, can be found elsewhere [6,21–23]. In this work the ionic strength is assumed to be under the control of the analyst, and the effects of ionic strength are not investigated in detail.

The electrophoretic mobility is dependent on the properties of the compound. The temperature of the separation medium is also important, as it affects the viscosity (the viscosity of water changes by approximately 2%/°C in the range from 20 to 40°C [23]). In practice, the electrophoretic mobility (μ_{ep}) is calculated from experimental results as follows:

$$\mu_{ep} = \frac{lL}{V}\left(\frac{1}{t_{mig}} - \frac{1}{t_0}\right) \tag{2}$$

where l is the effective length of the capillary (inlet to detector), L is the total length of the capillary, V is the applied potential and t_{mig} and t_0 are the migration time of the analyte and the migration time of an uncharged solute, respectively. Thus, in order to accurately determine the electrophoretic mobility t_0 must be measured, and the capillary dimensions must also be known accurately. In practice, the determination of electrophoretic mobility requires accurate knowledge and control of the capillary dimensions.

The migration time is easily determined experimentally. It can be expressed as:

$$t_{mig} = \frac{lL}{V(\mu_{ep} + \mu_{eo})} \tag{3}$$

where μ_{eo} is the electroosmotic mobility, which is defined as

$$\mu_{eo} = \frac{\epsilon\zeta}{\eta} \tag{4}$$

where ϵ is the dielectric constant of the separation medium and ζ is the zeta potential of the capillary surface. Looking at Eqs. 1, 3 and 4, one can see that the migration time is affected by the capillary dimensions, the zeta potential (ζ) of the silica surface, and the temperature of the system (affecting the viscosity, the dielectric constant and the zeta potential). Thus, it can be seen that migration time is affected by all of the problematic factors.

The use of relative migration time (RMT),

$$t_{rel} = \frac{t_{mig}}{t'_{mig}} \tag{5}$$

where primed values are for a reference standard run with the analyte, does eliminate the effects of the viscosity and the capillary dimensions, as can be seen by combining Eqs. 1 and 3 through 5:

$$t_{rel} = \frac{\epsilon\zeta + \dfrac{q'}{6\pi r'}}{\epsilon\zeta + \dfrac{q}{6\pi r}} = \frac{a + \dfrac{q'}{r'}}{a + \dfrac{q}{r}} \tag{6}$$

where a ($a = 6\pi\epsilon\zeta$) is independent of analyte characteristics, but is dependent on the zeta potential. This assumes that the solution–analyte viscosity is identical to the solution–surface viscosity, which is justified under most operating conditions [3]. It also assumes that the analyte and the reference material experience the same viscosity, which is true unless there is temperature drift or gradient in buffer composition which causes one to encounter a higher or lower average viscosity than the other. Relative migration time does depend on the zeta potential, although this appears in the numerator and denominator of the equation and thus its effects should be limited. Still, this could impair the ability of this parameter to permit the transfer of methodology. Temperature effects on RMT should be limited to the consequent changes in the zeta potential and dielectric constant.

Analysis of Eq. 6 by differentiation with respect to the electroosmotic flow leads one to the conclusion that variations in RMT caused by changes in the electroosmotic flow can be minimized by selecting a reference material with similar electrophoretic mobility to that of the analyte. This would also help with the effects of gradients or temperature drift during the run.

Consider the relative electrophoretic mobility (RM). This is most simply defined as:

$$\mu_{rel} = \frac{\frac{q}{r}}{\frac{q'}{r'}} = \frac{qr'}{q'r} \tag{7}$$

and is calculated from the experimental parameters:

$$\mu_{rel} = \frac{t'_{mig}\,(t_0 - t_{mig})}{t_{mig}\,(t_0 - t'_{mig})} \tag{8}$$

Eq. 7 reveals that this parameter depends only on the properties of the analyte and the reference standard. Eq. 8 reveals that no experimental parameters such as column dimensions etc. are required for the determination of the RM. The migration times of a nonionic solute, a reference standard, and the analyte must be determined. The chemical (pK_a) and electrophoretic properties (q) of the analyte and the reference materials should match as closely as possible to negate the effects of non-ideality on the electrophoretic mobility. The temperature must be constant during the run so that both the analyte and the reference material experience the same average temperature. Likewise, electroosmotic flow must either be large enough to permit measurement of t_0, or small enough that t_0 can be eliminated from Eq. 8.

With either Eq. 6 or Eq. 8 it can be shown that when electroosmotic flow is minimal (i.e. t_0 is very large) the relative migration time (t_{rel}) is the inverse of the relative electrophoretic mobility (μ_{rel}).

In the approach of Vespalec et al. [5], the actual mobility of the analyte, μ_x, is calculated from the known mobilities of two reference standards and the experimentally determined migration times:

$$\mu_x = \mu_{ep}'' + (\mu'_{ep} - \mu_{ep}'')\frac{t'_{mig}\,(t_{mig}'' - t_{mig})}{t_{mig}\,(t_{mig}'' - t'_{mig})} \tag{9}$$

Due to differences in the effects of ionic strength on the mobility of compounds with different charge, this approach should work best when the reference materials have the same charge as the analytes and/or when the standard electrophoretic mobilities are determined under conditions nearly the same as those used for the analysis. This parameter may, in fact, perform better than the relative mobility, since the reference standards can be chosen such that the analyte falls between them in mobility and migration time. It is certainly a better choice when electroosmotic flow is significant (preventing t_0 from being eliminated from Eq. 8) but not measurable, since no determination of electroosmotic flow (or t_0) is necessary.

Eq. 9 essentially reduces to Eq. 8 when μ_{ep}'' is set to 0, and t_{mig}'' is thus equal to t_0. This is not entirely true, since in Eq. 9 μ'_{ep} refers to the known electrophoretic mobility of the reference compound under a given set of standard conditions, and the calculated μ_x is thus the mobility of the analyte under the same set of standard conditions. In practice, this difference amounts only to μ_x being directly proportional to μ_{rel}.

When two migration reference materials with mobility are used μ_x is a unique parameter. An advantage of this parameter is that when the reference materials and the analytes have similar chemical and electrophoretic properties (same charge) the value for a given compound should not depend on the reference materials used, whereas relative mobility is specific to a given analyte and reference material.

3. Experimental

A Spectra-Physics Model 1000 CE was used for all studies. The instrument was controlled with an IBM PS/2 Model 70 386 PC equipped with Spectraphoresis version 1.03 data acquisition and control software. All electropherograms were collected at both 210 and 255 nm.

All chemicals were purchased in the highest grade possible. Sodium hydroxide, sodium chloride, sodium tetraborate, boric acid, and acetone were obtained from E. Merck (Darmstadt, Germany). Anthraquinone-2-sulfonic acid, *p*-toluene-sulfonic acid, salicylic acid and phthalic acid, which were used as test analytes, were obtained from Aldrich (Steinheim, Germany).

The fused-silica capillary was purchased from LC Packings (Emmen, Netherlands), and was sourced from Polymicro Technologies, USA. The capillary had a 75 μm internal diameter, and a total length of 70 cm (effective length of 63 cm). The capillary was rinsed when installed with 1 *M* NaOH for 5 min at 50°C, 20 min at 40°C with 0.1 *M* NaOH, 20 min at 40°C with millipore water, and 30 min at 30°C with the run buffer. Before each run, the capillary was rinsed for 3 min with the buffer at the run temperature, and after each run the capillary was washed for 2 min with the run buffer at the run temperature. At the end of each day, the capillary was rinsed for 30 min at the run temperature with millipore water. At the beginning of each day, the capillary was rinsed first for 10 min at 40°C with 0.01 *M* NaOH, followed by millipore water for 10 min at 40°C, and finally by run buffer for 30 min at the run temperature. Each day, a blank run was performed with the run buffer before any actual runs were performed.

A 0.02 *M* borate buffer, pH 8.2, was prepared in millipore water as follows: a 0.02 *M* boric acid solution was titrated to pH 8.2 using a 0.005 *M* solution of sodium tetraborate (0.02 *M* in borate). The buffer was vacuum filtered through a 0.45-μm filter before use. For higher ionic strength measurements, sodium chloride was added to the buffer at the indicated concentrations. No further pH adjustment or filtrations were made after addition of the sodium chloride.

Stock solutions of the test analytes were prepared by dissolving 15 to 20 mg of the compound in 10.00 ml of the borate buffer. These stock solutions were stored at 4°C when not in use. Run solutions were prepared by adding 10 μl of the stock solution of interest and 20 μl of pure acetone to 1.2 ml of buffer solution in a sample vial. The final concentration of test analytes was thus 12–16 ppm.

Electrophoretic measurements were made using applied potentials of 10, 20, or 30 kV and temperature settings of 30, 40, or 50°C. At least three measurements were made at each condition. At each new condition the migration order of the test analytes was reconfirmed by consecutive addition of the analytes to the run sample vial or by the relative intensities of the peaks at the two wavelengths. Measurements at a given potential and applied temperature were not all made consecutively. In most cases a given condition was returned to after several runs at other conditions, and/or on different days. A total of 40 electropherograms were collected at the various conditions over a period of 9 days.

4. Results and discussion

A typical electropherogram of a mixture of the four test analytes is presented in Fig. 1, showing the 210-nm trace. The migration order is indicated. Acetone, used as a marker for the electroosmotic flow, does not appear in Fig. 1 as it is not detected at 210 nm. Electropherograms run at the same conditions, on consecutive injec-

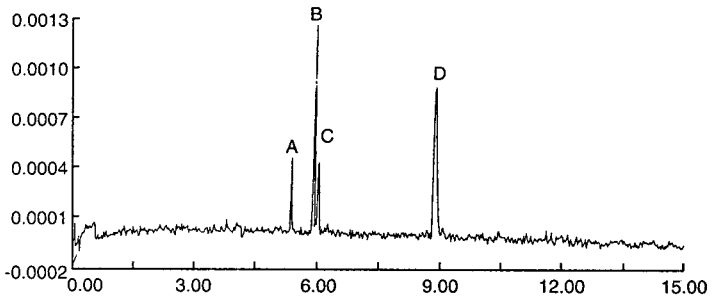

Fig. 1. Typical electropherogram, monitored at 210 nm. Peaks: A = anthraquinone-2-sulfonic acid, B = p-toluene sulfonic acid, C = salicylic acid, D = phthalic acid.

tions, are presented in Fig. 2. This figure illustrates limitations in the migration repeatability.

The electropherogram of these compounds provides the necessary features to test the utility of the various qualitative parameters. All of the compounds have pK_a values less than 5.5 (pK_{a2} for phthalic acid) and are fully ionized at pH 8.2. *p*-Toluene-sulfonic acid and salicylic acid have similar migration times, testing the ability to distinguish between compounds with similar migration characteristics. Phthalic acid has a charge of −2 and much greater mobility than anthraquinone-2-sulfonic acid which has a charge of −1, allowing the parameters to be tested with respect to migration time and testing their range of applicability. The effects of non-ideality on the electrophoretic mobility are expected to show for compounds with different charge. For relative migration time and relative mobility, anthraquinone-2-sulfonic acid was employed as the migration reference material. For actual mobility measurements, anthraquinone-2-sulfonic acid and phthalic acid were used as the reference migration materials. Because of the −2 charge on phthalic acid, its utility as a reference material for the analytes with −1 charge is questionable. We have tested the significance of this problem by repeating some of the studies using anthraquinone-2-sulfonic acid and salicylic acid as reference materials. The average electrophoretic mobility for these compounds at 30°C and 30 kV was used for the actual mobility calculations.

4.1. Migration time

Plotted in Fig. 3 are the migration times for a series of runs in which the applied potential was kept constant at 30 kV and the temperature was varied from 30 to 50°C. It can be seen from this plot that the migration time varies significantly with temperature, as expected. It can also be

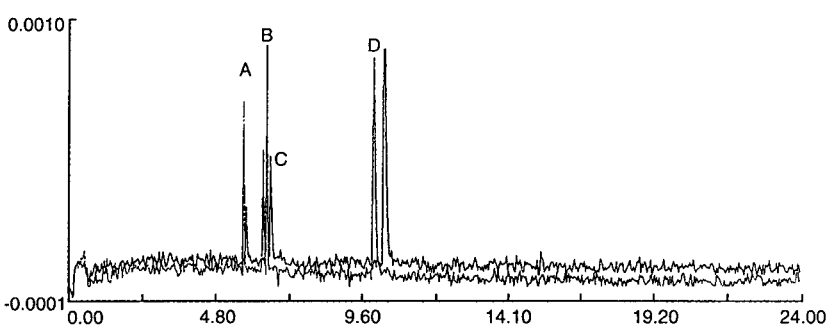

Fig. 2. Consecutive electropherograms at 20 kV applied potential and 30°C, monitored at 210 nm. Peaks: A = anthraquinone-2-sulfonic acid, B = *p*-toluene-sulfonic acid, C = salicylic acid, D = phthalic acid.

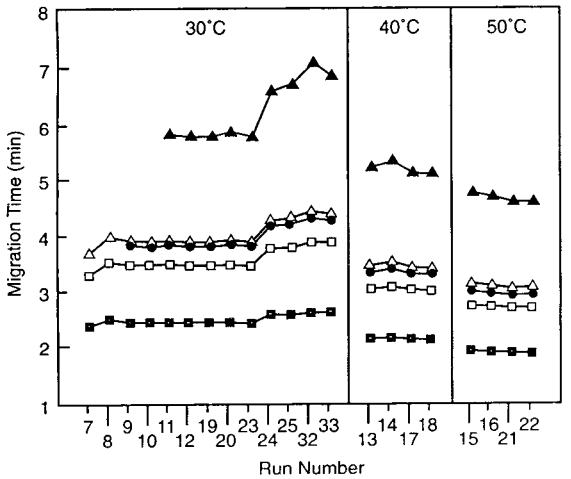

Fig. 3. Migration times as a function of the run number for the four analytes and acetone (t_0) at 30 kV and 30, 40, and 50°C. (■) acetone; (□) anthraquinone-2-sulfonic acid; (●) *p*-toluene-sulfonic acid; (△) salicylic acid; (▲) phthalic acid.

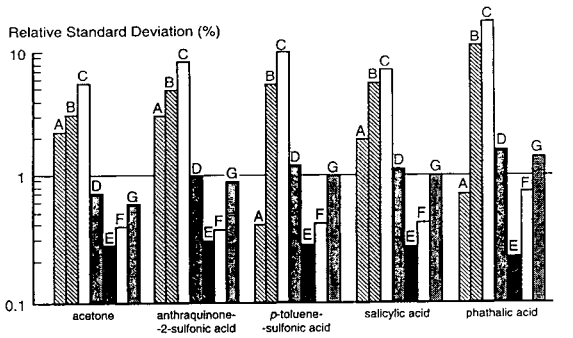

Fig. 4. Relative standard deviations in migration time for each analyte under the seven sets of analysis conditions. A = 30 kV, 30°C; B = 30 kV, 40°C; C = 30 kV, 50°C; D = 20 kV, 30°C; E = 20 kV, 40°C; F = 10 kV, 30°C; G = 10 kV, 40°C. Plotted on a semilogarithmic scale.

seen that there is significant variability in the migration times within a given temperature range. In fact, it would be impossible to determine whether a single peak in an unknown sample represented *p*-toluene-sulfonic acid or salicylic acid using migration time alone. It is important to notice the pattern in the variations. The fluctuations are always in the same direction, although they are not of the same magnitude. This implies that a common phenomenon, probably the electroosmotic flow, is causing these variations.

The data presented in Fig. 4 confirm the observations made from Fig. 3. There is a lot of variability in these results within a given condition, with the worst cases being 10–20% R.S.D. On the other hand, in the best cases, the precision was very good (<0.2% R.S.D.).

The poor precision is aggravated by the fact that the data were collected on different days and by the fact that the runs within a day were not made consecutively, but runs with different conditions fell between them. Often, the R.S.D. for a series of runs made consecutively at the same condition was very good (below 0.2%), but it was observed to be as high as 2%. The average migration time was observed to change by as much as 11% between days, when the analyses were otherwise run at the same conditions.

Analysis of covariance for the logarithm of the migration time (the logarithm was used to equalize the variance between analytes) for all of the separations run at 30 kV indicated that the type of analyte, the temperature and the run number all make highly significant contributions to the variance. Including the 10 and 20 kV data indicated that the applied potential also makes a highly significant contribution.

For a given temperature and applied potential, the inverse of the migration time was found to be highly correlated ($r^2 \geq 0.980$, as high as 0.9998) with the inverse of t_0. This is the expected behavior when the variations in migration time are caused solely by variations in electroosmotic flow.

An interesting result emerging from the statistical analysis is that the slopes of the plot of the logarithm of the migration time vs. the temperature are not significantly different for the five analytes. The slope of these plots (-0.0109 ± 0.0004) is similar to the slope of a plot of the logarithm of the viscosity of water with respect to the temperature (-0.0082) in the range from 30 to 50°C (data obtained from Ref. [24]). Changes in the viscosity appear to be the dominant factor, but do not sufficiently account for the observed slope. The difference may be the result of changes in the dielectric constant,

zeta potential or solvation brought on by changes in the temperature.

4.2. Electrophoretic mobility

Fig. 5 shows the data for electrophoretic mobility for the same data set as presented in Fig. 3. It can be seen that the electrophoretic mobility is also temperature dependent, but that it is in general more precise than migration time for a given temperature setting. The electroosmotic mobility is observed to vary significantly, with a pattern similar to that for the migration times (Fig. 3). This indicates that the common phenomenon which causes the poor precision in migration time for a given condition is the electroosmotic flow, probably due to zeta potential effects. These variations in electroosmotic mobility are not mirrored by variations in the electrophoretic mobilities.

Again, these observations are confirmed with study of Fig. 6. It can be seen that the relative standard deviations for electroosmotic mobility are often greater than one. The high variability in the electroosmotic flow is not reflected in the electrophoretic mobility values, which generally have an R.S.D. of less than one.

Analysis of covariance of the electrophoretic

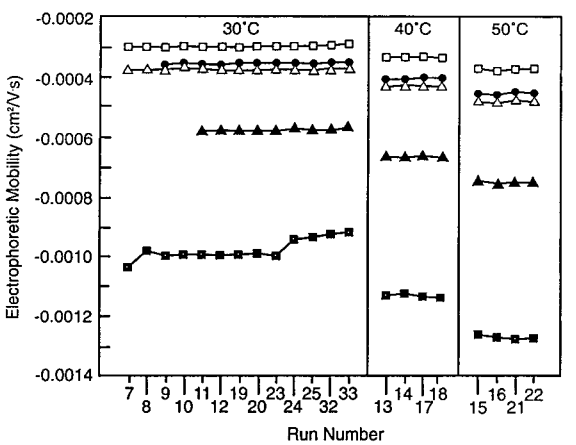

Fig. 5. Electrophoretic and electroosmotic mobilities at 30 kV and 30, 40, or 50°C, as a function of run number. (■) acetone; (□) anthraquinone-2-sulfonic acid; (●) *p*-toluene-sulfonic acid; (△) salicylic acid; (▲) phthalic acid.

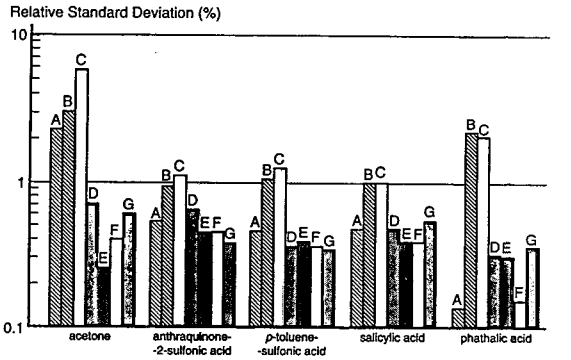

Fig. 6. Relative standard deviations in electrophoretic mobility for each of the analytes under seven sets of analytical conditions. Study conditions as in Fig. 4. Plotted on a semilogarithmic scale.

mobility indicated that the temperature and the analyte make the greatest contributions to the variance. The applied potential also makes a significant contribution, but its absolute contribution is minor. This may be the result of Joule heating, which is a function of the applied potential and affects the working temperature in the capillary. The run number also makes a minor, but significant, contribution. No reproducible correlation was observed between the electrophoretic mobility and t_0 or $1/t_0$, indicating that the electrophoretic mobility is unaffected by electroosmotic flow.

As was observed for migration time, there were differences between the mobilities measured on different days when the same conditions were used which affected the results reported in Fig. 6. These differences are not statistically significant, and since the data was collected on only two days no analysis of variance could be performed to determine the relative contributions to the variance. However, the changes in electrophoretic mobility between the two days are in the same direction and of nearly the same relative magnitude for all of the analytes. This must be caused by a real phenomenon, and is most likely due to differences in actual temperature between days. Although the temperature setting and reading were the same, these data indicate that there were still differences in temperature that affected the mobilities.

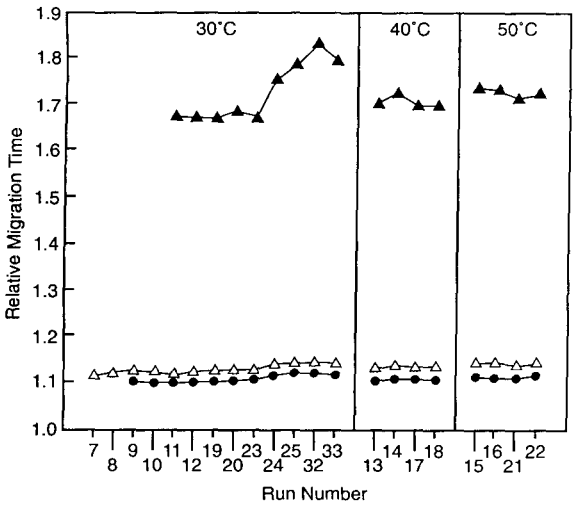

Fig. 7. Relative migration time at 30 kV and 30, 40, and 50°C, as a function of the run number. (●) *p*-Toluene-sulfonic acid; (△) salicylic acid; (▲) phthalic acid.

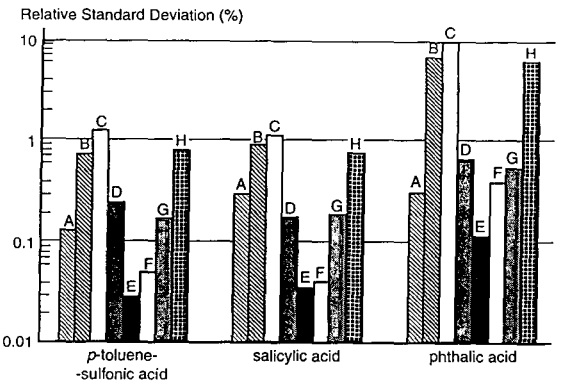

Fig. 8. Relative standard deviations in relative migration time for three analytes. Conditions of analysis as in Fig. 4. H = All conditions combined. Plotted on a semilogarithmic scale.

4.3. Relative migration time

Fig. 7 shows the results for relative migration time (RMT) using anthraquinone-2-sulfonic acid as a reference standard, for the same data as presented in Fig. 3. What can be seen here is that the RMT is not affected to a high degree by the temperature of the system. This was predicted by Eq. 6. Additionally, it can be seen that there remains some variation in the RMT within a given condition, especially for phthalic acid.

Fig. 8 presents the R.S.D. data for all the conditions. In this case we can also report an overall data set which takes into account the results for all conditions on all days, since the RMT should be independent of the conditions. The R.S.D. values are quite good for salicylic acid and *p*-toluene-sulfonic acid ($\leq 1\%$), but rather poor for phthalic acid (up to 10%). This is probably the result of the dependence, discussed in the Theory section, of the reproducibility of this parameter on the difference between the mobility of the analyte and the reference material. Phthalic acid has the greatest difference in mobility, and shows the poorest results. Also, when the electrophoretic mobility of the analyte is similar in magnitude but opposite in direction to the electroosmotic flow, small changes in the electroosmotic flow have a large effect on the migration time. The effect may also be caused by temperature drift, since this would cause phthalic acid to experience a different average temperature than the other analytes. It is also notable that the pattern of the plots follows that for electroosmotic mobility (Fig. 5) for each of the analytes. This indicates that the RMT is not completely free from the effects of variations in electroosmotic flow, as seen in Eq. 6.

Analysis of covariance for the data set collected at 30 kV indicates that only the type of analyte contributes significantly to the variance in the data set. The temperature and the run number do not significantly contribute. For a given applied potential and temperature, the inverse of the natural logarithm of the RMT was found to be highly correlated ($r^2 \geq 0.92$, as high as 0.999) with the inverse of t_0. This is as one would expect when the variation in RMT is caused solely by variations in electroosmotic flow.

The zeta potential and dielectric constant do depend on the temperature, so one might expect that the RMT would be affected to a greater extent by changes in temperature. This is a further indication that the effects of changes in the temperature are dominated by viscosity influences.

The ratio of the migration time of the analyte

to t_0 was also evaluated. In spite of earlier reports [13], this parameter behaved very poorly, showing poor repeatability within a given condition, and poor overall reproducibility. This probably results from the large difference in mobility between the analyte and the reference standard when this approach is used.

4.4. Relative electrophoretic mobility

Presented in Fig. 9 are the results for relative electrophoretic mobility, using anthraquinone-2-sulfonic acid as the migration standard. It can be seen from this figure that the RM is independent of temperature, and that it is reproducible over a range of analytical conditions. This is confirmed when the data are presented in Fig. 10. The R.S.D.s for this parameter are very good ($\leq$1.4%), even for cases where all data are included. The R.S.D.s do appear to increase from salicylic acid to phthalic acid, which is not unexpected, since the difference in mobility and migration time between the reference standard and the analyte also increases. This may also be the result of variations or drift in the temperature of the system during the analytical runs. The between-day or between-condition variations

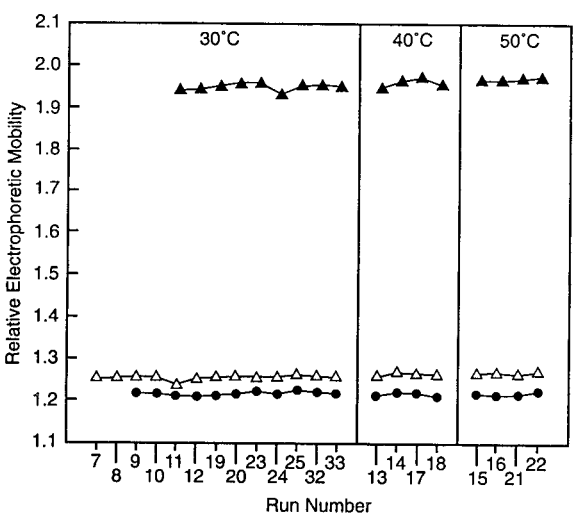

Fig. 9. Relative electrophoretic mobilities at 30 kV and 30, 40 and 50°C, as a function of the run number. (○) *p*-Toluene-sulfonic acid; (△) salicylic acid; (▲) phthalic acid.

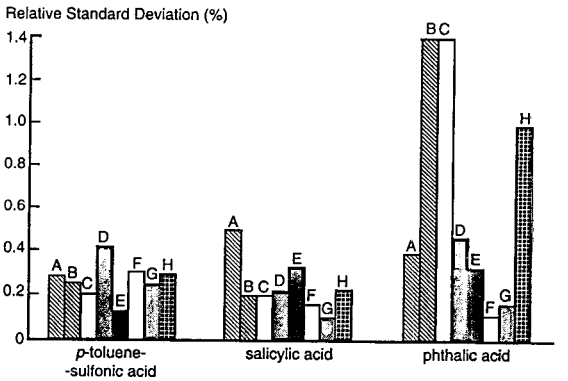

Fig. 10. Relative standard deviations in relative electrophoretic mobilities for three analytes. Conditions as in Fig. 4. H = All conditions combined. Plotted on a linear scale.

which were problematic for the other parameters were not observed for the RM.

Analysis of covariance indicated that all of the parameters (analyte, applied potential, temperature and run number) make significant contributions to the variance. The analyte contributes by far the greatest amount to the total variance. The temperature can not be considered significant with 95% confidence, but is significant at the 90% confidence level. However, these results must be considered with respect to the trivial overall variance in the data set, which results in high significance being assigned to only minor variations. No correlation between RM and t_0 or $1/t_0$ was observed.

4.5. Actual mobility

The actual mobility, calculated using anthraquinone-2-sulfonic acid and phthalic acid as reference standards, also provides very good results, as can be seen from Figs. 11 and 12. The precision of these results is equivalent to that for the relative electrophoretic mobility results for these analytes. There is no evidence that they are better, as might be expected since the mobilities of the two analytes are between those of the two reference standards.

Because phthalic acid has a charge of −2, it may be expected that it would not perform well as a reference standard for compounds such as *p*-toluene-sulfonic acid and salicylic acid, which

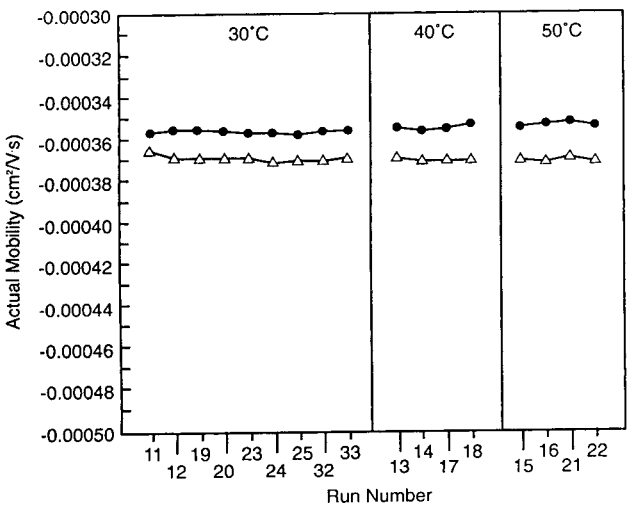

Fig. 11. Actual mobility for *p*-toluene-sulfonic acid and salicylic acid at 30 kV and 30, 40 and 50°C, plotted as a function of the run number. (●) *p*-Toluene-sulfonic acid; (△) salicylic acid.

each have a charge of −1. To investigate this, we have calculated the actual mobility of *p*-toluene-sulfonic acid using anthraquinone-2-sulfonic acid and salicylic acid as reference materials. The overall average actual mobility and reproducibility using these two reference materials ($3.56 \pm 0.02 \cdot 10^{-4}$ $cm^2\ V^{-1}\ s^{-1}$) were not significantly different from the results obtained with anthraquinone-2-sulfonic acid and phthalic acid as reference materials ($3.58 \pm 0.02 \cdot 10^{-4}$ $cm^2\ V^{-1}\ s^{-1}$). This indicates that, under the conditions of this study, when the ionic strength of the analysis buffer is not significantly different from the ionic strength of the buffer used for determination of the standard mobilities, the identity and even the charge of the reference materials is not a significant factor in determining the actual mobilities of the analytes.

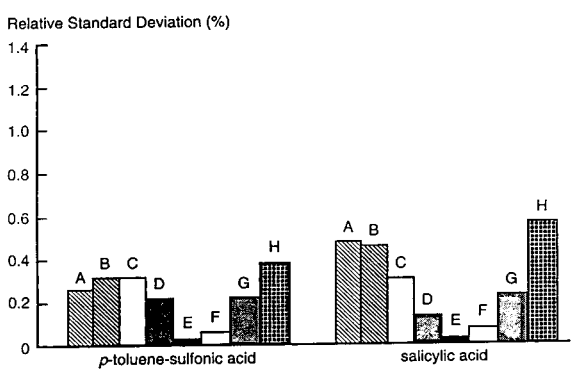

Fig. 12. Relative standard deviations in actual mobility for *p*-toluene-sulfonic acid and salicylic acid. Analysis conditions as in Fig. 4. H = All conditions combined. Plotted on a linear scale, at the same scale as Fig. 11.

Analysis of covariance for this data set was not performed. Due to the small variance in the data set the results were expected to mirror those of the relative migration time. No correlation was observed between the actual mobility and t_0 or $1/t_0$.

4.6. Ionic strength

It remains a question what the effect of the ionic strength of the separation buffer, and differences between the ionic strength of the sample and the buffer, would have on these parameters. Ionic strength directly affects the electroosmotic flow, and thus is expected to have a direct effect on the migration times and an indirect effect on the relative migration times. Additionally, the ionic strength may affect the charge or solvation of the analytes and has an effect on the electrophoretic mobility [6,21–23]. Differences in the ionic strength of the run buffer might be expected to have an effect on the relative parameters if the standards and the analytes react differently to the change in solvation. Additionally, a difference between the sample and run buffers might be expected to affect these parameters since immediately after injection the electric field in the sample and separation regions of the capillary will be different.

We have conducted only preliminary studies, in which the conductivity of the run buffer was doubled by addition of 5 m*M* sodium chloride. While the migration times were affected drastically and failed to stabilize, the other parameters showed no statistically significant change. This represents only preliminary work, and a more complete study of the effects of ionic strength should be conducted.

5. Conclusions

In many cases, especially for consecutive runs, the results for migration time are actually encouraging. This is not always the case, as is seen for some of the data sets and in the literature. The dependence of migration time on so many factors which are at best under limited control, such as the zeta potential, temperature, column dimensions and buffer composition, makes the use of this qualitative parameter difficult. Transfer of methodology and results would also be difficult using migration time as a qualitative measure.

Electrophoretic mobility is quite precise for a given set of conditions. This precision is probably due to its greatest advantage: independence of electroosmotic flow and zeta potential. Its dependence on temperature, which may be the cause of day-to-day variability, is a significant drawback. Another significant limitation is the need to know the capillary dimensions accurately.

Relative migration time is independent of the temperature, voltage, and capillary dimensions. However, it does not show the repeatability or reproducibility of other relative parameters, and can only be used under limited conditions. This is a result of its limited dependence on the zeta potential at the silica surface. This dependence also means that the parameter is dependent on the capillary supplier, conditioning procedure, and buffer composition. When it is used, the reference material should be chosen to have an electrophoretic mobility similar to that of the analyte, as this minimizes the effects of variations in electroosmotic flow.

The relative mobility and actual mobility show the greatest promise for providing a qualitative parameter with the qualities of the capacity factor in chromatography. They are independent of all parameters which the operator does not control. Actual mobility can best be used when there is significant electroosmotic flow, but it is not great enough to permit measurement. Actual mobility may have the added advantage that the value measured for a given compound should not depend on the reference materials used, making the approach more general. This was the case under the limited conditions of this study.

A significant limitation of the relative parameters is the need for a migration standard to be added to the sample. This requires the selection of a migration standard which does not interfere with the analysis, which may be difficult when the sample is complex. Relative mobility suffers from the additional complication that t_0 must be determined, and actual mobility suffers from the fact that it requires the addition of two reference standards, and that the electrophoretic mobility of these standards must be known.

Most of the problems with precision reported here can be traced to variations in the electroosmotic flow, as a direct result of variations in the chemistry at the fused-silica surface. This problem must be addressed to permit convenient application of CE in regulatory environments. Another problem which seemed to aggravate the poor precision was the lack of reproducibility in the temperature of the system on a day-to-day basis.

Overall, successful operation within a laboratory with a given instrument is certainly possible with migration time and standards when the system is equilibrated with the buffer, temperature, etc. This may, however, take a long time to achieve [4,25], slowing method development and the generation of results. When methods are to be transferred between instruments and laboratories, and a definitive qualitative assignment must be (quickly) made then a relative parameter should be employed. Relative mobility and actual mobility outperform relative migration time. Actual mobility should be employed in the case where electroosmotic flow is significant, but is too low to allow measurement.

List of symbols

Following is a list of symbols used in the text in the order in which they appear. Primed symbols in the text refer to the value for a migration reference material, double primed values refer to a second migration reference material.

μ_{ep}	Electrophoretic mobility
q	Effective molecular charge
r	Effective molecular radius
η	Buffer viscosity
l	Effective capillary length
L	Total capillary length
V	Applied potential
t_{mig}	Migration time
t_0	Migration time of an uncharged compound
μ_{eo}	Electroosmotic mobility
ϵ	Dielectric constant of the separation buffer
ζ	Zeta potential at the internal capillary wall
t_{rel}	Relative migration time
μ_{rel}	Relative electrophoretic mobility
μ_x	Actual electrophoretic mobility

References

[1] W.G. Kuhr and C.A. Monnig, Anal. Chem., 64 (1992) 389R.
[2] H. Engelhardt, W. Beck, J. Kohr and T. Schmitt, Angew. Chem. Int. Ed. Engl., 32 (1993) 629.
[3] T.T. Lee and E.S. Yeung, Anal. Chem., 63 (1991) 2842.
[4] S.C. Smith, J.K. Strasters and M.G. Khaledi, J. Chromatogr., 559 (1991) 57.
[5] R. Vespalec, P. Gebauer and P. Boček, Electrophoresis, 13 (1992) 677.
[6] J.L. Beckers, F.M. Everaerts and M.T. Ackermans, J. Chromatogr., 537 (1991) 407.
[7] K.D. Altria and Y.L. Chanter, J. Chromatogr., 652 (1993) 459.
[8] K.D. Altria, R.C. Harden, M. Hart, J. Hevizi, P.A. Hailey, J.V. Makwana and M.J. Portsmouth, J. Chromatogr., 641 (1993) 147.
[9] K.D. Altria, D.M. Goodall and M.M. Rogan, Electrophoresis, 15 (1994) 824.
[10] K.D. Altria, N.G. Clayton, M. Hart, R.C. Harden, J. Hevizi, J.V. Makawana and M.J. Portsmouth, Chromatographia, 39 (1994) 180.
[11] H. Siren, J.H. Jumppanen, K. Manninen, M.-L. Riekkola, Electrophoresis, 15 (1994) 779.
[12] T.T. Lee, R. Dadoo and R.N. Zare, Anal. Chem., 66 (1994) 2694.
[13] N. Chen, L. Wang and Y. Zhang, J. Liq. Chromatogr., 16 (1993) 3609.
[14] H. Watzig, Chromatographia, 33 (1992) 445.
[15] M.S. Bello, M. Chiari, N. Nesi, P.G. Rhigetti and M. Saracchi, J. Chromatogr., 625 (1992) 232.
[16] S. Terabe, T. Katsura, Y. Akaeda, Y. Ishihama and K. Otsuka, J. Microcol. Sep., 5 (1993), 23.
[17] J.H. Knox and K.A. McCormack, Chromatographia, 38 (1994) 207.
[18] J.W. Jorgenson, 15th International Symposium on Capillary Chromatography, Riva del Garda, Italy, 1993.
[19] E.S. Ahuja and J.P. Foley, Analyst, 119 (1994) 353.
[20] P.G.H.M. Muijselaar, H.A. Claessens and C.A. Cramers, Anal. Chem., 66 (1994) 635.
[21] J.C. Reijenga and E. Kenndler, J. Chromatogr. A, 659 (1994) 403.
[22] M.A. Survay, D.M. Goodall, S.A.C. Wren and R.C. Rowe, J. Chromatogr., in press.
[23] P.W. Atkins, Physical Chemistry, 3rd ed., W.H. Freeman and Co., New York, NY, 1986, p. 595.
[24] D.R. Lide (Editor), CRC Handbook of Chemistry and Physics, 74th ed., 1993–1994.
[25] C. Schwer and E. Kenndler, Anal. Chem., 63 (1991) 1801.

ELSEVIER

Journal of Chromatography A, 718 (1995) 167–175

JOURNAL OF CHROMATOGRAPHY A

Determination of critical micelle concentration by capillary electrophoresis. Theoretical approach and validation

J.C. Jacquier[a,b], P.L. Desbène[a,b,*]

[a] *Laboratoire d'Analyse des Systèmes Organiques Complexes, Université de Rouen, IUT, 43 rue St Germain, 27000 Evreux, France*

[b] *IFRMP, Université de Rouen, 76821 Mont Saint Aignan Cedex, France*

First received 28 December 1994; revised manuscript received 26 April 1995; accepted 26 April 1995

Abstract

The aim of this study was the determination of the critical micelle concentration (CMC) of the most commonly employed anionic surfactant in micellar electrokinetic chromatography, sodium dodecyl sulphate (SDS), using capillary electrophoresis, i.e., under the operating conditions of the electrophoretic separation (pH, ionic strength, temperature, etc.). The effective electrophoretic mobility of a neutral compound, resulting from the solvophobic and micellar contributions, appeared to be a well adapted parameter for the study of the micellization process of anionic surfactants. In fact, the theoretical treatment of the evolution of this parameter as a function of the total surfactant concentration allowed the identification of a sharp change in slope at the cmc, and therefore to establish capillary electrophoresis as a new analytical tool for the determination of critical micelle concentrations. In the experimental case of an electrolytic solution consisting of 5 mmol l^{-1} borax, the observed value of the cmc of SDS (5.29 mmol l^{-1}) was in total agreement with the literature data when the sodium concentration in the solution was the same.

1. Introduction

The optimisation of the analytical conditions in micellar electrokinetic chromatography (MEKC) has been an important field of research since 1984 and has allowed the resolution of a number of diverse organic matrices. Most of these studies dealt with the optimization of the operating conditions (nature and concentration of the electrolytic salt, nature and concentration in organic solvent) concerning the relative interactions of the solutes between the micellar and the aqueous phases. However, few authors examined the influence of these operating parameters on the evolution or the existence of the micellar phase. As the study of the micellization process is a key parameter in the optimization of the analytical conditions in MEKC, the determination of the critical micelle concentration under electrophoretic conditions proves to be essential.

Taking into account the complexity of the electrolytic media used in MEKC, the different physico-chemical properties used for the determination of the critical micelle concentration (cmc) (surface tension, conductivity, etc.) appear to be not well adapted or even inappropriate. The micellar solubilization, which can be easily accessible using capillary electrophoresis,

* Corresponding author, at the Evreux address.

0021-9673/95/$09.50
SSDI 0021-9673(95)00512-9

seems to be an appropriate method for the study of micellar systems as it is essentially due, like micellization, to the hydrophobic effect. The solubility in water of a hydrophobic molecule is strongly improved in the presence of a surfactant above its critical micelle concentration.

This micellar solubilization method for the determination of critical micelle concentrations is based on the measurement of the concentration of a poorly water soluble compound in the presence of increasing concentrations of surfactant. Below the cmc, the sample solubility will remain virtually the same as without surfactant. Above the cmc, one will observe a tremendous increase in the amount of solubilized additive with increase in the micelle concentration [1]. Moreover, this study can be done very simply with a UV–visible spectrophotometer if the solute studied contains a chromophore.

The inherent defaults of this micellar solubilization technique are linked with the use of an additive in the water–surfactant pseudo-biphasic system which can play the role of a catalyst of the micellar process, e.g., as an impurity of the surfactant does. Indeed, the cmc values obtained with this technique are known to be lower than those obtained with techniques that do not require an additive, e.g., measurement of the surface tension. Nevertheless, this systematic error can be minimized if the concentration of the additive is negligible, as in capillary electrophoresis, for example.

However, the principal interest in this technique is its universality, with regard to the nature of the studied surfactant (anionic, cationic, nonionic) or the nature of the aqueous phase (presence of neutral salts, of organic solvents, etc.).

2. Theoretical

Considering we are in the presence of the aqueous phase, the micellar pseudo-phase and the capillary wall, which represents a solid phase on which surfactant molecules are adsorbed, three equilibrium constants can be established: K_{mic}, the equilibrium constant of the solute between the aqueous phase and the micelles (micellar solubilization constant); K_{ads}, the equilibrium constant of the solute between the aqueous phase and a stationary phase constituted of surfactant molecules adsorbed on the capillary wall; and K_{solv}, the equilibrium constant of the solute between the aqueous phase and the monomeric surfactant molecules (solvophobic partition constant). Under these conditions, Fig. 1 shows schematically the exchanges involved in MEKC.

The adsorption of cationic surfactant molecules on the fused-silica capillary wall is a very important phenomenon, as it has been shown to be responsible for an inversion of the electroosmotic flow [2]. Nevertheless, in the case of anionic surfactants, it seems that the ionic repulsion between the hydrophilic moieties of the surface-active molecules and the silanol groups is strong enough to prevent any adsorption, and the zeta potential remains constant [3].

In the framework of our study, which involved sodium dodecyl sulphate (SDS), the only equilibria present were therefore the partition of the solute N between the aqueous phase and the monomeric surfactant molecules S on the one hand (Eq. 1), and the partition of the solute between the aqueous phase and the micellar pseudo-phase M on the other (Eq. 2). Under these conditions, two equilibria appear to be sufficient to describe the system fully, as we can omit the study of the partition of the solute between the micellar pseudo-phase and the monomeric surfactant molecules:

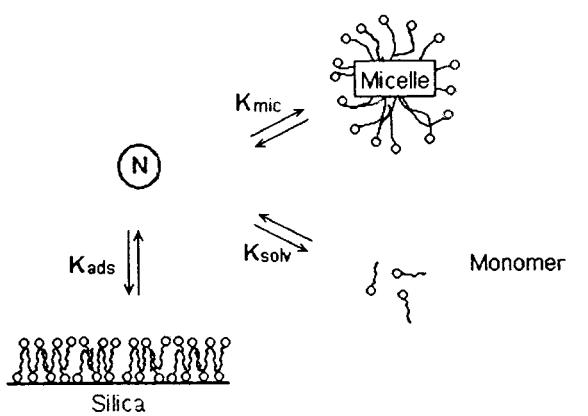

Fig. 1. Illustration of equilibria occurring in MEKC.

$$N + S \rightleftharpoons NS \qquad K_{solv} = \frac{x}{(1-x-y)[S]} \tag{1}$$

$$N + M \rightleftharpoons NM \qquad K_{mic} = \frac{y}{(1-x-y)[M]} \tag{2}$$

where x is the molar fraction of the solute associated with the monomeric surfactant through solvophobic interactions and y is the molar fraction of the solute in the micellar pseudo-phase. The micelle concentration [M] is expressed in moles of micelles per litre whereas [S] is expressed in moles of monomeric surfactants per litre. The total concentration C_T of surfactant introduced in the solution is therefore

$$C_T = [S] + n[M] \tag{3}$$

where n is the micellar aggregation number.

To be precise, an activity coefficient should have been introduced in Eqs. 1 and 2 to take into account the non-ideality inside these micellar aggregates. This introduction would nevertheless be only formal, as no data are available on the interaction between the solute and the surfactant in the micellar core [4].

Even though the partition involving the monomeric surfactant molecules is only rarely taken into account in the literature [5], this partitioning should not be neglected in the framework of a study on the effect of surfactant concentrations near or below the cmc. Under such conditions, the study by MEKC of the electrophoretic behaviour of chosen neutral molecules should lead to the elucidation of the micellization process.

The apparent mobility μ_{app} of a neutral solute will therefore be defined as the sum of the mobilities of the three components of the considered system (aqueous phase of mobility μ_{e0}, micellar pseudo-phase of mobility μ_{mic} and "solvophobic complex" of mobility μ_{solv}) weighted by the molar fraction of the solute in each of these "phases", i.e.,

$$\mu_{app} = (1-x-y)\mu_{e0} + x(\mu_{e0} - \mu_{solv}) + y(\mu_{e0} - \mu_{mic}) \tag{4}$$

or

$$\mu_{eff} = \mu_{e0} - \mu_{app} = x\mu_{solv} + y\mu_{mic} \tag{5}$$

where μ_{eff} is the effective electrophoretic mobility of the neutral solute, i.e., the mobility of the solute which is due only to the hydrophobic interactions with the surfactant molecules, whatever their nature (monomers or micelles).

If one expresses this mobility as a function of the equilibrium constants and the concentrations in monomeric and in micellar surfactant (Eqs. 1 and 2), one obtains, considering the two equilibria to be independent as a first approximation, i.e., the molar fraction of the solute associated with the monomeric surfactant, written as

$$x = \frac{K_{solv}[S]}{1 + K_{solv}[S]}$$

and, in an identical manner the molar fraction of the solute in the micellar pseudo-phase, written as

$$y = \frac{K_{mic}[M]}{1 + K_{mic}[M]}$$

Therefore,

$$\mu_{eff} = \frac{K_{solv}[S]}{1 + K_{solv}[S]} \cdot \mu_{solv} + \frac{K_{mic}[M]}{1 + K_{mic}[M]} \cdot \mu_{mic} \tag{6}$$

Therefore, it is possible to analyse the evolution of the effective electrophoretic mobility μ_{eff} of a neutral compound N as a function of the total concentration C_T of surfactant using Eq. 6 and considering three concentrations ranges, as follows.

(a) $C_T <$ cmc: solvophobic solubilization zone. In this case, the total surfactant concentration is reduced to $C_T = [S]$ and the equation for the effective mobility μ_{eff} is

$$\mu_{eff} = \frac{K_{solv}C_T}{1 + K_{solv}C_T} \cdot \mu_{solv} \tag{7}$$

Fig. 2a represents the theoretical evolution of such a mobility for a compound with a partition constant $K_{solv} = 5$ mol^{-1} l when the mobility of the "solvophobic complex" μ_{solv} is fixed at $5 \cdot 10^{-9}$ m^2 V^{-1} s^{-1}, the cmc being arbitrary established as 10^{-2} mol l^{-1} (arbitrary values in the order of experimental magnitudes).

(b) $C_T >$ cmc: "micellar" solubilization zone.

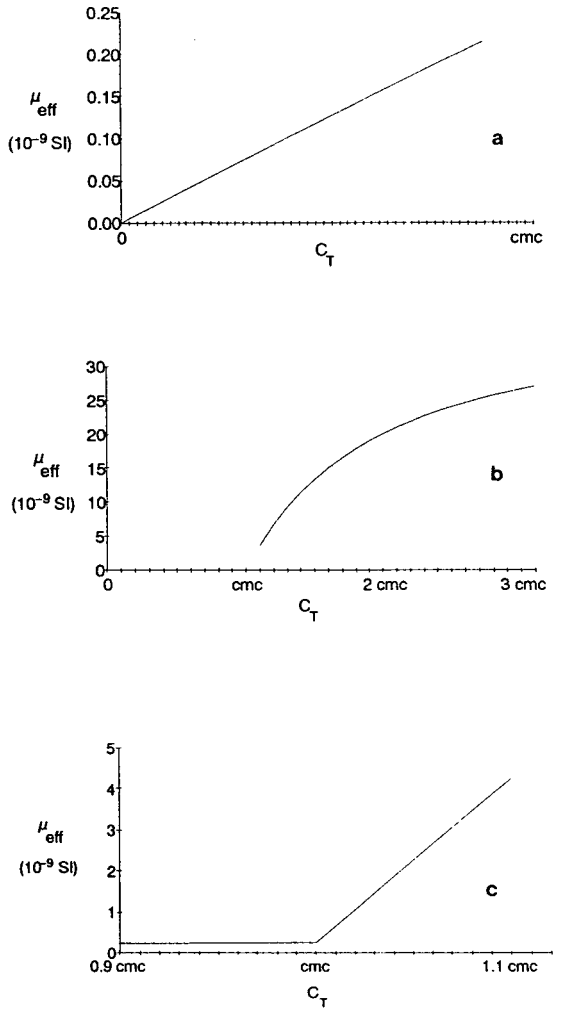

Fig. 2. Theoretical evolution of the effective mobility of a neutral compound as a function of the total surfactant concentration (see text for parameter values adopted for simulation). (a) Surfactant concentration below the cmc; (b) surfactant concentration above the cmc; (c) surfactant concentration near the cmc.

For such concentrations above the cmc, the concentration of monomeric surfactants remains approximately constant at the value at the cmc. Hence Eq. 3 can be expressed as $C_T = \text{cmc} + n[\text{M}]$. Under such conditions, the contribution to the effective mobility due to the solvophobic effect will remain constant (μ_{cmc}) as a function of the total surfactant concentration and equal to

$$\mu_{cmc} = \frac{K_{solv} \cdot \text{cmc}}{1 + K_{solv} \cdot \text{cmc}} \cdot \mu_{solv} \tag{8}$$

The formation of micelles in the electrophoretic medium will correspond to a micellar solubilization, of which the contribution to the effective mobility is translated into

$$\frac{K_{mic}(C_T - \text{cmc})/n}{1 + K_{mic}(C_T - \text{cmc})/n} \cdot \mu_{mic} \tag{9}$$

The effective mobility will therefore be equal to the sum of these two contributions, i.e.,

$$\mu_{eff} = \frac{K_{solv} \cdot \text{cmc}}{1 + K_{solv} \cdot \text{cmc}} \cdot \mu_{solv} + \frac{K_{mic}(C_T - \text{cmc})/n}{1 + K_{mic}(C_T - \text{cmc})/n} \cdot \mu_{mic} \tag{10}$$

In this surfactant concentration zone, the micellar contribution is much more important than the solvophobic contribution, on the one hand because of the much greater partition constant, but also because of an important micellar mobility. Fig. 2b represents the theoretical evolution of the effective mobility of a compound of which the equilibrium constant K_{mic} is equal to 100 S.I. units while μ_{mic} is fixed at $40 \cdot 10^{-9}$ m^2 V^{-1} s^{-1}. As in Fig. 2a, the equilibrium constant $K_{solv} = 5$ mol^{-1} l when the mobility of the "solvophobic complex" μ_{solv} is fixed at $5 \cdot 10^{-9}$ m^2 V^{-1} s^{-1}, the cmc being arbitrary established at 10^{-2} mol l^{-1} and the micellar aggregation number at 100.

(c) $C_T \approx$ cmc: micellization zone. For such a total surfactant concentration, none of the two terms in Eq. 6 can be neglected. Nevertheless, because of the very low micellar concentration in the solution, the term $K_{mic}[\text{M}]$ is negligible compared to 1. In the same way, because of the very low value of the solvophobic equilibrium constant K_{solv}, the term $K_{solv}[\text{S}]$ is also negligible compared to 1. Under such conditions, Eq. 6 reduces to

$$\mu_{eff} = K_{solv}[\text{S}]\mu_{solv} + K_{mic}[\text{M}]\mu_{mic} \tag{11}$$

According to Phillips [6], any property ϕ of the solution expressed as an equation of the form

$$\phi = A[\text{S}] + B[\text{M}] \tag{12}$$

where A and B are, proportionality constants, has a third derivative, with respect to the total concentration, equal to zero at the cmc and should therefore show, at the cmc, a maximum change in the slope of the curve of the evolution of this property as a function of the total surfactant concentration. This condition is necessary for the evolution of a property of the solution to translate the micellar aggregation as a radical change in the composition of the solution, i.e., the appearance of a new phase in solution.

In such a concentration zone, the effective mobility of a neutral compound then satisfies well the general condition of Phillips, as can be seen in Fig. 2c (the different constants being used for the establishment of this theoretical curve are the same as those used previously).

Hence the evolution of the electrophoretic mobility μ_{eff} of a neutral compound N as a function of the total surfactant concentration C_T in the solution appears to be a new method for the study of the micellization process.

3. Experimental

3.1. Reagents

Buffer and sample solutions were prepared with water purified by reverse osmosis and filtered using a Milli Ro + Milli Q system (Millipore, Molsheim, France). The reagent used as the electrolyte, i.e., borax, was of analytical-reagent grade (99%) from Aldrich (La Verpillère, France). SDS was of 99% purity and purchased from Sigma (Saint Quentin Fallavier, France). The compound used for the validation of the method, i.e., naphthalene, was of 99% purity from Aldrich. For the determination of the electroosmotic flow, we used acetonitrile of analytical-reagent grade from Aldrich.

3.2. Apparatus

All experiments were carried out on a P/ACE 2100 system (Beckman, Fullerton, CA, USA) monitored by a PS/2 computer (IBM, Greenock, UK), using P/ACE software (Beckman). Data collection was performed with the same software.

Samples were loaded by a 1-s pressure injection into a fused-silica capillary (57 cm × 50 μm I.D.). UV detection at 214 nm was performed through the capillary at 50 cm from the inlet. The pH values of the electrolytes were measured using a Beckman Model Φ pH meter at the temperature of the analyses. The separations were performed three to five times for each SDS concentration value studied in order to ensure good reproducibility of the measurements.

3.3. Buffer preparation

Stock solutions of borax ($5 \cdot 10^{-3}$ mol l^{-1}) and of surfactant (SDS) ($30 \cdot 10^{-3}$ mol l^{-1}) were prepared daily. Different SDS concentrations were then obtained by mixing these two solutions.

4. Results and discussion

In order to validate the method for the determination of the cmc, several experimental problems had to be solved concerning the nature of the sample and the control of the temperature.

4.1. Problem of the introduction of a neutral compound

The visualization of the evolution of the electrophoretic mobility at very low surfactant concentrations in the electrophoretic media imposes the choice of a neutral and very lipophilic compound. Indeed, the more important the equilibrium constants K_{solv} and K_{mic}, the more dramatic will be the change in the slope of the curve of the electrophoretic mobility as a function of the total surfactant concentration at the cmc, and therefore the easier and more precise will be the determination of this concentration.

Nevertheless, such a compound will be poorly soluble, if not insoluble, in the aqueous phase. This lack of solubility will lead to a low efficiency of the electrophoretic system and to uncertainty

in the measurement of retention times. Moreover, concerning the biphasic system, this lack of solubility will probably result in a shift in the micellization equilibrium and therefore lead to systematic errors in the cmc value.

It was therefore very important to find a compound of low polarity, but not insoluble in water, with a high molar absorptivity in UV–visible spectrophotometry and of sufficiently low residence time in the micellar core that its presence does not interfere with the dynamics of the biphasic system.

With regard to these requirements, different solutes can be considered. Table 1 summarizes the characteristics of a few solutes arranged in lipophilic order.

From Table 1, it is clear that benzene is not lipophilic enough to visualize the evolution of the biphasic system. The use of linear alkylbenzenes which are more lipophilic and with a linear geometric structure close to that of the surfactant molecule, can nevertheless be considered. However, this kind of molecules will not have a high enough molar absorptivity to allow their injection in small amounts, which is a necessary condition to prevent any perturbation of the system. Pyrene and anthracene are compounds of strong lipophilicity and with high molar absorptivities. Nevertheless, their water solubility is very low and they have to be injected in concentrations such that their detection is impossible. Further, biphenyl does not have a high enough molar absorptivity to be detected under its solubility limit in water.

Naphthalene seems to correspond to the ideal solute: it has medium lipophilicity, a high molar absorptivity over a large wavelength range and a low residence time in the SDS micellar core compared with the lifetime of the micelles (1.8–50 ms [9]). Therefore, naphthalene will be the only sample considered further here.

The injection of a 10^{-4} mol l^{-1} solution of naphthalene will probably not perturb the biphasic system, but will still allow the detection of this compound. The amounts injected were nevertheless reduced to the minimum allowed by the instrument, i.e., with the application of a 0.5 bar pressure for 1 s. The hydrodynamic injection mode was preferred here to the electrokinetic mode as it is independent of the nature of the electrophoretic media. The amount injected was therefore not biased when the concentration of bulk salt or surfactant was modified.

4.2. Temperature control problem

According to the instrument's specification, the temperature in the capillary is well controlled and regulated when the power dissipated in the capillary is up to 5 W m^{-1}. However, for security reasons, we adjusted the voltage applied through the capillary so the power did not exceed 2 W/m^{-1}, and the electric field was kept constant for an experimental set. These precautions allowed us to obtain consistent and reproducible results, even with a change in the capillary length.

These two crucial points having been established, we then proceeded to the evaluation of

Table 1
Characteristics of the solutes

Solute	Solubility in water (mol l^{-1})	Residence time in micelles (μs)[a]	$\lambda_{max}(\varepsilon)$ (nm)[b]
Benzene	$2.3 \cdot 10^{-2}$	0.23	204 (8800)
Naphthalene	$2.2 \cdot 10^{-4}$	4	221 (117 000)
Biphenyl	$4.1 \cdot 10^{-5}$	10	201 (46 500)
Pyrene	$6.0 \cdot 10^{-7}$	243	252 (220 000)
Anthracene	$2.2 \cdot 10^{-7}$	59	241 (88 000)

[a] Time taken for a fraction of 63% of the probe molecules to escape the SDS micelles [7].
[b] Wavelength for which the molar absorptivity ε (l mol^{-1} cm^{-1}) is maximum [8].

the method for the determination of critical micelle concentrations and applied it to SDS.

4.3. Validation of the analytical method

In order to validate the method, we plotted the evolution of the electrophoretic mobility of naphthalene as a function of the SDS concentration. To do so, we used a simple electrolyte which satisfied two conditions: to contain ions in sufficient amounts to conduct the electric current, and to have pH buffer characteristics so as to maintain constant the ionization state of the silanol groups on the capillary wall.

Among the most commonly employed inorganic salts in MEKC, borax (sodium tetraborate) seemed the most appropriate. From very low concentrations ($<10^{-3}$ mol l^{-1}), this salt leads to aqueous solutions of pH 9.2 at 25°C. An aqueous solution of $5 \cdot 10^{-3}$ mol l^{-1} borax allows one to work at constant pH, keeping the ionic strength of the solution low (10 mequiv. l^{-1}).

Fig. 3 shows the general evolution of the electrophoretic mobility of naphthalene as a function of the SDS concentration under these simple electrolytic conditions. The general shape of this graph shows a dramatic change in slope at an SDS concentration of ca. $5 \cdot 10^{-3}$ mol l^{-1}. In order to measure this concentration value with more accuracy, we studied the part of the graph corresponding to surfactant concentrations between $3 \cdot 10^{-3}$ and $8 \cdot 10^{-3}$ mol l^{-1} (Fig. 4).

The values of the electrophoretic mobility of naphthalene in this concentration range are given in Table 2. The values given are means calculated from three independent electropherograms for each SDS concentration. From these data, and according to the theoretical representation in Fig. 2c, two linear regression curves were plotted: one for SDS concentrations between $3 \cdot 10^{-3}$ and $5.2 \cdot 10^{-3}$ mol l^{-1}, with the equation $\mu_{eff} = -0.193 \cdot 10^{-9} + 0.189 \cdot 10^{-6}$ [SDS], and for SDS concentrations between $5.4 \cdot 10^{-3}$ and $8 \cdot 10^{-3}$ mol l^{-1}, with the equation $\mu_{eff} = -30.048 \cdot 10^{-9} + 5.834 \cdot 10^{-6}$ [SDS]. The intersection of these two lines allows one to evaluate the cmc and the contribution to the electrophoretic mobility of the "solvophobic complex" (μ_{cmc}) at and above this concentration, i.e., cmc $= 5.29 \cdot 10^{-3}$ mol l^{-1} and $\mu_{cmc} = 0.807 \cdot 10^{-9}$ m^2 V^{-1} s^{-1}.

The hypotheses made for the theoretical approach for the determination of the cmc using this new technique (Eq. 11) were based on,

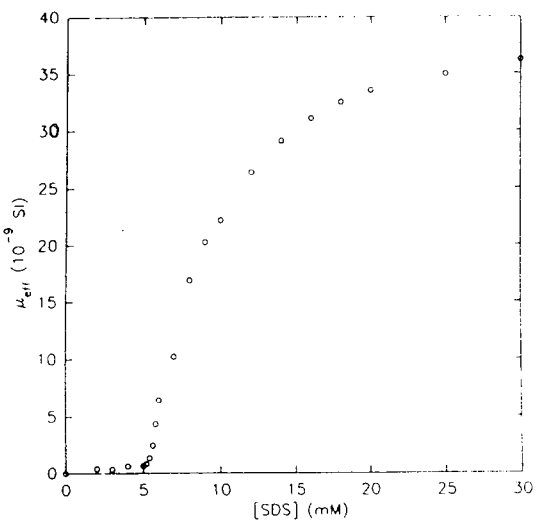

Fig. 3. Graph of the evolution of the electrophoretic mobility of naphthalene as a function of the SDS concentration. Bulk salt: $5 \cdot 10^{-3}$ mol l^{-1} borax.

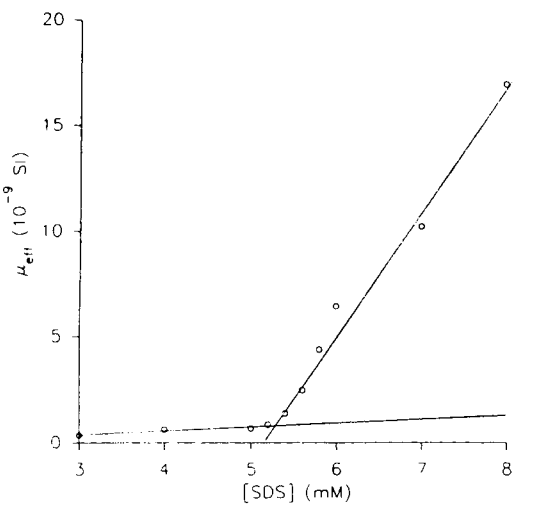

Fig. 4. Graph of the evolution of the electrophoretic mobility of naphthalene as a function of the SDS concentration near the cmc. Bulk salt: $5 \cdot 10^{-3}$ mol l^{-1} borax.

among other things, a low value of the partition constant of the solute between the "aqueous phase" and the surfactant monomers (K_{solv}). The low values of the electrophoretic mobility of naphthalene under the cmc, which are translated on the corresponding electropherograms into a quasi-co-elution of naphthalene and the electroosmotic flow, verify this assumption.

Another verification of this point is the relatively high electrophoretic mobility of the SDS molecule, determined under the same analytical conditions using indirect fluorimetric detection [10], even if this value is overestimated for the "solvophobic complex". The value of K_{solv} should then be of the order of 0.1 mol l^{-1} and the term $K_{solv}[S]$ is therefore negligible compared to 1.

Another important assumption made in the theoretical approach was the independence of the two partition equilibria. This independence is true, on the one hand, for surfactant concentrations under the cmc, by the absence of micelles in the electrophoretic medium and, de facto, the absence of micellar solubilization. On the other hand, for high surfactant concentrations ($[SDS] > 8 \cdot 10^{-3}$ mol l^{-1}), this independence can be verified if the evolution of the electrophoretic mobility of naphthalene can be expressed by Eq. 10, which can be rearranged to

$$\frac{1}{(\mu_{eff} - \mu_{cmc})} = \frac{1}{\mu_{mic}} + \frac{n}{\mu_{mic} K_{mic} (C_T - cmc)} \quad (13)$$

where μ_{cmc} is the contribution to the electrophoretic mobility of the "solvophobic complex" (μ_{cmc}) at and above the cmc.

The values of μ_{cmc} and cmc having been deduced from Fig. 4 and Table 2, it is therefore possible to evaluate the value of μ_{mic} and the value of the ratio K_{mic}/n (Fig. 5). The excellent correlation coefficient of this curve ($\rho > 0.9993$) allows one to validate the assumption concerning the independence of the two partition equilibria, as well as the values deduced from this curve, i.e., $\mu_{mic} = 42.27 \cdot 10^{-9}$ m^2 V^{-1} s^{-1} and $K_{mic}/n =$ 227 S.I. units which are well above the values of the corresponding parameters for the solvophobic partition. This last observation appears to be a supplementary element in the validation of the independence of these two partitions, simply because of the predominance of one over the other, depending on the concentration zone studied.

Table 2
Average values of the electrophoretic mobility of naphthalene as a function of the SDS concentration near the cmc (bulk salt: 5 mmol l^{-1} borax)

[SDS] (mmol l^{-1})	μ_{eff} (10^{-9} m^2 V^{-1} s^{-1})
3	0.346
4	0.625
5	0.667
5.2	0.835
5.4	1.36
5.6	2.45
5.8	4.36
6	6.43[a]
7	10.2
8	16.9

[a] This value was not used in the calculations.

To conclude on the validation of the theoretical approach, it seemed of interest to replot the curve for the evolution of the electrophoretic mobility of naphthalene as a function of the total surfactant concentration (Fig. 6) from the values of the different parameters deduced from the

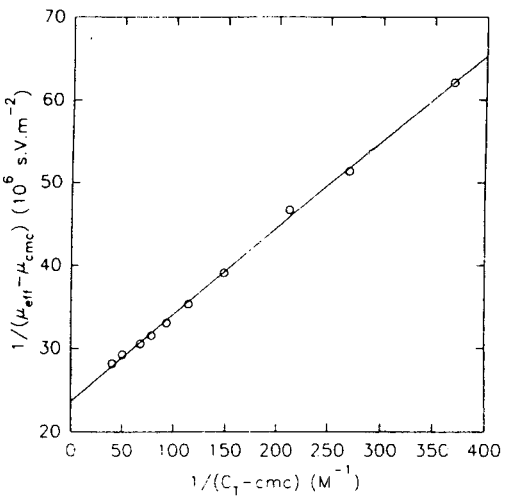

Fig. 5. Evolution of $1/(\mu_{eff} - \mu_{cmc})$ as a function of $1/(C_T - cmc)$ for surfactant concentrations above $8 \cdot 10^{-3}$ mol l^{-1} ($y = 23.66 \cdot 10^6 + 10.42 \cdot 10^3 x$; $\rho > 0.9993$).

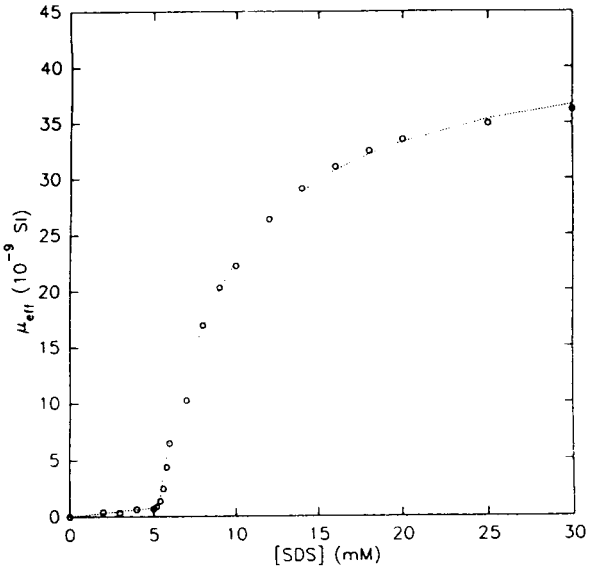

Fig. 6. Comparison between (symbols) the experimental and (line) the theoretical evolution of the electrophoretic mobility of naphthalene as a function of the total SDS concentration. Electrolyte: $5 \cdot 10^{-3}$ mol l^{-1} borax.

analysis of the experimental graph in Fig. 3. Fig. 6 shows a perfect fit between the experimental and the deduced theoretical values, and therefore validates without ambiguity this new technique as a method for the determination of the cmc. Moreover, the so-deduced cmc value ($5.29 \cdot 10^{-3}$ mol l^{-1}) is identical with that reported in the literature [11], using surface tension measurements, under the same experimental conditions (25°C, $[Na^+] = 0.01$ mol l^{-1}). This perfect fit not only from the theoretical but also the experimental point of view confirms capillary electrophoresis as the technique of choice for micellization process studies.

5. Conclusion

The results obtained in this study establish capillary electrophoresis as a preferred technique for the determination of the cmc of anionic surfactants, as it is not only rapid but also easy to carry out and, above all, is readily automatable.

Based on studies of the micellization process in various aqueous solutions, we intend, in the near future, to proceed to the evaluation of the cmc of SDS in various electrophoretic media used in MEKC, i.e., concerning inorganic salts, borax and the sodium salts of phosphoric acid at different concentrations and pH values, and concerning organic solvents, methanol, ethanol, acetonitrile and acetone, which cover a broad lipophilic range and are therefore the most widely employed, either to adjust the aqueous phase lipophilicity, to increase the selectivity of the chromatographic system or to modify the retention time window. Moreover, we shall attempt to widen the fields of application of this technique for the determination of cmc to anionic surfactants with different structures and to cationic and neutral surfactants.

References

[1] P. Mukerjee and K.J. Mysels, Critical Micelle Concentrations of Aqueous Surfactant Systems, NSRDS-NBS 36, National Bureau of Standards, Washington, DC, 1971.
[2] S.A. Swedberg, J. Chromatogr., 503 (1990) 449.
[3] S. Terabe, K. Otsuka and T. Ando, Anal. Chem., 57 (1985) 834.
[4] C. Treiner, Composés Tensioactifs en Solution aqueuse, Phénomènes d'Interface Agents de Surface, Technip, Paris, 1983, Ch. 3.
[5] Y. Walbroel and J.W. Jorgenson, Anal. Chem., 58 (1986) 479.
[6] J.N. Phillips, Trans. Faraday Soc., 51 (1955) 561.
[7] M. Almgren, F. Grieser and J.K. Thomas, J. Chem. Soc., Faraday Trans. 1, 75 (1979) 1674.
[8] H.H. Perkampus, UV–VIS Atlas of Organic Compounds, VCH, Weinheim, 2nd ed., 1992.
[9] E.G. Aniansson and S.N. Wall, J. Phys. Chem., 78 (1974) 1024.
[10] J.C. Jacquier, C. Morin and P.L. Desbène, unpublished results.
[11] D. Stigter, in Physical Chemistry, Enriching Topics for Colloids and Surface Science, IUPAC Commission I.6, Theorex, La Jolla, CA, 1975, Ch. 12.

ELSEVIER

Journal of Chromatography A, 718 (1995) 177–185

JOURNAL OF CHROMATOGRAPHY A

Simple double-beam absorption detection systems for capillary electrophoresis based on diode lasers and light-emitting diodes

Wei Tong, Edward S. Yeung*

Ames Laboratory-U.S.D.O.E. and Department of Chemistry, Gilman Hall, Iowa State University, Ames, IA 50011, USA

First received 4 May 1995; accepted 7 June 1995

Abstract

Simple double-beam absorption detection systems for capillary electrophoresis (CE) based on diode lasers and light-emitting diodes (LEDs) are developed. Using digital normalization, the intensity fluctuations are greatly reduced and a relative standard deviation of the background noise of 10^{-5} to 10^{-6} can be achieved. The detection performance is thus improved over those of commercial CE systems. For the diode-laser-based system, the gain in detectability results from both a reduction in intensity fluctuations and a better optical coupling of the laser beam with the small capillary tube, maximizing the effective optical path length. The improvement in the LED-based system is largely due to the excellent stability of the LED augmented by double-beam cancellation of the baseline fluctuations. Indirect absorption detection for cationic and anionic species are also demonstrated, extending the applicability of the system.

1. Introduction

Capillary electrophoresis (CE) is one of the fastest growing separation techniques today [1,2]. Various detection methods, including absorption, fluorescence, electrochemistry, and mass spectrometry, have been used for CE [3]. Because of their versatility and simplicity, absorption detectors are still the most popular. However, it has been an inherent weakness in absorption detection that the concentration limit of detection (LOD) is poor. This is due to the high background noise level due to low light intensities, the very short optical path length, and the poor optical coupling resulting from the small capillary size. These need to be improved for further development of absorption detection in CE.

Recently, we demonstrated a double-beam laser absorption detection scheme in CE using a novel electronic circuit to reduce the background noise [4]. A practical noise-to-signal ratio of $1 \cdot 10^{-5}$ in intensity is achieved. Further applications of this system were demonstrated for UV-absorption detection [5], indirect absorption detection [6], and high-performance liquid chromatography (HPLC) [7,8]. Diode lasers have the advantage of small size, low cost, and low noise [9]. Recently, diode lasers have been used in fluorescence detection for LC [10] and CE [11,12]. A diode-laser-based absorption detector using a lock-in amplifier was also reported [13]. In the present study, a very simple diode-laser-based double-beam absorption detection system is demonstrated. The two well-correlated laser

* Corresponding author.

0021-9673/95/$09.50
SSDI 0021-9673(95)00638-9

beams reflected from a glass window were used as signal and reference beams, respectively. With a standard A/D interface and subsequent renormalization, the background fluctuations are largely canceled out. The detectability is improved over commercial double-beam CE systems and is close to that of our previous study with an electronic noise-canceler.

In addition, it is well known that light-emitting diodes (LEDs) are an exceptionally stable light source [14]. Recently, LEDs with ultra-high intensities at a variety of wavelengths (ranging from blue to red, with spectral bandwidth from 20 to 100 nm) have become commercially available from several manufacturers. They have been used as a light source for absorption [15], fluorimetric titration [16], and fluorimetry [17]. However, there have not been any reports using LED as the light source for optical detection in CE. In fact, the combination of extremely high stability, reasonably high intensity, small size, low cost, and very long lifetime makes the LED an attractive source for further improvement of absorption detection in CE. We report here a new absorption detection system based on LED. Despite the difficulty of optical focusing and the poor coupling of the beam with a small-diameter capillary, the detection limit is still close to that of the diode-laser-based system.

Since a large number of analytes lack proper chromophores for UV–Vis detection after CE, indirect absorption detection has been employed as a "universal' approach [18]. Except for a few [6,19] examples, indirect detection schemes in CE are operated in the UV. However, sensitivity and applicability of indirect UV detection can be adversely affected by the absorption of the UV light by analytes and/or by matrix constituents in the sample [19]. For this reason, the application of the present systems for indirect detection in the visible range is also evaluated.

2. Experimental

A schematic diagram of the diode-laser-based double-beam absorption detector for CE is shown in Fig. 1A. The light source was a 10-mW LAS200-670-10 (670 nm) or LAS200-635-10 (635 nm) diode laser (Lasermax, Rochester, NY,

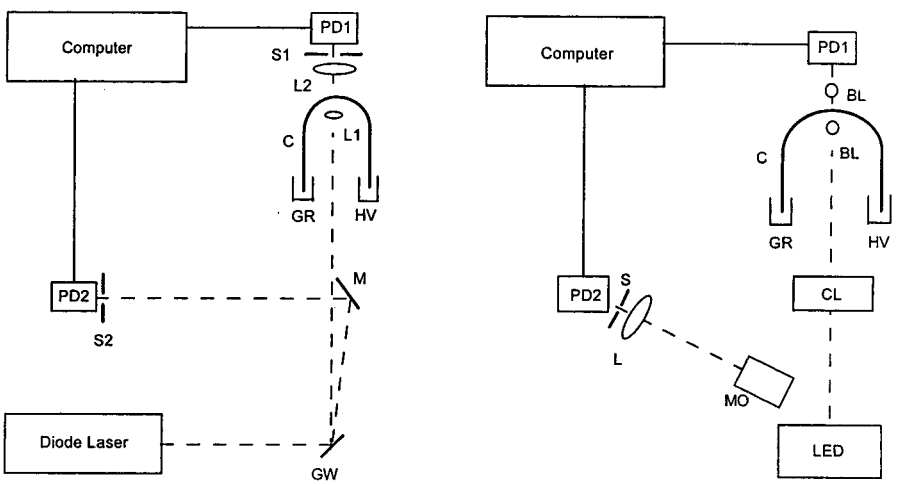

Fig. 1. Experimental setups of double-beam absorption detection for CE. (A) Diode-laser-based system. GW, glass window; M, mirror; S1 and S2, apertures; L1, 1-cm focal length lens; L2, 3.5-cm focal length lens; PD1 and PD2, photodiodes; C, capillary; HV, high-voltage power supply; GR, ground. (B) LED-based system. CL, camera lens; MO, microscope objective; BL, ball lens; S, aperture; L, lens; others are the same as in (A).

USA) powered by a 9-V battery or a home-made power stabilizer. Two photodiodes (BPW34, Siemens) were used as signal- and reference-beam detectors. The laser beam was reflected by the two surfaces of a glass window (BK7). One of the two reflected beams was reflected by a mirror (Newport) and passed through a 5-mm aperture before reaching a photodiode, PD2. The signal beam was focused by a 1-cm focal length lens onto the detection window of the capillary. The capillary was mounted on a precision $x-y$ positioner (Newport, 462 Series) for fine adjustment relative to the focal point. The transmitted signal beam through the capillary was collected by a 3.5-cm focal length lens. After passing through a 5-mm aperture, the signal beam was monitored by a photodiode, PD1. Low-pass (1 Hz) filters were employed at both photodiodes to limit the output bandwidth.

The schematic setup for the LED-based system is shown in Fig. 1B. The source LEDs used were AND130CR (peak wavelength 660 nm) and HLMP-3950 (peak wavelength 565 nm) (Hewlett-Packard). Power was supplied to the LEDs by a 12-V car battery in series with a 500-Ω current-limiting resistor. The d.c. forward current in the LED was 20 mA. The LEDs were "aged" by operating for about a week at 20 mA to eliminate the initial low-frequency noise component that is common to freshly manufactured devices [17]. Unlike the unidirectional laser source, the LEDs have certain view angles (16° for AND130CR and 24° for HLMP-3950), which make them difficult to be focused by conventional lenses. A 24-mm focal length wide-angle camera lens (Tamron, Japan) was used to focus the beam spot down to a diameter of 1 mm. The spot was further focused by a pair of ball lenses from a commercial CE system (Spectraphoresis 1000, Spectra Physics, Mountain View, CA, USA) before reaching the signal detector, PD1. The capillary detection window was positioned between the two ball lenses. PD1 was put very close to the ball lens to collect more light. The reference beam was collected by a microscope objective lens close to the LED and was focused onto the reference detector, PD2, by a lens. The same photodiodes as those in the diode-laser-based system were used for the LED-based system. However, different combinations of resistors and capacitors were used to maintain an RC time constant of 1 s. Signal and reference data were acquired at 5 or 10 Hz by the two channels of a 24-bit A/D conversion interface (ChromPerfect, Justice Innovation, Palo Alto, CA, USA). The data was stored in an IBM/PC-compatible computer for subsequent renormalization.

A high-voltage power supply (Glassman, Whitehouse Station, NJ, USA) was used to supply high voltage across the capillary. A commercial double-beam CE system (Spectraphoresis 1000, Spectra Physics, Mountain View, CA, USA) operated at the same wavelength was used for comparison. The capillaries used for direct detection were fused-silica 75 μm I.D. and 360 μm O.D. (Polymicro Technologies, Phoenix, AZ, USA) with various lengths. The capillaries were flushed with 0.1 M NaOH overnight, followed by equilibration with the running buffer for one day. For indirect detection, 50 μm I.D. DB-1 capillaries (J&W Scientific, Folsom, CA, USA) were used. The DB-1 capillaries were equilibrated with the running buffer for one day before use. The sample solutions were injected hydrodynamically by raising the analyte vial 15 cm above the ground buffer reservoir for 7 s. The analytes for indirect detection were dissolved in the running buffer for injection.

The running buffer for direct CE detection was 10 mM disodium phosphate (Fisher, Fair Lawn, NJ, USA) at different pHs. The running buffer for indirect CE detection of cations was adapted from Ref. [19], and contained 0.12 mM methyl green in 1 mM tris(hydroxymethyl)aminomethane (Tris) and 2.5 mM acetic acid (pH 3.9). For indirect detection of anions, the running buffer was 20 mM permanganate (pH 7.0). Oxazine-1 perchlorate was obtained from Kodak (Rochester, NJ, USA), methyl green (zinc chloride salt) from Aldrich (Milwaukee, WI, USA), malachite green from Exciton (Dayton, OH, USA), Tris from Fisher, and bromothymol blue from J.T. Baker (Philipsburg, NJ, USA). All solutions and buffers were filtered with a 22-μm cutoff cellulose acetate filter before

use. The water was deionized with a water purification system (Millipore, Milford, MA, USA).

3. Results and discussion

3.1. Background noise cancellation

Successful cancellation of background noise can be achieved only if the optical characteristics of the signal and reference channels are truly identical. Therefore, how to split the laser beam to obtain two closely correlated or co-fluctuating beams is an important consideration. The signal beam here passed through a capillary filled with running buffer (10 m*M* phosphate, pH 10.4). Beam splitters, beam displacers and glass windows were examined for this purpose. It was found that the two reflected laser beams from the two surfaces (front and back) of a glass window were the best correlated (Fig. 2A). These two beams are also quite stable, with the residual noise approaching the resolution limit of the A/D board. Therefore, some digitization noise exists. However, the A/D interface (ChromPerfect) used to monitor the beams is actually asynchronous in operation. This can be confirmed by monitoring the same signal from a waveform generator via the two channels. Therefore, simply subtracting or dividing the reference data points from the signal data points does not

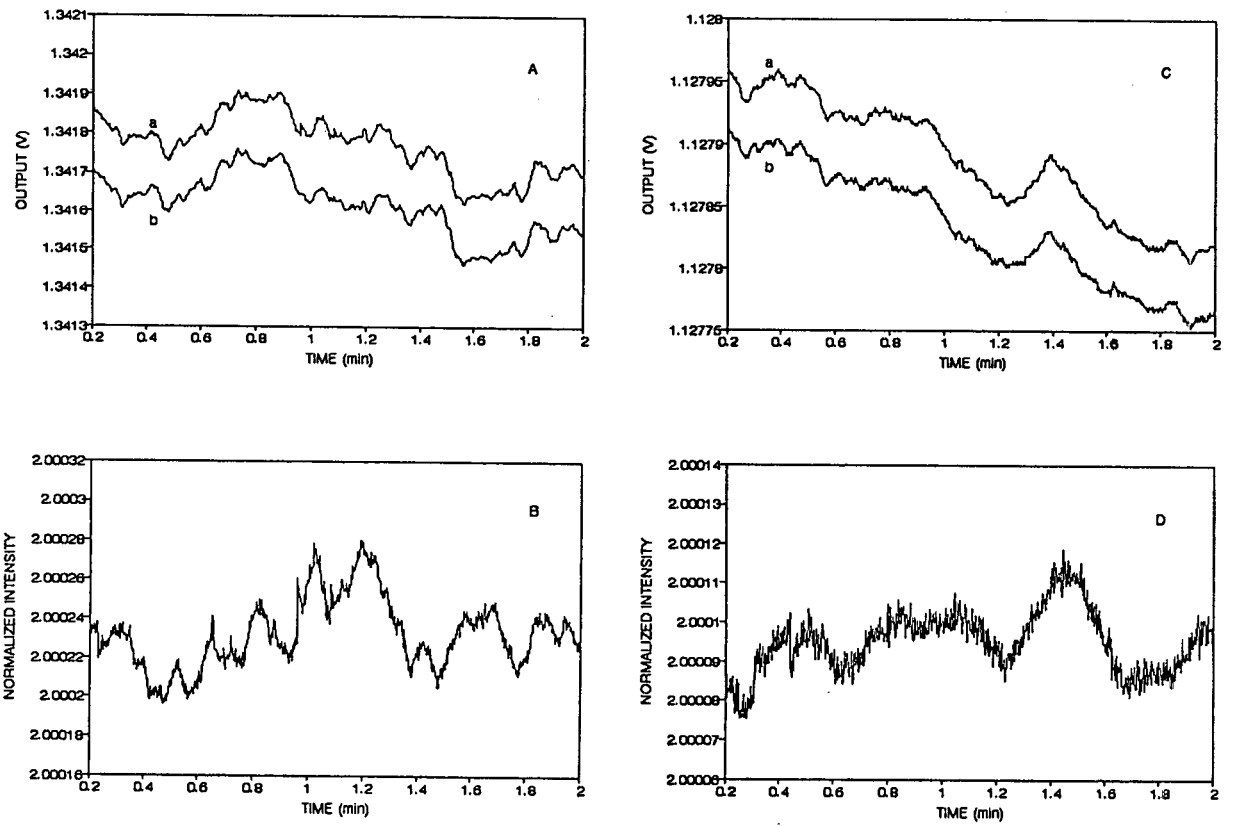

Fig. 2. Background noise of diode laser and LED. (A) Signal (a) and reference (b) beams for diode laser before cancellation. (B) Output intensity of (A) after cancellation by Eq. 1. (C) Signal (a) and reference (b) beams for LED before cancellation. (D) Output intensity of (C) after cancellation by Eq. 1.

give the best cancellation. What we did was to use the sum of the two adjacent data points in channel a (interpolation) and divide that by the data point in channel b to get the normalized output intensity, I:

$$I = (a_i + a_{i+1})/b_i \quad (1)$$

Here a_i and a_{i+1} are the ith and $(i+1)$th data points in channel a, and b_i is the ith data point in channel b. This has an averaging effect and the resulting background noise showed a relative standard deviation of $1 \cdot 10^{-5}$. The high-resolution A/D conversion is critical here. The residual peaks observed in Fig. 2B were most likely due to the asynchronous movements of the optical components for the two beams. So, the ruggedness of the setup is very important. From another point of view, this also proves that the proposed cancellation scheme is suitable for cancellation of correlated noise components. With this simple system (Fig. 1), the possibility of mechanical movements can be reduced compared to a complicated setup. He–Ne and Ar lasers were also tested with the same setup. The cancellation results were less impressive. This is largely due to the inherent instability of these laser systems. One needs to account for the higher-frequency fluctuations by sampling the two beams at a higher rate for proper cancellation.

For the LED-based system, obtaining the signal and reference beams is not so easy. Many beam-splitting techniques do not apply simply because the beam from the LED is not unidirectional, like the laser beam. In this case, the reference beam is collected by putting a microscope objective very close to the LED. The two beams thus obtained are also quite well correlated (Fig. 2C). Since the LED appears to be more stable but is at a lower intensity than the diode laser, there is more digitization noise before (Fig. 2C) and after (Fig. 2D) cancellation. Despite this, the background noise still has a relative standard deviation of only $3.6 \cdot 10^{-6}$. As we will discuss later, this noise can be further eliminated by averaging and smoothing after normalization.

3.2. Direct absorption detection

As a demonstration, the separation of oxazine-1 and bromothymol blue was performed in our diode-laser system (Fig. 3). The baseline is stable and the peaks are sharp, indicating the lack of broadening due to the detector. When the concentration of oxazine-1 was reduced ($6.7 \cdot 10^{-8}$ M) to approach its detection limit, the peak was hardly distinguishable from the background noise (Fig. 4A) if merely the signal-channel data is plotted (e.g., single beam). However, after our double-beam renormalization scheme the oxazine-1 peak is several times above the background noise level (Fig. 4B). This shows the effectiveness of this noise-cancellation technique.

The absorbance of an analyte in CE should be predictable from Beer's law. For small absorbance, Beer's law can be written as:

$$|\Delta I|/I_0 = 2.303\epsilon bc = 2.303A \quad (2)$$

where $|\Delta I|$ is the absolute intensity change caused by absorption, I_0 is the initial intensity without analyte, ϵ is the molar absorptivity of the analyte, b is the optical path length, c is the analyte concentration, and A is the absorbance

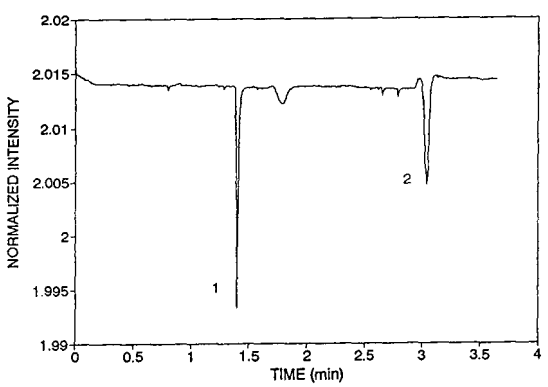

Fig. 3. Electropherogram of a mixture of oxazine-1 (1) and bromothymol blue (2) with injected concentrations of $7 \cdot 10^{-6}$ and $2 \cdot 10^{-5}$ M, respectively. The running potential was 18 kV. The running buffer was 10 mM phosphate at pH 10.4. A 75 μm I.D., 360 μm O.D. capillary with 50 cm total length and 38 cm to the detector was used.

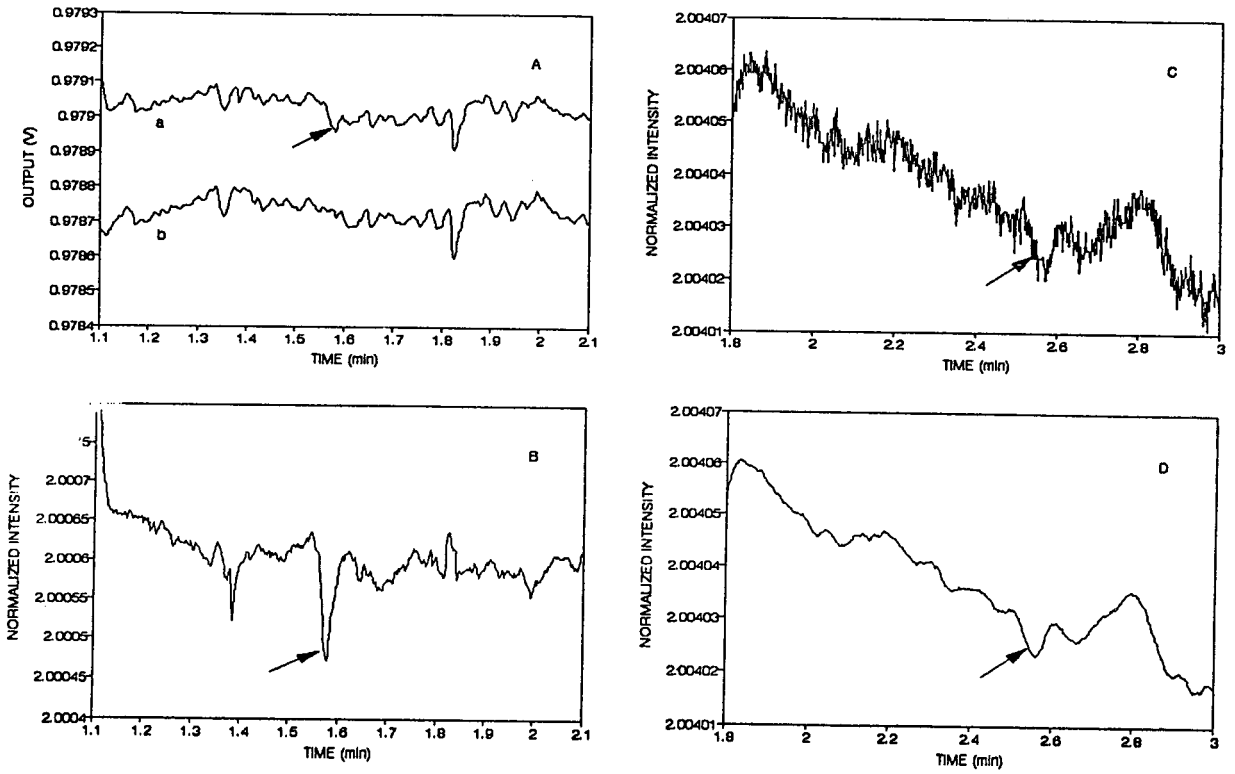

Fig. 4. Electropherogram of $6.7 \cdot 10^{-8}$ *M* oxazine-1 (injected). For (A) and (B), the diode-laser-based system was used and the conditions were the same as those in Fig. 3. (A) Raw data of signal channel before cancellation, and (B) after cancellation. For (C) and (D), the LED-based system was used. The running potential was 20 kV and the capillary length was 70 cm total and 55 cm to the detector. Other conditions were the same as those in Fig. 3. (C) After cancellation, (D) data in (C) after ten-point box-car smoothing.

of the analyte in the capillary. In our diode-laser-based system, the capillary was inclined 30° from the vertical direction to minimize multiple reflection. The actual optical path length is therefore 87 μm. The molar absorptivity of oxazine-1 at pH 10.4 was measured in a spectrometer to be $6.43 \cdot 10^4$ l mol^{-1} cm^{-1}. According to Beer's law, the theoretical absorbance of $6.7 \cdot 10^{-8}$ *M* of oxazine-1 in the capillary is $3.75 \cdot 10^{-5}$. From Fig. 4B, ΔI for oxazine-1 is about $1.7 \cdot 10^{-4}$ and I_0 is about 1.99. From Eq. 2, the absorbance, *A*, is calculated to be $3.7 \cdot 10^{-5}$, which matches the theoretical value very well. This means that the laser beam passed through the center of the capillary and the full diameter of the capillary was utilized as the optical path length. This is actually not surprising because the laser beam can be focused down to a few micrometers and superior optical coupling can be achieved easily. However, in the LED-based CE system such coupling cannot be realized because of the limitations of the light source. Fig. 4C is the electropherogram of $6.7 \cdot 10^{-8}$ *M* oxazine-1 from the LED-based CE system. After ten-point smoothing, the oxazine-1 peak is more clearly visible (Fig. 4D). But this peak height is not predicted by Beer's law. This shows that the beam did not all pass through the diameter of the capillary. Since the LED appears to be more stable than the diode laser, the background noise level is lower in the LED-based CE system. This results in a similar detection limit to that of the diode-laser-based system. However, with LEDs we have a better choice of wavelengths suitable for

different analytes, from blue to red in the visible range. LEDs are also less expensive. For the same reason as for LEDs, the peak heights from the commercial system are also not predicted by Beer's law. Fig. 5 is the electropherogram of $2 \cdot 10^{-7}$ *M* oxazine-1 from the commercial CE system. The absorbance observed here is only $3 \cdot 10^{-5}$. Better focusing in the diode-laser system accounts for about four times improvement in the absorbance measured. This effect will be even more dramatic for smaller-diameter capillaries [6].

In our previous study, $2 \cdot 10^{-8}$ *M* malachite green was detectable at 632.8 nm (He–Ne laser) with an electronic noise-canceler [4]. In the simple system reported here, $7 \cdot 10^{-8}$ *M* of injected malachite green also gives good signal-to-noise ratio at 635 nm (diode laser), which is very close to 632.8 nm. But the whole scheme is simplified and the requirements are much less critical. Again, this result is well predicated by Beer's law.

3.3. Indirect detection

For practical applications, the 635 and 670 nm wavelengths provided by the diode laser are not broadly useful. Even with LEDs, which can cover most of the visible range, the wavelengths are still long compared to most chromophores. Fortunately, the same system is applicable to universal detection via indirect absorption as well [6]. Fig. 6A is the electropherogram of several cations obtained by the diode-laser-based system. From our previous study, the limit of detection (LOD) for indirect absorption detection can be written as:

$$LOD = \Delta A/[(TR)\epsilon b] \quad (3)$$

where ΔA is the absorbance noise, ϵ is the molar absorptivity of the background chromophore,

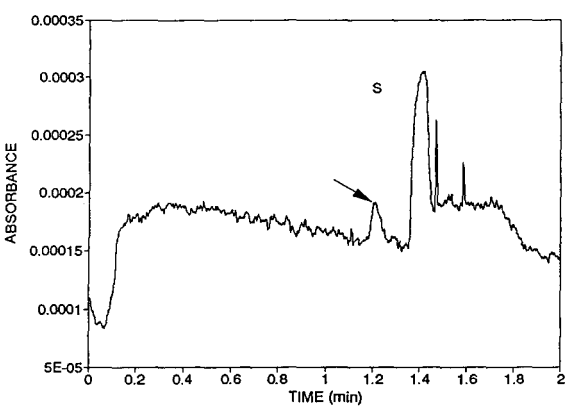

Fig. 5. Electropherogram of $2 \cdot 10^{-7}$ oxazine-1 (injected) from a commercial CE system. The running potential was 15 kV. The total and effective lengths of the capillary were 44 and 35 cm, respectively. Other conditions were the same as in Fig. 3. S, system peak.

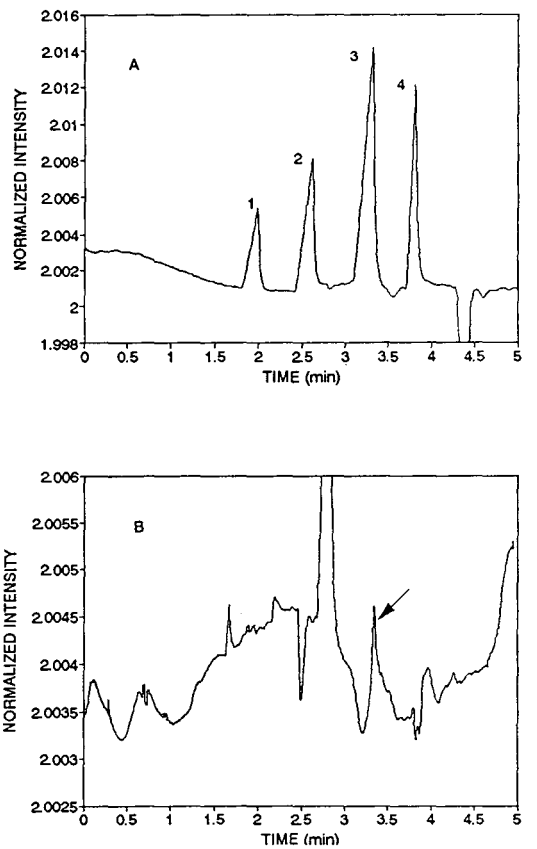

Fig. 6. Electropherograms for the indirect detection of cations in the diode-laser-based system. The running buffer was 0.12 m*M* methyl green in 1.0 m*M* Tris and 2.5 m*M* acetic acid (pH 3.9). The applied potential was 28 kV. A 50 μm I.D. DB-1 capillary with 55 cm total length and 40 cm to the detector was used. (A) Separation of cations (1, $5.2 \cdot 10^{-4}$ *M* K^+; 2, $3.2 \cdot 10^{-4}$ *M* Ca^{2+}; 3, $9.6 \cdot 10^{-5}$ *M* Na^+; and 4, $8.8 \cdot 10^{-5}$ *M* Li^+). (B) Detection limit of Li^+ ($3.5 \cdot 10^{-6}$ *M*).

and TR is the transfer ratio (the number of chromophore molecules transferred or displaced by one analyte molecule). The electropherogram of $3.5 \cdot 10^{-6}$ *M* Li^+ is shown in Fig. 6B. Here, the intensity noise is about $5 \cdot 10^{-4}$, which corresponds to $8.7 \cdot 10^{-5}$ absorbance units. The molar absorptivity of methyl green in the same running buffer at 635 nm is measured to be $2.32 \cdot 10^4$ l mol^{-1} cm^{-1}. Because methyl green carries two positive charges, the transfer ratio for Li^+ is 0.5 to maintain charge balance. If a signal-to-noise ratio of 2 is used as the criterion, the theoretical detection limit is $3.7 \cdot 10^{-6}$ *M*. From Fig. 6B, the peak due to $3.5 \cdot 10^{-6}$ *M* Li^+ can still be recognized by our system, which is quite close to the predicted value. For the other cations in Fig. 6A, the peaks are lower than that of Li^+ at the same concentration. This probably because the transfer ratio is lower than that predicted by simple charge balance.

From Eq. 3, it can be inferred that the LOD does not depend on the concentration of the background chromophore. Although increasing the chromophore concentration can make the indirect detection peak sharper [20], this at the same time will increase the background fluctuations caused by heating or increased interaction with the capillary wall. The LOD will be improved by choosing chromophores with larger ϵ. However, intense chromophores often have large conjugated aromatic ring systems. The mobilities of such molecules usually do not match those of the analytes (e.g., small inorganic anions). Also, such molecules often have relatively large adsorptive interactions with the capillary wall and cause baseline fluctuations. As a result, the actual detection limit is not improved much.

The same CE systems can be also applied to the indirect detection of anions. Boçek and coworkers [19] reported chlorophenol red–Tris and indigo carmine–Tris as background electrolytes for the indirect detection of anions. We found that permanganate can be used as the background electrolyte to avoid large baseline fluctuation caused by large dye molecules. Permanganate is quite similar to the chromate buffer for indirect UV detection reported by Jones and Jandik [21]. It has smaller fluctuation, better match of the mobility with small anions, and is quite stable at neutral or weakly basic environments. Fig. 7A is the electropherogram showing indirect detection of several anions using a green-LED-based CE system. As can be seen from Fig. 7B, the intensity-noise level is about $5 \cdot 10^{-5}$, which corresponds to $\Delta A = 1.1 \cdot 10^{-5}$. This is much lower than that using large dye molecules as the running buffer. The molar absorptivity at 567 nm is measured to be $1.24 \cdot 10^3$ l mol^{-1} cm^{-1}. According to Eq. 3, the theoretical detection limit at an S/N of 2 is $3.4 \cdot 10^{-6}$ *M*. From Fig. 7B, $4.6 \cdot 10^{-5}$ *M* ClO_3^- gives an S/N of 7.5, which corresponds to a detection limit of $1.2 \cdot 10^{-5}$ *M* at an S/N of 2. This is three

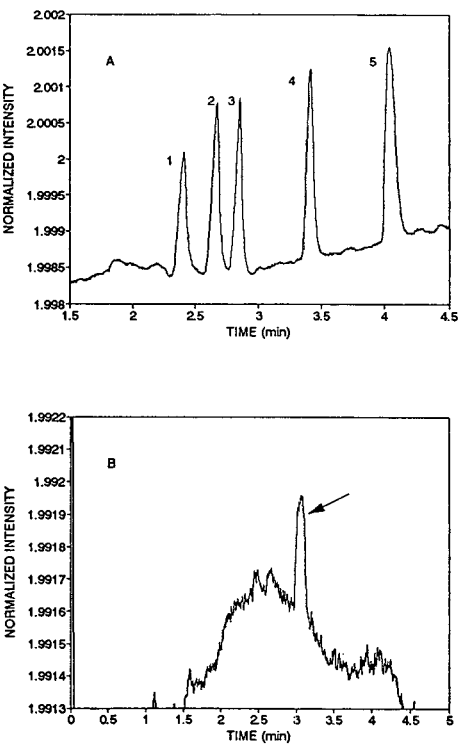

Fig. 7. Electropherograms for the indirect detection of anions in the LED-based system. The running buffer was 20 m*M* permanganate (pH 7.0). The applied potential was 27 kV. A 50 μm I.D. DB-1 capillary with 55 cm total length and 40 cm to the detector was used. (A) Separation of anions (1, $4.6 \cdot 10^{-4}$ *M* Cl^-; 2, $2.6 \cdot 10^{-4}$ *M* SO_4^{2-}; 3, $5.0 \cdot 10^{-4}$ *M* NO_3^-; 4, $4.6 \cdot 10^{-4}$ *M* ClO_3^-; and 5, $5.2 \cdot 10^{-4}$ *M* F^-). (B) Electropherogram of $4.6 \cdot 10^{-5}$ *M* ClO_3^-.

times poorer than the theoretical value. The reason is still the poor coupling of the LED beam with the small-diameter capillary, which cannot assure that all the light rays pass through the center of the capillary.

4. Conclusions

Diode-laser- and LED-based double-beam absorption detection systems for CE using digital cancellation were demonstrated. The background noise was reduced substantially. Better optical coupling of the laser beam with the small capillary is achieved for the diode-laser-based system. Both systems also benefited from the excellent intensity stability of the diode laser and the LED. The detectability is improved over the commercial double-beam CE system. The many wavelengths available for different LEDs make them versatile. Although LEDs are not strictly monochromatic, the linear correlation coefficient for the calibration curve can still be 0.999. Indirect detection can make the system more universally applicable. With the availability of shorter-wavelength diode lasers in the future, we believe these systems will find even broader application.

Acknowledgements

The authors thank Q. Xue and Q. Li for helpful discussions. The Ames Laboratory is operated for the U.S. Department of Energy by Iowa State University under Contract No. W-7405-Eng-82. This work was supported by the Director of Energy Research, Office of Basic Energy Sciences, Division of Chemical Sciences.

References

[1] M. Albin, P.O. Grossman and S.E. Morning, Anal. Chem., 65 (1993) 489A.
[2] C.A. Monnig and R.T. Kennedy, Anal. Chem., 66 (1994) 280R.
[3] A.G. Ewing, R.A. Wallingford and T.M. Olefirwicz, Anal. Chem., 61 (1989) 292A.
[4] Y. Xue and E.S. Yeung, Anal. Chem., 65 (1993) 1988.
[5] Y. Xue and E.S. Yeung, Appl. Spectrosc., 48 (1994) 502.
[6] Y. Xue and E.S. Yeung, Anal. Chem., 65 (1993) 2923.
[7] Z. Rosenzweig and E.S. Yeung, J. Chromatogr., 645 (1993) 201.
[8] Z. Rosenzweig and E.S. Yeung, Appl. Spectrosc., 47 (1993) 1175.
[9] T. Imasaka and N. Ishibashi, Anal. Chem., 62 (1990) 363A.
[10] A.J.G. Mank, H. Lingeman and C. Gooijer, Trends Anal. Chem., 11 (1992) 210.
[11] T. Higashijima, T. Fuchigami, T. Imasaka and N. Ishibashi, Anal. Chem., 64 (1992) 711.
[12] T. Fichigami and T. Imasaka, Anal. Chim. Acta, 291 (1994) 183.
[13] S.J. Williams, E.T. Bergstrom, D.M. Goodall, H. Kawazumi and K.P. Evans, J. Chromatogr., 636 (1993) 39.
[14] J. Pawliszyn, Rev. Sci. Instrum., 58 (1987) 245.
[15] T. Imasaka, T. Kamikubo, Y. Kawabata and N. Ishibishi, Anal. Chim. Acta, 153 (1983) 261.
[16] O.S. Wofbeis, B.P.H. Schaffar and E. Kaschnitz, Analyst (London), 111 (1986) 1331.
[17] B.W. Smith, B.T. Jones and J.D. Winefordner, Appl. Spectrosc., 42 (1988) 1469.
[18] P. Jandik and G. Bonn, Capillary Electrophoresis for Small Molecules and Ions, VCH, New York, 1993.
[19] Z. Mala, R. Vespalec and P. Boçek, Electrophoresis, 15 (1994) 1526.
[20] G.J.M. Bruin, A.C. van Asten, X. Xu and H. Poppe, J. Chromatogr., 608 (1992) 97.
[21] W.R. Jones and P. Jandik, J. Chromatogr., 608 (1992) 385.

ELSEVIER

Journal of Chromatography A, 718 (1995) 187–193

JOURNAL OF CHROMATOGRAPHY A

Micellar electrokinetic capillary chromatography of limonoid glucosides from citrus seeds

Vinayagum E. Moodley[1], Dulcie A. Mulholland, Mark W. Raynor*

Department of Chemistry and Applied Chemistry, University of Natal, King George V Ave., Durban 4001, South Africa

First received 9 March 1995; revised manuscript received 7 June 1995; accepted 7 June 1995

Abstract

This report presents the results of an investigation into the application of micellar electrokinetic capillary chromatography (MECC) for the analysis of limonoid glucosides in a citrus seed extract. MECC based on sodium dodecyl sulphate (SDS) was used to provide highly efficient separations of the closely related structures. A phosphate–borate buffer containing SDS was used to optimize the separation conditions for a mixture containing standard compounds of the glucosides of limonin, obacunone and nomilin. The study showed that MECC analysis of limonoid glucosides requires minimal sample clean-up steps and achieves excellent separations within a relatively short analysis time. The technique developed was used to quantify two limonoid glucosides in a methanol extract of the seeds of *Citrus nobilis* (nartjie) and *Citrus limon* (lemon).

1. Introduction

Limonoids are a group of chemically related triterpene derivatives which are isolated from plants of the *Meliaceae, Rutaceae* and *Cneoraceae* families. These limonoids are one of the two major bitter principles found in *Citrus*. Thirty seven limonoid aglycones have been isolated from *Citrus* and its hybrids and of these limonin is the major cause of the bitterness in citrus juices. It has been shown recently that limonoids also occur in fruit tissues and seeds of *Citrus* as nonbitter glucoside derivatives [1]. The names and structures of the major limonoid glucosides which have been isolated from *Citrus* are shown in Fig. 1. This discovery has explained the natural debittering process that occurs in fruit during the late stages of fruit growth and maturation. Limonoids have been shown to exhibit anticancer activity in laboratory animals [2–4] and antifeedant activity against insects and termites [5,6]. Citrus seeds contain a high concentration of limonoid glucosides and could therefore be utilized as a source of these important compounds.

Analysis of limonoid glucosides in citrus juices using thin layer chromatography (TLC) [7] and high-performance liquid chromatography (HPLC) [8] have been reported. Limonoid glucosides in citrus seeds have also been analyzed recently using TLC and HPLC [9]. However, the use of HPLC is restricted by the longer clean-up steps required, interference from flavonoids, the lengthy analysis time (at least 35 min) and unsatisfactory resolution between two of the five major limonoid glucosides. The purpose of

* Corresponding author.

[1] Present address: Department of Chemistry, M.L. Sultan Technikon, P.O. Box 1334, Durban 4000, South Africa.

0021-9673/95/$09.50
SSDI 0021-9673(95)00648-6

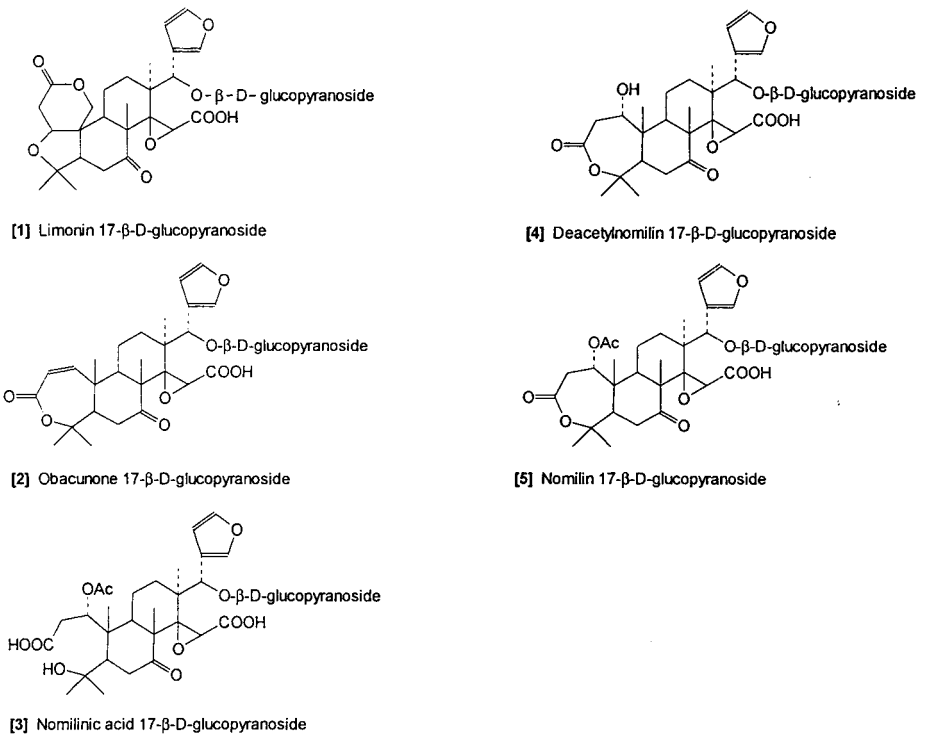

Fig. 1. Structures of the major limonoid glucosides present in *Citrus*.

this study was to establish a simple capillary electrophoretic (CE) procedure for the separation and quantitation of limonoid glucosides in citrus seeds.

Capillary electrophoretic techniques offer very high separation efficiencies, relatively short analysis times and represent an attractive alternative to HPLC methods [10]. Although CE has been applied to the analysis of a wide variety of complex mixtures [11–13], it is limited to the separation of ionic substances. However, in micellar electrokinetic capillary chromatography (MECC), a buffer solution that contains a surfactant (e.g., SDS) at, or above, its critical micelle concentration (cmc) is used as the electrophoretic medium. As a result, a pseudo stationary phase is produced, enabling the separation of both charged and neutral solutes in a single analysis according to differential distribution of the solutes between the aqueous and micellar phases. MECC based on micellar solubilization was first reported in 1984 by Terabe et al. [14]. Since then the technique has been well documented for a wide variety of applications [15–18]. We report for the first time a novel MECC method for the rapid, reproducible and efficient analysis of limonoid glucosides in citrus seeds.

2. Experimental

2.1. Materials

Citrus nobilis and *Citrus limon* were obtained locally. The seeds were dried in a refrigerator for 3 days and then ground finely in a coffee grinder.

2.2. Sample extraction

The seed meals of *Citrus nobilis* (12.0 g) and *Citrus limon* (9.0 g) were extracted for 24 h with refluxing *n*-hexane in a Soxhlet extractor to remove oils and non-glucosylated limonoids. The seed material was thereafter extracted for a further 24 h with refluxing methanol in a Soxhlet

extractor. The methanol extract was evaporated to dryness and the residue was re-extracted with 6 ml of methylene chloride–water (1:1). The water fraction contained the limonoid glucosides and was analyzed directly.

2.3. Reagents and chemicals

The separation buffer consisted of 20 m*M* sodium dihydrogen phosphate (BDH, Poole, UK), 12 m*M* disodium tetraborate (BDH) and 35 m*M* sodium dodecyl sulphate (Sigma, St. Louis, MO, USA) and was prepared in doubly deionised water (Millipore Corp., USA). All samples and standards were filtered through a 0.45-μm syringe filter (Lida, Kenosha, USA). All chemicals were of analytical-reagent grade.

2.4. Standards of limonoid glucosides

In this study, standards of the 17-β-D-glucopyranosides of limonin, obacunone and nomilin were used. They were isolated and characterised by nuclear magnetic resonance, infra-red and mass spectroscopic techniques.

2.5. Instrumentation

The qualitative and optimization experiments were carried out on a laboratory built CE system and the quantitative experiments were performed on a Beckman P/ACE System 2000 (Beckman Instruments, Palo Alto, CA, USA). The laboratory built system consisted of a 0–30 kV high voltage power supply (Series 230, Bertan High Voltage, Hicksville, NY, USA) and a variable-wavelength UV detector (Spectrasystem UV 1000, Spectra-Physics, San Jose, CA, USA) that was fitted with an on-column capillary cell (Model 9550-0155, Linear Instruments, NV, USA). The platinum electrodes were housed in a perspex box which was equipped with an interlock for operator safety. Fused-silica capillaries (50 μm I.D., 220 μm O.D.) were obtained from SGE (Melbourne, Australia). The capillary length was 68 cm (43 cm from the injection end to the detector window). The separations were carried out at ambient temperature and detection was at 210 nm. The electropherograms were recorded with an electronic integrator (Model SP 4200, Spectra-Physics). Hydrodynamic injections were made by lowering the vial at the detector end by 4 cm below its normal position and inserting the upstream end of the capillary into the sample vial for 5 s.

The Beckman system consisted of a 0–30 kV high-voltage built-in power supply, a selectable fixed-wavelength UV detector, a temperature-controlled column cartridge (75 μm I.D.) and an autosampler. The capillary length was 50 cm (43.5 cm from the injection end to the detector window). All experiments were carried out at 25°C at a constant voltage of 25 kV. Injections were made using the pressure mode for 2 s each and the peaks were monitored at 214 nm. The Gold software for system controlling and data handling was used. The electropherograms were recorded on an IBM PS/2 Model 55 SX computer.

2.6. Calibration graphs

The calibration graphs were obtained from standard solutions containing limonin glucoside and nomilin glucoside in the concentration range 0.15–1.5 mg/ml in doubly deionised water. Since only a small amount of obacunone glucoside standard was available it was excluded from the quantitative study.

3. Results and discussion

Preliminary experiments were conducted to separate the limonoid glucosides using capillary zone electrophoresis (CZE) conditions. CZE was unable to resolve limonin and obacunone glucoside in the pH range 6.0–7.5. The upper limit of the pH was set at 7.5 because nomilin glucoside is converted to obacunone glucoside at a pH greater than 7.5 [19].

The three limonoid glucoside standards were estimated from pH measurements to have pK_a values close to 4.3. The difference in ionization of the carboxylic group in the limonoid skeletons was not great enough to allow differentiation

among the electrophoretic mobilities of limonin and obacunone glucosides. However, nomilin glucoside had a sufficiently different charge-to-mass ratio to be well separated from the other two (Fig. 2A).

The technique which gave successful separations of these compounds was MECC (Fig. 2B,C). The separation mechanism is primarily based on differences in hydrophobic interactions for all of the compounds, as well as differences in their electrophoretic mobilities. The effect of SDS concentration on the separation of the three limonoid glucoside standards is shown in Fig. 3. The overall decrease in the migration time values of limonin and nomilin glucosides in the concentration range 0–50 m*M* SDS may indicate an increase in the temperature of the capillary [20,21] or perhaps less interaction between the SDS micelles and these two glucosides. However, obacunone glucoside showed increased migration times as the concentration of SDS was increased, and was increasingly separated from limonin glucoside but tended to migrate closer to nomilin. The increase in migration time of obacunone glucoside relative to the other two is probably due to the increased hydrophobicity of obacunone glucoside compared with limonin glucoside or nomilin glucoside. As can be seen in Fig. 3, the best separation was obtained at an SDS concentration of 32 m*M*.

The migration times obtained for the components present in the *Citrus limon* extract at different pH values are shown in Fig. 4. As expected, the migration times decrease with an increase in buffer pH due to an increase in the electroosmotic flow velocity. At a pH of 6.0 the migration times were excessively high and the peaks were broadened. The peak shape improved as pH was increased from 6.5 to 7.5.

The separation of the limonoid glucosides in *Citrus limon* is shown in Fig. 5 at three different pH values. As can be seen excellent baseline separations were obtained at pH 6.5 and 7.0. Since the analysis time was approximately 2 min shorter at pH 7.0, this condition was chosen for subsequent analysis of the citrus extracts. Furthermore, during pH optimization studies at 25 kV, current fluctuations were experienced on

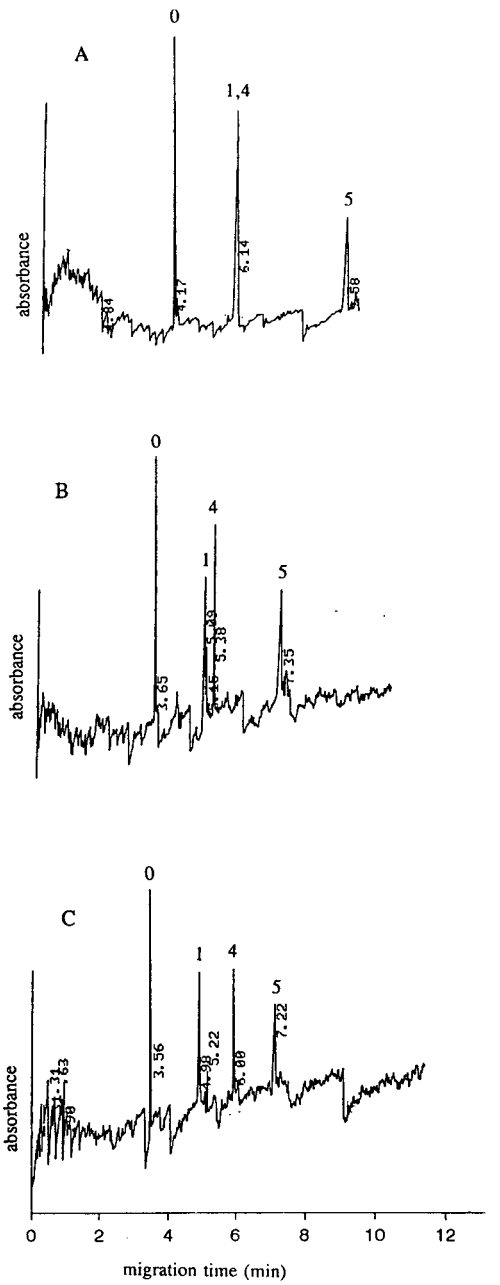

Fig. 2. Electropherograms of a mixture of limonoid glucoside standards showing the separation at (A) 0 m*M* SDS, (B) 10 m*M* SDS, (C) 30 m*M* SDS. Conditions: pH 7.0; 20 m*M* NaH_2PO_4; 12 m*M* $Na_2B_4O_7$; 25 kV; 43 cm (detection point); 68 cm (total length) × 50 μm I.D. untreated fused-silica capillary. Peaks: 0 = formamide (neutral marker); 1 = limonin glucoside; 4 = obacunone glucoside; 5 = nomilin glucoside.

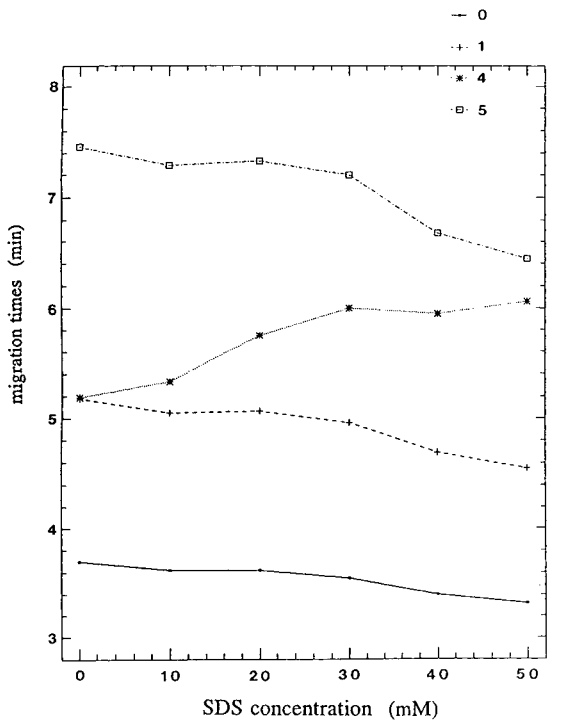

Fig. 3. Variation of migration time of limonoid glucoside standards with SDS concentration. Conditions and numbers as in Fig. 2.

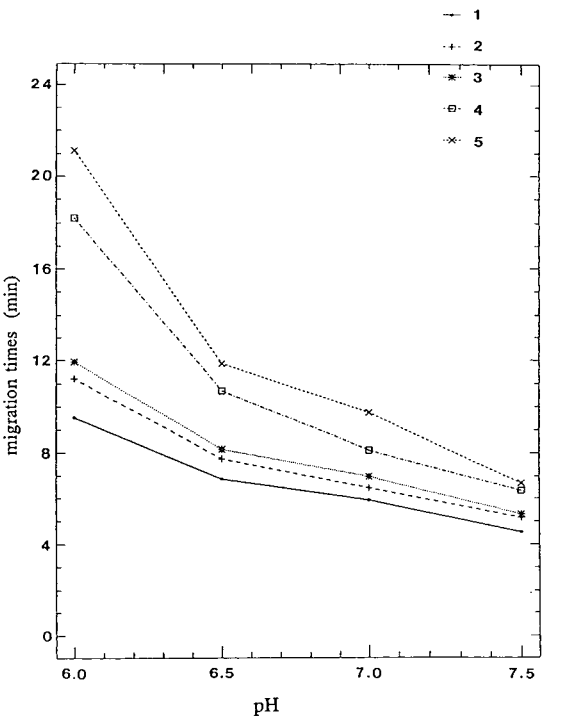

Fig. 4. Effect of pH on the migration time of limonoid glucosides in *Citrus limon*. Conditions: 32 m*M* SDS; 22 kV; other separation conditions as in Fig. 2. Peaks: 1 = limonin glucoside; 2 = unidentified; 3 = unidentified; 4 = obacunone glucoside; 5 = nomilin glucoside.

the laboratory built system at pH 7.5. It was therefore necessary to lower the applied voltage to 22 kV when separations were done at a pH of 7.5. Peaks 1, 4 and 5 were identified by comparison of the migration times with the three standards that were available. The separation of the limonoid glucosides in *Citrus limon* and *Citrus nobilis* is shown in Fig. 6 together with the separation of a standard solution containing limonin, obacunone and nomilin glucosides. Good separations were obtained for both extracts and except for the relative amounts of the glucosides, the electropherograms are very similar.

The water fraction of the methylene chloride–water extract of *Citrus limon* and *Citrus nobilis* was analyzed for limonin glucoside and nomilin glucoside. Quantitative information was obtained by using the external standard method. The peak areas were normalized by dividing the peak area by the migration time. The calibration graphs for limonin glucoside and nomilin glucoside showed good linearity in the concentration range 150–1500 μg/ml.

For the regression equation $y = ax + b$, where x is the concentration of limonoid glucosides (μg/ml) and y is the normalized peak area, the correlation coefficients (r) were as follows: for limonin glucoside, $y = 12.2167 \cdot 10^{-5}x + 283.3000 \cdot 10^{-5}$ ($r = 1.000$); for nomilin glucoside, $y = 11.3359 \cdot 10^{-5}x - 62.3250 \cdot 10^{-5}$ ($r = 0.999$). The results of the quantitation for limonin glucoside and nomilin glucoside are shown in Table 1. The results are within the expected limits of these compounds in citrus seeds found by other methods [19].

The recovery of limonoid glucosides was tested by adding known amounts of limonin and nomilin glucosides to a sample water fraction of

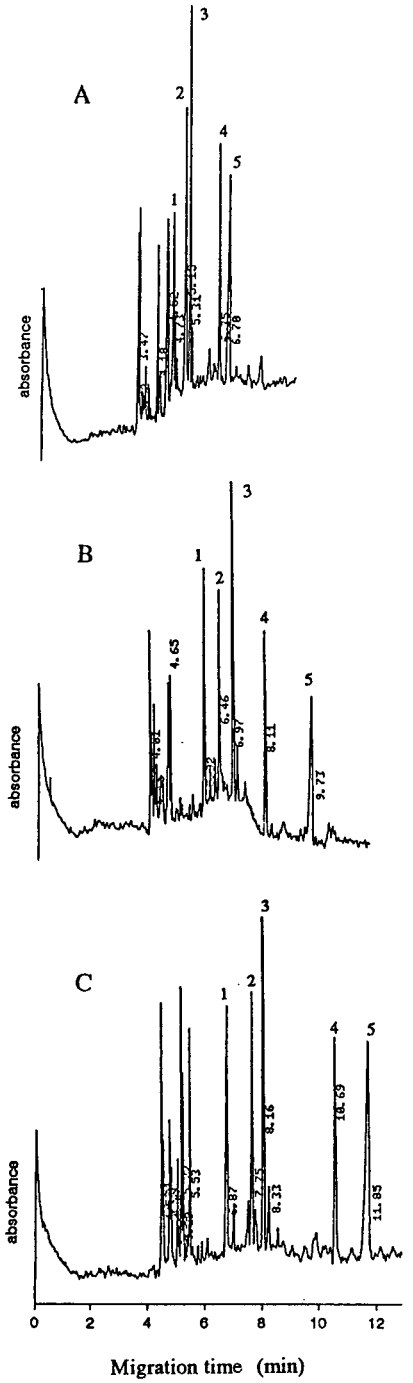

Fig. 5. Electropherogram of limonoid glucosides in *Citrus limon*. (A) pH = 7.5; (B) pH = 7.0; (C) pH = 6.5. Conditions: 32 m*M* SDS; 22 kV; other separation conditions as in Fig. 2. Peak numbers as in Fig. 4.

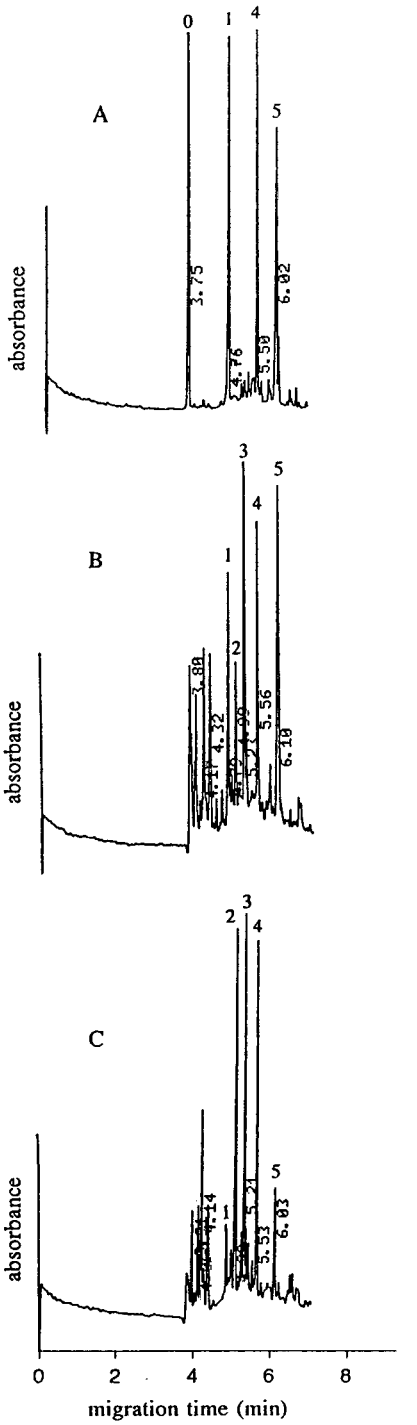

Fig. 6. (A) Electropherogram of limonoid glucoside standards. (B and C) Electropherograms of *Citrus limon* and *Citrus nobilis*, respectively. Conditions: 32 m*M* SDS; other separation conditions as in Fig. 2. Peak numbers as in Fig. 4.

Table 1
Results of the determination of some limonoid glucosides in seeds of Nartjie (*Citrus nobilis*) and Lemon (*Citrus limon*)

17-β-D-Glucopyranoside of	Concentration[a] (mg per g of dried seed)	
	Nartjie	Lemon
Limonin	0.523 ± 0.006	0.19 ± 0.02
Nomilin	0.45 ± 0.03	0.440 ± 0.005

[a] Average values of 3 injections.

Citrus nobilis containing known levels of these compounds (see Table 1). The recovery of the limonoid glucosides by the MECC method described gave recoveries of 94.1% for limonin glucoside and 93.5% for nomilin glucoside. Precision tests for limonin glucoside and nomilin glucoside were carried out on the Beckman P/ACE 2000 instrument. The coefficients of variation of the migration time for limonin glucoside and nomilin glucoside (9 injections) were 0.92% and 1.35%, respectively. The coefficient of variation for the normalized peak areas for limonin glucoside and nomilin glucoside were 1.92% and 7.98%, respectively. These results indicate that MECC is sufficiently sensitive for the reproducible determination of limonoid glucosides in citrus seeds.

The study has shown that MECC can be applied successfully to separate limonoid glucosides. The analysis of some of the major limonoid glucosides present in citrus seeds demonstrates the applicability of the proposed method. Further, the technique offers high separation efficiencies, rapid analyses, low running costs and is aqueous rather than organic solvent based. All these are advantages over traditional chromatographic procedures.

Acknowledgements

The authors thank Mr. Walter Deppe (Department of Chemical Pathology, University of Natal) for the use of the Beckman System 2000 (Model P/ACE) for the quantitative part of the work and thank the Foundation for Research Development, Pretoria, South Africa and the University of Natal Research Fund for financial assistance.

References

[1] S. Hasegawa, R.D. Bennett, Z. Herman, C.H. Fong and P. Ou, Phytochemistry, 28 (1989) 1717.
[2] L.K.T. Lam and S. Hasegawa, Nutr. Cancer, 12 (1989) 43.
[3] L.K.T. Lam, Y. Li and S. Hasegawa, J. Agric. Food Chem., 37 (1989) 378.
[4] E.G. Miller, R. Fanous, F.R. Hidalgo, W.H. Binnie, S. Hasegawa and L.K.T. Lam, Carcinogen, 10 (1989) 1535.
[5] A.R. Alford and M.D. Bentley, J. Econ. Entomol., 79 (1987) 35.
[6] A.R. Alford, J.A. Cullen, R.H. Stoch and M.D. Bentley, J. Econ. Entomol., 80 (1987) 575.
[7] C.H. Fong, S. Hasegawa, Z. Herman and P. Ou, J. Food Sci., 54 (1989) 1505.
[8] Z. Herman, C.H. Fong, P. Ou and S. Hasegawa, J. Agric. Food Chem., 38 (1989) 1860.
[9] H. Ohta, C.H. Fong, M. Berhow and S. Hasegawa, J. Chromatogr., 639 (1993) 295.
[10] A. Loreglan, C. Scremin, M. Schiavon, A. Marcello and G. Palú, Anal. Chem., 66 (1994) 2981.
[11] H. Stuppner, S. Sturn and G. Konwalinka, J. Chromatogr., 609 (1992) 375.
[12] T.K. McGhie, J. Chromatogr., 634 (1993) 107.
[13] M.B. Amran, M.D. Lakkis, F. Lagarde, M.J.F. Leroy, J.F. Lopez-Sanches and G. Rauret, Fresenius J. Anal. Chem., 345 (1993) 420.
[14] S. Terabe, K. Otsuka, K. Ichikawa, A. Tsuchiya and T. Ando, Anal. Chem., 56 (1984) 111.
[15] P. Pietta, P. Mauri, R. Maffei Facino and M. Carini, J. Pharm. Biomed. Anal., 10 (1992) 1041.
[16] S. Michaelson, P. Moller and H. Sørensen, J. Chromatogr., 608 (1992) 363.
[17] J. Vindevogel, P. Sandra and L. Verhagen, J. High Resol. Chromatogr., 13 (1990) 295.
[18] P. Piergiorgio, C. Gardana and M. Pierluigi, J. High Resol. Chromatogr., 15 (1992) 136.
[19] S. Hasegawa, C.H. Fong, Z. Herman and M. Miyake, in Flavor Precursors, R. Teranishi, G.R. Takeoka and M. Guntert (Eds.), ACS Symp. Ser., Vol. 490, American Chemical Society, Washington, DC, USA, 1992, p. 87.
[20] S. Terabe, K. Otsuka and T. Ando, Anal. Chem., 57 (1985) 834.
[21] K.H. Row, W.H. Griest and M.P. Maskarinec, J. Chromatogr., 409 (1987) 193.

ELSEVIER

Journal of Chromatography A, 718 (1995) 195–202

JOURNAL OF CHROMATOGRAPHY A

Analysis of the glycoforms of human recombinant factor VIIa by capillary electrophoresis and high-performance liquid chromatography

Niels Kristian Klausen*, Troels Kornfelt

Protein Chemistry, Biologics Development, Novo Nordisk A/S, Niels Steensensvej 1, DK-2820 Gentofte, Denmark

First received 10 March 1995; revised manuscript received 6 June 1995; accepted 9 June 1995

Abstract

The carbohydrate-dependent microheterogeneity of recombinant coagulation factor VIIa (rFVIIa) has been characterized by capillary electrophoresis (CE) of the native protein and by high-performance liquid chromatography (HPLC) of tryptic peptides and of oligosaccharides released by hydrazinolysis.

The development of the CE analysis is reported here. We have found that application of 1,4-diaminobutane (putrescine) as additive to the CE separation buffer is essential for the separation of the various glycoforms. Under optimum conditions rFVIIa migrates as a cluster of six peaks or more. By CE of neuraminidase-treated rFVIIa a faster-moving double peak is observed. This indicates that the separation obtained is primarily based upon the different content of N-acetyl-neuraminic acid of the oligosaccharide structures in rFVIIa.

By reversed-phase HPLC of tryptic digested neuraminidase treated rFVIIa the glycopeptides containing the heavy chain N-glycosylated site elute as two peaks compared to the four peaks corresponding to glycopeptides with 0 to 3 N-acetyl-neuraminic acids seen for untreated rFVIIa.

In high-pH anion-exchange HPLC of the oligosaccharides released from native rFVIIa by hydrazinolysis the major peaks elute as oligosaccharides with 1 or 2 N-acetyl-neuraminic acids. Oligosaccharides released from neuraminidase treated rFVIIa elute earlier compared to oligosaccharides from native rFVIIa, but separated into several peaks, indicating heterogeneity for the oligosaccharide structures without N-acetyl-neuraminic acid.

1. Introduction

Factor VII is a single-chain, vitamin K-dependent plasma glycoprotein that participates in the extrinsic pathway of blood coagulation. By the activation of factor VII to factor VIIa the peptide chain is cleaved between Arg152 and Ile153, resulting in a two-chain molecule consisting of a light chain (AA 1–152) and a heavy chain (AA 153–406) linked through one disulphide bond [1]. Human recombinant blood coagulation factor VII has been obtained from a mammalian expression system and has in its activated form (rFVIIa) been purified and characterized [1]. rFVIIa is post-translationally modified in several ways, including γ-carboxylation, O-glycosylation at Ser52 and Ser60 and N-glycosylation at Asn145 and Asn322 [1,2]. At Ser52 three different structures, $(Xyl)_{0-2}$-Glc-, and at Ser60 a single Fuc have been found [2].

Each N-glycosylated site in eukaryotic glycoproteins is associated with several different oligo-

* Corresponding author.

0021-9673/95/$09.50
SSDI 0021-9673(95)00656-7

saccharide structures, also referred to as N-glycosylation microheterogeneity [3]. A glycoprotein with multiple N-glycosylated sites, therefore, consists of a population of glycoforms [3,4]. Since separation of such a glycoprotein into its individual glycoforms is not readily attainable [4], characterization of the glycosylation of glycoproteins has been performed after initial enzymatic or chemical cleavage [5–12]. A common approach for characterization of glycoprotein glycosylation has been proteolytic digestion followed by glycopeptide analysis using reversed-phase high-performance liquid chromatography (RP-HPLC) with detection by UV absorbance [5] or mass spectrometry [6]. Another approach has been to release the oligosaccharides by enzymatic [7,8] or chemical cleavage [8,9] and to analyze the oligosaccharides by high-pH anion-exchange HPLC (HPAEC) with pulsed amperometric detection (PAD) [7,8], by mass spectrometry [10], or by NMR [11,12].

HPLC separation of native glycoproteins with multiple N-glycosylated sites into fractions differing in the glycosylation is not readily attainable [3] and has to our knowledge only been obtained in a few cases. Frenz et al. [13] used anion-exchange HPLC to separate recombinant human deoxyribonuclease I glycoforms according to extent and positions of phosphorylation. In addition, some separation according to sialylation was obtained.

During the past three to four years several papers have been published concerning the application of capillary electrophoresis (CE) for the analysis of the carbohydrate-mediated heterogeneity of various glycoproteins. Some of the published work has been reviewed [14]. Relatively few glycoproteins have been addressed in the published articles, but separation of the glycoforms has been achieved using various analytical conditions. Capillary zone electrophoresis (CZE), as well as capillary isoelectric focusing and micellar electrokinetic capillary chromatography have been applied [15–23]. CZE using various buffers of both basic and acidic pH values seems to be the most preferred technique, probably due to its simplicity. Recent studies [24–26] have indicated that CZE using α,ω-diaminoalkanes like 1,4-diaminobutane (putrescine) as buffer additive may be general applicable for the separation of glycoforms.

In several papers it has been demonstrated that addition of 1,3-, 1,4- or 1,5-diaminoalkanes to the running buffer improves the resolution of proteins and polypeptides [27–31]. The beneficial effect of these polyethylenediamines is obviously due to a binding to the fused-silica wall. Thereby the electroendosmotic flow (EOF), as well as the interaction between the solutes and the capillary wall, is reduced. Whereas low levels (maximum 5 mM) of putrescine or cadaverine (1,5-diaminopentane) have been used in some cases [27–29], Bullock and Yuan [30] found that about ten times higher concentrations of 1,3-diaminopropane (30–60 mM) were best for the separation of a series of six basic proteins. These conditions have also proven useful in a subsequent paper on recombinant human protein interleukin-4 [31].

It is apparent from the above-cited literature that analysis of the carbohydrate-dependent microheterogeneity of glycoproteins is not readily attainable by use of HPLC while several good results have been obtained in recent years by use of various CE techniques. CZE seems to be the most preferred technique, probably due to its simplicity. While HPLC is of limited success with regard to separation of the glycoforms of native glycoproteins, various HPLC separation modes are essential for the characterization and purification of glycopeptides and oligosaccharides.

In the study presented here, we have investigated the separation of glycoforms of native rFVIIa by CE using a phosphate buffer with putrescine as buffer additive. The effect of other buffer parameters is also investigated. Native and neuraminidase treated rFVIIa are characterized by CE, RP-HPLC of tryptic glycopeptides, and HPAEC of released oligosaccharides.

2. Experimental

2.1. Materials

rFVIIa was expressed and purified at Novo Nordisk A/S (1). Trypsin (bovine, T-1005),

Neu5Ac (A-2751) and putrescine dihydrochloride (1,4-diaminobutane, 2HCl) were from Sigma (St. Louis, MO, USA). Neuraminidase was from Boehringer Mannheim (Mannheim, Germany) for rFVIIa and from Oxford GlycoSystems (X-5011, Oxford, UK) for the oligosaccharides. The reagent kit (I-4011) used for the hydrazinolysis and the oligosaccharide standards (C-335300, C-224300 and C-124300) were from Oxford GlycoSystems (Oxford, UK). All other chemicals were of analytical grade.

2.2. Neuraminidase treatment of r-factor VIIa and purified oligosaccharides

Removal of Neu5Ac was done by incubation of rFVIIa or purified oligosaccharide with neuraminidase in 50 m*M* sodium acetate, 5 m*M* calcium chloride, pH 4.8, for 3 h at room temperature. The enzyme–substrate ratio was 1:5 for rFVIIa and 1 U per approximately 100 pmol for the oligosaccharides.

2.3. Preparation and separation of r-factor VIIa tryptic peptides

rFVIIa samples (1 mg/ml) were digested with trypsin (enzyme/substrate ratio 1:100) in 50 m*M* Tris buffer, 5 m*M* $CaCl_2$, pH 7.5, for 20 h at 37°C. Digestion was terminated by addition of glacial acetic acid, adjusting the pH to approximately 3.5. The digestion product (25 μl) was analyzed using RP-HPLC: HPLC equipment, Waters; column, Nucleosil C_{18} column (250 × 4 mm, particle size 7 μm, pore diameter 12 nm, Macherey-Nagel 720042); column temperature, 30°C; detection, 215 nm; flow-rate, 1.5 ml/min; eluent A, 0.065% (by volume) trifluoroacetic acid in water; eluent B, 0.05% (by volume) trifluoroacetic acid in 90% acetonitrile in water. Gradient for heavy chain glycopeptides, 6–41% eluent B for 49 min; gradient for light chain glycopeptides, 0–16% eluent B for 40 min.

The elution positions of the glycosylated peptides by the RP-HPLC analysis were identified as previously described [33].

2.4. Preparation and separation of rFVIIa oligosaccharides

Samples of rFVIIa (1 mg/ml) were dialyzed against 0.1% trifluoroacetic acid, lyophilized and hydrazinolyzed on a GlycoPrep1000 (Oxford GlycoSystems, UK), using standard procedure. The dried oligosaccharide pools were resuspended in water and analyzed, using HPAEC–PAD: HPLC equipment, Waters; column, CarboPac PA100 (250 × 4 mm) with a CarboPac PA100 Guard (50 × 4 mm) (Dionex, USA); column temperature, ambient; detection, pulsed amperometric with pulse potentials and durations 0.05 V/300 ms, 0.80 V/200 ms, −0.06 V/600 ms, working at 1 μA full scale; flow-rate, 1.0 ml/min; gradient, 7.5 m*M* to 150 m*M* sodium acetate in 150 m*M* sodium hydroxide for 50 min.

2.5. Sample preparation prior to CE

A change of the buffer of the rFVIIa samples (1 mg/ml) to 50 m*M* sodium acetate, 5 m*M* calcium chloride, pH 4.8, was done in some of the experiments. Buffer exchange was performed either by dialysis (M_r 8000 cutoff) or size-exclusion chromatography (NAP10 column, Pharmacia, Sweden).

2.6. Capillary electrophoresis–instrumentation and operation

The capillary electrophoresis was performed using a Waters Quanta 4000 capillary electrophoresis system. Fused-silica capillaries (75 μm I.D.; 356 μm O.D.) from Polymicro Technologies (Phoenix, AZ, USA) with a total length of 88 or 45 cm were used. Sample introduction was done by hydrostatic injection (siphoning) for 10 s at the anode. UV detection at 214 nm took place 7.5 cm from the cathodic end of the capillary. To avoid excessive heating of the buffer in the capillary the field strength was chosen so that the current did not exceed 100 μA.

Before analysis the capillary was equilibrated with the separation buffer. Washing with dilute sodium hydroxide between runs had no beneficial effect and was therefore avoided. At chang-

ing from buffer containing putrescine to pure buffer the capillary was washed with 1 *M* HCl followed by 1 *M* NaOH, distilled water and finally equilibrated with the new buffer.

As marker for the electroosmotic flow 0.1% benzylalcohol was used. The buffer solution in the electrode vessels was renewed at least once a day.

3. Results and discussion

3.1. Effect of putrescine on CE of rFVIIa

Inspired by the results achieved using putrescine as a buffer additive for CE of glycoproteins, we tested the effect on rFVIIa. CE analysis of rFVIIa in 100 m*M* phosphate buffer, pH 9.0, containing 0, 5 and 25 m*M* putrescine, respectively, is shown in Fig. 1. In phosphate buffer without putrescine (top panel) rFVIIa migrates as a single symmetrical peak followed by a slightly skewed peak representing the sample buffer glycylglycine. Although a separation of rFVIIa into at least two components is clearly visible using 5 m*M* putrescine (middle panel), optimal resolution requires about 25 m*M* putrescine (bottom panel). Addition of putrescine has two effects on the electrophoretic peak pattern. The EOF is markedly reduced and simultaneously rFVIIa is separated into a cluster of peaks. The reduction of the EOF is most probably due to a partial neutralization of the fused-silica surface of the capillary, which is strongly negative at pH 9.0 due to ionization of the silanol groups. It is noteworthy that the optimum concentration of putrescine is about ten times higher compared to what was found to be optimal for ovalbumin [26] and r-HuEPO [24]. Increasing the concentration of putrescine to 50 m*M* prolongs the migration time of rFVIIa even further without any improvement in the resolution of the peak cluster (not shown). This indicates that the resolution of rFVIIa into several close-eluting peaks is only for a part due to a reduction of EOF. Ion-pair formation between putrescine and negatively charged groups of the glycoprotein probably plays also an important role.

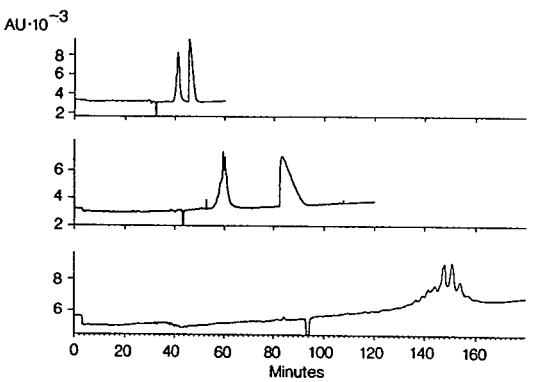

Fig. 1. Capillary electrophoretic separation of rFVIIa glycoforms using putrescine as buffer additive. The separations were performed in an 88-cm long capillary using 100 m*M* phosphate, pH 9.0, and a separation voltage of 10 kV. Top panel: 0 m*M* putrescine; rFVIIa migrates in front of glycylglycine. Middle panel: 5 m*M* putrescine; rFVIIa migrates in front of glycylglycine. Bottom panel: 25 m*M* putrescine.

3.2. Significance of the CE separation buffer substance

The beneficial effect of borate for the resolution of mono- and oligosaccharides as well as glycosylated peptides has been reported [32]. In a study on ovalbumin [26] it was likewise concluded that application of a borate buffer played an important role in the separation of ovalbumin glycoforms.

We have compared the separation of rFVIIa using 100 m*M* phosphate, 25 m*M* putrescine, pH 8.0, respectively 100 m*M* borate, 12.5 m*M* putrescine, pH 8.0, as running buffer. It was necessary to reduce the concentration of putrescine in the borate buffer as the migration time of rFVIIa became too long with 25 m*M*. We observed that replacement of phosphate with borate resulted in longer migration times and the resolution of the peak cluster became worse. We cannot tell, however, whether some complexation between borate and the glycostructures of rFVIIa also takes place. However, it does not improve the separation of the glycoforms. These

observations are in agreement with the findings of Taverna et al. [20] in their studies on rtPA glycopeptides. Further, they support the idea that the resolution induced by addition of putrescine is not only caused by a reduction of the electroosmotic flow but also by ion-pair formation with rFVIIa itself.

3.3. Optimization of the CE separation buffer pH

The influence of buffer pH was investigated in the pH interval 7–9. Optimum separation was achieved around pH 8. At pH ca. 7 the resolution was more or less lost. The reason for this could be that rFVIIa carries a low electrical net charge at this pH. By CE analysis in pure phosphate buffer, pH ca. 7 (without putrescine), rFVIIa behaves in a similar manner (not shown). The separation was not improved when buffer pH was raised to about 9.

3.4. Repeatability of the CE separation of rFVIIa glycoforms

Fig. 2, which shows run nos. 2, 4, 6 and 8 out of eight consecutive runs of the same FVIIa sample, using the same separation buffer, clearly demonstrates that the repeatability of the separation is excellent. However, frequent replacement of the separation buffer was required. With extensive use of the same separation buffer we observed that the resolution gradually became worse. Simultaneously the UV background was increased and the analyte turned yellow. An electrochemical oxidation of putrescine into a six-membered cyclic azo-structure is a possible explanation of these observations.

3.5. Specificity of putrescine

To test whether the separation obtained by adding putrescine to the phosphate buffer was a specific effect of putrescine, we repeated the analysis replacing putrescine with cadaverine (1,5-diaminopentane). Analysis of the rFVIIa sample using respectively putrescine and cadaverine as buffer additive is shown in Fig. 3. Clearly the separation pattern obtained by either of the two additives is essentially the same. This indicates that not only putrescine but probably a larger group of α,ω-diaminoalkanes are potential ion-pair reagents.

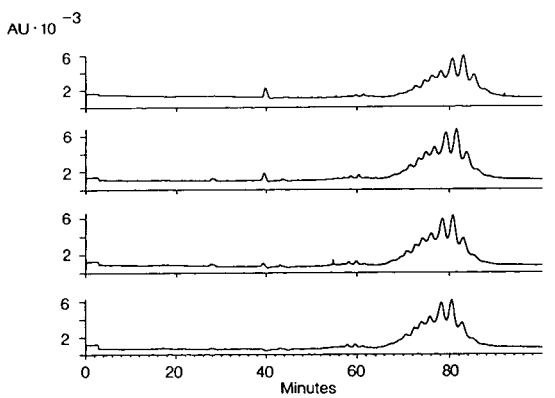

Fig. 2. Repeatability of the separation of rFVIIa glycoforms by capillary electrophoresis. The figure shows from top to bottom analysis nos. 2, 4, 6 and 8 of the same sample. The separation buffer was 100 m*M* phosphate, 25 m*M* putrescine, pH 8.0. A voltage of 4.5 kV was applied on a 45-cm long capillary.

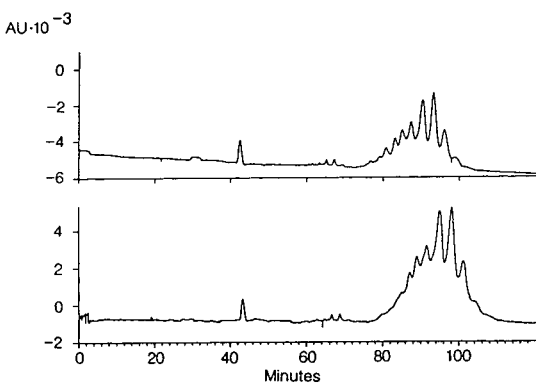

Fig. 3. Separation of rFVIIa glycoforms by capillary electrophoresis in a 45-cm long capillary using 100 m*M* phosphate buffer, pH 8.0, containing either 25 m*M* putrescine (upper panel) or 25 m*M* cadaverine (lower panel) as buffer additive. The separation was performed in a 45-cm long capillary and with a voltage of 4–5 kV.

3.6. CE analysis of native and neuraminidase treated rFVIIa

As the separation in free zone electrophoresis is based upon differences in the mass-to-charge ratio of the analytes, it was assumed that the observed resolution of rFVIIa was related to the different content of Neu5Ac of the individual glycoforms. Studies on rtPA [18] and r-HuEPO [24] supported this assumption. The CE analysis of rFVIIa before and after treatment with neuraminidase is shown in Fig. 4. It is obvious that the removal of Neu5Ac gives a much simpler peak profile of rFVIIa and a shorter migration time than the native protein. By removal of the Neu5Ac residues positioned terminally on the oligosaccharide structures a reduction is obtained in the net negative charge of the individual glycoforms as well as in the charge heterogeneity of the glycoform population. Reduction of the net negative charge leads to an increase in migration rate and reduction in charge heterogeneity results in a peak profile that is much less broad, and both effects are observed for rFVIIa (Fig. 4). This supports the idea that the peak cluster represents glycoforms of rFVIIa having different numbers of Neu5Ac residues. Some heterogeneity of neuraminidase treated rFVIIa is obviously still present. Since extended neuraminidase treatment gave no further change in the peak profile (not shown), it is concluded that the remaining heterogeneity is not caused by incomplete removal of Neu5Ac.

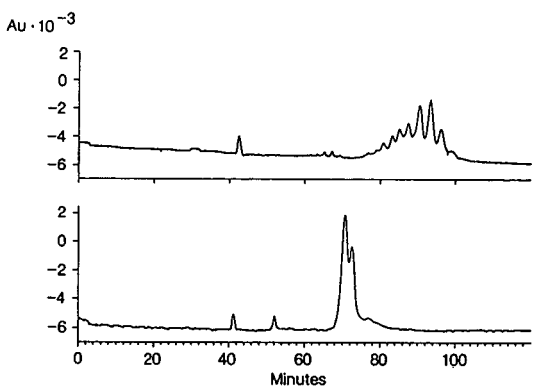

Fig. 4. Capillary electrophoresis of rFVIIa before and after treatment with sialidase. The separation was performed in 100 m*M* phosphate with 25 m*M* putrescine, pH 8.0, using a 45-cm long capillary and a voltage of 5 kV. Top panel: native rFVIIa. Bottom panel: sialidase treated rFVIIa.

3.7. RP-HPLC analysis of tryptic Asn322 glycopeptides from native and from neuraminidase treated rFVIIa

In RP-HPLC of the tryptic peptides from native rFVIIa, the glycopeptides containing the Asn322 glycosylation site elute as several distinct peaks (Fig. 5). These glycopeptide peaks have previously been characterized to be the rFVIIa glycopeptide fragment 317–326 (i.e. Val-Gly-Asp-Ser-Pro-Asn(glycosylated)-Ile-The-Glu-Tyr) and the separation has been shown to be based on the content of Neu5Ac in the oligosaccharide structures linked to the peptide so that with increasing retention time the number of Neu5Ac residues decrease [33]. In comparison, the tryptic Asn322 glycopeptides from neuraminidase treated rFVIIa elute as two peaks only (Fig. 5). Since we have no indication of incomplete removal of Neu5Ac, separation by RP-HPLC analysis of the desialylated glycopeptides is apparently based on other differences in the oligosaccharide structures than the content of Neu5Ac. Similar results have been obtained by RP-HPLC of the Asn145 glycopeptides (not shown).

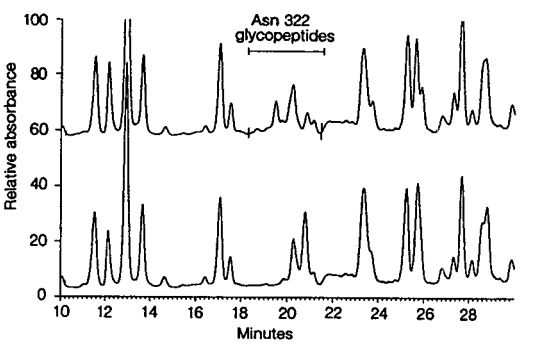

Fig. 5. Reversed-phase HPLC separation of tryptic peptides from native rFVIIa (top) and from neuraminidase treated rFVIIa (bottom). The peaks corresponding to the glycopeptides containing the heavy chain N-glycosylated site Asn322 are marked Asn322 glycopeptides. The separation conditions are described in Section 2.3.

3.8. HPAEC/PAD analysis of oligosaccharides from native and from neuraminidase treated rFVIIa

The HPAEC analysis of the oligosaccharides released from rFVIIa samples was performed at high pH using conditions similar to those originally described by Townsend and co-workers [7,34]. Using HPAEC it is possible to obtain a separation not only based on the content of Neu5Ac in the oligosaccharides but, in addition, a further separation based on the oxyanion formation of the neutral part of the oligosaccharides [5,7,8,34]. In HPAEC of the oligosaccharides from native rFVIIa and of the oligosaccharides from desialylated rFVIIa separation into 5–8 peaks is obtained for both samples (Fig. 6). The oligosaccharide peaks OS-A and OS-B (Fig. 6) were collected and subjected to neuraminidase treatment. While untreated OS-A and OS-B eluted as expected from the preparative run, the neuraminidase treated oligosaccharides for both oligosaccharides resulted in two peaks, one coeluting with Neu5Ac and one coeluting with a corefucosylated biantennary reference structure (not shown) (OS-C). Based on the relative amounts of Neu5Ac found after neuraminidase treatment, it is concluded that OS-A and OS-B are corefucosylated biantennary structures with two and one Neu5Ac residues, respectively. It is noteworthy that rFVIIa glycosylation shows considerably microheterogeneity also with regard to the desialylated structures (Fig. 6).

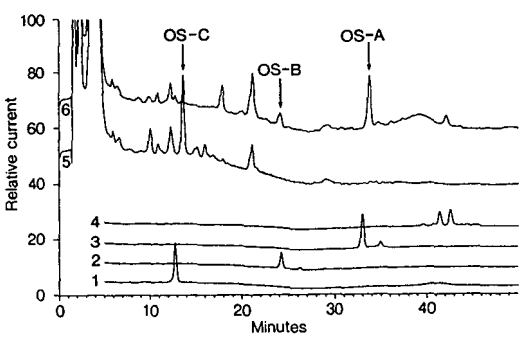

Fig. 6. High-pH anion-exchange HPLC separation of from top to bottom: (trace 6) oligosaccharides from native rFVIIa, (trace 5) oligosaccharides from neuraminidase treated rFVIIa, (trace 4) trisialylated triantennary oligosaccharide standard (C-335300), (trace 3) disialylated biantennary oligosaccharide standard (C-224300), (trace 2) monosialylated biantennary oligosaccharide standard (C-124300), (trace 1) Neu5Ac. Two oligosaccharides, labelled OS-A and OS-B, from native rFVIIa were purified and characterized as described in the text. The peak labelled OS-C corresponds to the desialylated forms of OS-A and OS-B. The oligosaccharide standards contain oligosaccharides with Neu5Ac linked either α2–3 or α2–6, and can therefore give more than one peak. Detection was pulsed amperometric. The separation conditions are described in Section 2.4.

4. Conclusion

Separation of the glycoforms of rFVIIa into six peaks or more has been obtained by CE, using phosphate as separation buffer with 1,4-diaminobutane as buffer additive. The separation has been shown to be related primarily to differences in the content of Neu5Ac of the rFVIIa glycoforms. Techniques for RP-HPLC separation of the rFVIIa tryptic glycopeptides containing the N-glycosylated sites and for HPAEC separation of the rFVIIa oligosaccharides released by hydrazinolysis have been established. The CE and the HPLC separations have been used for characterization of native and neuraminidase treated rFVIIa. Although the neuraminidase treatment, as expected, reduces the heterogeneity, significant peak separation is obtained by all three analyses for the neuraminidase treated sample. Characterization of this heterogeneity will be the subject of further studies using the potentials of CE and HPLC.

Acknowledgements

The authors wish to thank Anne-Lis Morsing Boeje and Mette Marie Thomsen for their excellent technical assistance.

Abbreviations

rFVIIa	Activated recombinant human factor VII

RP-HPLC	Reversed-phase high-performance liquid chromatography
HPAEC	High-pH anion-exchange chromatography
PAD	Pulsed amperometric detection
CE	Capillary electrophoresis
CZE	Capillary zone electrophoresis
EOF	Electroendosmotic flow
Neu5Ac	N-Acetyl-neuraminic acid
r-HuEPO	Recombinant human erythropoietin
rtPA	Recombinant tissue plasminogen activator

References

[1] L. Thim, S. Bjoern, M. Christensen, E.M. Nicolaisen, T. Lund-Hansen, A.H. Pedersen and U. Hedner, Biochemistry, 27 (1988) 7785–7793.

[2] S. Bjoern, D.C. Forster, L. Thim, F.C. Wiberg, M. Christensen, Y. Komiyama, A.H. Pedersen and W. Kisiel, J. Biol. Chem., 266 (1991) 11051–11057.

[3] R.A. Dwek, C.J. Edge, D.J. Harvey and M.R. Wormald, Ann. Rev. Biochem., 62 (1993) 65–100.

[4] R.B. Parekh and T.P. Patel, TIBTECH, 10 (1992) 276–280.

[5] J.S. Rohrer, G.A. Cooper and R.R. Townsend, Anal. Biochem., 212 (1993) 7–16.

[6] A.W. Guzzetta, L.J. Basa, W.S. Hancock, B.A. Keyt and W.F. Bennett, Anal. Chem., 65 (1993) 2953–2962.

[7] R.R. Townsend, M.R. Hardy, D.A. Cumming, J.P. Carver and B. Bendiak, Anal. Biochem., 182 (1989) 1–8.

[8] P. Hermentin, R. Witzel, R. Doenges, R. Bauer, H. Haupt, T. Patel, R.B. Parekh and D. Brazel, Anal. Biochem., 206 (1992) 419–429.

[9] T. Patel, J. Bruce, A. Merry, C. Bigge, M. Wormald, A. Jaques and R. Parekh, Biochemistry, 32 (1993) 679–693.

[10] M. Nimtz, W. Martin, V. Wray, K.-D. Klöppel, J. Augustin and H.S. Conradt, Eur. J. Biochem., 213 (1993) 39–56.

[11] P.A. Haynes, M. Batley, R.J. Peach, S.O. Brennan and J.W. Redmond, J. Chromatogr., 581 (1992) 187–193.

[12] S.B. Yan, Y.B. Chao and H. Van Halbeek, Glycobiology, 3 (1993) 597–608.

[13] J. Frenz, C.P. Quan, J. Cacia, C. Democko, R. Bridenbaugh and T. McNerney, Anal. Chem., 66 (1994) 335–340.

[14] M.V. Novotny and J. Sudor, Electrophoresis, 14 (1993) 373–389.

[15] F. Kilár and S. Hjertén, Electrophoresis, 10 (1989) 23–29.

[16] F. Kilár and S. Hjertén, J. Chromatogr., 480 (1989) 351–357.

[17] F. Kilár and S. Hjertén, J. Chromatogr., 638 (1993) 269–276.

[18] K.W. Yim, J. Chromatogr., 559 (1991) 401–410.

[19] S.-L. Wu, G. Teshima, J. Cacia and W.S. Hancock, J. Chromatogr., 516 (1990) 115–122.

[20] M. Taverna, A. Baillet, D. Biou, M. Schlüter, R. Werner and D. Ferrier, Electrophoresis, 13 (1992) 359–366.

[21] P.D. Grossman, J.C. Colburn and H.H. Lauer, Anal. Chem., 61 (1989) 1186–1194.

[22] P.M. Rudd, I.G. Scragg, E. Coghill and R.A. Dwek, Glycoconjugate J., 9 (1992) 86–91.

[23] A.D. Tran, S. Park, P.J. Lisi, O.T. Huynh, R.R. Ryall and P.A. Lane, J. Chromatogr., 542 (1991) 495–471.

[24] E.F. Watson and F. Yao, Anal. Biochem., 210 (1993) 389–393.

[25] E.F. Watson and F. Yao, J. Chromatogr., 630 (1993) 442–446.

[26] J.P. Landers, R.P. Oda, B.J. Madden and T.C. Spelsberg, Anal. Biochem., 205 (1992) 115–124.

[27] H.H. Lauer and D. McManigill, Anal. Chem., 58 (1986) 166–170.

[28] F.S. Stover, B.L. Haymor and R.J. McBeath, J. Chromatogr., 470 (1989) 241–250.

[29] V. Rohlicek and Z. Deyl, J. Chromatogr., 494 (1989) 87–89.

[30] J.A. Bullock and L.-C. Yuan, J. Microcol. Sep., 3 (1991) 241–248.

[31] J. Bullock, J. Chromatogr., 633 (1993) 25–244.

[32] S. Hoffstetter-Kuhn, A. Paulus, E. Gassmann and H.M. Widmer, Anal. Chem., 63 (1991) 1541–1547.

[33] P.L. Weber, T. Kornfelt, N.K. Klausen and S.M. Lunte, Anal. Biochem., 225 (1995) 135–142.

[34] M.R. Hardy and R.R. Townsend, Proc. Natl. Acad. Sci. USA, 15 (1988) 3289–3293.

ELSEVIER

Journal of Chromatography A, 718 (1995) 203–210

JOURNAL OF CHROMATOGRAPHY A

Separation of tryptophan and related indoles by micellar electrokinetic chromatography with KrF laser-induced fluorescence detection

King C. Chan*, Gary M. Muschik, Haleem J. Issaq

SAIC Frederick, National Cancer Institute, Frederick Cancer Research and Development Center, P.O. Box B, Frederick, MD 21702, USA

First received 23 March 1995; revised manuscript received 24 May 1995; accepted 13 June 1995

Abstract

Micellar electrokinetic chromatography (MEKC) was applied for the separation of tryptophan and related indoles. Using a 5 m*M* sodium borate buffer (pH 9.2) containing 50 m*M* sodium dodecyl sulfate and 5% acetonitrile, eleven indoles were baseline separated in under 17 min. Most of the indoles were detected at the n*M* level by native fluorescence using KrF laser-induced fluorescence (LIF), which was approximately 100 times more sensitive than UV absorption detection at 200 nm. Preliminary results show that the MEKC–LIF with direct sample injection is a feasible method for assessing indole profiles in diluted urine and serum.

1. Introduction

In humans, tryptophan (TRP) is metabolized by two major pathways, either through kynurenine or a series of indoles [1]. Among the indoles (Fig. 1), 5-hydroxytryptamine (5-HT, serotonin) is pharmacologically the most active indole amine. These indoles are known to have important physiological and pathological properties. Abnormal metabolism of TRP has been observed in patients with bladder cancer [2], carcinoid syndrome [3], alcoholism [4], liver cirrhosis [5], psychiatric diseases [6], HIV infection [7], and acute rejection after renal transplant [8]. Therefore, measurement of TRP and/or its metabolites is essential in investigating and monitoring disease status.

High-performance liquid chromatography (HPLC) with various detection schemes has been widely used to determine TRP and related indoles in biological samples [9,10]. Using pre-column fluorescent derivatization with methoxyacetaldehydyde [11], phenylglyoxal [12,13], or 9-hydroxymethyl-β-carboline [14], TRP in serum, plasma, or brain tissue was selectively detected. Post-column fluorescent derivatization with benzylamine was also used for the selective detection of 5-hydroxyindoles in urine and serum [15,16]. However, these derivatization steps are not convenient and may not be quantitative. In general, TRP indoles have been detected mostly by electrochemistry [17–23] or native fluorescence [24,25]. Combinations of UV, electrochemical, or native fluorescence detection were

* Corresponding author.

SSDI 0021-9673(95)00675-3

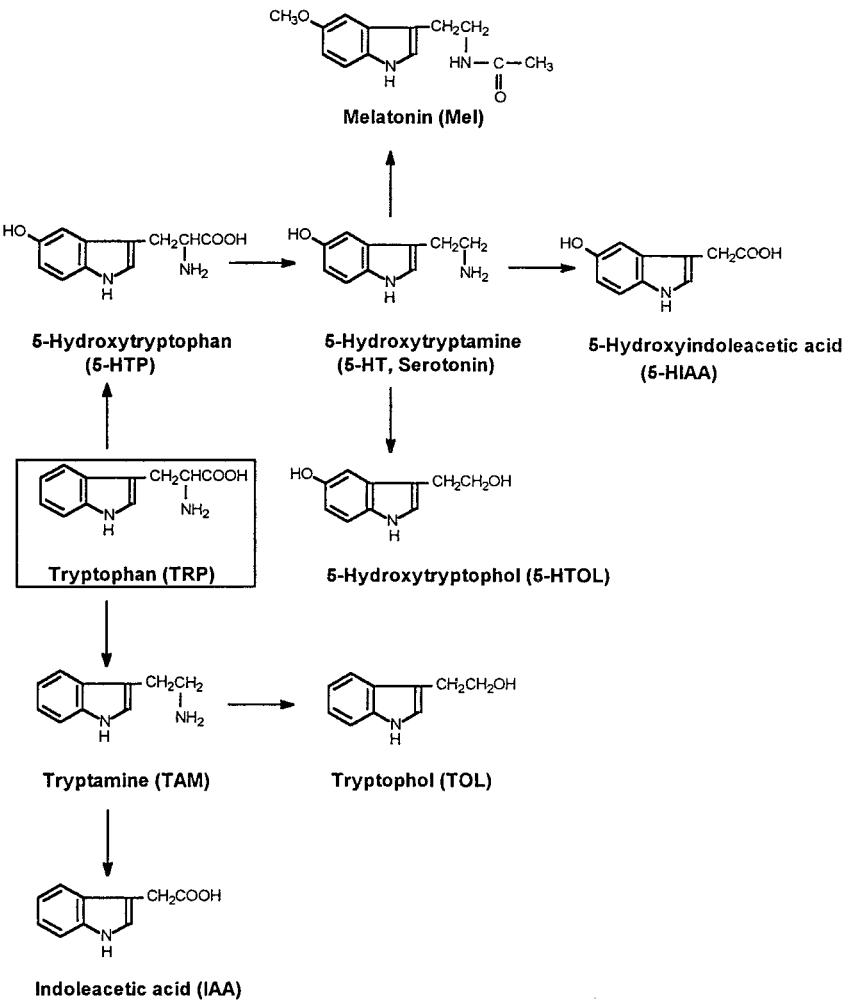

Fig. 1. Metabolic pathways of tryptophan.

also reported [8,26]. Gas chromatography–mass spectrometry (GC–MS) was also used to determine 5-hydroxyindoleacetic acid (5-HIAA) and indoleacetic acid (IAA) in biological samples, but the sample clean-up procedures before derivatization for GC separation were tedious [27].

Recent advances in capillary electrophoresis (CE) have made it an attractive separation tool alternative to HPLC [28]. CE has the advantages of versatility, rapid analysis, low-mass detectability, high-efficiency separation, and ease of operation. Among various CE modes, capillary zone electrophoresis (CZE) and micellar electrokinetic chromatography (MEKC) are widely used to separate charged and neutral molecules, respectively. When CE is coupled to laser-induced fluorescence (LIF), detection of attomole amounts is achieved [29].

The aim of this study was to apply MEKC for the separation of TRP and its indolic metabolites. Since TRP-related indoles fluoresce when

excited by UV light (Fig. 2), the detection sensitivity of the indoles using LIF with a KrF laser (248 nm) as the excitation source was evaluated. Finally, the feasibility of using MEKC–LIF for achieving indole profiles in urine and serum was investigated.

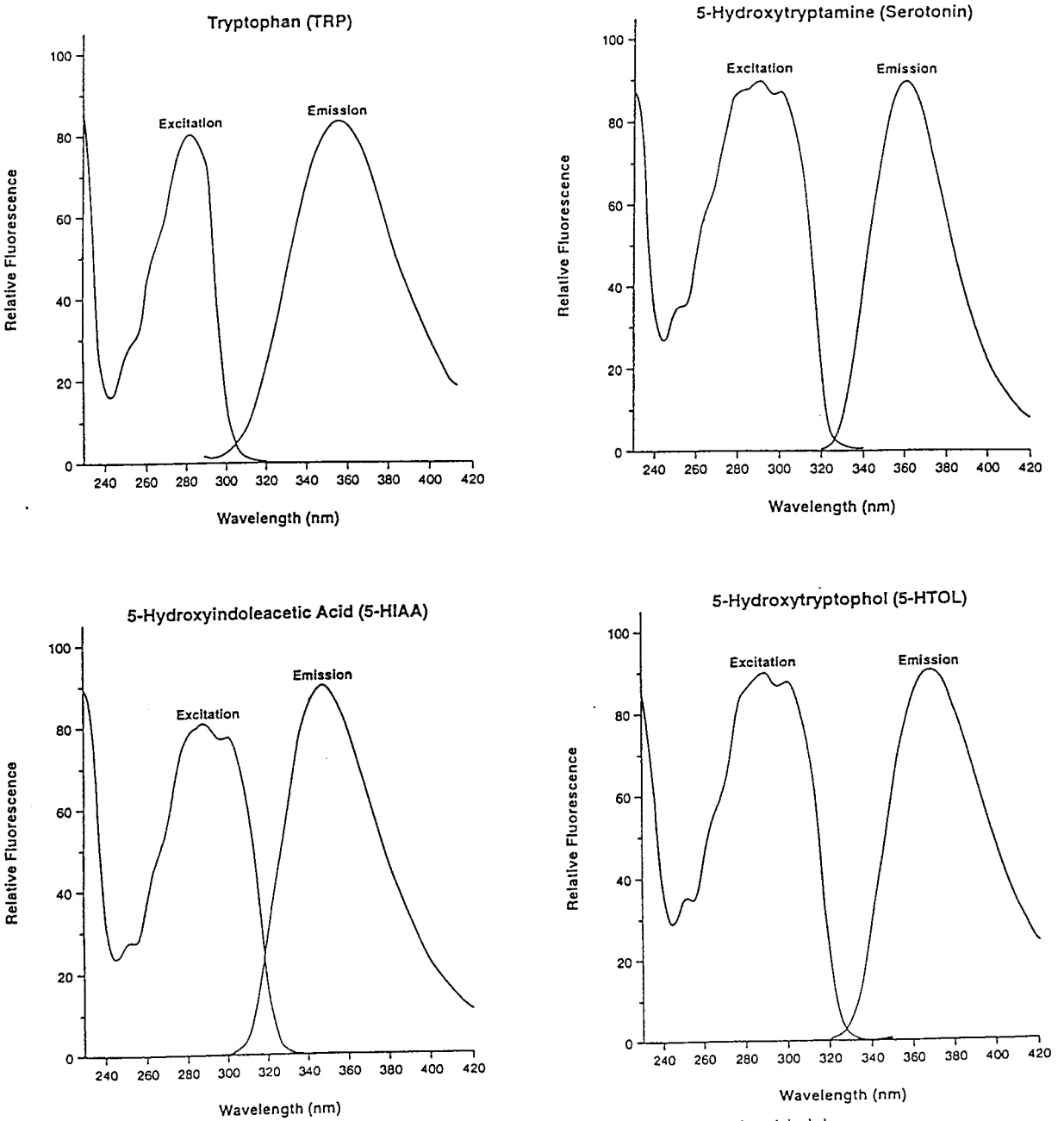

Fig. 2. Excitation and emission spectra of tryptophan and some related indoles.

2. Experimental

2.1. Apparatus

Experiments using UV detection were carried out with a Beckman P/ACE 2050 CE systems. Separations were performed at 25°C with a 67 cm × 50 μm I.D. (60 cm to detector) fused-silica capillary (Polymicro Technologies, Phoenix, AZ, USA). Each new capillary was washed with 0.1 *M* NaOH and deionized water each for 15 min before use. Samples were injected into the capillary by applying pressure (0.5 p.s.i. = 3447.38 Pa) for 5 s. The capillary was then flushed with the running buffer for 1 min between runs.

In the LIF experiments, high voltage and pressure for CE operations were supplied by a Crystal 310 CE module obtained from ATI/Unicam (Boston, MA, USA). Separations were performed at room temperature with a 67 cm × 50 μm I.D. (60 cm to detector) fused-silica capillary. Samples were injected into the capillary by applying pressure (30 mbar) for 6 s. The home-built LIF detection system was described previously [30]. Fluorescence excitation was provided by a compact, pulsed laser operating at 248 nm (Model GX-500, Potomac, Lanham, MD, USA). The laser beam was first passed through an interference filter centered at 248 nm and then focused onto a capillary with a 50-mm focal-length bi-convex lens. The emission was collected at a 90° angle to the incident laser beam with a 10×, N.A. = 0.5, microscope objective (Carl Zeiss, Thornwood, NY, USA). After passing through an UG-1 bandpass filter (Melles Griot, Irvine, CA, USA), the collected emission was detected by a photomultiplier tube (PMT, Model 70680, Oriel, Stratford, CT, USA). The current output of the PMT was fed into a boxcar averager (Model 4100, EG&G, Princeton, NJ, USA) and its voltage output was displayed on a PC computer via an A/D interfacing module (Model 406, Beckman Instruments, Fullerton, CA, USA). In a typical experiment, a laser pulse rate of 1 kHz with an averaged excitation power of 0.5 mW was used. Excitation and emission spectra of the indoles (in water) were obtained with a Perkin-Elmer LS3 spectrofluorometer.

2.2. Chemicals

TRP, 5-hydroxytryptophan (5-HTP), 5-HIAA, 5-hydroxytryptophol (5-HTOL), 5-HT, IAA, 5-methoxytrytophan (5-MTP), tryptophol (TOL), melatonine (MEL), tryptamine (TAM), and N-acetyl-tryptophan (NAT) were obtained from Sigma (St. Louis, MO, USA). A stock solution of individual indole was prepared in methanol (2 mg/ml) and stored at −20°C when not in use. The injected standard mixture was prepared by mixing the individual stock, followed by dilution with water. Sodium tetraborate and sodium dodecyl sulfate (SDS) was obtained from Fluka (Ronkonkoma, NY, USA). Urine and serum samples were diluted 200-fold with water before injections.

3. Results and discussion

The tryptophan metabolites contain either acidic, basic, neutral, or zwitterionic groups. Partial separations of some of indoles were achieved by CZE using a 5 m*M* sodium borate buffer (pH 9.2), as shown in Fig. 3A. The basic indoles (TAM and 5-HT) migrated first, while the acidic indoles (5-HIAA and IAA) migrated last. TRP, 5-HTP, and 5-MTP were not separated due to their similar electrophoretic mobilities. Also, the neutral indoles (5-HTOL, MEL, TOL) all migrated as one peak because uncharged molecules are not separated by CZE. MEKC was developed initially for the resolution of neutral molecules [31]. The method is based on the differential affinities of analytes for the hydrophobic core of micelles which serves as a pseudo-stationary phase for separation. Because the TRP-related indoles have different natures, they were effectively separated by MEKC. Using a borate buffer containing 50 m*M* SDS, ten of the eleven indoles were separated (Fig. 3B). In comparison to CZE, 5-HT and TAM migrated last in MEKC, probably due to the strong electrostatic interaction between the negatively charged SDS micelles and the positively charged 5-HT and TAM.

The addition of an organic solvent is commonly used to enhance resolution in MEKC [32–34].

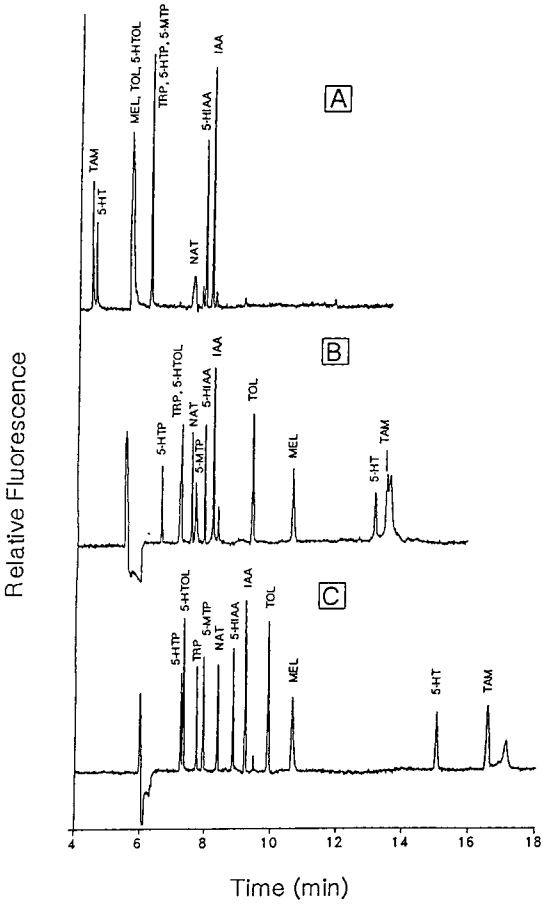

Fig. 3. Electropherograms for the separation of eleven tryptophan-related indoles using different buffers. Buffers: (A) 5 m*M* sodium borate (pH 9.2); (B) 5 m*M* sodium borate (pH 9.2) and 50 m*M* SDS; and (C) 5 m*M* sodium borate (pH 9.2), 50 m*M* SDS, and 5% acetonitrile. Capillary: 67 cm × 50 μm. Voltage: 20 kV.

Organic solvent reduces electroosmotic flow by increasing the viscosity of the running buffer, consequently widening the migration window. In this study, addition of 5% acetonitrile to the micellar buffer allowed the separation of TRP from 5-HTOL, and improved the resolution of most indoles (Fig. 3C). The distributions of NAT and 5-MTP into the SDS micelles were also affected by acetonitrile, resulting in their migration order reversal. In addition, the 5-MTP peak was sharpened, which was probably due to its higher solubility in organic solvent. All of the eleven indoles were baseline separated in about 17 min. Although these indoles also were separated by HPLC [3], the analysis time was rather long (ca. 50 min).

When excited by UV light, TRP and its related indoles fluoresce with excitation and emission maximums at ca. 288 nm and 350–370 nm, respectively (Fig. 2). Since the KrF laser operates at 248 nm, it is not an ideal excitation source for the indoles. Nevertheless, TRP was detected at the n*M* level by KrF-LIF in our previous CZE study using a 75 μm I.D. capillary [30]. In this MEKC study with a 50-μm capillary, high sensitivity detection for the indoles was also obtained. Fig. 4A shows the KrF-LIF detection of 90 ng/ml of each indole, which is about 100-fold more sensitive than the absorption detection at 200 nm (Fig. 4B). In Fig. 4A, the signal-to-noise ratio (*S*/*N*) ranged from 62 to 190, which

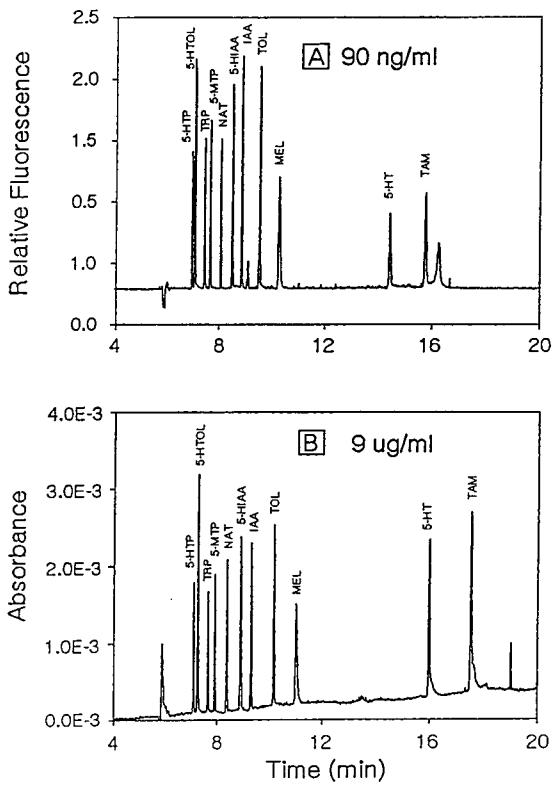

Fig. 4. Detections of tryptophan and related indoles. (A) KrF-LIF detection, 90 ng/ml of each indole; and (B) UV detection (200 nm), 9 μg/ml of each indole. Buffer: 5 m*M* sodium borate (pH 9.2), 50 m*M* SDS, and 5% acetonitrile. Capillary: 67 cm × 50 μm. Voltage: 20 kV.

Table 1
The limits of detection of tryptophan and related indoles using KrF-LIF detection

	Analyte	LOD (n*M*)
1	5-HTP	7.4
2	5-HTOL	5.5
3	TRP	7.3
4	5-MTP	5.6
5	NAT	6.1
6	5-HIAA	5.8
7	IAA	5.5
8	TOL	6.3
9	MEL	8.7
10	5-HT	13.7
11	TAM	11.9

Buffer: 5 m*M* sodium borate (pH 9.2), 50 m*M* SDS, and 5% acetonitrile. Capillary: 67 cm × 50 μm. Voltage: 20 kV. Signal-to-noise ratio = 2.

correspond to the limits of detection (LOD) ranging from 5.5 to 13.7 n*M* for the indoles ($S/N = 2$, Table 1). The detection sensitivity is expected to improve with an UV laser operating at 284 nm [35], which is currently not available in this laboratory.

Kema et al. [3] have recently used HPLC to assess the indoles profiles in urine, platelet-rich plasma, and gut-tissue, and they found that the amounts of TRP, 5-HIAA, and 5-HT in carcinoid patients were significantly different from that of normal patients. Alternatively, it is also feasible to use MEKC to obtain the indole profiles in biological samples. Fig. 5A shows the MEKC electropherogram of a diluted normal urine sample with direct sample injection. A few major peaks were observed. The TRP and 5-HIAA peaks in the urine were tentatively identified by matching the migration times of standards and by spiking the sample with standards (Fig. 5B). Other indoles in the diluted normal sample were not detected because of their low concentrations. Fig. 6A shows the MEKC electropherogram of a diluted normal serum with direct sample injection. The broad peak at 11 min was serum protein. As with the urine sample, TRP in the serum sample was tentatively identified by matching the migration times of standards and by spiking (Fig. 6B). The fluores-

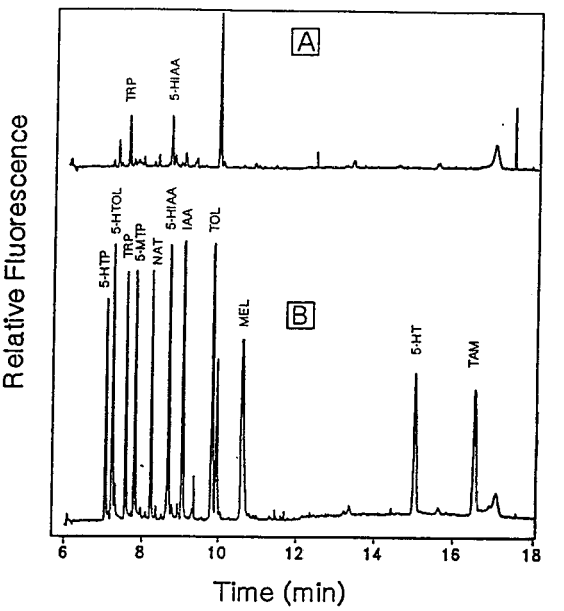

Fig. 5. Electropherograms for the MEKC of (A) urine, and (B) urine fortified with 90 ng/ml of each indole standard. The urine was diluted 200-fold with water before injection. Running conditions were the same as in Fig. 4A.

cence intensity of an emitting molecule is easily affected by the matrix, which may be significant for the direct injection of biological samples. Since diluted samples (200-fold) were used in this study, the above-mentioned effect was minimal, as judged by the similar fluorescence intensity of the indoles in the standard and spiked samples. Also, serum protein did not interfere with the detection of the indoles because most of them were separated from the protein.

4. Conclusion

MEKC using SDS micelles is a suitable method for the separation of TRP and related indoles. Most of the indoles were detected by native fluorescence at the n*M* level using KrF-LIF, which eliminates the need for chemical derivatization to obtain sensitive detection. Preliminary results show that MEKC–LIF is a feasible method for assessing the indole profiles in biological samples such as urine and serum.

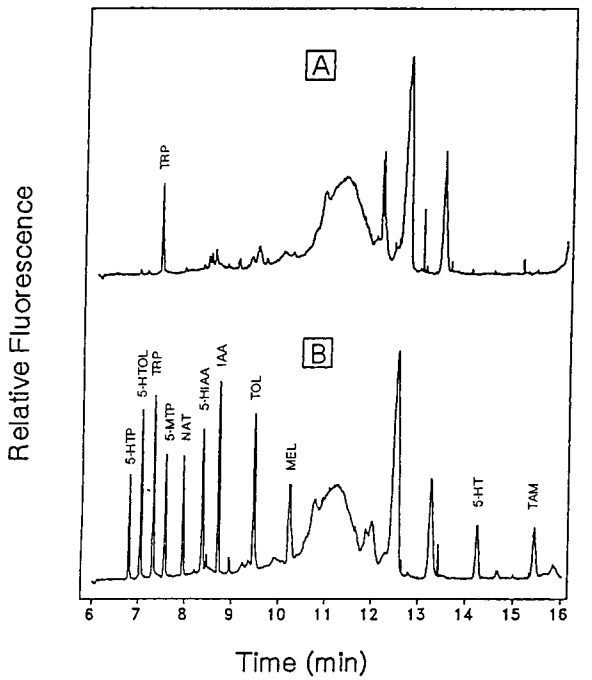

Fig. 6. Electropherograms for the MEKC of (A) serum, and (B) serum fortified with 90 ng/ml of each indole standard. The serum was diluted 200-fold with water before injection. Running conditions were the same as in Fig. 4A.

Studies involving pathological samples and quantitation are being investigated.

Acknowledgement

The content of this publication does not necessarily reflect the views or policies of the Department of Health and Human Services, nor does mention of trade names, commercial products, or organizations imply endorsement by the U.S. Government.

References

[1] C.R. Scriver, A.L. Beaudet, W.S. Sly and D. Valle (Editors), The Metabolic Basis of Inherited Disease, McGraw-Hill, New York, 6th ed., 1989, p. 2515.
[2] M. Bizzarri, A. Catizone, M. Pompei, L. Chiappini, L. Curini and A. Lagana, Biomed. Chromatogr., 4 (1990) 24.
[3] I.P. Kema, A.M.J. Schellings, C.J.M. Hoppenbrouwers, H.M. Rutgers, E.G.E. deVries and F.A.J. Muskiet, Clin. Chim. Acta, 221 (1993) 143.
[4] L. Branchey, S. Shaw and C.S. Lieber, Life Sci., 29 (1981) 2751.
[5] E. Rocchi, F. Farina, M. Silingardi and G. Casalgrandi, J. Chromatogr., 380 (1986) 128.
[6] R.B. Minderaa, G.M. Anderson, F.R. Volkmar, G.W. Akkerhuis and D.J. Cohen, Biol. Psychiatry, 22 (1987) 933.
[7] D. Fuchs, A. Forsman, L. Hagberg, M. Larsson, G. Norkrans, G. Reibnegger, E.R. Werner and H. Wachter, J. Interferon. Res., 10 (1990) 599.
[8] E.W. Holmes, P.M. Russell, G.J. Kinzler and E.W. Bermes, Jr., Clin. Chim. Acta, 227 (1994) 1.
[9] P.M.M. VanHaard and S. Pavel, J. Chromatogr., 429 (1988) 59.
[10] A.C. Deacon, Ann. Clin. Biochem., 31 (1994) 215.
[11] H. Iizaka and T. Yajima, Biol. Pharm. Bull., 16 (1993) 103.
[12] E. Kojima, M. Kai and Y. Ohkura, J. Chromatogr., 612 (1993) 187.
[13] E. Kojima, M. Kai and Y. Ohkura, Anal. Sci., 9 (1993) 25.
[14] S. Inoue, T. Tokuyama and K. Takai, Anal. Biochem., 132 (1983) 468.
[15] J. Ishida, R. Iizuka and M. Yamaguchi, Analyst, 118 (1993) 165.
[16] J. Ishida, R. Iizuka and M. Yamaguchi, Clin. Chem., 39 (1993) 2355.
[17] F.C. Cheng, J.S. Kuo, W.H. Chang and D.J. Juang, J. Chromatogr., 617 (1993) 227.
[18] F.C. Cheng, L.L. Yang, F.M. Chang, L.G. Chia and J.S. Kuo, J. Chromatogr., 582 (1992) 19.
[19] M. Radjaipour, H. Raster and H.M. Liebich, Eur. J. Clin. Chem. Clin. Biochem., 32 (1994) 609.
[20] A. Helander, O. Beck, M. Wennberg, T. Wikstrom and G. Jacobsson, Anal. Biochem., 196 (1991) 170.
[21] N.E. Zoulis, D.P. Nikolelis and C.E. Efstathiou, Analyst, 115 (1990) 291.
[22] Y. Sagara, Y. Okatani, S. Yamanaka and T. Kiriyama, J. Chromatogr., 431 (1988) 170.
[23] D.D. Koch and P.T. Kissinger, J. Chromatogr., 164 (1979) 441.
[24] I. Morita, M. Kawamoto, M. Hattori, K. Eguchi, K. Sekiba and H. Yoshida, J. Chromatogr., 529 (1990) 367.
[25] J.D. Jong, U.R. Tjaden, E. Visser and W.H. Meijer, J. Chromatogr., 419 (1987) 85.
[26] I. Morita, M. Kawamoto and H. Yoshida, J. Chromatogr., 576 (1992) 334.
[27] B.A. Davis, D.A. Durden and A.A. Boulton, J. Chromatogr., 374 (1986) 227.
[28] C.A. Monnig and R.T. Kennedy, Anal. Chem., 66 (1994) 280R.
[29] H.E. Schwartz, K.J. Ulfelder, F.-T.A. Chen and S.L. Pentoney, Jr., J. Cap. Elec., 1 (1994) 36.
[30] K.C. Chan, G.M. Janini, G.M. Muschik and H.J. Issaq, J. Liq. Chromatogr., 16 (1993) 1877.

[31] S. Terabe, K. Otsuka, K. Ichikawa, A. Tsuchiya and T. Ando, Anal. Chem., 56 (1984) 111.
[32] R.O. Cole and M.J. Sepaniak, LC–GC, 10 (1992) 380.
[33] R.D. Holland and M.J. Sepaniak, Anal. Chem., 65 (1993) 1140.
[34] T. Yashima, A. Tsuchiya, O. Morita and S. Terabe, Anal. Chem., 64 (1992) 2981.
[35] H.T. Chang and E.S. Yeung, Anal. Chem., 67 (1995) 1079.

ELSEVIER

Journal of Chromatography A, 718 (1995) 211–215

JOURNAL OF CHROMATOGRAPHY A

Use of capillary zone electrophoresis in an investigation of peptide uptake by dairy starter bacteria ☆

Ian L. Moore[a], Graham G. Pritchard[a], Don E. Otter[b,*]

[a] *Department of Chemistry and Biochemistry, Massey University, Palmerston North, New Zealand*

[b] *Food Science Section, New Zealand Dairy Research Institute, Private Bag 11029, Palmerston North, New Zealand*

First received 7 February 1995; revised manuscript received 31 May 1995; accepted 8 June 1995

Abstract

A capillary zone electrophoresis (CZE) method to separate the peptide series val-gly$_n$, where n is 1 to 4, has been evaluated and compared to separation by reversed-phase high-performance liquid chromatography (RP-HPLC). The method was able to quantitate peptides present at very low concentrations (down to 0.05 mM) with high reproducibility and accuracy and was capable of separating peptides differing in size by only a single glycine residue. It could also separate the peptides val-gly and leu-gly which differed in only a single side-chain methylene group. The method was fast, required small sample volumes, and proved to be superior to RP-HPLC. The suitability of the CZE method to analyze peptide uptake by dairy starter bacteria is discussed.

1. Introduction

In the manufacture of cheese from milk, starter bacteria (*Lactococcus lactis*) convert large amounts of lactose to lactic acid, acidifying the milk and facilitating the formation of milk curds. For these starter bacteria to grow to the high cell densities required to sustain this lactic acid production they must obtain peptides and amino acids from the hydrolysis of the casein milk protein [1]. The metabolites are acquired by the activity of a complex proteolytic system, a key step of which is the transport of the casein-derived peptides into the bacterial cell [2,3]. It is presently not known whether the relatively large peptides (average length 11 residues) produced by the initial degradation of casein by a cell-wall-associated proteinase can be transported into the cell intact or only after further degradation by extracellular peptidases.

The rate of peptide transport into whole cells is generally calculated by measuring the uptake of synthetic peptides by the starter bacteria. Whilst reversed-phase high-performance liquid chromatography (RP-HPLC) has been used previously for the analysis of changes in the levels of these peptides [4–6] this method is slow, requires relatively large sample volumes and often cannot resolve closely related peptides.

The present paper reports the use of a capillary zone electrophoresis (CZE) method to separate and measure synthetic peptides belonging to the homologous series val-gly$_n$, where n is from 1 to 4. The peptide series was based on valine as this amino acid is essential to the growth of the *L. lactis* strain used in this study [7]. For the

* Corresponding author.

☆ Presented at the *3rd International Symposium on Capillary Electrophoresis, York, 24–26 August 1994.*

0021-9673/95/$09.50
SSDI 0021-9673(95)00654-0

purposes of this study on peptide uptake, the analytical method used was required to resolve peptides from background interference, to differentiate between peptides differing in size by only one amino acid residue and to differentiate between peptides differing by only one side-chain group. The ability of a CZE method to fulfil these criteria was examined.

2. Experimental

2.1. Chemicals

All buffers, glucose and trifluoroacetic acid (TFA) were of analytical grade or better and were obtained from either BDH Chemicals (Poole, UK) or Sigma (St. Louis, MO, USA). Water was purified by reverse osmosis followed by deionization (Milli-Q, Millipore, Bedford, MA, USA). The peptides val-gly, val-gly_2 and leu-gly were obtained from Sigma; the remaining peptides (val-gly_3 and val-gly_4) were synthesized using an Applied Biosystems (Foster City, CA, USA) 430A peptide synthesizer.

2.2. Peptide uptake experiment

Peptide uptake experiments were performed by growing bacterial cells (*Lactococcus lactis*) in a chemically defined medium until the mid-exponential phase (4 h) and then suspending them in phosphate buffer solution. After maintaining the cells in buffer for 10 min, glucose was added to a final concentration of 0.2%. After a further 15 min the peptide(s) of interest was added (final concentration 1 m*M*). Samples were taken over a 60 to 120 min time course and TFA (final concentration 1%) was added to each sample to stop further peptide uptake. The cells were then removed by centrifugation (MSE Microcentaur bench centrifuge at 11 600 *g* for 5 min) and the supernatant frozen until analyzed by HPLC or CE.

2.3. Capillary electrophoresis

Capillary zone electrophoresis (CZE) was performed on an Applied Biosystems 270A-HT CE system (Foster City, CA, USA) using a PE Nelson 900 series interface and a PE Nelson TurboChrom 3.3 software package (Cupertino, CA, USA) for data acquisition and analysis, respectively. The uncoated capillary (72 cm total length, 50 cm effective length and 50 μm internal diameter) was supplied by Applied Biosystems. Filtered samples were injected at the anode using vacuum (17 kPa) for 2.5 s. The buffer system was 20 m*M* sodium citrate, pH 2.5, at 30°C and the separation voltage was 30 kV with detection by absorbance at 200 nm. Between injections the capillary was flushed for 2 min (68 kPa) consecutively with 0.1 *M* NaOH, Milli-Q water and buffer to retain separation reproducibility.

2.4. HPLC

Reversed-phase HPLC (RP-HPLC) was performed on a Philips PU4100 HPLC (Philips, Eindhoven, Netherlands) with a Vydac (Hesperian, CA, USA) 218TP C_{18} column (250 × 4.6 mm I.D.; pore size, 10 μm; pore diameter, 30 nm). The eluate was monitored by absorbance at 220 nm using a Philips PU4110 UV–Vis detector. Samples were separated using an isocratic gradient of 0.1% TFA in Milli-Q water.

3. Results and discussion

3.1. Comparative analysis of val-gly_3 using RP-HPLC and CZE

The RP-HPLC chromatogram of the separation of val-gly_3 from the other components present in the supernatant of the bacterial cell suspension is shown in Fig. 1a. Due to its low hydrophobicity the val-gly_3 peptide interacted weakly with the reversed-phase matrix and eluted soon after the non-retained material. Whilst the val-gly_3 peak was resolved from the other peaks, there was considerable background noise which reduced the sensitivity. There was also interference from other peptides leaked from the bacterial cells and, when other val-gly_n peptides were used, some overlap with these other peptides (data not shown).

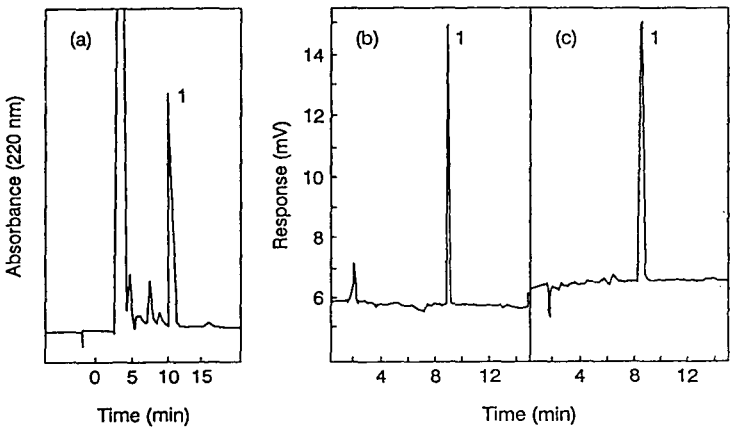

Fig. 1. Separation of val-gly$_3$ by (a) RP-HPLC, (b) CZE and (c) CZE in the presence of 1% TFA. Conditions for chromatography and CE were as in the Experimental section. Peak 1 was val-gly$_3$.

In contrast to the RP-HPLC chromatogram, the CZE electropherogram (Fig. 1b) showed that migration of the val-gly peptide through the capillary was retarded by the separation conditions such that it was well resolved from other material found in the cell suspension and that it was a very sharp peak. When 1% TFA was included in the samples taken from the bacterial cell suspension to inhibit further peptide uptake, the separation of the val-gly$_3$ peptide was not seriously affected (Fig. 1c). Whilst the val-gly$_3$ peak was not as sharp as in the absence of TFA, there was still good resolution and reproducibility.

The CZE method, therefore, gave excellent separation of the tetrapeptide val-gly$_3$ from contaminating material both in the presence and absence of 1% TFA. It also had the advantages over the RP-HPLC method of having a total assay time, including washing and regenerating the capillary, of 20 min compared with 60 min for the RP-HPLC method, and of requiring only small amounts of sample (20 μl for CZE versus 100–200 μl for RP-HPLC).

Overall these results reinforce previous studies that have compared the use of CZE and RP-HPLC to separate peptides [8,9]. The two methods are best described as orthogonal with the CZE selectivity based on peptide charge and mass and the RP-HPLC separation based on the relative hydrophobicity of the peptides. Whilst this provides a degree of complementarity between the two techniques, in the present case the CZE method was deemed to be superior to RP-HPLC due to its quicker separation, greater resolution and higher sensitivity.

3.2. Separation of peptides differing in size by one amino acid

When determining what size of peptides could be transported into the bacterial cell it was deemed to be essential that the assay method should be able to accurately separate peptides which differed in size by as little as one amino acid residue. Using the CZE method (Fig. 2) there was baseline separation of a series of val-gly$_n$ peptides where $n = 1$ to 4. This series was generated during the synthesis of the pentapeptide val-gly$_4$ with the peptides val-gly, val-gly$_2$ and val-gly$_3$ appearing as contaminants that resulted from the incomplete coupling to the solid-phase. As neither val nor gly have a charged side-chain, the separation was presumed to be based on both the change in the charge-to-size ratio of the peptide and changes in the local hydrophobic environment as successive gly residues are introduced.

3.3. Separation of peptides differing by one amino acid

The ability of dipeptides structurally related to val-gly to inhibit the uptake of val-gly was

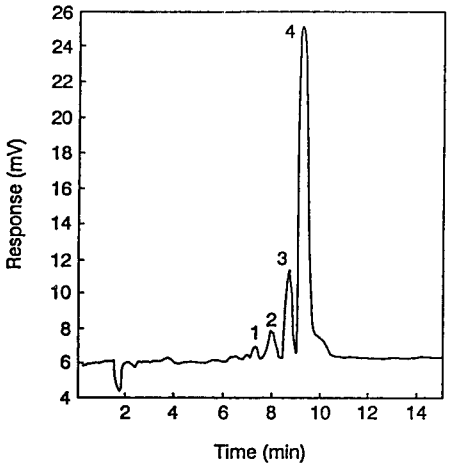

Fig. 2. Separation of the peptide series val-gly$_n$ where n is 1 to 4 by CZE. Conditions for electrophoresis were as in the Experimental section. Peaks: 1 = val-gly, 2 = val-gly$_2$, 3 = val-gly$_3$ and 4 = val-gly$_4$.

investigated to provide evidence for competition between peptides for a single peptide transport system.

The ability of the CZE method to separate the dipeptides val-gly and leu-gly is shown in Fig. 3. Although these two dipeptides differ in only a single side-chain methylene group they could be resolved, presumably due to the slight difference in their relative hydrophobicity. Whilst baseline resolution of the two peaks was not fully achieved, the migration times were very reproducible and, in the absence of 1% TFA, the peaks were a lot sharper and the resolution higher (data not shown).

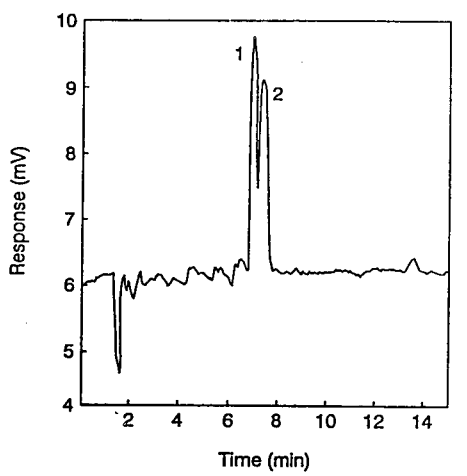

Fig. 3. Separation of val-gly and leu-gly by CZE. Electrophoresis was performed as described in the Experimental section. Peaks: 1 = val-gly, 2 = leu-gly.

3.4. Time course of peptide uptake

Another requirement of the analytical method was the ability to quantitate peptide uptake by the bacterial cells during a time-course experiment. In Fig. 4a a series of electropherograms taken during a 100-min val-gly$_3$ peptide uptake experiment have been overlaid. There was excellent reproducibility in the elution times of the solvent peak at approximately 1.8 min and the val-gly$_3$ peak at approximately 8.2 min. Accurate measurement of the val-gly$_3$ levels were possible down to very low peptide levels as the background noise was low. This high sensitivity was apparent in the plot of val-gly$_3$ concentration against incubation time (Fig. 4b), which showed a linear uptake of the peptide over an 80-min period and down to very low peptide concentrations (<0.05 mM).

4. Conclusion

Capillary zone electrophoresis is an excellent method for measuring peptide uptake by bacterial cell suspensions as it has the ability to resolve peptides that differ by a single gly residue, it can resolve peptides that differ in only one single side-chain methylene group and it has a high degree of reproducibility of peak areas between repeat samples, thus enabling a quantitative measurement of very low concentrations of peptide to be determined and hence the rate of peptide uptake to be calculated. The CZE method has the advantages over RP-HPLC of having a faster analysis time, requiring a smaller sample volume and also being able to resolve the peptides of interest from other compounds which coeluted with these peptides when using HPLC.

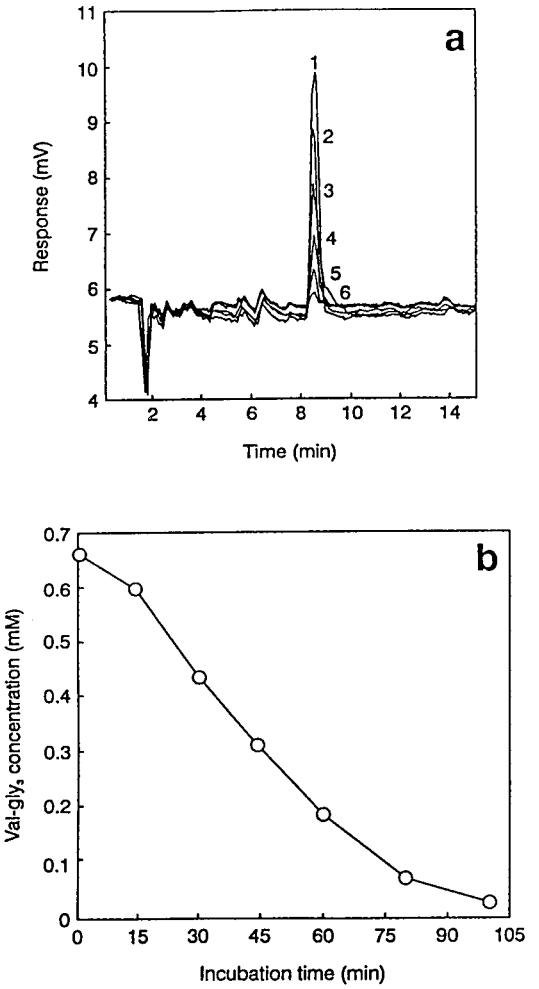

Fig. 4. Time-course of val-gly$_3$ uptake by bacterial cells. Uptake experiments and CE were performed as described in the Experimental section. Samples in (a) were taken at times: 1 = 15 min, 2 = 30 min, 3 = 45 min, 4 = 60 min, 5 = 80 min and 6 = 100 min. Val-gly$_3$ concentrations (b) were calculated from the peak areas and the initial val-gly$_3$ concentration.

References

[1] O.E. Mills and T.D. Thomas, N.Z. J. Dairy Sci. Technol., 15 (1981) 43.
[2] E.J. Smid, Ph.D. Thesis, University of Groningen, Groningen, Netherlands, 1991.
[3] S. Tynkkynen, G. Buist, E. Kunji, J. Kok, B. Poolman, G. Venema and A. Haandrikman, J. Bacteriol., 175 (1993) 7523.
[4] Y.K. Zhang, N. Chan and L. Wang, Biomed. Chromatogr., 7 (1993) 75.
[5] E. Ylidez, G. Grübler, S. Hörger, H. Zimmermann, H. Echner, S. Stoeva and W. Voelter, Electrophoresis, 13 (1992) 683.
[6] A. van Boven and W.N. Konings, Biochimie, 70 (1988) 535.
[7] B. Reiter and J.D. Oram, J. Dairy Res., 29 (1962) 63.
[8] H.J. Issag, G.M. Janini, I.Z. Atamna, G.M. Mushik and J. Lukszo, J. Liq. Chromatogr., 15 (1992) 1129.
[9] L.M. Castognola, L. Cassano, R. Rabino, D.V. Rossetti and F.A. Bassi, J. Chromatogr., 572 (1991) 51.

ELSEVIER

Journal of Chromatography A, 718 (1995) 217–225

JOURNAL OF CHROMATOGRAPHY A

Determination of morphine and related alkaloids in crude morphine, poppy straw and opium preparations by micellar electrokinetic capillary chromatography

V. Craige Trenerry[a,*], Robert J. Wells[b], James Robertson[c]

[a]*S.A. Regional Laboratory, Australian Government Analytical Laboratories, 338–340 Tapleys Hill Road, Seaton 5023, Australia*

[b]*Australian Government Analytical Laboratories, 1 Suakin Street, Pymble, N.S.W. 2073, Australia*

[c]*Australian Federal Police, Weston, A.C.T. 2611, Australia*

First received 14 March 1995; revised manuscript received 23 May 1995; accepted 13 June 1995

Abstract

A rapid method for the determination of morphine and related alkaloids in crude morphine, poppy straw and opium preparations by micellar electrokinetic capillary chromatography (MEKC) has been developed. Morphine, codeine, thebaine, oripavine, papaverine, narcotine, narceine, cryptopine and salutaridine were separated in less than 10 min using a 70 cm × 50 μm I.D. uncoated fused-silica capillary column with a buffer consisting of 10% dimethylformamide, 90% 0.05 *M* cetyltrimethylammonium bromide, 0.01 *M* potassium dihydrogen orthophosphate, 0.01 *M* sodium tetraborate, pH 8.6. An applied voltage of −25 kV and a temperature of 28°C gave the best separation of the alkaloids. Pholcodine was used as the internal standard. The compounds were detected by UV at 254 nm. The levels of morphine and related alkaloids determined by MEKC were in good agreement with those determined by high-performance liquid chromatography (HPLC). The coefficients of variation for area calculation (%C.V.) for multiple sample and standard injections by MEKC were slightly greater than for HPLC but were still acceptable (morphine content of poppy straw: %C.V. MEKC 1.7%, %C.V. HPLC 0.3%).

1. Introduction

Analytical procedures based on the relatively new technique of micellar electrokinetic capillary chromatography (MEKC) are rapidly gaining acceptance as rugged analytical methods that are suitable for use in analytical laboratories with high sample throughput [1–6]. In MEKC, the electrophoretic buffer is modified with an ionic surfactant to provide a phase for chromatographic separation [7]. MEKC separations exhibit superior resolution to high-performance liquid chromatography (HPLC) separations, have the same order of repeatability and are faster and less costly to operate than HPLC methods [8]. Both anionic and cationic surfactants have been used as micelle modifiers to separate mixtures that cannot be easily separated using traditional capillary zone electrophoresis (CZE) [8]. Sodium dodecyl sulphate (SDS) and cetyltrimethylammonium bromide (CTAB) are often used as surfactants for

* Corresponding author.

0021-9673/95/$09.50
SSDI 0021-9673(95)00670-2

MEKC. The addition of an organic solvent (e.g. methanol, acetonitrile, dimethylsulphoxide) to the buffer can also affect the separation of complex mixtures [8].

Weinberger and Lurie [9] separated a wide range of illicit substances by MEKC with a phosphate–borate buffer modified with acetonitrile and SDS. This separation showed the excellent separating potential and resolving power of MEKC. We recently reported the separation and quantitation of diacetylmorphine (heroin), acetylcodeine, O^6-monoacetylmorphine, morphine, codeine, papaverine and narcotine and a number of other compounds found in illicit heroin seizures by MEKC using a phosphate–borate buffer modified with CTAB and acetonitrile. The compounds were separated in less than 13 min and the method was far superior to the isocratic HPLC method that was currently used in our laboratory for the routine testing of illicit heroin seizures [1]. We extended this work to the separation of a number of components of illicit cocaine seizures [2]. Both illicit heroin and cocaine seizures could be analysed with the same electrophoretic conditions: the settings on the UV detector were all that needed to be altered. A small change in the acetonitrile content of the buffer gave complete separation of other naturally occurring alkaloids as well as additives/adulterants of the illicit cocaine seizures.

The success of our work with heroin and cocaine prompted us to extend this work to the analysis of crude morphine, poppy straw and opium preparations. High-performance liquid chromatography (HPLC) with UV–Vis detection as the determinative step is the method of choice for the quantitative determination of morphine and related alkaloids found in crude morphine preparations, poppy straw and opium [10–12]. However, the run times are reasonably long. It was of interest to see if MEKC would give a superior separation of the alkaloids found in crude morphine, poppy straw and opium preparations and provide a faster and less costly analysis with comparable quantitative results to HPLC [10].

2. Experimental

2.1. Reagents

Morphine, codeine, papaverine hydrochloride, narceine, cryptopine, salutaridine, thebaine, oripavine and pholcodine were obtained from the Curator of Standards, Australian Government Analytical Laboratories (N.S.W., Australia). Cetyltrimethylammonium bromide was obtained from Sigma Chemical (St. Louis, MO, USA). The poppy straw was a gift from Glaxo Australia (Port Fairy, Vic., Australia). All other chemicals and solvents were AR grade or HPLC grade and used without further purification.

2.2. MEKC buffer

Amounts of 0.05 *M* CTAB buffers were prepared by dissolving 0.92 g CTAB in 50 ml of a 1:1 mixture of 0.01 *M* sodium tetraborate and 0.01 *M* potassium dihydrogen orthophosphate. The pH of the solution was 8.6. Then 2.5 ml of dimethylformamide was added to 22.5 ml of the buffer and the solution filtered through a 0.8-μm PTFE filter disc before use.

2.3. Apparatus

MEKC

The samples were analysed with an uncoated fused-silica capillary column (70 cm × 50 μm I.D.) with an effective length to the detector of 45 cm (Polymicro Technologies, AZ, USA), using an Isco Model 3140 Electropherograph (Isco, Lincoln, NE, USA) operating at −25 kV and at 28°C. The sample solutions were loaded under vacuum (vacuum level 2, 10 kPa · s) and the alkaloids were detected at 254 nm at 0.005 AUFS (absorbance units full scale). The detector response was linear to 1 mg/ml for morphine and codeine, and 0.2 mg/ml for oripavine, thebaine, papaverine and narcotine. The capillary was flushed with running buffer for 2 min between analyses. Also, the running buffer was replaced after 20 analyses. The capillary was cleaned on a weekly basis by washing with 0.1 *M*

sodium hydroxide for 10 min followed by de-ionised water for 10 min before filling with running buffer. Electropherograms were recorded with either the ICE Data Management and Control Software supplied with the Electropherograph or a HP 3350 Laboratory Data System (Hewlett-Packard, Palo Alto, CA, USA). Peak areas were used in the calculations.

HPLC

The analyses were performed with a Model 501 HPLC pump, Model 712 WISP and a Model 484 tunable absorbance UV detector using a 250 × 4.6 mm stainless-steel column filled with 10-μm Spherisorb CN packing material equipped with a CN pre-column. A mobile phase consisting of a 100:10:5 mixture of 1% w/v aqueous ammonium acetate (adjusted to pH 5.8 with 10% acetic acid), acetonitrile and dioxane at a flow-rate of 1.5 ml/min was used for the analyses. The compounds were detected at 254 nm at 0.05 AUFS.

Peak areas obtained from a HP 3350 Laboratory Data System (Hewlett-Packard) were used in the calculations.

2.4. Samples and standards for MEKC and HPLC

Samples

The crude morphine preparations were dissolved in 0.01 *M* HCl. For MEKC analysis, pholcodine was added as an internal standard at a final concentration of 0.4 mg/ml.

Opium and opium dross was extracted using the procedure of Srivastava and Maheshawari [13]. Essentially, 1 g of opium was extracted with 20 ml of 2.5% acetic acid and then made up to volume (100 ml) with water. For the opium dross, 1 g of sample was extracted with 2.5% acetic acid (5 × 20 ml) and the solutions combined. The solutions were filtered and 20 ml added to 60 ml of water. The pH of the solution was adjusted to 9.2 with concentrated ammonia solution and the solution was then extracted with chloroform (6 × 50 ml). The chloroform was dried over sodium sulphate and the solvent removed in vacuo with a rotary evaporator. The residue was dissolved in 5 ml of 0.05 *M* HCl. Then 1 ml of this solution was diluted to 5 ml with de-ionised water for MEKC and HPLC analysis. For MEKC analysis, pholcodine was added as an internal standard at a final concentration of 0.4 mg/ml.

The poppy straw was extracted with (a) lime-water, (b) 5% acetic acid solution and (c) soxhlet extraction with 30% ethanol in chloroform.

(a) Lime-water extraction [14]. An amount of 100 ml of de-ionised water was added to 8 g of finely milled poppy straw and 2 g of calcium hydroxide and the mixture shaken vigorously for 25 min. The mixture was filtered and 20 ml was diluted with 60 ml of de-ionised water. The pH of the solution was adjusted to 9.2 with 10% acetic acid and then extracted with 25% ethanol in chloroform (5 × 50 ml). Care had to be exercised to avoid the formation of emulsions. The combined extracts were washed with de-ionised water (2 × 30 ml) and then dried with sodium sulphate. The solvent was removed in vacuo with a rotary evaporator. The residue was dissolved in 25 ml of 0.05 *M* HCl. For MEKC analysis, 9 ml of the solution was diluted with 1 ml of internal standard solution (4 mg/ml) and filtered before analysis. For HPLC analysis, 1 ml of the solution was diluted to 5 ml with de-ionised water.

(b) Acetic acid (5%) extraction [13]. An amount of 100 ml of 5% acetic acid was added to 8 g of finely milled poppy straw and the mixture shaken vigorously for 25 min. The mixture was filtered and 20 ml was diluted with 60 ml of de-ionised water. The pH of the solution was adjusted to 9.2 with concentrated ammonia solution and then extracted with chloroform (5 × 50 ml). The combined extracts were washed with de-ionised water (2 × 30 ml) and then dried with sodium sulphate. The solvent was removed in vacuo with a rotary evaporator. The residue was dissolved in 25 ml of 0.05 *M* HCl. Then 1 ml of this stock solution was diluted to 5 ml with de-ionised water for HPLC analysis. For MEKC analysis, 9 ml of the stock solution was diluted with 1 ml of

internal standard solution (4 mg/ml) and filtered before analysis.

(c) ethanol in chloroform (30%) extraction. An amount of 8 g of finely milled poppy straw was extracted with 120 ml of 30% ethanol in chloroform in a soxhlet extractor for 6 h. Then 25 ml was removed and taken to dryness with a rotary evaporator. The residue was dissolved in 10 ml 0.05 *M* HCl. Then 2 ml of this stock solution was diluted to 5 ml with de-ionised water for HPLC analysis. For MEKC analysis, 0.5 ml of internal standard solution (4 mg/ml) was added to 2 ml of the stock solution and the volume made to 5 ml with de-ionised water and filtered before analysis.

Standards

Standard solutions were prepared in 0.01 *M* HCl for both MEKC and HPLC. The solutions were filtered before analysis. Pholcodine was added as the internal standard at a final concentration of 0.4 mg/ml for MEKC analyses. No internal standard was used for the HPLC analyses.

3. Results and discussion

The separation and quantitation of the components of illicit heroin seizures (heroin, acetylcodene, O^6-monoacetylmorphine, morphine, codeine, papaverine and narcotine) by MEKC was accomplished using a 75 cm × 75 μm I.D. uncoated fused-silica capillary column with a buffer consisting of 10% acetonitrile–90% 0.05 *M* CTAB, 0.01 *M* potassium dihydrogen orthophosphate, 0.01 *M* sodium tetraborate, pH 8.6 [1]. Morphine and codeine, the major alkaloids found in *Papaver somniferium* poppies, were reasonably well separated, as were the alkaloids papaverine and narcotine. Thebaine and oripavine are two other important alkaloids found in various amounts in poppy straw, opium and crude morphine preparations [12,14]; however, they are not found in illicit heroin seizures as they rearrange when the crude morphine/opium is converted to heroin with hot acetic anhydride [15]. Narceine, cryptopine and salutaridine are also present in various amounts in *Papaver somniferium* poppies. Initial attempts to separate the alkaloids on a 50-μm uncoated fused-silica column with the buffer used for the analyses of illicit heroin seizures were encouraging. Increasing the amount of acetonitrile to 12.5% resulted in near-baseline separation of the alkaloids (Fig. 1C). The separation of the alkaloids, except for oripavine and cryptopine, was maintained over twenty repetitive injections. Pholcodine was well separated from the other alkaloids and was therefore suitable for use as the internal standard. Other organic modifiers were then tried in an attempt to achieve baseline separation of the alkaloids. Optimum separation was achieved when the acetonitrile was replaced with 27.5% methanol as the modifier (Fig. 1B). The separation was maintained over twenty repetitions. With this buffer, codeine migrated before morphine, however, the separation of oripavine and thebaine was not as pronounced. The run time for the separation increased from 10 to 15 min with this buffer. Dioxane and tetrahydrofuran were unsuitable as organic modifiers as morphine and codeine could not be completely separated. The buffer containing tetrahydrofuran was particularly unsuitable as the migration times of the alkaloids changed dramatically over repeated injections of the standard solution.

One of the features of CZE is that the buffers are transparent in the low UV range (210–220 nm). Detection at these wavelengths allows for increased sensitivity and has been exploited on a number of occasions [8]. Acetonitrile, methanol, dioxane and tetrahydrafuran are often the first choices as organic modifiers as buffers containing these solvents are UV transparent at 210–220 nm. Dimethylformamide, dimethylsulphoxide and hexamethylphosphoramide can also be used as organic modifiers but absorb UV light in the low UV range (<240 nm) and so have limited use when optimum sensitivity is required. In this work, the alkaloids were detected at 254 nm and so these compounds could be used as organic modifiers. Various amounts of these solvents with the CTAB buffer were tried. Optimum separation of the alkaloids was obtained with buffers

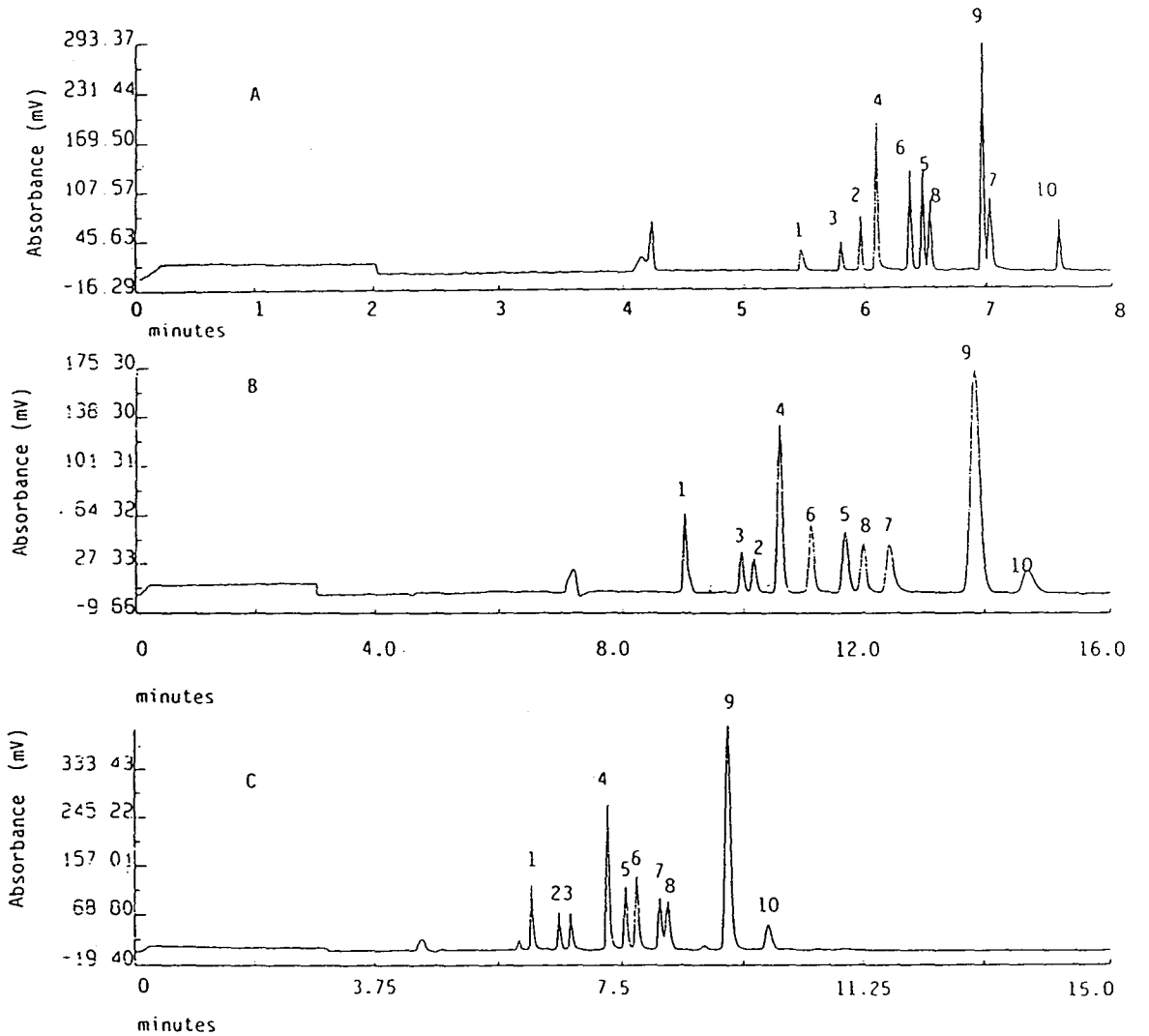

Fig. 1. Separation of (1) pholcodine, (2) morphine, (3) codeine, (4) salutaridine, (5) oripavine, (6) cryptopine, (7) narceine, (8) thebaine, (9) papaverine and (10) narcotine using a mixture of (A) 10% dimethylformamide (DMF) and 90% of a buffer consisting of 0.05 *M* CTAB and a 1:1 mixture of 0.01 *M* potassium dihydrogen orthophosphate and 0.01 *M* sodium tetraborate, pH 8.6, (B) 27.5% CH_3OH and 72.5% of a buffer consisting of 0.05 *M* CTAB and a 1:1 mixture of 0.01 *M* potassium dihydrogen orthophosphate and 0.01 *M* sodium tetraborate, pH 8.6, and (C) 12.5% CH_3CN and 87.5% of a buffer consisting of 0.05 *M* CTAB and a 1:1 mixture of 0.01 *M* potassium dihydrogen orthophosphate and 0.01 *M* sodium tetraborate, pH 8.6.

containing 20% dimethylsulphoxide, 5% hexamethylphosphoramide and 10% dimethylformamide. The buffer containing 10% dimethylformamide as the organic modifier gave the best separation of the ten alkaloids (Fig. 1A). This separation was extremely reproducible over twenty repetitive injections of a standard solution. Also, the separation of the alkaloids was quite consistent over the pH range 8.4 to 8.8, except for narceine, which migrated before papaverine below pH 8.5, and oripavine, which comigrated with cryptopine at pH 8.5 (Fig. 2). Minimal separation was seen when both dimethylformamide and CTAB were absent from the buffer. The addition of 0.05 *M* CTAB gave partial separation of the alkaloids, but complete

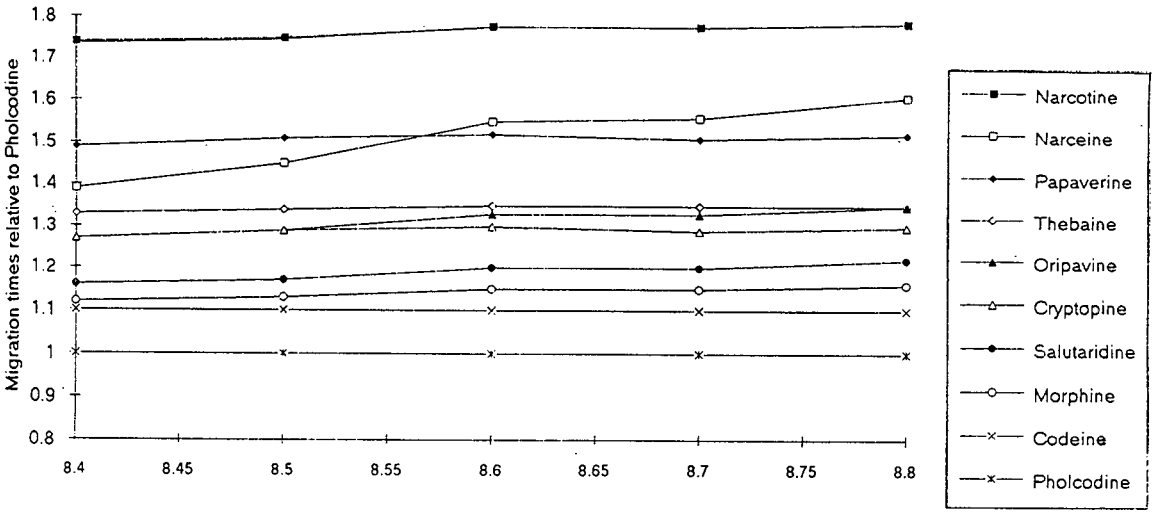

Fig. 2. Migration times of opium alkaloids relative to the internal standard using a buffer consisting of 10% DMF and 90% of 0.05 *M* CTAB and a 1:1 mixture of 0.01 *M* potassium dihydrogen orthophosphate and 0.01 *M* sodium tetraborate, pH 8.6. Results show change in migration times with variations of buffer pH.

separation was not achieved until the buffer contained 10% dimethylformamide.

The instrument repeatability data for area calculation (%C.V.) for seven consecutive injections of a number of standards of different concentrations were acceptable and are displayed in Table 1.

A number of crude morphine preparations that were available from a previous study [15] were analysed by MEKC and by HPLC [10]. The levels of the various alkaloids in the samples and the instrument repeatability for area calculation (%C.V.) data for seven repetitive injections for one sample are listed in Table 2. In general, there was a good agreement for the levels of the alkaloids determined by MEKC and HPLC in the samples. The MEKC run time was much faster than the HPLC run time (12 compared to 25 min). The amounts of the minor components of crude morphine preparations and the instrument repeatability data for area calculation (%C.V.) were more accurately determined by analysing more-concentrated solutions. The excellent separation of the alkaloids was main-

Table 1
Coefficient of variation for area calculation (%C.V.) for MEKC for standard solutions of varying concentrations

Concentration (mg/ml)	C.V. (%)					
	Codeine	Morphine	Oripavine	Thebaine	Papaverine	Narcotine
0.01	–	–	10	12	4.3	–
0.02	10	8.0	3.6	6.1	4.4	7.8
0.05	4.8	4.3	2.4	2.1	1.5	3.5
0.1	2.4	1.7	2.4	1.7	1.8	1.8
0.2	–	–	1.4	3.2	0.9	2.7
0.5	3.8	2.5	–	–	–	–
1.0	2.4	2.9	–	–	–	–

Buffer consisting of 10% DMF and 90% 0.05 *M* CTAB and a 1:1 mixture of 0.01 *M* potassium dihydrogen orthophosphate and 0.01 *M* sodium tetraborate, pH 8.6. %C.V. data obtained from seven replicate injections.

Table 2
Comparison of the quantitative results (%) and the %C.V. for area calculation for MEKC and HPLC for samples of crude morphine, poppy straw, opium and opium dross using a buffer consisting of 10% DMF and 90% 0.05 *M* CTAB and a 1:1 mixture of 0.01 *M* potassium dihydrogen orthophosphate and 0.01 *M* sodium tetraborate, pH 8.6. %C.V. data obtained from seven replicate injections of standard solutions

Sample	Codeine (%)		Morphine (%)		Oripavine (%)		Thebaine (%)		Papaverine (%)		Narcotine (%)	
	MEKC	HPLC	MEKC	HPLC	MEKC	HPLC	MEKC	HPLC	MEKC	HPLC	MEKC	HPLC
1-70	3.9	3.6	85.4	81.6	1.6	1.4	2.0	2.0	–	–	–	–
%C.V.[1]	9.0	0.6	4.3	0.3	4.1	0.8	6.4	0.9				
%C.V.[2]	1.8	–	–	–	0.9	–	1.0	–				
1-44C	5.5	5.9	62.4	58.2	1.6	1.9	1.4	1.4	–	–	–	–
1-49	1.0	0.8	67.3	61.9	–	–	–	–	–	–	–	–
1-54E	1.5	1.4	95.5	93.2	0.4	0.4	–	–	–	–	–	–
Poppy straw[3]	0.1	0.1	0.9	0.9	0.01	0.01	0.05	0.05	–	–	–	–
Poppy straw[4]	0.1	0.1	1.2	1.2	0.01	0.01	0.02	0.02	–	–	–	–
Opium[5]	5.3	4.7	11.5	9.9	–	–	2.0	1.7	0.5	0.4	0.4	0.6
Dross[5]	1.7	1.6	2.9	2.9	–	–	0.2	0.2	0.6	0.6	0.9	0.9

[1] 11.4 mg/10ml 0.01 *M* HCl.
[2] 51.5 mg/10ml 0.01 *M* HCl.
[3] Soxhlet extraction.
[4] Lime-water extraction.
[5] Acetic acid extraction.

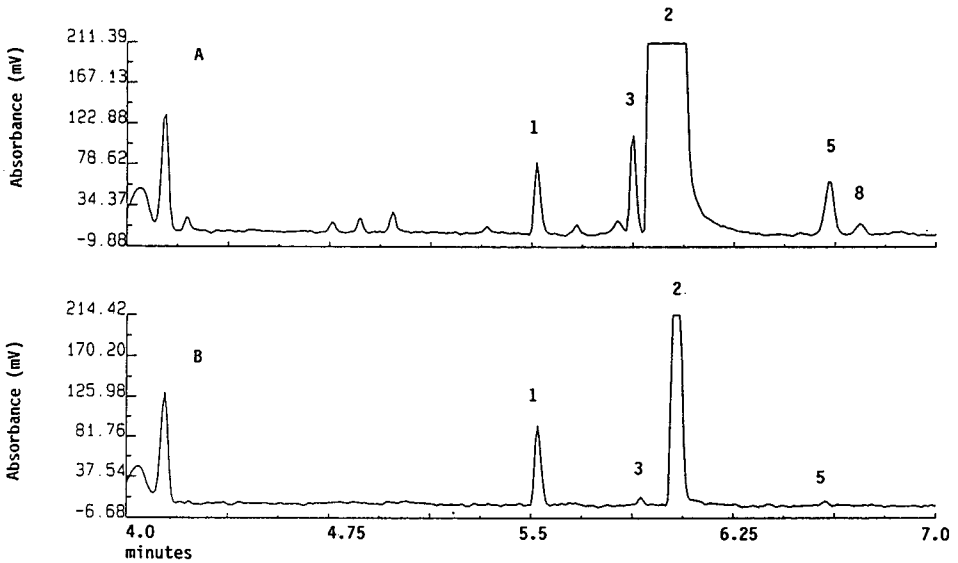

Fig. 3. Separation of morphine and related substances using a buffer consisting of 10% DMF and 90% of 0.05 *M* CTAB and a 1:1 mixture of 0.01 *M* potassium dihydrogen orthophosphate and 0.01 *M* sodium tetraborate, pH 8.6, for (A) a solution containing 15 mg/ml of sample 1-54 and (B) a solution containing 1 mg/ml of sample 1-54. Peak assignments as for Fig. 1.

tained even when a solution containing 15 mg/ml of crude morphine was loaded onto the column. The instrument repeatabilities (%C.V.) for codeine (3.1%) and oripavine (3.0%) in sample 1-54E were quite satisfactory for the low levels in the sample. The partial electropherograms showing the separation of codeine, morphine and oripavine in sample 1-54E at sample concentrations of 1 and 15 mg/ml are displayed in Fig. 3.

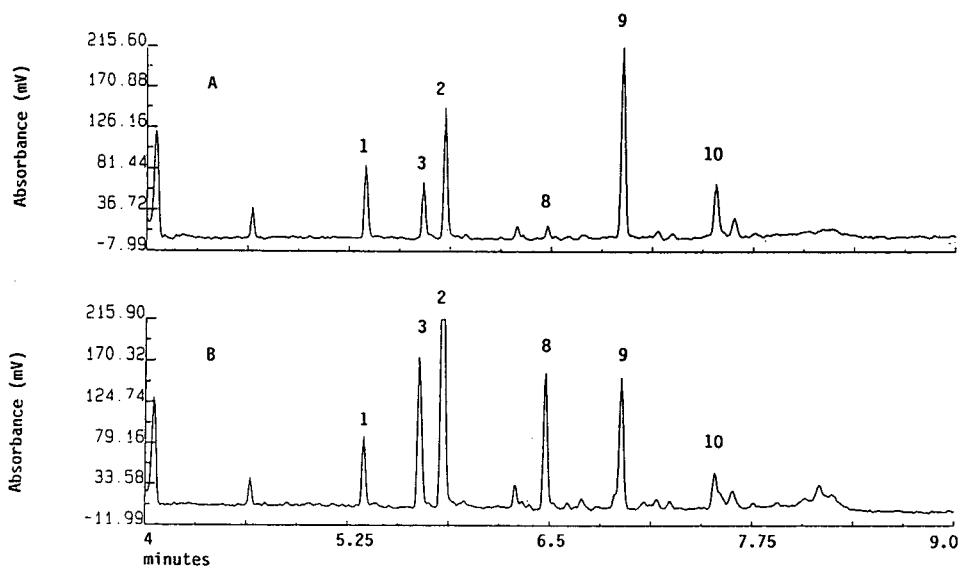

Fig. 4. Separation of morphine and related substances using a buffer consisting of 10% DMF and 90% of 0.05 *M* CTAB and a 1:1 mixture of 0.01 *M* potassium dihydrogen orthophosphate and 0.01 *M* sodium tetraborate, pH 8.6, for (A) a sample of opium dross and (B) a sample of opium. Peak assignments as for Fig. 1.

The procedure was then extended to the analysis of a sample of poppy straw, opium and opium dross. The materials were extracted with either lime-water, acetic acid or ethanol–chloroform and analysed by MEKC and HPLC. The levels of the alkaloids determined by MEKC and HPLC are displayed in Table 2 and are in good agreement. The different levels of alkaloids extracted from the poppy straw with the lime-water and the solvent extraction were due to the different extraction conditions used. Similar alkaloid profiles were obtained when the poppy straw was extracted with acetic acid. Partial electropherograms showing the excellent separation of the alkaloids in the opium and opium dross extracts are displayed in Fig. 4.

4. Conclusion

A rapid method for the separation and determination of alkaloids present in crude morphine, poppy straw and opium preparations by MEKC is described. The instrument repeatability for area calculation was acceptable, and the levels of the alkaloids in the samples were in good agreement with the levels determined by HPLC. The MEKC procedure is also faster and less costly to operate than the HPLC method.

Acknowledgements

The authors are grateful to the National Institute of Forensic Science, Forensic Drive, Macleod, Victoria 3085, Australia for the partial funding of this work and to Glaxo Australia for providing a sample of milled poppy straw and the Australian Government Analyst for his permission to publish.

References

[1] V.C. Trenerry, R.J. Wells and J. Robertson, J. Chromatogr. Sci., 32 (1994) 1.
[2] V.C. Trenerry, R.J. Wells and J. Robertson, Electrophoresis, 15 (1994) 103.
[3] I. Pant and V.C. Trenerry, Food Chem., 53 (1995) 219.
[4] C.O. Thompson and V.C. Trenerry, Food Chem., 53 (1995) 43.
[5] P.A. Marshall, V.C. Trenerry and C.O. Thompson, J. Chromatogr. Sci., (1995) in press.
[6] V.C. Trenerry, R.J. Wells and J. Robertson, J. Chromatogr. A, 708 (1995) 169.
[7] S. Terabe, K. Otsuka, K. Ichikawa, A. Tsuchiya and T. Ando, Anal. Chem., 56 (1984) 111.
[8] S.F.Y. Li, Capillary Electrophoresis, Principles, Practice and Applications, J. of Chromatogr. Library Ser., Vol. 52, Elsevier, Amsterdam, Netherlands, 1992.
[9] R. Weinberger and I.S. Lurie, Anal. Chem., 63 (1991) 823.
[10] Y. Nobuhara, S. Hirano, K. Namba and M. Hashimoto, J. Chromatogr., 190 (1980) 251.
[11] L.W. Doner and A.-F. Hsu, J. Chromatogr., 253 (1982) 120.
[12] P. Gomez-Serranillos, E. Carretero and A. Villar, Phytochem. Anal., 5 (1994) 5.
[13] V.K. Srivastava and M.L. Maheshawari, J. Assoc. Off. Anal. Chem., 64 (1985) 801.
[14] I. Dainis and M. Ronis, Australian Government Analytical Laboratories, National Research Report No. 106, 1983.
[15] I. Dainis, M. Ronis and V.C. Trenerry, Australian Government Analytical Laboratories, National Research Report No. 116, 1984.

ELSEVIER

Journal of Chromatography A, 718 (1995) 227–232

JOURNAL OF CHROMATOGRAPHY A

Determination of chloride complex of Au(III) by capillary zone electrophoresis with direct UV detection

Besnik Baraj[1], Ana Sastre*, Arben Merkoçi[1], María Martínez

Chemical Engineering Department, Universitat Politècnica de Catalunya, ETSEIB, Diagonal 647, E-08028 Barcelona, Spain

First received 24 March 1995; revised manuscript received 7 June 1995; accepted 9 June 1995

Abstract

Capillary zone electrophoresis was used for the determination of gold(III) chloride using direct UV detection at 220 nm. By using a capillary column 70 cm long, the optimum applied voltage was found to be around −7 kV; carrier solution containing 0.1 *M* HCl and 0.4 *M* NaCl was used as an additive. At this pH, the electroosmotic flow-rate appears to be almost zero. The effects of chloride concentration and the applied voltage on determination efficiency are discussed. Heat generation appeared negligible as the electric current and migration time were reproducible. The analytical performance is discussed in terms of the detection limit, linearity and reproducibility. A single trial was performed in 18 min. Under these conditions, Pd(II) and Pt(IV) can also be determined; the order of mobility in the electropherogram was as follows: $PdCl_4^{2-} > PtCl_6^{2-} > AuCl_4^-$. The method was applied to the monitoring of Au concentration during a study of $AuCl_4^-$ transport through solid-supported liquid membranes.

1. Introduction

In the last 5 years, the number of applications of capillary zone electrophoresis (CZE) has increased greatly, but the number of papers discussing CZE separations of inorganic cations has remained relatively low [1–3]. This technique offers rapid and efficient separation, being more matrix-independent than other existing techniques. Several ligands have been proposed for CZE analysis, including cyanide [4–6], EDTA [7,8], 8-hydroxyquinoline-5-sulfonic acid [9] and α-hydroxyisobutyric acid [10]. In each case, methods using a mainly basic or slightly acidic medium were described. Methods employed for the determination of Au are both numerous and heterogeneous [11–14]. Many use dyes as complexing agents following an extraction step, which makes the procedure time consuming and tedious. Atomic absorption spectrometry (AAS) or inductively coupled plasma spectrometry is currently used [15,16].

In a study by Aguilar et al. [6], cyanide was used as a ligand for the determination of gold(I) and silver(I) at pH 9.6 by CZE. The samples and carrier solution were prepared with almost the same conductivity, and consequently the stacking effect was not used. In addition, the ionic strength (0.01 *M* NaCN) was much lower than in the present work.

In this paper, the determination of gold(III) as the $AuCl_4^-$ complex is described. The formation of the gold chloride complex is supported by using HCl and NaCl in the carrier solution (pH

* Corresponding author.

[1] On leave from Faculty of Natural Sciences, Tirana University, Tirana, Albania.

0021-9673/95/$09.50
SSDI 0021-9673(95)00655-9

1) and in sample preparation (pH 1–2). A high ionic strength is usually undesirable since Joule heat is generated. To avoid this effect, a relatively moderate voltage was applied (below −10 kV). Enhancement of the detection limits was achieved by using stacking conditions.

The choice of low pH and high chloride concentration has two distinct advantages: (a) the gold(III) chloride complex is the predominant species and (b) as gold samples are normally dissolved in a strongly acidic medium, their determination by this procedure is convenient. The method was applied to the monitoring of Au concentration during a study of $AuCl_4^-$ transport through solid-supported liquid membranes. Results obtained by CZE were compared with those of AAS analysis.

2. Experimental

2.1. Instrumentation

An ISCO (Lincoln, NE, USA) Model 3850 integrated capillary electrophoresis system equipped with high voltage up to 30 kV and reversible polarity was used. Samples were introduced by applying a 3.4 kPa vacuum at the detector end of the capillary. Separations were performed with an unmodified fused-silica capillary column, 70 cm (50 cm to the UV detector) × 0.05 mm I.D. A Model 4270 integrator (Spectra-Physics, San José, CA, USA), was used to record all data. A Shimadzu UV-240 UV–Vis recording spectrophotometer was used to record the absorption spectra of the gold(III) chloride complex. The pH and the conductivity of the solutions were monitored with a Crison-Digilab 517 pH meter and a Crison 525 conductimeter, respectively. A Perkin-Elmer Model 2380 AAS system was used to determine the total concentration (by flame) of Au in the samples.

2.2. Reagents and solutions

A chloride stock standard solution of Au(III) was purchased from Merck. All other reagents were of analytical-reagent grade from Merck. Purified (18 MΩ) water, obtained using a Millipore Milli-Q water-purification system, was used to prepare all solutions. All solutions were filtered through a 0.45-μm membrane filter and degassed by ultrasound.

The carrier solution contained 0.1 *M* HCl and 0.4 *M* NaCl (conductivity ca. 65 mS cm^{-1}) and the samples were prepared with 10–70% carrier solution (conductivity 8–50 mS cm^{-1}).

2.3. Procedure for electrophoresis

The capillary tube was rinsed several times with deionized water, then equilibrated with carrier solution for 40 min before the first run. Both ends were dipped into two separate beakers filled with the same carrier solution. The sample solution was introduced into the cathodic end of the capillary by vacuum injection. Lastly, a negative voltage was applied. For determination of the electroosmotic flow-rate, negative and positive voltages were applied (using methanol as a marker). When finished, the CZE system must be cleaned carefully as the carrier solution used is corrosive.

3. Results and discussion

3.1. Gold chloride complex

Gold(III) produces species which are generally stable. Thus, gold(III) forms mixed complexes of chloride and hydroxide [17,18], depending on the pH and chloride concentration. The distribution diagram of Au(III), H^+ and Cl^- species in Fig. 1 shows that $AuCl_4^-$ is the predominant species at pH 1–2 for Cl^- concentrations higher than 0.01 *M* [19,20]. The absorption spectrum of this species (in 0.1 *M* HCl) showed a maximum around 220 nm, which is suitable for CZE determination with a UV detector.

3.2. CZE separation

In order to prevent hydrolysis of the chloride complex of Au(III), the pH of the carrier electrolyte was kept around 1 (0.1 *M* HCl), while 0.4

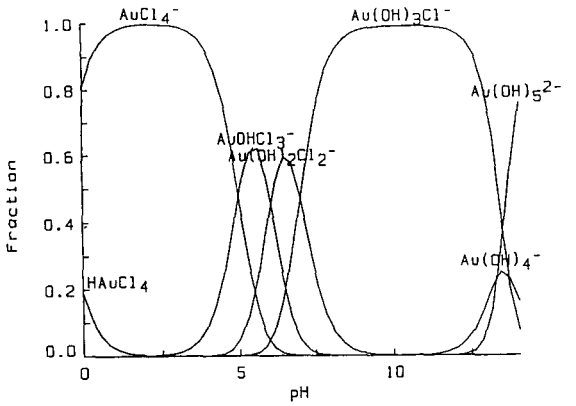

Fig. 1. Distribution species–pH diagram. Total gold(III) concentration, 10 μg ml^{-1}; 0.1 *M* Cl^-.

M sodium chloride was used as an additive. At such a high ionic strength, some optimization of the applied voltage was required to obtain low noise and a stable electric current, which could be affected by Joule heat generation. It was observed that it was not possible to increase the voltage beyond −10 kV, as the electric current was beyond the instrument limit. In addition, at −10 kV applied voltage we noted an up-scale excursion of the baseline (detector drift). A voltage of −7 to −8 kV proved to be the best compromise between the applied voltage, migration time, sensitivity and baseline noise. We also noted that at −7 kV applied voltage the reproducibility of the migration time was very good and the current through the capillary was fairly stable (190 μA). This means that under the conditions used the Joule heating was negligible.

Gold samples were prepared in 10–70% carrier solution. Consequently, in all cases the conductivity of the sample was lower than that of the carrier solution, allowing the possibility of working in stacking conditions [21,22]. Under the conditions used (pH ≈ 1), silanols on the capillary wall become more protonated as the buffer pH is made more acidic, thereby reducing the charge on the capillary walls. Correspondingly, the electroosmotic flow should also be minimal or approach zero [23,24]. This was confirmed by the fact that we were not able to detect the methanol injected (as a marker) even when applying a positive or negative voltage. Thus, the electrophoretic mobility rate of $AuCl_4^-$ at pH 1, neglecting any small residual electroosmotic mobility, can be estimated using the equation

$$\mu_{ep} = LL_d/Vt_m \quad (1)$$

where L is the capillary length, L_d is the capillary length to the detector cell, V is the applied voltage and t_m is the observed migration time. According to Eq. 1, the electrophoretic mobility of $AuCl_4^-$ is $-4.5 \cdot 10^{-4}$ cm^2 V^{-1} s^{-1}.

Working at high ionic strength and low pH should yield a more reproducible separation, since changes in ionic strength and pH can cause significant changes in the magnitude of the electroosmotic flow. In contrast, separations that depend solely on the electrophoretic mobility are not subject to these flow variations [23]. The applied voltage can be increased when using a carrier solution containing 0.1 *M* Cl^-. Consequently, the migration time of the gold complex will be shorter. Under these conditions the samples have to be prepared in 100% carrier solution to avoid the instability of the $AuCl_4^-$, but the system will not work under stacking conditions, which improve the sensitivity and resolution.

It is also possible to determine Pd(II) and Pt(IV) simultaneously at 270 nm (to be published elsewhere), while at 220 nm all three can be determined simultaneously (Fig. 2). Nevertheless, the sensitivity of Pd(II) at this wavelength is about twice that at 270 nm, while the sensitivity of Pt(IV) is approximately three times lower.

3.3. *Calibration graph, detection limit and reproducibility*

Several calibration graphs were obtained by changing the concentration of the carrier solution (10–70%) in the prepared standards. At high sample-solution conductivity, the peak is broad and the sampling time is therefore limited. From preliminary experiments the following upper limits were selected: 20-s sampling time for samples containing 50–70% carrier solution

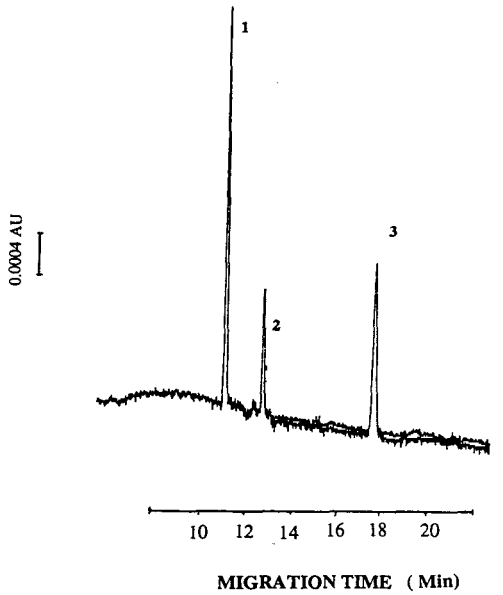

Fig. 2. Electropherogram obtained for a mixture of standard chloride complexes of Pd(II), Pt(IV) and Au(III). Conditions: capillary, 70 cm (50 cm to detector); carrier solution, 0.1 *M* HCl–0.4 *M* NaCl; voltage, −7 kV; UV detection at 220 nm; sampling time, 10 s. Sample contained 40% carrier solution. Peaks: 1 = Pd(II), 5 μg ml^{-1}; 2 = Pt(IV), 10 μg ml^{-1}; 3 = Au(III), 4 μg ml^{-1}.

and 50 s for the rest. Fig. 3 shows that by decreasing the concentration of carrier solution in the sample, the peaks obtained are sharper, owing to the improvement achieved through stacking conditions. A linear relationship between the peak area or peak height and gold concentration in the range 0.5–25 μg/ml was observed under all conditions for the calibration graphs tested ($r = 0.991$–0.999). The good correlation indicates that this method can be used for samples having a conductivity in the range 8–50 mS cm^{-1} (10–70% carrier solution in the sample). In the case where the gold sample is prepared in less than 10% carrier solution, a decrease in the area of the $AuCl_4^-$ peak was observed owing to the formation of hydrolysis species, which occurs at higher pH and lower chloride concentration [19]. For samples prepared in more than 70% of carrier solution, however, the peak was broad owing to the high sample conductivity (Fig. 3, peak 1). The detection limits for the different experiments performed are given in Table 1. A factor of two is often used in CZE to calculate the detection limit relative to the baseline noise; we used a factor of three [25]. A linear relationship was

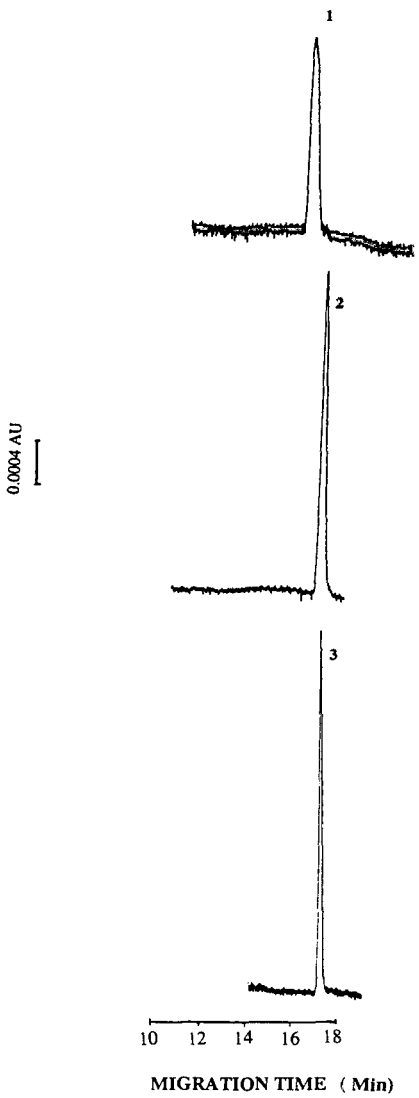

Fig. 3. Electropherograms of $Au(Cl)_4^-$ standard samples prepared at different concentrations of carrier solution. Conditions: sampling time, 20 s; other conditions as in Fig. 2. Sample preparation: (peak 1) 5 μg ml^{-1} Au(III) dissolved in carrier solution; (peak 2) 5 μg ml^{-1} Au(III) containing 50% carrier solution; (peak 3) 4 μg ml^{-1} Au(III) containing 10% carrier solution.

Table 1
Detection limits (DL) of gold at different concentrations of carrier solution in the sample (C) and injection times (t)

C (%)	t (s)	DL (μg mol^{-1})
10	50	0.07
20	50	0.08
30	50	0.11
40	20	0.19
50	20	0.20
70	20	0.29

Experimental conditions: −7 kV, 220 nm; fused-silica capillary (70 cm × 0.05 mm I.D.).

observed between the slopes of the regression equations (found to be related to peak height) of the calibration graphs and the composition of the carrier solution.

Table 2 summarizes some results for the reproducibilities obtained for different concentrations of gold and carrier solution in the sample. The relative standard deviations of peak heights and peak areas for successive injections were found to be less than 4.2%, and for the migration time it was below 0.87% ($n = 10$). Good reproducibilities were observed under all conditions used, but the sensitivity appeared to increase when the carrier solution content in the sample was decreased. This is because stacking conditions were met to a greater extent, so the sampling injection time could consequently be increased to obtain sharp peaks.

3.4. Application

The method was applied to the monitoring of gold(III) concentration during a study of $AuCl_4^-$ transport through a solid-supported liquid membrane. In these experiments, gold was selectively transported and concentrated using two-compartment cells containing two aqueous phases separated by a hydrophobic membrane, impregnated with an organic phase permeable to gold. One of the compartments (feed solution) contained gold(III) and 0.5–1 M sodium chloride (pH 2) and the other compartment contained a stripping solution.

Fig. 4 shows the electropherogram of a sample after appropriate dilution. For comparison, the same sample was analysed by CZE according to the described procedure and by flame AAS. The values obtained were 2.50 and 2.46 μg ml^{-1} using the CZE and AAS techniques, respectively, i.e., not significantly different. The first peak in Fig. 4 is NO_3^- (a contaminant), which was confirmed by using a standard addition method.

Acknowledgements

This work was supported by CICYT (Spanish Ministry of Education and Science) project AMB 93-0482 and MAT 93-0621-C03-02. B. Baraj and A. Merkoçi gratefully acknowledge CICYT and

Table 2
Relative standard deviations of peak area (R.S.D.-A), peak height (R.S.D.-h) and migration time (R.S.D.-t) of $AuCl_4^-$ at different concentrations of carrier solution in the sample (C) and injection times (t)

C (%)	Au (μg ml^{-1})	t (s)	R.S.D.-A (%)	R.S.D.-h (%)	R.S.D.-t (%)
40	5	10	3.36	1.90	0.78
40	5	20	1.56	0.95	0.80
40	2	20	1.90	3.40	0.67
30	5	20	3.37	2.20	0.75
30	3	50	1.10	2.70	0.42
30	3	20	2.30	3.20	0.87
20	5	20	3.25	0.56	0.54
20	3	50	4.20	4.10	0.30

Other conditions as in Table 1.

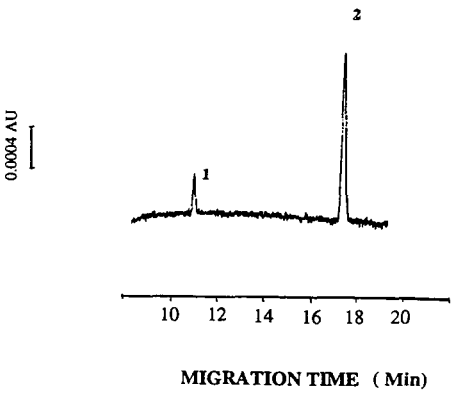

Fig. 4. Electropherogram of 2.5 μg ml^{-1} Au(III) sample. Sample preparation: dilution with 0.025 *M* HCl, injection; other conditions as in Fig. 3. Peaks: 1 = NO_3^- (contaminant), 2 = $AuCl_4^-$.

CIRIT, respectively, for the fellowships they received.

References

[1] C.A. Monning and R.T. Kennedy, Anal. Chem., 66 (1994) 280R–314R.
[2] S.F.Y. Li, Capillary Electrophoresis: Principles and Application, Elsevier, Amsterdam, 1993.
[3] M.L. Marina and M. Torre, Talanta, 41 (1994) 1411–1433.
[4] M. Aguilar, X. Huang and R.N. Zare, J. Chromatogr., 480 (1989) 427–431.
[5] W. Buchberger, O.P. Semanova and A.R. Timerbaev, J. High Resolut. Chromatogr., 16 (1993) 153–156.
[6] M. Aguilar, A. Ferran and M. Martinez, J. Chromatogr., 635 (1993) 127–131.
[7] S. Motomizu, M. Oshima, S. Matsuda, J. Obata and H. Tanaka, Anal. Sci., 8 (1992) 619–625.
[8] B. Baraj, M. Martinez, A. Sastre and M. Aguilar, J. Chromatogr. A, 695 (1995) 103–111.
[9] D.F. Swaile and M.J. Sepaniak, Anal. Chem., 63 (1991) 179–184.
[10] M. Koberta, M. Konkowski, P. Joungberg, W.R. Jones and A. Weston, J. Chromatogr., 602 (1992) 335–340.
[11] H. Onishi, Mikrochim. Acta, 1 (1959) 9–17.
[12] T.M. Cotton and A.A. Woolf, Anal. Chim. Acta, 22 (1960) 192–194.
[13] R. Kuroda, Y. Hayshibe and K. Yoshitsuka, Fresenius' J. Anal. Chem., 336 (1990) 494–497.
[14] I.A. Blyum, N.N. Pavlova and F.P. Kalupina, Zh. Anal. Khim., 26 (1971) 55–64.
[15] R. Hahn and M. Ikramuddin, At. Spectrosc., 6 (1985) 77–78.
[16] J.C. Van Loon, M.S. Szeto, W.W. Howson and I.A. Levin, At. Spectrosc., 5 (1984) 43–45.
[17] F.A. Cotton and G. Wilkinson, Advanced Inorganic Chemistry, a Comprehensive Text, Wiley, New York, 5th ed., 1988.
[18] E. Hogfeldt, Stability Constants of Metal-Ion Complexes, Part A: Inorganic Ligands (IUPAC Chemical Data Series, No. 21), Pergamon Press, Oxford, 1982.
[19] C.F. Baes and R.E. Mesmer, The Hydrolysis of Cations, Wiley, New York, 1976.
[20] I. Puigdomenech, TRITA-00K-3010, Royal Institute of Technology, Stockholm, 1983.
[21] D.S. Burgin and R.L. Chien, Anal. Chem., 63 (1991) 1046–1050.
[22] R.L. Chien and D.S. Burgi, J. Chromatogr., 559 (1991) 141–152.
[23] R.M. McCormick, Anal. Chem., 60 (1988) 2322–2328.
[24] P. Jandik and G. Bonn, Capillary Electrophoresis of Small Molecules and Ions, VCH, New York, 1993.
[25] I.C. Miller and J.N. Miller, Statistics for Analytical Chemistry, Wiley, Chichester, 2nd ed., 1988.

ELSEVIER

Journal of Chromatography A, 718 (1995) 233–237

JOURNAL OF CHROMATOGRAPHY A

Short communication

Migration behavior of niacin derivatives in capillary electrophoresis

Shunitz Tanaka[a,*], Kokoro Kodama[a], Takashi Kaneta[b], Hiroshi Nakamura[a]

[a]*Division of Material Science, Graduate School of Environmental Earth Science, Hokkaido University, Sapporo 060, Japan*
[b]*Department of Chemical Science and Technology, Faculty of Engineering, Kyushu University, Hakozaki, Fukuoka 812, Japan*

First received 5 April 1995; revised manuscript received 30 May 1995; accepted 2 June 1995

Abstract

The migration behaviour of niacin derivatives was investigated by capillary zone electrophoresis (CZE) and micellar electrokinetic chromatography (MEKC). When the pH of the buffer solution is lower than the pK_a of the pyridine ring in the niacin derivatives, they are positively charged by protonation on the pyridine ring and migrate electrophoretically. The mobilities of niacin derivatives in CZE were controlled by the pH of the migrating buffer. Good separation of thirteen niacin derivatives was achieved at pH 2.8. Further, to shorten the analytical time and to achieve a more complete separation, an investigation by MEKC using sodium dodecyl sulfate micelles was performed. All thirteen niacin derivatives were eluted within 30 min and a satisfactory separation was achieved.

1. Introduction

Niacin (nicotinic acid) is a type of vitamin that is widely distributed in animals and vegetables. It is converted into NAD (nicotinamide adenine dinucleotide) and NADH (nicotinamide adenine dinucleotidic acid), which behave as coenzymes for many redox enzymes in the cells. Niacin leads to many derivatives by an in vivo metabolic pathway. Consequently, to establish in detail the dynamic behaviour of niacin in vivo, an analytical technique with high resolution and sensitivity for these derivatives is required [1]. Previously, we have reported that some niacin derivatives could be separated by capillary tube isotachophoresis (cITP) [2]. However, cITP could not offer a complete separation. Niacin derivatives have a pyridine ring in their structure, and most of them behave similarly as weak bases. The small difference in the electrophoretic mobilities makes it difficult to separate them by cITP.

Capillary electrophoresis (CE) has attracted interest in many areas recently because of the high resolution. Capillary zone electrophoresis (CZE), one of the separation modes of CE, is a powerful separation technique for many ionic substances. CZE has a high resolution for ionic species but not for non-ionic species. For the separation of non-ionic species, micellar electrokinetic chromatography (MEKC) can be applied [3,4]. Therefore, the separations of many substances have been attempted by using CE. The separation of water- or fat-soluble vitamins has been performed by using CZE and MEKC [5–9]. However, investigations of the migration behaviour of niacin derivatives in detail have not yet been reported.

* Corresponding author.

0021-9673/95/$09.50
SSDI 0021-9673(95)00634-6

In this study, the migration behaviour of niacin derivatives was investigated by CZE and MEKC. First we attempted to separate niacin derivatives on the basis of proton dissociation equilibrium at the pyridine ring in the CZE mode. The electrophoretic mobilities were calculated from the migration times. Further, the migration behaviour of the niacin derivatives in buffer containing sodium dodecyl sulfate (SDS) was investigated by MEKC, and their distribution coefficients into SDS micelles were evaluated.

2. Experimental

2.1. Apparatus

A polyimide-coated fused-silica capillary (70 cm × 50 μm I.D.) was purchased from GL Science (Tokyo, Japan). A Model HCZE-30PNO.25 high-voltage power supply (Matsusada Precision Devices, Shiga, Japan) was used for applying high voltages. An ISCO (Lincoln, NE, USA) CV^4 variable-wavelength absorbance detector was used to measure the absorbance at 185 or 210 nm on the column at a position 20 cm from the negative end of the capillary. The measurements of migration times and recording of electropherograms were carried out with a Model D-2500 Chromato-Integrator (Hitachi, Tokyo, Japan). The sample solution was introduced into the capillary by raising the positive end of the capillary about 4 cm higher than the other end. The electroosmotic velocities of the bulk solution and the electrophoretic velocities of SDS micelles were calculated from the signals of methanol and Sudan III, respectively.

2.2. Reagents

All reagents were of analytical-reagent grade. β-Picoline, 3-pyridinemethanol, isonicotinic acid hydrazide, pyridine-3-aldehyde, 3-acetylpyridine, N-methylnicotinamide, thionicotinamide, nicotinic acid ethyl ester, nicotinic acid and pyridine-3-sulfonic acid were purchased from Tokyo Kasei (Tokyo, Japan), pyridine, nicotinamide, Sudan III and SDS from Wako (Osaka, Japan) and 6-aminonicotinamide from Sigma (St. Louis, MO, USA).

Sample solutions were prepared by dissolving the above reagents in water at 50–100 m*M*, except for thionicotinic acid and 6-aminonicotinic acid, which were dissolved in hydrochloric acid, and nicotinic acid, which was dissolved in potassium hydroxide solution. Mixed samples were prepared by mixing equal volumes of each solution.

Buffer solutions were prepared by mixing 0.02 *M* chloroacetic acid solution (pH 2.8) or 0.02 *M* potassium phosphate solution (pH 7.0) or 0.02 *M* boric acid solution (pH 9.1) with 0.01 *M* potassium hydroxide solution in order to adjust the pH to the required value. A buffer solution of pH 5.0 was prepared by mixing 0.02 *M* acetic acid with 0.02 *M* sodium acetate solution. For MEKC, SDS was dissolved in 0.02 *M* boric acid–0.01 *M* potassium hydroxide buffer solution. The buffer solution passed through a 0.2-μm cellulose acetate filter (Toyo Roshi Kaisha) prior to use. The solutions of niacin derivatives were stored in a refrigerator.

3. Results and discussion

3.1. CZE separation

First, the migration behaviour of niacin derivatives was investigated by CZE. The relationship between the pH of the migrating buffer and the electrophoretic mobility of niacin derivatives obtained in the CZE mode is shown in Fig. 1. When 0.02 *M* borate buffer (pH 9.1) was used as the migrating solution, most of the niacin derivatives (**1–11**) were eluted at the same velocity as the electroosmotic flow (EOF). Because these niacin derivatives are electrically neutral in this buffer solution, the electrophoretic mobility is zero. Therefore, these substances move at the same velocity and no separation could be achieved. On the other hand, nicotinic acid (**12**) and pyridine-3-sulfonic acid (**13**) were eluted after methanol. They have a strong acid dissocia-

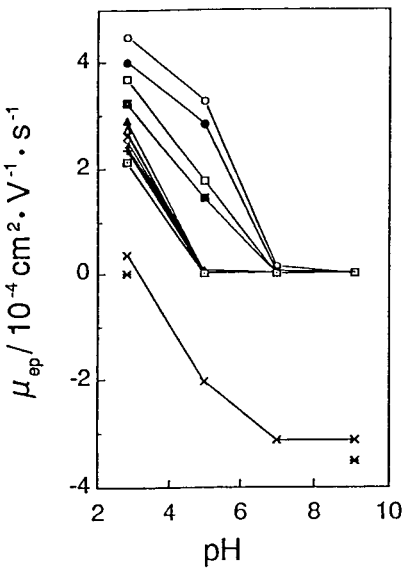

Fig. 1. Effect of the pH on electrophoretic mobility. Buffers: pH 2.8, chloroacetic acid; pH 5.0, acetic acid; pH 7.0, phosphoric acid; pH 9.1, boric acid. Voltage, 15 kV; capillary length, 70 cm. Compounds: ○ = pyridine (**1**); ● = β-picoline (**2**); □ = 3-pyridinemethanol (**3**); ■ = 6-aminonicotinamide (**4**); ▲ = pyridine-3-aldehyde (**5**); △ = isonicotinic acid hydrazide (**6**); ◆ = 3-acetylpyridine (**7**); ◇ = nicotinamide (**8**); + = thionicotinamide (**9**); ┼ = N-methylnicotinamide (**10**); ⊡ = nicotinic acid ethyl ester (**11**); × = nicotinic acid (**12**); ✳ = pyridine-3-sulfonic acid (**13**).

tion group which is negatively charged at this pH. Therefore, they migrated electrophoretically in the opposite direction to the EOF. The electrophoretic mobilities of the niacin derivatives, except nicotinic acid and pyridine-3-sulfonic acid, increased with decreasing pH. When the pH of the buffer solution is lower than the pK_a of the pyridine ring in the niacin derivatives, they are positively charged by protonation on the pyridine ring. The degree of ionization depends on the pK_a of these species. The electrophoretic mobilities of the niacin derivatives can be controlled on the basis of the acid dissociation equilibrium. The pK_a values of the niacin derivatives used in this study are about 3–5 [10].

A good separation of the thirteen niacin derivatives was achieved at low pH (2.8). At pH 2.8, the electrophoretic mobilities of nicotinic acid (**12**) and pyridine-3-sulfonic acid (**13**) are nearly zero. The positive charge due to protonation of the pyridine ring is neutralized by the negative charge of the strong acid dissociation groups, and therefore the net charge of these substances is close to zero. Pyridine-3-sulfonic acid migrated with the EOF and was detected at this pH. However, pyridine-3-sulfonic acid was not eluted at pH 7 and 5. The migration behaviour of this compound at various pH values can be considered as follows. The EOF at pH 9.1 is so fast that pyridine-3-sulfonic acid can be eluted even if it has a negative charge to migrate electrophoretically in the opposite direction to the EOF. At pH 2.8, although the EOF is slow, pyridine-3-sulfonic acid can be eluted because the electrophoretic mobility in the opposite direction to the EOF is zero, as mentioned previously. However, the electrophoretic mobility of negatively charged pyridine-3-sulfonic acid in the opposite direction to the EOF is larger than the EOF at pH 5 and 7. Therefore, pyridine-3-sulfonic acid was not eluted to the detector side and could not be detected at these pH values.

Fig. 2 shows the electropherograms at pH 9.1 and 2.8. At pH 9.1, most of the niacin derivatives except nicotinic acid (**12**) and pyridine-3-sulfonic acid (**13**) could not be separated, whereas at pH 2.8, the thirteen niacin derivatives were separated completely. The elution order seems to follow approximately the pK_a order. However, about 50 min were required for the elution of all the niacin derivatives including pyridine-3-sulfonic acid (**13**). At low pH, the EOF becomes small and it therefore becomes difficult to detect neutral and negatively charged species at low pH. Similar investigations were carried out at lower pH. More peaks than the number of sample species were observed at pH 2.0. These peaks were assumed to originate from the reaction products between niacin derivatives in the acidic medium.

It was found that the separation of niacin derivatives by CZE was improved by controlling the pH. However, in the CZE mode, a longer migration time was required for the detection of all the niacin derivatives and broadening of the peak of pyridine-3-aldehyde also occurred.

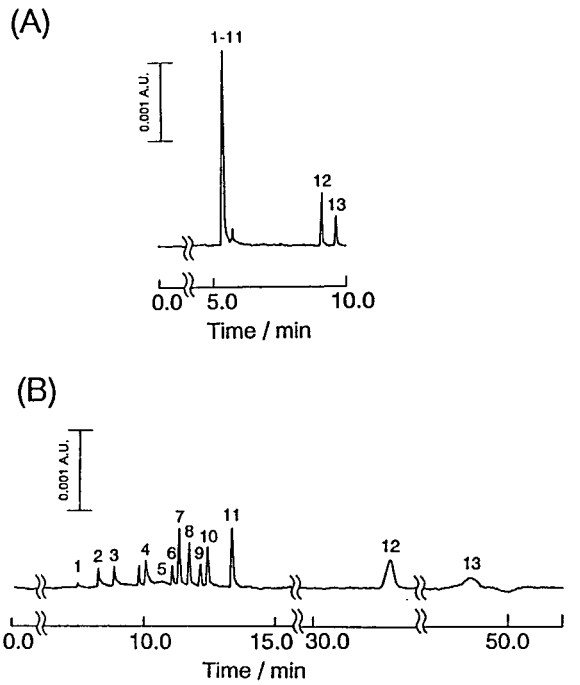

Fig. 2. Electropherograms of the niacin derivatives at pH 9.1 and 2.8. Buffers: (A) pH 9.1, boric acid; (B) pH 2.8, chloroacetic acid. Voltage, 15 kV; capillary length, 70 cm. Peak numbers correspond to the compounds in Fig. 1.

3.2. MEKC separation

To shorten the analytical time and achieve a more complete separation, investigations using buffers with various SDS concentrations were performed. The chromatogram of the thirteen niacin derivatives with 0.15 *M* SDS is shown in Fig. 3. All niacin derivatives (**1–13**) were eluted within 30 min and a satisfactory separation was achieved. The elution order in MEKC differed considerably from that in CZE; the distribution of the derivatives into the micelles seems to determine the elution order.

The relationship between the capacity factor and SDS concentration was studied. It has been reported that the capacity factor, k', of an electrically neutral species in the MEKC mode could be calculated from the migration time [2,3]. Fig. 4 shows the dependence of the capacity factor on SDS concentration. For the calculation of the distribution coefficients, the value

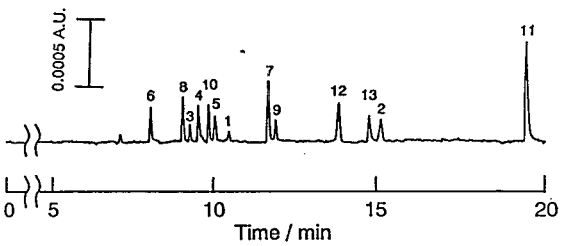

Fig. 3. Electrokinetic separation of niacin derivatives in the presence of SDS. Micellar solution: 0.15 *M* SDS in 0.02 *M* borate–0.01 *M* KOH (pH 9.1). Capillary length, 70 cm; voltage, 15 kV; current, 30 μA. Peak numbers correspond to the compounds in Fig. 1.

reported by Shinoda and Soda [11] was used for the partial specific volume of the SDS micelles. A linear relationship was observed for most of the niacin derivatives. The distribution coefficients calculated from the slopes of these plots are summarized in Table 1. However, reasonable slopes for nicotinic acid and pyridine-3-sulfonic acid were not obtained. With this buffer (pH 9.1), nicotinic acid and pyridine-3-sulfonic acid are negatively charged, and SDS is also negatively charged. Therefore, these compounds

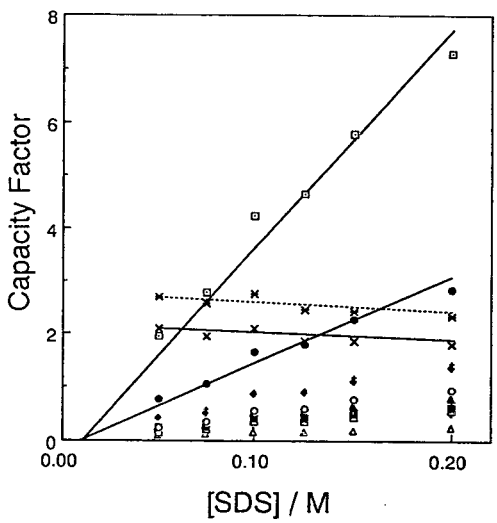

Fig. 4. Dependence of capacity factor on SDS concentration. Micellar solution: SDS in 0.02 *M* borate–0.01 *M* KOH (pH 9.1). Voltage, 15 kV; current, 11 μA at 0.05 *M*, 19 μA at 0.10 *M*, 24 μA at 0.125 *M*, 30 μA at 0.15 *M*, 38 μA at 0.20 *M*; capillary length, 70 cm. Symbols as in Fig. 1.

Table 1
Distribution coefficients (K) calculated from slopes of plots of k' vs. SDS concentration

No.	Compound	K[a]
11	Nicotinic acid ethyl ester	151.8
2	β-Picoline	59.6
13	Pyridine-3-sulfonic acid	–
12	Nicotinic acid	–
9	Thionicotinamide	29.9
7	3-Acetylpyridine	28.6
1	Pyridine	20.0
5	Pyridine-3-aldehyde	16.7
10	N-Methylnicotinamide	15.0
4	6-Aminonicotinamide	12.3
3	3-Pyridinemethanol	11.7
8	Nicotinamide	4.50
6	Isonicotinic acid hydrazide	3.73

[a] Partial specific volumes ($\bar{v}$) were used to calculate distribution coefficients (K); $\bar{v} = 0.8721$ ml g^{-1}.

hardly distribute into the micellar phase because of the electrical repulsion.

4. Conclusion

The migration behaviour of some niacin derivatives was investigated by CZE and MEKC. In the CZE mode, the separation of niacin derivatives was improved by controlling the pH, and the separation of thirteen niacin derivatives was achieved at pH 2.8. A more satisfactory separation of the niacin derivatives was obtained within 30 min by MEKC with a migration buffer containing 0.15 M SDS. The distribution efficiencies of the niacin derivatives into the SDS micelles were evaluated.

References

[1] T. Kobayashi (Editor), Vitamin Handbook, Vol. 2, Kagaku Dojin, 1989, p. 75 (in Japanese).
[2] S. Tanaka, T. Kaneta, H. Yoshida and H. Ohtaka, J. Chromatogr., 521 (1990) 158–162.
[3] S. Terabe, K. Otsuka, K. Ichikawa, A. Tsuchiya, T. Ando, Anal. Chem., 56 (1984) 111–113.
[4] S. Terabe, K. Otsuka and T. Ando, Anal. Chem., 57 (1985) 834–841.
[5] S. Boonkerd, M.R. Detaevernier and Y. Michotte, J. Chromatogr. A, 670 (1994) 209–214.
[6] H. Nishi, N. Tsumagari, T. Kakimoto and S. Terabe, J. Chromatogr., 465 (1989) 331–343.
[7] U. Jegle, J. Chromatogr. A, 652 (1993) 495–501.
[8] C.P. Ong, C.L. Ng, H.K. Lee and S.F.Y. Li, J. Chromatogr., 547 (1991) 419–428.
[9] H. Nishi, N. Tsumagari and S. Terabe, Anal. Chem., 61 (1989) 2434–2439.
[10] D.D. Perrin (Editor), Dissociation Constants of Organic Bases in Aqueous Solution, Butterworths, London, 1965.
[11] K. Shinoda and T. Soda, J. Phys. Chem., 67 (1963) 2072–2074.

PUBLICATION SCHEDULE FOR THE 1996 SUBSCRIPTION

Journal of Chromatography A

MONTH	Oct. 1995	Nov. 1995	Dec. 1995[a]	
Journal of Chromatography A	715/1	715/2 716/1 + 2 717/1 + 2	718/1 718/2	The publication schedule for further issues will be published later.
Bibliography Section				

[a] Vol. 701 (Cumulative Indexes Vols. 652–700) expected in December.

INFORMATION FOR AUTHORS

(Detailed *Instructions to Authors* were published in *J. Chromatogr. A*, Vol. 657, pp. 463–469. A free reprint can be obtained by application to the publisher, Elsevier Science B.V., P.O. Box 330, 1000 AH Amsterdam, Netherlands.)

Types of Contributions. The following types of papers are published: Regular research papers (full-length papers), Review articles, Short Communications, Discussions and Letters to the Editor. Short Communications are usually descriptions of short investigations, or they can report minor technical improvements of previously published procedures; they reflect the same quality of research as full-length papers, but should preferably not exceed five printed pages. Discussions (one or two pages) should explain, amplify, correct or otherwise comment substantively upon an article recently published in the journal. Letters to the Editor (max. two printed pages) bring up ideas, comments, opinions, experiences, advice, disagreements, insights, etc. For Review articles, see inside front cover under Submission of Papers.

Submission. Every paper must be accompanied by a letter from the senior author, stating that he/she is submitting the paper for publication in the *Journal of Chromatography A*.

Manuscripts. Manuscripts should be typed in **double spacing** on consecutively numbered pages of uniform size. The manuscript should be preceded by a sheet of manuscript paper carrying the title of the paper and the name and full postal address of the person to whom the proofs are to be sent. As a rule, papers should be divided into sections, headed by a caption (*e.g.*, Abstract, Introduction, Experimental, Results, Discussion, etc.). All illustrations, photographs, tables, etc., should be on separate sheets. Manuscripts should be accompanied by a 5.25- or 3.5-in. disk. Your disk and (**exactly matching**) printed version (printout, hardcopy) should be submitted together to the accepting editor or Editorial Office **according to their request**. Please specify the type of computer and word-processing package used (do not convert your textfile to plain ASCII). Ensure that the letter "l" and digit "1" (also letter "O" and digit "0") have been used properly, and format your article (tabs, indents, etc.) consistently. Characters not available on your word processor (Greek letters, mathematical symbols, etc.) should not be left open but indicated by a unique code (*e.g.* gralpha, @,#, etc., for the Greek letter α). Such codes should be used consistently throughout the entire text. Please make a list of such codes and provide a key. Do not allow your word processor to introduce word splits and do not use a "justified" layout. Please adhere strictly to the general instructions on style/arrangement and, in particular, the reference style of the journal. Further information may be obtained from the Publisher.

Abstract. All articles should have an abstract of 50–100 words which clearly and briefly indicates what is new, different and significant. No references should be given.

Introduction. Every paper must have a concise introduction mentioning what has been done before on the topic described, and stating clearly what is new in the paper now submitted.

Experimental conditions should preferably be given on a *separate* sheet, headed "Conditions". These conditions will, if appropriate, be printed in a block, directly following the heading "Experimental".

Illustrations. The figures should be submitted in a form suitable for reproduction, drawn in Indian ink on drawing or tracing paper. Each illustration should have a caption, all the *captions* being typed (with double spacing) together on a *separate sheet*. If structures are given in the text, the original drawings should be provided. Coloured illustrations are reproduced at the author's expense. The written permission of the author and publisher must be obtained for the use of any figure already published. Its source must be indicated in the legend.

References. References should be numbered in the order in which they are cited in the text, and listed in numerical sequence on a separate sheet at the end of the article. Please check a recent issue for the layout of the reference list. Abbreviations for the titles of journals should follow the system used by *Chemical Abstracts*. Articles not yet published should be given as "in press" (journal should be specified), "submitted for publication" (journal should be specified), "in preparation" or "personal communication".

Vols. 1–651 of the *Journal of Chromatography*; *Journal of Chromatography, Biomedical Applications* and *Journal of Chromatography, Symposium Volumes* should be cited as *J. Chromatogr.* From Vol. 652 on, *Journal of Chromatography A should be cited* as *J. Chromatogr. A* and *Journal of Chromatography B: Biomedical Applications* as *J. Chromatogr. B.*

Dispatch. Before sending the manuscript to the Editor please check that the envelope contains four copies of the paper complete with references, captions and figures. One of the sets of figures must be the originals suitable for direct reproduction. Please also ensure that permission to publish has been obtained from your institute.

Proofs. One set of proofs will be sent to the author to be carefully checked for printer's errors. Corrections must be restricted to instances in which the proof is at variance with the manuscript.

Reprints. Fifty reprints will be supplied free of charge. Additional reprints can be ordered by the authors. An order form containing price quotations will be sent to the authors together with the proofs of their article.